

AD-758 590

**HEAT-TRANSFER MEASUREMENTS IN SHORT-
DURATION HYPERSONIC FACILITIES**

D. L. Schultz, et al

Advisory Group for Aerospace Research and
Development
Paris, France

February 1973

DISTRIBUTED BY:

NTIS

National Technical Information Service
U. S. DEPARTMENT OF COMMERCE
5285 Port Royal Road, Springfield Va. 22151

-AD 758590

AGARD-AG-165

1

AGARD-AG-165

AGARD

ADVISORY GROUP FOR AEROSPACE RESEARCH & DEVELOPMENT

7 RUE ANCELLE 92200 NEUILLY SUR SEINE FRANCE

AGARDograph No. 165

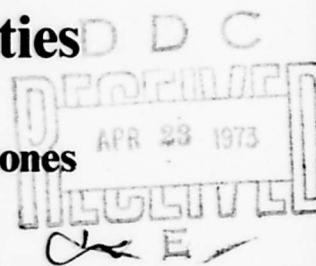
on

Heat-transfer Measurements in Short-duration Hypersonic Facilities

by

D.L.Schultz and T.V.Jones

This document has been approved
for public release and sale; its
distribution is unlimited.



NORTH ATLANTIC TREATY ORGANIZATION

Reproduced by
**NATIONAL TECHNICAL
INFORMATION SERVICE**
U S Department of Commerce
Springfield VA 22151



**DISTRIBUTION AND AVAILABILITY
ON BACK COVER**

**NORTH ATLANTIC TREATY ORGANIZATION
ADVISORY GROUP FOR AEROSPACE RESEARCH AND DEVELOPMENT
(ORGANISATION DU TRAITE DE L'ATLANTIQUE NORD)**

**AGARDograph No.165
HEAT-TRANSFER MEASUREMENTS IN SHORT-DURATION
HYPERSONIC FACILITIES**

by

**D.L.Schultz and T.V.Jones
Department of Engineering Science, University of Oxford, Gt. Britain**

THE MISSION OF AGARD

The mission of AGARD is to bring together the leading personalities of the NATO nations in the fields of science and technology relating to aerospace for the following purposes:

- Exchanging of scientific and technical information;
- Continuously stimulating advances in the aerospace sciences relevant to strengthening the common defence posture;
- Improving the co-operation among member nations in aerospace research and development;
- Providing scientific and technical advice and assistance to the North Atlantic Military Committee in the field of aerospace research and development;
- Rendering scientific and technical assistance, as requested, to other NATO bodies and to member nations in connection with research and development problems in the aerospace field;
- Providing assistance to member nations for the purpose of increasing their scientific and technical potential;
- Recommending effective ways for the member nations to use their research and development capabilities for the common benefit of the NATO community.

The highest authority within AGARD is the National Delegates Board consisting of officially appointed senior representatives from each member nation. The mission of AGARD is carried out through the Panels which are composed of experts appointed by the National Delegates, the Consultant and Exchange Program and the Aerospace Applications Studies Program. The results of AGARD work are reported to the member nations and the NATO Authorities through the AGARD series of publications of which this is one.

Participation in AGARD activities is by invitation only and is normally limited to citizens of the NATO nations.

The material in this publication has been reproduced
directly from copy supplied by AGARD or the author.

Published February 1973

533.6.011.6 : 533.6.011.55
533.6.071



*Printed by Technical Editing and Reproduction Ltd
Harford House, 7-9 Charlotte St. London. W1P 1HD*

PREFACE

This is the first of several AGARDographs commissioned by the Fluid Dynamics Panel to deal with instrumentation techniques used in hypersonic short-duration facilities and with related topics. Since one of the reasons for the development of such facilities was the need for experimental data on the extremely high heat-transfer rates that a body experiences in re-entry conditions, the measurement of heat transfer constitutes a particularly appropriate initial subject area; moreover, the methods to be described are also applicable to a variety of problems other than those of hypersonic flow.

An important feature of this AGARDograph is the unified treatment that it accords to the theory underlying heat-transfer gauges of various types. In addition, a detailed analysis is given of the magnitude of the errors in the values of heat-transfer rate deduced from the observation. Constructional considerations are discussed fully; physical data and design charts are included.

A subsequent AGARDograph will cover the subject of force measurements in short-duration facilities. Of a complementary character, a later AGARDograph is being planned to describe measurement methods used in various types of rapidly varying flow other than those produced in shock tunnels and similar short-duration facilities.

Dr R.C.Pankhurst
Fluid Dynamics Panel Member

HEAT-TRANSFER MEASUREMENTS IN SHORT-DURATION HYPERSONIC FACILITIES

D.L.Schultz and T.V.Jones

CONTENTS

	<u>Page</u>
<u>INTRODUCTION</u>	1
1 <u>ONE-DIMENSIONAL ANALYSIS OF HEAT TRANSFER GAUGES</u>	4
2 <u>GAUGES OPERATING ON THE SEMI-INFINITE PRINCIPLE</u>	6
a. Variation of Surface Temperature with Time and Heat Transfer Rate	6
b. Measurement of Surface Temperature with Thermocouples, Thin Film Resistance Thermometers and Semiconductor Resistance Thermometers	9
c. Errors Introduced by the Presence of the Surface Sensor	12
d. Thermal Properties of Substrate Materials	19
d(i) Variation with Temperature	19
d(ii) Effect of the Variation of Thermal Properties on Calculated Heat Transfer Rates	21
e. Calibration Techniques	23
e(i) Electrical Discharge Calibration of Thin Film Heat Transfer Gauges	23
e(ii) Thermal Radiation Techniques	25
e(iii) Errors Introduced by Non-Uniformity in Thin Film Thickness	26
e(iv) Standard Heat Transfer Gauges	29
f. Construction of Thin Film and Thermocouple Gauges	30
g. Analysis of Data from Thin Film Heat Transfer Gauges	35
g(i) Numerical Computation	35
g(ii) Analogue Circuits	37
h. Practical Circuits for use with Thin Film Heat Transfer Gauges	40
3 <u>CALORIMETER GAUGES</u>	41
a. The Ideal Calorimeter and Limitations of the Simple Theory	41
b. One-Dimensional Analyses	41
b(i) Equation for Surface Temperature Rise	41
b(ii) Calorimeter without Substrate	42
b(iii) Calorimeter with Substrate	43
c. The Rose Calorimeter Gauge	45
d. Thin Skin Calorimeter Models	47
d(i) Elementary Principles	47
d(ii) The Variation of Calorimeter Properties with Temperature	48
d(iii) Conduction Effects	48
d(iv) Construction Techniques for Thin Skin Models	51
e. Capsule and 'Slug' Calorimeter Gauges	53
f. Thick Wall Calorimeters	56
g. Total Calorimeters	58
4 <u>PYROELECTRIC HEAT TRANSFER GAUGES</u>	59
5 <u>MEASUREMENT OF RADIATIVE HEAT TRANSFER</u>	61
a. Instruments Based on Thin Film Gauges	61
b. Circular Disc Radiometers	63

6	<u>OPTICAL METHODS</u>	
a.	Principles	66
b.	Surface Temperature Measurements	67
b(i)	Temperature Sensitive Colour-Change Paints	67
b(ii)	Phase-Change Coatings	67
b(iii)	Liquid Crystals	68
b(iv)	Thermographic Phosphors	68
b(v)	Infra-Red Emission	69
c.	The Determination of Heat Transfer Rates from Optically Recorded Surface Temperatures	70

7	<u>THE ERRORS IN DEDUCED HEAT TRANSFER RATE ARISING FROM A SURFACE TEMPERATURE DISCONTINUITY DUE TO THE PRESENCE OF AN ISOLATED HEAT TRANSFER GAUGE</u>	72
---	---	----

	<u>REFERENCES</u>	75
--	-------------------	----

	<u>APPENDICES</u>	82
A-1	Characteristics of Thermocouples 0 - 800°C	
A-2	Thermal Properties of Electrical Insulators at 300 K	
A-3	Thermal Properties of Metals at 300 K	

	<u>NOMENCLATURE</u>	84
--	---------------------	----

FIGURES

PRINCIPAL ABBREVIATIONS

A.A.S.U.	Dept of Aeronautics and Astronautics, Southampton University, U.K.
A.E.D.C.	Arnold Engineering Development Centre, Tullahoma, U.S.A.
A.F.B.	Wright Patterson Air Force Base, Ohio, U.S.A.
A.R.C.	Aeronautical Research Council, U.K.
B.R.L.	Ballistics Research Laboratory, Aberdeen Proving Ground, Maryland.
C.A.L.	Cornell Aeronautical Laboratory, Buffalo, New York.
D.F.V.L.R.	Deutsche Forschungs- und Versuchsanstalt für Luft- und Raumfahrt, Germany.
G.E.C.	General Electric Company, Philadelphia, U.S.A.
I.C.	Imperial College of Science and Technology, London, U.K.
L.T.V.	Ling Temco Vought Aerospace Corp., Dallas, Texas.
N.O.L.	Naval Ordnance Laboratory, Maryland, U.S.A.
T.P.R.C.	Thermophysical Properties Research Centre, Purdue, U.S.A.
O.N.E.R.A.	Office National d'Études et de Recherches Aerospatiales, France
U.T.I.A.S.	University of Toronto Institute of Aerospace Sciences, Canada.
V.K.I.	Von Kármán Institute, Rhode-St-Genèse, Belgium.

INTRODUCTION

Much of the early research on high-enthalpy, high-Mach-number flows was accomplished in shock tubes in which the flow duration was of order ten microseconds. Valuable information was obtained from such experiments, however, since the main problems associated with re-entry bodies having ballistic trajectories concerned the stagnation region. For these problems Mach number simulation is not so important as the attainment of the correct enthalpy. Stagnation temperatures up to 6000 K and pressures up to 11 MN/m^2 may be obtained in shock tubes operated in the straight through mode with cold hydrogen at 100 MN/m^2 as the driver, and the use of a combustion driver at a maximum pressure of 100 MN/m^2 to raise the driver gas sound speed enables conditions of 10,000 K and 9.5 MN/m^2 to be reached, thus increasing the range of simulation and permitting a 7 km/s re-entry body with a ballistic trajectory to be studied down to impact. In straight-through shock tubes the flow duration is a function of the driver and driven tube lengths and in facilities used for bluff body research the flow duration was typically 20 to $40 \mu\text{s}$. In such flow durations it is possible to measure heat transfer rates and pressure distributions, although the main emphasis in early work was naturally on heat transfer rates, since pressure distributions were less likely to be affected by real gas effects and could therefore be measured in perfect-gas facilities. Although it is theoretically possible to increase the flow duration in straight-through shock tubes by lengthening both the driver and driven tube the attenuation of the primary shock wave reduces the benefits to be gained and few high enthalpy shock tubes have been constructed with lengths greater than about 30 m, with flow durations of about $30 \mu\text{s}$. More importantly the shock attenuation causes severe spatial non-uniformity of gas properties behind the incident shock wave since the gas immediately behind the shock and first to pass over the model has been processed by a weaker shock than that which passed through the gas nearer to the contact surface. Allowance for such non-uniformity can be made but the reliability of the data obtained is reduced. At shock Mach numbers below about 4 the shock attenuation is a less severe problem and the theoretical advantages of increasing the tube lengths can be realised.

Expansion of the gas behind the incident shock wave was first employed at Cornell Aeronautical Laboratories to produce hypersonic flow Mach numbers at stagnation temperatures up to 6000 K. The starting processes in the nozzles of such simple expansion shock tunnels leads to a reduction in the flow duration, which is already short; to overcome this limitation, tunnels operating in the 'reflected shock' mode (in which the high-pressure and high-temperature gas behind a reflected shock is used as a reservoir) were proposed by Cornell Aeronautical Laboratory (1). The flow duration in such tunnels can extend to 15 ms and working section Mach numbers between 6 and 24 have been achieved. Operation in the 'tailored interface' mode (in which reflections from the contact surface are prevented by matching of the sound speeds on either side of the contact surface) enables the flow duration to be further extended until the limitation is ultimately imposed by the length of the driver section. Beginning with the pioneering work at Cornell Aeronautical Laboratory the concept of the tailored interface shock tunnel has been extended and applied in a large number of facilities so that it now represents one of the commonest forms of operation. Although pure hydrogen at room temperature, when used as a driver gas, will only provide tailoring conditions at a shock Mach number of 6, which results in a stagnation temperature of about 3200 K, the limit may be lowered by the use of suitable nitrogen-hydrogen dilution mixtures as shown by Woodley and others (2).

At about the same time that shock tunnels operating in the reflected-shock mode were being developed in the United States the gun tunnel became established as an alternative hypersonic facility. Cox and Winter (3) laid the foundations for a facility which has since been developed at Imperial College, London (4), Oxford University and Southampton University (5) and at other centres. This relatively simple device has the advantages

of a longer running time, typically 30 to 50 ms, which enables detailed studies of boundary layer transition, boundary layer profiles and other phenomena to be made. Gun tunnels, however, appear to have been less useful in the investigation of real gas effects since their mode of operation has been typically at stagnation temperatures below 1200 K and generally at temperatures just high enough to avoid condensation in the working section.

Two further similar devices employing free pistons for gas compression have also had an important effect on the progress of hypersonic research. The first, the free piston tunnel R4CH developed by Leuchter at ONERA (6), employs isentropic compression of a preheated gas to attain temperatures up to 1700 K. A 1.5 kg piston is accelerated slowly in a compression tube of length 10 m and volume 0.11 m^3 to achieve final pressures of 25 MN/m^2 and flow durations between 0.2 s at $M = 7$ and 0.5 s at $M = 14$. The flow duration in this tunnel enables many conventional techniques to be employed for the measurement of aerodynamic quantities such as forces although heat transfer rates are obtained from thin wall calorimeter gauges whose response is transient in nature. The second type of free piston compressor is the 'Longshot' originally developed by Perry at Republic Aviation (7) and subsequently installed at the von Karman Institute for Fluid Dynamics. In this device a 0.125 m^3 volume of gas is compressed by a heavy piston, 2.3 to 8.8 kg, and the resulting high pressure gas is trapped in a reservoir by an array of 48 non-return valves. Extremely high pressures may be obtained from this ballistic piston compression process, 400 MN/m^2 being the current limit with a planned increase to 1350 MN/m^2 . Since the gas is trapped at constant volume the pressure falls during the tunnel running time and the analysis of the data must take this into account. A continuous measurement of dynamic pressure enables corrections to be made to free flight determinations of forces and moments, which have been one of the major contributions from this facility.

Arc heated tunnels, which form an important part of the range of hypersonic facilities, were first developed at A.E.D.C., Tullahoma (8) as short duration facilities with flow durations up to about 30 ms. The energy for these first tunnels was derived from inductor or capacitor storage systems. Their advantages at that time were the high stagnation pressures which could be obtained by virtue of the nature of the reservoir itself, a closed volume, which could be stressed to withstand pressures up to 170 MN/m^2 at temperatures after arc discharge of 8000 K. The use of such intermittent arc driven tunnels has become widespread and five large installations are in use in the United States and in France. Arc heaters have been employed for tunnels with longer flow durations than is common in the 'hotshots' described above. Tunnels have been built with flow durations ranging from 15 s for the N.O.L. high energy facility, which operates at a stagnation pressure of 6.7 MN/m^2 , to continuous operation for lower pressure systems such as the PK2 plasma tunnel at D.F.V.L.R. Porz Wahn in which the stagnation pressure is 1 MN/m^2 .

The very high stagnation temperatures and pressures which may be obtained in short duration facilities is of course the main reason for their widespread use at hypersonic speeds but their performance must be compared with conventional hypersonic tunnels which are capable of continuous or near continuous operation. A broad classification of hypersonic facilities has been attempted in Fig. 1. It will be seen that there is a considerable amount of overlap in flow duration at the lower end of the time scale and in particular between about 1 and 20 ms. In this regime both straight-through and reflected shock tunnels (1), gun tunnels, (3), (4), and the V.K.I. 'Longshot', (9), are available and in these facilities most aerodynamic tests may be made although the shorter times around 1 ms permit only simple studies such as heat transfer rate. At the upper end of the scale (at about 20 to 40 ms) the flow duration is adequate for multicomponent balances, free flight techniques and detailed pressure distribution.

Intermittent arc facilities ('Hotshot' tunnels), the ONERA free piston adiabatic compressor R4CH and Ludwig tubes, (10), (11), span the range between 0.1 and 0.5 s and

in the last case the tunnel stagnation temperature may be up to 1100 K for $M = 9$ operation in the D.F.V.L.R. 0.5 m Ludwig tube at Göttingen. Between the upper end of these intermittent tunnels and the lower end of the operating time scale of hypersonic blowdown tunnels only one facility is at present capable of operation at high stagnation temperature, the N.O.L. hypervelocity tunnel (12). This tunnel is capable of 1 to 4 s operation at stagnation temperatures of 2800 K. Several blowdown tunnels are capable of high stagnation temperatures but in general the upper Mach number is limited to about 15.

A comparison of the various types of hypersonic tunnels may be made on the basis of Reynolds number. Although the test core is often substantially smaller than the tunnel exit, a comparison based on tunnel exit dimension indicates the size of the tunnel as well as its working pressure. Such a comparison is shown in Fig. 2 where it will be seen that, with the exception of the 0.75 m diameter M 16-20 blowdown tunnel at Wright Patterson A.F.B., most high-Reynolds-number, high-Mach-number facilities are essentially of the short duration type. The exceptions are seen in the N.O.L. hypervelocity tunnel whose Re_D is 10^8 at $M = 10$ and the 0.75 m continuous hypersonic tunnel at Wright Patterson A.F.B. with Re_D between 1.5 and 2.5×10^6 at Mach numbers between 16 and 22.

This volume is the first of several AGARDographs which it is hoped will review the techniques available for making measurements in short duration and rapidly varying flows. Since the extreme aerodynamic heating undergone by re-entry bodies was one of the phenomena which stimulated the development of short-duration hypersonic tunnels it is appropriate that the measurement of heat transfer rate should be the subject to be treated. Perhaps few other techniques developed especially to meet the demands of short duration flows have found such widespread application or encouraged the use of intermittent techniques in general to the same extent as have fast response heat flux gauges which were originally proposed by Vidal at Cornell Aeronautical Laboratory (13). Indeed the measurement of heat transfer rate is easier in almost all transient facilities than in continuous hot tunnels because in a continuous tunnel the model must be internally cooled to establish the temperature gradient from which the heat transfer rate is deduced, it must be capable of withstanding the recovery temperature continuously, and if the model has a large thermal capacity the tunnel itself must be operated for an extended period to achieve uniform conditions within the model. In transient facilities, on the other hand, the model never attains an equilibrium temperature and it is the nature of its approach to such thermal equilibrium that enables the heat flux rate to be determined. Thus models may be constructed from relatively simple materials including thermal insulators such as quartz and conductors such as metals, and used in flows whose stagnation temperatures may approach 15,000 K. The sudden onset of the high temperature flow results in a rapid rise in the model's surface temperature and a variety of transducers is employed to measure this temperature-time history.

The literature on heat transfer measurements in transient facilities is extensive but there have been to date no publications which have attempted to provide a unified theoretical treatment. One of the objects of the present monograph, therefore, is to demonstrate that the analysis of many types of heat transfer gauge may be approached from a single theoretical model of transient heat conduction in a two-layered medium. Accordingly section 1 is concerned with the theoretical derivation of the temperature at any point within a layered medium comprising two separate substances in thermal contact. The solution, in terms of integral transforms, enables the temperature to be determined as a function of time for prescribed heat transfer rates. The analysis of the many types of heat transfer transducer may then be obtained quite simply by applying the appropriate boundary conditions. A thin-film resistance thermometer heat-transfer gauge, for example, consists of a two-layered material in which the front surface material is a thin conducting sheet mounted on a semi-infinite material of low thermal conductivity (section 2.a). A thin wall calorimeter model (section 3.b) is analysed by allowing a finite thickness conducting element to be backed by a material of negligible

thermal conductivity. By including the effects of thermal conductivity in the substrate in this latter case it has been possible (section 3 b (iii)) to apply the unified theoretical approach to the investigation of the effects of heat losses on the frequently used 'thick film' heat transfer gauges (called 'Rose' gauges in this monograph after the originator). The analysis of the errors which arise in the use of heat transfer gauges has been aimed at predicting effects (such as that due to the presence of the thin film in section 2.c) on the measured heat transfer rate, which is the error which the user wants to know, rather than effects on the surface temperature. The effect of non-linearities in thermocouple sensitivities and of the variation of thermal properties of the metallic and insulating components of the transducers is also discussed and the likely effects on the overall accuracy is assessed.

Other types of heat transfer transducer also dealt with in the present volume include radiation gauges suitable for use in aerodynamic facilities (section 5). Section 6 is devoted to optical methods in which the surface temperature is indicated by thermosensitive paints, pyrographic phosphors or liquid crystals. Finally section 7 deals with the effect of any surface temperature discontinuity due to the presence of a heat transfer gauge on the inferred heat transfer coefficient.

Throughout the monograph the aim has been to emphasise the fundamental processes of heat conduction which govern the function of each transducer and to demonstrate the transient response time, sensitivity and possible errors which characterise each technique. It is hoped that sufficient practical details have been given for new techniques to be used with confidence. Methods of data analysis have been discussed in some detail in the case of the thin-film resistance thermometer, for instance, including a critical appraisal of all the electrical analogue circuits commonly used in conjunction with this form of transducer (section 2.g(ii)). Several charts have been devised to assist in the design of thin film gauges and calorimeter gauges for a wide range of expected heat transfer rates and flow durations. Any errors noticed in the published literature were corrected in the preparation of the monograph.

It is hoped that the monograph will fulfil the role of a useful reference source for the expert, bringing together some of the widely scattered information to which he constantly needs to refer. In addition, the very powerful heat transfer measurement techniques now available for exploiting the advantages of short duration wind tunnels will find application in other research fields.

1. ONE-DIMENSIONAL ANALYSIS OF HEAT TRANSFER GAUGES

The basic time dependent problem of both thin film gauges (i.e. those relying on conduction in a semi-infinite medium) and calorimeter gauges is that of conduction into a slab of material (medium 1) mounted on a semi-infinite extent of another material (medium 2) as shown in Fig. 3. In the case of a thin film gauge this slab is a thin metallic film deposited on the surface of the medium 2 in order to monitor the surface temperature. It is desired that the film is of such a thickness that it does not affect the temperature history of the substrate surface. On the other hand a calorimeter gauge employs a relatively thick slab as medium 1; the temperature of this is measured using thermocouples mounted at some point in the slab and it is necessary to know how this measured temperature is related to those throughout the slab. Furthermore it is necessary to deduce how much heat is lost from the slab into any backing material or supporting structure on which it is necessary to mount the calorimeter.

In this section therefore the basic equations common to the above situations are set out; these will subsequently be expanded in later sections dealing with specific problems. In order to determine the response time of gauges, for example, the following equations are solved for the particular case of a step function input of heat transfer rate.

The differential equations governing heat flow in the two media are:

$$\frac{\partial^2 T_1}{\partial x^2} = \frac{1}{\alpha_1} \frac{\partial T_1}{\partial t} \quad (1)$$

$$\frac{\partial^2 T_2}{\partial x^2} = \frac{1}{\alpha_2} \frac{\partial T_2}{\partial t} \quad (2)$$

The temperature is T at a distance x from the surface, at time t ;
 α is the diffusivity of the material defined in terms of the thermal conductivity, k , the density, ρ , and the specific heat, c , $\alpha = k/\rho c$. The suffices 1 and 2 refer to the slab and backing material respectively as shown in Fig.3. If the surface heat transfer rate is $\dot{q}_s(t)$, then:

$$-k_1 \frac{\partial T_1}{\partial x} = \dot{q}_s \text{ at } x = 0 \quad (3)$$

At the interface between regions 1 and 2, $x = l$:

$$k_1 \frac{\partial T_1}{\partial x} = k_2 \frac{\partial T_2}{\partial x} \text{ and } T_1 = T_2 \quad (4)$$

Also $T_2 = 0$ at $x = \infty$.

Taking the Laplace transforms, denoted by $\bar{}$ we obtain:

$$\frac{\partial^2 \bar{T}_1}{\partial x^2} = \frac{p}{\alpha_1} \bar{T}_1 \quad (5)$$

$$\frac{\partial^2 \bar{T}_2}{\partial x^2} = \frac{p}{\alpha_2} \bar{T}_2 \quad (6)$$

which give the general solutions:

$$\bar{T}_1 = A e^{x(p/\alpha_1)^{1/2}} + B e^{-x(p/\alpha_1)^{1/2}} \quad (7)$$

$$\bar{T}_2 = C e^{x(p/\alpha_2)^{1/2}} + D e^{-x(p/\alpha_2)^{1/2}} \quad (8)$$

Transforming the boundary conditions of Eqs (3) and (4) we have:

$$-k_1 \frac{\partial \bar{T}_1}{\partial x} = \bar{q}_s \text{ at } x = 0 \quad (9)$$

$$k_1 \frac{\partial \bar{T}_1}{\partial x} = k_2 \frac{\partial \bar{T}_2}{\partial x} \text{ at } x = l \quad (10)$$

$$\bar{T}_2 = 0 \text{ at } x = \infty \quad (11)$$

and using these to eliminate the constants from Eqs (7) and (8) we obtain:

$$\bar{T}_1 = \frac{\bar{q}_s \sqrt{\alpha_1} \left[(1+a) e^{-(x-l)\sqrt{p/\alpha_1}} + (1-a) e^{(x-l)\sqrt{p/\alpha_1}} \right]}{k_1 \sqrt{p} \left[(1+a) e^{l\sqrt{p/\alpha_1}} - (1-a) e^{-l\sqrt{p/\alpha_1}} \right]} \quad (12)$$

$$\bar{T}_2 = \frac{2 \bar{q}_s \sqrt{\alpha_1} e^{(l-x)\sqrt{p/\alpha_2}}}{k_1 \sqrt{p} \left[(1+a) e^{l\sqrt{p/\alpha_1}} - (1-a) e^{-l\sqrt{p/\alpha_1}} \right]} \quad (13)$$

where

$$a = \sqrt{\frac{\rho_2 c_2 k_2}{\rho_1 c_1 k_1}}$$

The transformed time derivatives of temperature are given by the equation

$$\frac{\partial \bar{T}}{\partial t} = p \bar{T} \quad (14)$$

These solutions (Eqs (12), (13) and (14) are applied to the problems that arise in the following sections which in general involves inverting the transformed quantities and using numerical techniques or expanding in approximate forms.

This set of transformed equations forms the basis for the unified treatment of all types of calorimeter heat transfer gauges, thin film gauges and thick wall transducers and are thus the central feature of the present monograph. The process of inverting these transformed equations is simplified in the thin film gauge for example by allowing l to tend to zero. For the calorimeter gauge l is finite and a is usually much less than unity so that a second form of simplification is possible.

2 GAUGES OPERATING ON THE SEMI-INFINITE PRINCIPLE

One of the heat transfer gauges most commonly used in short duration facilities is the thin film resistance thermometer. The surface temperature is determined from the change of resistance of the film and the heat transfer rate is inferred from the application of Eqs (12) and (13) in the preceding section. The surface temperature of the model may in fact be determined by a variety of methods employing surface thin film thermocouples, semiconductor resistance thermometers or by the use of thermosensitive paints but to a large extent the basic theory will be the same. It is the object of this section to determine the magnitude of the surface temperature rise which occurs under different conditions of heat transfer rate and flow duration, the effect of the thermal properties of the substrate on this rise and the thickness of the substrate which must be employed to ensure that simple one-dimensional theory may be applied.

2.a Variation of Surface Temperature with Time and Heat Transfer Rate

Assuming in the first instance that the surface measuring film has negligible effect on the heat conduction process, the surface temperature of the substrate may be found by putting $l=0$ in Eq(13). The temperature of the substrate then becomes:

$$\bar{T}_x = \frac{1}{\sqrt{\rho c k}} \frac{\bar{q}_s}{\sqrt{p}} e^{-x\sqrt{p}} \quad (15)$$

where $(\rho c k)$ and α refer to the substrate properties.

At the surface, $x=0$,

$$\bar{T}_s = \frac{1}{\sqrt{\rho c k}} \frac{\bar{q}_s}{\sqrt{p}} \quad (16)$$

and inverting the transform,

$$T_s = \frac{1}{\sqrt{\pi} \sqrt{\rho c k}} \int_0^t \frac{\dot{q}_s(\tau) d\tau}{(t-\tau)} \quad (17)$$

Alternatively the heat transfer rate at the surface may be obtained from Eq (16) in the form

$$\begin{aligned}\bar{q}_s &= \bar{T}_s \sqrt{\rho} \sqrt{eck} \\ &= \rho \bar{T}_s \frac{1}{\sqrt{\rho}} \sqrt{eck}\end{aligned}\quad (18)$$

Inverting Eq(18) yields:

$$\dot{q}_s = \frac{\sqrt{eck}}{\sqrt{\pi}} \int_0^t \frac{dT(\tau)}{(t-\tau)^{1/2}} d\tau \quad (19)$$

This form is inconvenient for data reduction since it involves the differential of the surface temperature and the presence of noise will make the determination of Eq (19) difficult. Integrating Eq (19) by parts with $T(t) - T(\tau) = Z$,

$$\dot{q}_s = \sqrt{\frac{eck}{\pi}} \left\{ \frac{1}{2} \left[\frac{-2Z}{(t-\tau)^{1/2}} \right] + \int_0^t \frac{Z d\tau}{(t-\tau)^{3/2}} \right\}$$

For $\tau = 0$, $T(\tau) = 0$;

hence:

$$\dot{q}_s = \sqrt{\frac{eck}{\pi}} \left[\frac{T(t)}{\sqrt{t}} + \int_0^t \frac{T(t) - T(\tau)}{(t-\tau)^{3/2}} d\tau \right] \quad (20)$$

This is the form of the solution which is most convenient for data analysis when the heat transfer rate is not constant. In this form there is, however, a singularity in the integral term at $t = \tau$ which will give rise to errors in the deduced value of \dot{q}_s . These errors will in general be larger for t small and numerical techniques which either reduce or avoid this difficulty are discussed in detail in section 2g(1).

If the heat transfer rate is, however, constant, Eq (17) above reduces to:

$$\bar{T}_s = \frac{2\dot{q}_s}{\sqrt{\pi}} \sqrt{\frac{t}{eck}} \quad (21)$$

and it is seen that under such conditions the surface temperature is parabolic in form. The first important criterion is then how thick the substrate should be to enable the above analysis to be applied. This depth may be obtained by considering the solution of the heat transfer equation for the temperature T_x at a depth x . If the surface is subjected to a step function of surface heat transfer \dot{q}_s whose Laplace transform is \dot{q}_s/ρ , the temperature may be obtained from Eq (15):

$$\bar{T}_x = \frac{\dot{q}_s}{\sqrt{eck}} \frac{e^{-x\sqrt{\frac{p}{\alpha}}}}{p^{3/2}} \quad (22)$$

Inversion of this expression gives

$$T_x = \frac{\dot{q}_s}{\sqrt{eck}} \left[\frac{2\sqrt{t}}{\sqrt{\pi}} e^{-\frac{x^2}{4\alpha t}} - \frac{x}{\sqrt{\alpha}} \operatorname{erfc} \sqrt{\frac{x^2}{4\alpha t}} \right] \quad (23)$$

$$\dot{q}_x = -k \frac{\partial T}{\partial x} = \dot{q}_s \operatorname{erfc} \sqrt{\frac{x^2}{4\alpha t}} \quad (24)$$

Introducing a dimensionless penetration depth $x^* = x/\sqrt{4\alpha t}$ and putting $x=0$ in Eq (23) to obtain the surface temperature

$$\frac{T_x}{T_s} = e^{-(x^*)^2} - \sqrt{\pi} x^* \operatorname{erfc} x^* \quad (25)$$

$$\frac{\dot{q}_x}{\dot{q}_s} = \operatorname{erfc} x^* \quad (26)$$

Values of T_x/T_s and \dot{q}_x/\dot{q}_s are plotted in Fig.4. The ratio $T_x/T_s = 0.01$ at $x^* = 1.50$ and $\dot{q}_x/\dot{q}_s = 0.01$ at $x^* = 1.07$.

It should be noted that the penetration depth is often quoted as $\sqrt{\alpha t}$, i.e. $x^* = 0.5$, but it will be seen that at this depth the heat transfer rate is 50% of its surface value and the temperature 35% of its surface value. Dimensions for heat transfer gauges calculated on the basis of a penetration distance $x^* = 0.50$ will therefore result in serious heat loss from the rear of the sensitive element. Thus the ratios T_x/T_s and \dot{q}_x/\dot{q}_s do not fall to 0.01 until $x = 3.16\sqrt{\alpha t}$ and $x = 3.74\sqrt{\alpha t}$ respectively. The penetration depth at which T_x/T_s and \dot{q}_x/\dot{q}_s are 1% of their surface values are plotted in Fig.5. for some commonly used metals and insulators assuming constant thermal properties. It will be seen that the two criteria yield depths so close to each other that a convenient rule of thumb would be $x = 4\sqrt{\alpha t}$. For most metals this would yield $x(\text{cm}) = 4\sqrt{t \text{ sec}}$ and for insulators $x(\text{cm}) = 0.3\sqrt{t \text{ sec}}$. For reasons of mechanical strength, insulating substrate heat transfer gauges should probably exceed 2 mm in thickness and are thus satisfactory for all flow durations less than 0.3 second (for a 1% heat loss at the rear face). In the case of metallic gauges working on the 'semi-infinite' principle lengths between 4 and 12 cm are required for blowdown tunnels with flow durations between 1 and 10 seconds respectively. Clearly in the longer gauges great care has to be taken that heat transfer does not occur between the gauge and wall by the use of suitable thermal insulation. Values of T_s as a function of t when $\dot{q} = 1 - 10^3 \text{ W/cm}^2$ are shown in Fig.6 for several substrate materials.

The various techniques which are commonly used for the measurement of surface temperature are the subject of the next section. For low heat transfer rates or short flow durations accompanied by high heat transfer rates it is convenient to use thermally insulating substrates so that the surface temperature rise is higher and larger electrical signals are obtained from all transducer types whether they be thermocouples or thin film resistance thermometers. For higher heat transfer rates or longer flow durations at reduced heat transfer rates the substrate may be metallic since the surface temperature rise may make it possible to employ surface thermocouples (e.g. copper-constantan) in which one arm of the junction is formed by the substrate (e.g. copper) itself.

The same basic theory developed in this section applies to all types of transducer operating on the semi-infinite principle but care must be taken in the design of metallic substrate units. Using simple one-dimensional semi-infinite heat conduction with constant heat transfer rate to a copper slug, for example, the surface temperature can be shown to be $T_s = 0.32/\dot{q}\sqrt{t}$, T_s °C, \dot{q} W/cm², t s, and the expression is plotted in Fig 7 with $\dot{q} = 1 \text{ W/cm}^2$ to 10 kW/cm^2 . This graph should be read in conjunction with Fig.5 in order to determine the thickness of the gauge required to restrict heat loss from the rear surface to 1% of input heat transfer rate. It is clear that transducer lengths may become excessive (10 cm for 10 sec flow duration) if high accuracy is sought although the rear of the slug may be curved to fit inside the model, provided care is taken to insulate it. The metallic slug has been used (14) for a wide range of heat transfer measurements down to 10 W/cm^2 , the lower limit being set by the thermocouple voltage. Fig.7 shows contours of constant thermocouple output between 0.1 and

and 10.0 mV for copper-constantan junctions. For thermocouple signals to be above 0.1 mV at low heat transfer rates, less than 10 W/cm^2 for instance, flow durations greater than 1 s are required.

2.b Measurement of Surface Temperature with Thermocouples, Thin Film Resistance Thermometers and Semiconductor Resistance Thermometers.

The surface temperature rise in the substrate discussed in the preceding section may be measured in several ways but the most common are the thin film resistance thermometer and the surface thermocouple. The thin film resistance thermometer has been used chiefly on insulating substrates but the thermocouple may be used on both insulating and conducting bases and in the latter case the base itself often forms one leg of the thermojunction. In both the thin film thermometer and thin film thermocouple errors may be introduced by the finite thickness and thermal conductivity of the metal layer; these errors are treated in detail in section 2.c.

A comparison of the sensitivities of the two types of surface temperature gauge, the thin film and the thin film thermocouple, may be made by reference to the following two tables.

Table 1
Temperature sensitivities of some common thermocouples

Metal Combinations	Sensitivity (0-55°C) $\mu\text{V/K}$
Copper-Constantan	40
Iron-Constantan	50
Chromel-Alumel	40
Platinum-Platinum/Rhodium(13% Rhodium)	6.0
Platinum-Platinum/Rhodium(10% Rhodium)	6.0
Chromel-Constantan	63

Table 2
Temperature sensitivities for some common resistance thermometers
for $V_0 = 1 \text{ V}$

Metal	Temperature Coefficient $\alpha_R, \text{K}^{-1} \times 10^3$	Sensitivity V/K
Aluminium	4.05	0.00405
Copper	3.90	0.00390
Gold	3.41	0.00341
Nickel	5.40	0.00540
Platinum	3.01	0.00301
Rhodium	3.30	0.00430
Silver	3.79	0.00379

The temperature sensitivities of the resistance thermometers in Table 2 have been compared at a constant value of mean film voltage, in this case 1.00 V, but the sensitivity is directly proportional to the mean film voltage since $\Delta V/V_0 = \alpha_R \Delta T$. It would thus appear that higher sensitivities could be obtained by operation at as high

a film voltage as possible, within the limits set by heat dissipation. To some extent this is the case and a figure of merit has been suggested by Metcalfe (15) whereby $\Delta V/\Delta T$ is compared when the films are dissipating equal power per unit area since this takes into account the differing resistivities of the materials. With the restriction of equal power the mean film voltage is then proportional to the square root of the resistivity and thus the overall sensitivity $\Delta V/\Delta T$ is proportional to $\sqrt{\epsilon_R \alpha_R}$. Metcalfe has suggested figures of merit for several commonly used thin film thermometers and his comparison is shown in Table 3 below using, however, the values of α_R from Table 2 where available.

Table 3
Figure of merit $\alpha_R \sqrt{\epsilon_R}$ for metals

Metal	Resistivity ϵ_R ohm cm $\times 10^6$	Temperature Coefficient α_R $K^{-1} \times 10^3$	$\alpha_R \sqrt{\epsilon_R}$ $K^{-1} \Omega^{1/2} cm^{1/2} \times 10^9$
Platinum	90.0	3.01	28.5
Gold	2.44	3.41	5.32
Nickel	11.1	5.40	17.95
Chromium	13.0	3.00	10.83
Copper	1.7	3.90	5.08
Iron	17.8	14.70	62.00

It will be seen that on the basis of this comparison platinum is better than all other metals with the exception of iron which has not been used so far for thin film thermometers. Nickel is also better than chromium and gold so that either platinum or nickel are recommended for this purpose. Silicon semiconductor resistance thermometers are now available with temperature coefficients of $0.0069 K^{-1}$ in miniaturised form with dimensions 1.5 mm x 0.5 mm suitable for fixing to both metal and insulating substrates. Reference is made to this type of temperature sensor in section 3.e where their use on calorimeter gauges is discussed. As surface thin film thermometers they would suffer from the relatively fragile nature of the lead connections but this restriction does not of course apply when the units are mounted on the rear face of calorimeter gauges. Although the temperature coefficient is not significantly greater than that of most of the metals quoted in Table 2 their resistance is very high, of order 5000 ohms. The power dissipation is limited to 50 milliwatts so that the supply current must not exceed 3.16 mA but this current will produce a voltage drop of 15.8 volts and the temperature sensitivity $\Delta V/\Delta T$ will be 0.109 volt/K about 50 times that of a platinum resistance thermometer.

Although the sensitivity of the thin film resistance thermometers listed above are much greater than those of the thermocouples there have been recent advances in semiconductor thermocouples which promise to reverse this situation. Thermocouples of 'p' and 'n' germanium junctions have been reported with sensitivities of $2.0 mV K^{-1}$ although at present their internal impedances are higher than those of thin film gauges and electrical interference difficulties would therefore be more serious although not necessarily insuperable. The advantages of the thermocouple system are the smaller sizes which may be attained in the thin film form and the relative simplicity of the electrical leads which, being inactive, may be made narrower than the leads for a thin film resistance thermometer. It is also possible to utilise the model itself as one leg of the thermojunction if it is made of a suitable material such as nickel. A thin layer of insulating material such as silicon dioxide is put down with a gap into which the other thermojunction metal penetrates, (see detail in Fig.8). Alternatively the model itself may be made thermally insulating and both legs of the thermojunction laid down on the surface by vacuum evaporation, (Fig.8(a)). The thickness of the insulating

layer must be sufficiently thick to appear 'semi-infinite' for the duration of the flow in the facility and it will be seen from Fig.5 that this dimension need be only 3 mm for a 1 second flow duration for quartz or Pyrex insulation. In the case of the solid metal model in which the model forms one arm of the thermojunction, however, it will be seen from Fig.5 that a thickness of 3 cm is required for the same flow duration if the model is to appear 'semi-infinite'. This thickness is excessive for a metal such as nickel and such techniques are more suitable for flow durations shorter than 1 second; a thickness of 3 mm would be satisfactory for a flow duration of 10 ms. An example of a semiconductor thermocouple gauge suitable for use in tunnels with a flow duration less than about 70 ms is shown in Fig.9. The substrate length is 0.5 cm of germanium with a surface thin film of gold approximately 1 micron thick bridging two bars of 'p' type and 'n' type germanium respectively. This type of gauge was developed by Dixon et al (16) for the measurement of low heat transfer rates of order 0.1 W/cm^2 . The scheme is outlined in Fig.9(a) where it will be seen that the temperatures T_1 and T_3 are equal as are T_2 and T_4 so that the effect of the lead wire connections is self cancelling. Thus only the thermal gradient ΔT established by the unsteady heat conduction within the semiconductor bars will affect the measured voltage ΔV . For the p-n germanium junction the measured sensitivity was 2 mV/K and the loop resistance was 1300 ohm. The samples were cut from material with resistivity of 0.25 ohm cm 'p' type and 2.5 ohm cm 'n' type and exhibited a deviation of less than 2% of 2mV over the temperature range from 5° to 50°C . This sensitivity is however the same as would be achieved with a conventional thin film gauge of platinum with a temperature coefficient of 0.002/K when operated with a mean film voltage of 1 volt.

With combinations of heat transfer rates and flow durations which result in elevations of substrate temperature above about 50°C the non-constancy of thermal properties reduces the accuracy of measurements made with conventional thin film resistance thermometers. This topic is dealt with in detail in section 2d(ii) and although there are techniques available for the correction of the data there are advantages in using metallic substrates operating in the semi-infinite mode. Heat transfer rates between 500 and 1000 W/cm^2 can cause severe thermal stresses in insulating substrates and the surface may 'spall', small pieces being ejected from the surface. Erosion due to particles in the flow may also be troublesome particularly in arc-heated facilities and in both of these situations metallic substrate thermocouples are useful. Reference to Fig.7 in section 2.a shows that the surface temperature rise of copper for instance is about 1/20th of that of quartz. Examples of surface thermocouples mounted on metal substrates are shown in Fig.10. The type shown, comprising an insulated constantan wire fixed coaxially with a Chromel-P tube has been described by Kendall and Dixon (17). The ends of the wire and tube are ground and polished so that no overlap of metal remains. The surface may be ground to the contour of the model before deposition of the chromium film. The surface is then vapour plated with chromium to a thickness of 1 to $1.5 \mu\text{m}$ establishing contact between the constantan and chromel. In all such vapour deposited thermojunctions the sensitivity must be carefully checked since the standard thermal emf constants may not be applicable. Thermal emf's of metal/metal-alloy thermocouples are generally less than the thermal emf's of bulk materials when prepared in thin film form. It is also necessary to avoid lateral temperature gradients so that the thermojunction records a unique temperature. In coaxial systems such as that described above this will only be achieved when both the diffusivity and thermal conductivities of the two materials are the same.

Although thin film surface thermocouples are relatively insensitive their response is less likely to be affected by severely eroding flows, for instance at the stagnation points of bluff bodies. Provided that their internal resistance is low compared with the input impedance of the measuring system, changes in thermocouple resistance due to erosion damage will not affect the measured output voltage. An example of chromel-constantan thermocouple deposited at the end of a Pyrex 7740 rod is shown in Fig.10(b)

from Kendall et al (17), & (18). Wires of chromel and constantan are carried through the Pyrex rod and films of the two materials are vapour deposited to form a thermojunction.

2.c Errors Introduced by the Presence of the Surface Sensor

Although the thin metallic layers deposited on the surface of an insulator to form either resistance thermometers or thermocouples have thicknesses typically between 0.01 and 0.1 μm they have an effect on the surface temperature history which cannot be neglected. An analysis of the effect of finite thickness metallic films was first presented by Vidal (13) although the study was confined to errors in surface temperature. Subsequently Maulard (19) examined the effect of the surface element on the value of the heat transfer rate which would be deduced from such surface temperature measurements but his simplifying assumptions have resulted in an overestimate of the fractional error $(\dot{q}_0 - \dot{q})/\dot{q}_0$ by a factor of $\pi/2$, (\dot{q}_0 being the heat transfer rate in the absence of the surface film and \dot{q} the measured heat transfer rate). It is, of course, this ratio which is of more interest to the user than the error in surface temperature although it is possible to obtain some idea of the errors involved from the analysis of the temperature behaviour.

In this section a rigorous analysis of the effect of the surface film is presented in a form which enables it to be applied to any metal/substrate combination. For the particular case of a platinum film on a Pyrex substrate the ratio \dot{q}/\dot{q}_0 is calculated in terms of the dimensionless time $\alpha t/l^2$. This is compared with an analysis following that of Vidal (13) of the ratio of surface temperatures with and without surface films of finite conductivity.

The heat transfer rate is found from the temperature history of the thin film by assuming that this is the same as the surface temperature T_s , of a semi-infinite insulator subject to the same heat transfer history and hence the heat transfer rate is given by the inversion formula;

$$\dot{q}_s = \sqrt{\frac{\rho_2 c_2 k_2}{\pi}} \left[\frac{T_s(t)}{t} + \int_0^t \frac{T_s(t) - T_s(\tau)}{(t - \tau)^{3/2}} d\tau \right] \quad (27)$$

which in terms of the Laplace transforms is:

$$\bar{\dot{q}}_s = \sqrt{\rho_2 c_2 k_2} \sqrt{p} \bar{T}_s \quad (28)$$

The above assumption can now be tested by putting into the above equation an exact solution for the average temperature within the thin film for a step function in surface heat transfer rate and seeing when the rate deduced from the equation above, \dot{q} , approaches the actual value, \dot{q}_0 . The average temperature is sensibly that measured by monitoring the resistance of the film as shown by Rose (20).

As shown previously in section 1 the temperature distribution within the thin film for a constant-heat transfer rate is given by Eq (12) with $\bar{\dot{q}}_s = \dot{q}_0/p$:

$$\bar{T}_i = \frac{\dot{q}_0 \sqrt{\alpha_i} \left[(1+a) e^{-(x-l)\sqrt{\frac{p}{\alpha_i}}} + (1-a) e^{(x-l)\sqrt{\frac{p}{\alpha_i}}} \right]}{k_i p^{3/2} \left[(1+a) e^{l\sqrt{\frac{p}{\alpha_i}}} - (1-a) e^{-l\sqrt{\frac{p}{\alpha_i}}} \right]} \quad (29)$$

Thus
$$\int_0^l \bar{T}_1 dx = \frac{\dot{q}_0 \alpha_1}{k_1 \beta^2} \left[1 - \frac{2a}{(1+a)e^{L\sqrt{\frac{\beta}{\alpha_1}}} - (1-a)e^{-L\sqrt{\frac{\beta}{\alpha_1}}}} \right] \quad (30)$$

and
$$\bar{T}_{av} = \frac{1}{l} \int_0^l \bar{T}_1 dx \quad (31)$$

Inserting \bar{T}_{av} from Eq (31) into Eq (28) for the heat transfer rate we have

$$\bar{q} = \frac{\sqrt{\rho_2 c_2 k_2} \dot{q}_0 \alpha_1}{k_1 l} \left[\frac{1}{\beta^{3/2}} - \frac{2a}{\beta^{3/2}} \frac{1}{(1+a)e^{L\sqrt{\frac{\beta}{\alpha_1}}} - (1-a)e^{-L\sqrt{\frac{\beta}{\alpha_1}}}} \right] \quad (32)$$

which on expanding the denominator of the second term becomes

$$\bar{q} = \frac{\sqrt{\rho_2 c_2 k_2} \dot{q}_0 \alpha_1}{k_1 l} \left[\frac{1}{\beta^{3/2}} - \frac{2a}{1+a} \sum_{n=0}^{\infty} \frac{1}{\beta^{3/2}} \left(\frac{1-a}{1+a} \right)^n e^{-(2n+1)L\sqrt{\frac{\beta}{\alpha_1}}} \right] \quad (33)$$

Taking the inverse transform of this equation we have

$$\frac{\dot{q}}{\dot{q}_0} = 2az \left[\frac{1}{\sqrt{\pi}} - \frac{2a}{1+a} \sum_{n=0}^{\infty} \left(\frac{1-a}{1+a} \right)^n \text{ierfc} \left(\frac{n+1/2}{z} \right) \right] \quad (34)$$

where
$$z = \frac{\sqrt{\alpha_1 t}}{l}$$

This series may be evaluated for small values of t directly from the above equation; for large times this is difficult because the series converges only slowly and a solution for large times may be found by approximating $\text{ierfc } x$ as,

$$\text{ierfc } x = \frac{1}{\sqrt{\pi}} (1+x^2) - x$$

In this case the approximate solution is, for t large,

$$\frac{\dot{q}}{\dot{q}_0} = 1 - \frac{1}{\sqrt{\pi} z} \left(\frac{1}{a} - \frac{a}{2} \right) \quad (35)$$

From this equation the time taken for the fractional error in the deduced value of \dot{q} to be reduced to y is given by:

$$t = \frac{l^2}{\pi y^2 \alpha_1} \left(\frac{2-a^2}{2a} \right)^2$$

A plot of \dot{q}/\dot{q}_0 versus Z is given in Fig.11 for $a = 0.1$. Fig.12 is a plot of \dot{q}/\dot{q}_0 again for $a = 0.1$; in this case the abscissa is in terms of $(t_{\mu s})/(l_{\mu m})^2$ i.e. for a $1 \mu m$ film, t is in microseconds. Thus we see that for a $1 \mu m$ film approximately $517 \mu s$ is required before the deduced heat transfer rate is within 5% of its correct value.

Maulard (19) has performed a calculation similar to that just examined. The average film temperature was calculated as in Eq (31) but the heat flux rate inferred from this average temperature was found from the following equation:

$$\dot{q} = \frac{\sqrt{\pi \rho_2 c_2 k_2}}{2} \cdot \frac{T_{av}}{\sqrt{t}}$$

This last step is only approximate and the full equation relating the heat flux rate to the surface temperature, Eq (28), should be used. Maulard produces an approximate value of $(\dot{q}_0 - \dot{q})/\dot{q}_0$ for t large, applicable when $a \ll 1$, giving:

$$\frac{\dot{q}_0 - \dot{q}}{\dot{q}_0} = \frac{\sqrt{\pi}}{2 a Z} \quad (36)$$

compared to that of Eq (35) which gives:

$$\frac{\dot{q}_0 - \dot{q}}{\dot{q}_0} = \frac{1}{\sqrt{\pi} a Z}$$

It would appear therefore that Maulard has overestimated the error in the inferred heat flux rate by a factor $\pi/2$.

The response times above are shorter than those evaluated by Vidal (13) for the actual temperature of the film which always lags the ideal temperature by a fixed amount. This is due to the fact that the inversion depends largely on the derivative of the temperature with respect to time as seen by Eq (28). Busing (21) has measured the film thickness achieved by painting techniques and has found these to be approximately $0.5 \mu\text{m}$ for single coat films. In this case approximately $100 \mu\text{s}$ is required before the accuracy in the deduced heat transfer rate reaches 5%. Care should therefore be taken in interpreting results with such thin films in very short duration flows, such as encountered behind the incident shock wave in straight-through shock tubes.

In order to investigate the effect of the metallic surface film on the surface temperature in the presence of a prescribed heat transfer rate Eqs (12) and (13) may be arranged, following Vidal as:

$$\bar{T}_1 = \frac{\sqrt{\alpha_1} \bar{q}_s e^{-x\sqrt{p/\alpha_1}}}{k_1 \sqrt{p}} \left[\frac{1 + \sigma e^{-2(l-x)\sqrt{p/\alpha_1}}}{1 - \sigma e^{-2l\sqrt{p/\alpha_1}}} \right] \quad (37)$$

$$\bar{T}_2 = \frac{(1+\sigma)\sqrt{\alpha_1} \bar{q}_s e^{-l\sqrt{p/\alpha_1}}}{k_1 \sqrt{p}} \left[\frac{e^{-(x-l)\sqrt{p/\alpha_2}}}{1 - \sigma e^{-2l\sqrt{p/\alpha_1}}} \right] \quad (38)$$

$$\text{where } \sigma = \left[\frac{\sqrt{e_1 c_1 k_1}}{\sqrt{e_2 c_2 k_2}} - 1 \right] \times \left[\frac{\sqrt{e_1 c_1 k_1}}{\sqrt{e_2 c_2 k_2}} + 1 \right]^{-1} = \frac{1-a}{1+a} \quad (39)$$

In this form these solutions for the transformed temperatures are not readily inverted. The denominator may, however, be expanded in series form for $\sigma < 1$ to give:

$$\bar{T}_1 = \frac{\sqrt{\alpha_1} \bar{q}_s}{k_1 \sqrt{p}} \left\{ e^{-x\sqrt{p/\alpha_1}} + \sum_{n=1}^{\infty} \sigma^n \left[e^{-(2nl+x)\sqrt{p/\alpha_1}} + e^{-(2nl-x)\sqrt{p/\alpha_1}} \right] \right\} \quad (40)$$

$$\bar{T}_2 = \frac{(1+\sigma)\sqrt{\alpha_1} \bar{q}_s e^{-(x-l)\sqrt{p/\alpha_2}}}{k_1 \sqrt{p}} \sum_{n=0}^{\infty} \sigma^n e^{-(2n+1)l\sqrt{p/\alpha_1}} \quad (41)$$

These expressions are now in a form which can be inverted to obtain solutions for the temperature T_1 and T_2 noting that the inverse transform of $(p)^{-\frac{1}{2}} e^{-\gamma(p)^{\frac{1}{2}}}$ is $(\pi t)^{-\frac{1}{2}} e^{-\gamma^2/(4t)}$ for $\gamma \geq 0$ and also employing the convolution theorem:

$$L^{-1}[f_1(p) f_2(p)] = \int_0^t F_1(t-\lambda) F_2 \lambda d\lambda$$

$$\begin{aligned} T_1 = & \frac{1}{k_1 \sqrt{\pi}} \int_0^t \frac{\dot{q}_s(\lambda)}{\sqrt{t-\lambda}} e^{-\frac{x^2}{4\alpha_1(t-\lambda)}} d\lambda \\ & + \frac{1}{k_1 \sqrt{\pi}} \sum_{n=1}^{\infty} \sigma^n \int_0^t \frac{\dot{q}_s(\lambda)}{\sqrt{t-\lambda}} \left[e^{-\frac{(2nl+x)^2}{4\alpha_1(t-\lambda)}} + e^{-\frac{(2nl-x)^2}{4\alpha_1(t-\lambda)}} \right] d\lambda \end{aligned} \quad (42)$$

$$T_2 = \frac{(1+\sigma)}{k_1} \sqrt{\frac{\alpha_1}{\pi}} \sum_{n=0}^{\infty} \sigma^n \int_0^t \frac{\dot{q}_s(\lambda)}{\sqrt{t-\lambda}} e^{-\left[\frac{(2n+1)\frac{l}{\sqrt{\alpha_1}} + \frac{x-l}{\sqrt{\alpha_2}}}{4(t-\lambda)} \right]} d\lambda \quad (43)$$

Eqs (42) and (43) are the exact solutions for the temperature in a semi-infinite body which comprises two thermally dissimilar materials whose thermal properties are such that $\sigma < 1$ or $\rho_1 c_1 k_1 < \rho_2 c_2 k_2$. If either T_1 or T_2 were known from experimental measurements it should be possible to calculate the unknown rate of heat transfer $\dot{q}(t)$ from the appropriate expression but the process would be complex and with certain simplifying assumptions the calculation of $\dot{q}(t)$ from temperature data may be made much more straightforward.

If it is assumed that (1) the thickness of region 1 is very small

(2) the thermal conductivity in region 1 is much greater than in region 2,

(3) the time intervals of interest are much greater than the characteristic time l^2/α_1 ,

then the temperature of the metallic film corresponds to the temperature of the front face of the semi-infinite insulator and Eq (42) becomes

$$T_1(t) = \frac{1}{k_1} \sqrt{\frac{\alpha_1}{\pi}} \left[\int_0^t \frac{\dot{q}_s(\lambda)}{\sqrt{t-\lambda}} d\lambda + \sum_{n=1}^{\infty} 2\sigma^n \int_0^t \frac{\dot{q}_s(\lambda)}{\sqrt{t-\lambda}} e^{-\frac{n^2 l^2}{\alpha_1(t-\lambda)}} d\lambda \right] \quad (44)$$

The three assumptions made above concerning the effect of the surface film would also suggest that the surface temperature would be dominated by the properties of the substrate (region 2) rather than by the properties of the metallic film (region 1). Thus the surface temperature would be similar to that of a homogeneous slab of material 2 with a correction term to account for the presence of region 1. Eq (44) assumes this form if the term

$$\frac{1}{k_1} \sqrt{\frac{\alpha_1}{\pi}} \sum_{n=1}^{\infty} 2\sigma^n \int_0^t \frac{\dot{q}_s(\lambda)}{\sqrt{t-\lambda}} d\lambda$$

is added and subtracted from the equation. With the added simplification that

$$1 + \sum_{n=1}^{\infty} 2\sigma^n = \frac{1+\sigma}{1-\sigma} = \sqrt{\frac{\rho_1 c_1 k_1}{\rho_2 c_2 k_2}}$$

Eq (44) becomes for $x=0$:

$$T_1(t) = \frac{1}{\sqrt{\pi \rho_2 c_2 k_2}} \int_0^t \frac{\dot{q}_s(\lambda)}{\sqrt{t-\lambda}} d\lambda - \frac{2}{\sqrt{\pi \rho_1 c_1 k_1}} \sum_{n=1}^{\infty} \sigma^n \int_0^t \frac{\dot{q}_s(\lambda)}{\sqrt{t-\lambda}} \left[1 - e^{-\frac{n^2 l^2}{\alpha_1(t-\lambda)}} \right] d\lambda \quad (45)$$

It will be noted at once that the first term of Eq (45) is the exact solution for the surface temperature of a homogeneous semi-infinite body of material 2 and the second term is a correction which accounts for the presence of the surface metallic film. A further simplification in the correction term can be achieved through integration of

the correction term:

$$\begin{aligned}
 & \frac{2}{\sqrt{\pi \rho_1 c_1 k_1}} \sum_{n=1}^{\infty} \sigma^n \int_0^t \frac{\dot{q}_s(\lambda)}{\sqrt{t-\lambda}} \left[1 - e^{-\frac{n^2 l^2}{\alpha_1(t-\lambda)}} \right] d\lambda \\
 &= \frac{2}{\sqrt{\pi \rho_1 c_1 k_1}} \sum_{n=1}^{\infty} \sigma^n \left\{ \int_0^t \dot{q}'_s(\lambda) \sqrt{t-\lambda} \left[1 - e^{-\frac{n^2 l^2}{\alpha_1(t-\lambda)}} \right] d\lambda \right. \\
 & \quad \left. + n l \sqrt{\frac{\pi}{\alpha_1}} \int_0^t \dot{q}'_s(\lambda) \left[1 - \operatorname{erf} \left(\frac{n l}{\sqrt{\alpha_1(t-\lambda)}} \right) \right] d\lambda \right\} \quad (46)
 \end{aligned}$$

Expanding the exponential and error functions in Eq (46) in their series form, and substituting Eq (46) in Eq (45), the solution for the surface temperature becomes:

$$\begin{aligned}
 T_1(t) &= \frac{1}{\sqrt{\pi \rho_2 c_2 k_2}} \int_0^t \frac{\dot{q}_s(\lambda)}{\sqrt{t-\lambda}} d\lambda - \frac{4}{k_1 \sqrt{\pi}} \sum_{n=1}^{\infty} \sigma^n \int_0^t \left\{ n l \sqrt{\pi} \right. \\
 & \quad \left. - \frac{n^2 l^2}{[\alpha_1(t-\lambda)]^{3/2}} + \frac{1}{6} \cdot \frac{n^4 l^4}{[\alpha_1(t-\lambda)]^{5/2}} - \dots \right\} \dot{q}'_s(\lambda) d\lambda \quad (47)
 \end{aligned}$$

If the thickness of the surface film l is sufficiently small it should be possible to neglect the series terms involving higher powers of the thickness and so obtain a first order thickness correction for the effects of region 1 on the surface temperature. In this way the solution for $T_1(t)$ is obtained as:

$$T_1(t) = \frac{1}{\sqrt{\pi \rho_2 c_2 k_2}} \int_0^t \frac{\dot{q}_s(\lambda)}{\sqrt{t-\lambda}} d\lambda - \dot{q}_s(t) \frac{l}{k_1} \left(\frac{\rho_1 c_1 k_1}{\rho_2 c_2 k_2} - 1 \right) \quad (48)$$

An estimate of the accuracy involved in the assumptions made above may be arrived at in the case of a constant heat transfer rate. For this case Eq (42) becomes:

$$\begin{aligned}
 T_1(t) &= 2 \dot{q}_s \sqrt{\frac{t}{\pi \rho_1 c_1 k_1}} e^{-\frac{x^2}{4 \alpha_1 t}} - \dot{q}_s \frac{x}{k_1} \left[1 - \operatorname{erf} \left(\frac{x}{2 \sqrt{\alpha_1 t}} \right) \right] \\
 & \quad + 2 \dot{q}_s \sqrt{\frac{t}{\pi \rho_1 c_1 k_1}} \sum_{n=1}^{\infty} \sigma^n \left[e^{-\frac{(2n l + x)^2}{4 \alpha_1 t}} + e^{-\frac{(2n l - x)^2}{4 \alpha_1 t}} \right] \\
 & \quad - \frac{\dot{q}_s}{k_1} \sum_{n=1}^{\infty} \sigma^n \left\{ (2n l + x) \left[1 - \operatorname{erf} \left(\frac{2n l - x}{2 \sqrt{\alpha_1 t}} \right) \right] \right. \\
 & \quad \left. + (2n l - x) \left[1 - \operatorname{erf} \left(\frac{2n l + x}{2 \sqrt{\alpha_1 t}} \right) \right] \right\} \quad (49)
 \end{aligned}$$

Eq (44), the solution for the surface temperature becomes, again for $\dot{q}(t)$ constant at $x=0$;

$$T_1(t) = 2 \dot{q}_s \sqrt{\frac{t}{\pi \rho_1 c_1 k_1}} \left[1 + 2 \sum_{n=1}^{\infty} \sigma^n e^{-\frac{n^2 l^2}{\alpha_1 t}} \right] - \dot{q}_s \frac{l}{k_1} \sum_{n=1}^{\infty} 4 n \sigma^n \left[1 - \operatorname{erf} \frac{n l}{\sqrt{\alpha_1 t}} \right] \quad (50)$$

Eq (48), the first order solution for the surface temperature then becomes:

$$T_s(t) = 2\dot{q}_s \sqrt{\frac{t}{\pi \rho_2 c_2 k_2}} - \dot{q}_s \cdot \frac{\ell}{k_1} \left[\frac{\rho_1 c_1 k_1}{\rho_2 c_2 k_2} - 1 \right] \quad (51)$$

Numerical evaluation of the three equations (49), (50) and (51) for the case of a platinum film on a fused quartz substrate has been made by Vidal (13) and the results are plotted in Fig.13 in terms of non-dimensional temperature $(k_1 T)/(\ell \dot{q}_s)$ versus non-dimensional time $\alpha_s t/\ell^2$. In addition the solution for a single insulating slab is shown for comparison, this being the first term in Eq (51).

The exact solution, Eq.(49) was evaluated for $x = \ell/2$ on the assumption that if the instrument were a thermocouple it would record the temperature mid-way through two equal thickness deposits, and if it were a resistance thermometer the average resistance would be the resistance of an element in the centre of the deposit. In the evaluation the series were continued until the last term affected the result by 0.05% or less.

Comparing Eqs (49) and (48) in Fig.13 it will be seen that the exact solution and the surface temperature $T_s(t)$ are nearly identical after a short time interval and it can be concluded that the surface temperature closely approximates the measured temperature corresponding to $x = \ell/2$. Comparing the results of the first order solution, Eq (51), with the solution for a solid quartz model it can be that the first order solution is the quartz solution with a more or less constant temperature lag which is determined by the thickness of the surface film and the relative thermal properties of the two materials.

Comparing the solution for the surface temperature and the first order solution in Fig.13 it can be seen that for relatively small values of non-dimensional time the first order solution gives substantially smaller values for the surface temperature than the exact solution. For non-dimensional times of the order of 1000, however, the discrepancy between the two solutions is acceptable. In the limit as $t \rightarrow \infty$ the first order solution and the exact solution approach the same value.

The data presented in Fig.13 can be summarised in tabular form for the case of a 1 micron thick platinum film on a fused quartz substrate. Table 4 indicates the serious discrepancy between the exact solution and the first order solution and between the exact and the solid insulator (homogeneous slab) solution for short times. For instance it can be seen that for the case of the 1 μm thick element the first order solution is acceptably accurate for times in excess of 50 μs while the solid insulator solution is still in error by 17% after 100 μs .

Table 4

Temperature errors resulting from first order and solid insulator approximations

1 μm platinum element on fused quartz

$\alpha_s t/\ell^2$	250	500	1000	1500	2000	2500
t μs	10	20	40	60	80	100
first order %	-23	-11	-5.4	-3.3	-2.8	-2.0
Solid insul.%	60	39	27.7	22.3	19.0	17.2

Although Table 4 indicates that the first order solution and the solid insulator solution are very inaccurate it should be noted that the error is a linear function of film thickness. For instance the error between the homogeneous solution and the first order solution is the temperature lag in Eq (51):

$$\dot{q}_s \frac{l}{k_1} \left[\frac{\rho_1 c_1 k_1}{\rho_2 c_2 k_2} - 1 \right]$$

This term can be made small in comparison with the surface temperature by making $\rho_1 c_1 k_1 \approx \rho_2 c_2 k_2$, by making k_1 as large as possible and by making l (the film thickness) as small as possible. It is undesirable to make $\rho_2 c_2 k_2$ too large since the detector sensitivity will be thereby reduced although there are advantages in this approach in the measurement of high heat flux rates when the surface temperature may exceed 100°C and non-linear effects in c_2 and k_2 become apparent. Examination of Table 5, reproduced from Vidal, shows that there is little advantage to be gained by the use of metals other than platinum and most by the use of very thin films, less than $1 \mu\text{m}$ thick. On the other hand a figure of merit for the sensitivity of films operated under conditions of constant power dissipation per unit area shows that platinum is at least as good as all but iron, see section 2.a.

Table 5

Thermal properties of commonly used metals relative to fused quartz

Surface Film	$\frac{\rho_1 c_1 k_1}{\rho_2 c_2 k_2} - 1$	$\frac{1}{k_1} \left(\frac{\rho_1 c_1 k_1}{\rho_2 c_2 k_2} - 1 \right)$
Aluminium	234	99
Copper	577	144
Gold	336	107
Nickel	142	170
Platinum	83	120
Steel	27	155

From the first order solution for the surface temperature, Eq (51):

$$T_i(t) = 2\dot{q}_s \sqrt{\frac{t}{\pi \rho_2 c_2 k_2}} - \Delta T$$

where $\Delta T = \frac{\dot{q}_s l}{k_1} \left[\frac{\rho_1 c_1 k_1}{\rho_2 c_2 k_2} - 1 \right]$

The solution for the surface temperature of an homogeneous solid is given by:

$$T_o = 2\dot{q}_s \sqrt{\frac{t}{\pi \rho_2 c_2 k_2}}$$

thus $\frac{T_i}{T_o} = 1 - \frac{l}{k_1} \left[\frac{\rho_1 c_1 k_1}{\rho_2 c_2 k_2} - 1 \right] \frac{2\sqrt{t}}{\sqrt{\pi \rho_2 c_2 k_2}}$

$$= 1 - \frac{\sqrt{\pi \rho_2 c_2 k_2}}{2k_1} \left[\frac{\rho_1 c_1 k_1}{\rho_2 c_2 k_2} - 1 \right] \left[\frac{l^2}{t} \right]^{1/2} \quad (52)$$

Thus the error in surface temperature may be expressed more conveniently in terms of t/l^2 in a similar manner to the error in heat transfer measurement. Values of the ratio T_i/T_o for platinum on quartz are shown on Fig. 12 together with associated errors in heat transfer measurement previously deduced.

The large errors in deduced heat transfer rate caused by the use of thin film resistance thermometers of $1 \mu\text{m}$ thickness can be clearly seen in Fig.12 and compared with the corresponding reductions in surface temperature. Fortunately the errors in heat transfer rate are less than those in surface temperature. For example with

a 1 μm film the error after 100 μs is approximately 11% in heat transfer rate compared with 18% in surface temperature. Both errors are reduced markedly by the use of thinner films since the thickness term appears squared. For a 0.1 μm film typical of vacuum deposited elements (see section 2f) the heat transfer rate is in error by 5% after 0.4 μs and 1% after 120 μs . The very gradual reduction in errors in both quantities with increasing time is clear from Fig.13 and caution must be exercised in the use of such gauges in shock tubes whose flow durations are less than 100 μs . On the other hand negligible errors will arise from this source in facilities whose flow duration exceeds 0.1 s. For the shock tunnel case in which flow durations are typically between 5 and 10 ms the errors arising from the use of 1 μm films are approximately 2% which is within the generally acceptable error level.

2.d Thermal Properties of Substrate Materials

If reliance is to be placed on quoted values for density, specific heat and thermal conductivity for the purpose of data reduction, then a material such as quartz has several advantages. Its thermal properties are reasonably well documented and samples from different sources, although showing variations (19) are sufficiently consistent for use to be made of this material as a substrate for thin film heat transfer gauges without resort to individual calibration except of course for the temperature coefficient of the metallic film itself.

The density of fused quartz at 20°C is between 2.20 and 2.21 g/cm^3 and there appears to be little variation from one sample to another. The specific heat at room temperature is between 0.73 and 0.78 $\text{J g}^{-1} \text{K}^{-1}$ (0.175 and 0.186 $\text{cal g}^{-1} \text{K}^{-1}$), the variation with temperature being shown in Fig.14. The variation of the thermal conductivity of fused quartz with temperature is shown in Fig.15 and the mean of the values quoted at 20°C is 0.01425 $\text{J cm}^{-1} \text{s}^{-1} \text{K}^{-1}$ (0.0034 $\text{cal cm}^{-1} \text{s}^{-1} \text{K}^{-1}$). The value of the thermal product $(\rho ck)^{1/2}$ thus has a mean value of 0.151 $\text{J cm}^{-2} \text{K}^{-1} \text{s}^{-1/2}$ at 20°C and it will be seen later (section 2.e(i)) that this is in close agreement with the figure obtained by calibration of thin film heat transfer gauges on quartz substrates using an electrical discharge technique. There are, however, as will be seen from Figs.14 and 15, quite marked variations in specific heat and thermal conductivity with temperature. These may become the cause of quite serious errors in the deduced heat transfer rate if the substrate temperature rises much above 100°C. The following two sections, 2.d(i) and 2.d(ii) present data on the currently available values of c and k as a function of temperature for both quartz and Pyrex (type 7740 Corning) and the likely effect on the inferred heat transfer rate.

2.d(i) Variation with Temperature

Some of the currently available thermal conductivity data for fused quartz extracted from Ref (23) are shown in Fig.15. It will be seen that there is a fair measure of agreement between the different measurements up to 400 K but between 400 K and 800 K there appears to be a consistent difference amounting to about 0.02 $\text{J s}^{-1} \text{cm}^{-1} \text{K}^{-1}$. At 300 K the mean value of 0.01425 $\text{J s}^{-1} \text{cm}^{-1} \text{K}^{-1}$ is in close agreement with the value of 0.01446 deduced by Hartunian and Varwig (24) from an electrical pulse calibration technique (see section 2.e(i)) in which the value of (ρck) is determined and k may be found by assuming values for ρ and c . The available data for the specific heat of fused quartz shows a high degree of consistency, Fig.14, and the mean value of 0.755 $\text{J g}^{-1} \text{K}^{-1}$ at 300 K is probably correct to within $\pm 3\%$. Using these data for the variation of specific heat and thermal conductivity it is possible to estimate the variation of the thermal product $(\rho ck)^{1/2}$ and this is shown in Fig.16 and compared with measurements at room temperature by Bogdan (25), Maulard (19), (22). Hartunian and Varwig (24) determined the variation of the thermal product over a temperature range 20° to 160°C and the agreement with the predicted value is seen to be good at least to 100°C. This general agreement over the temperature range normally encountered in thin

film heat transfer gauges and the excellent agreement obtained by all three groups at room temperature give confidence in the validity of the pulse calibration technique used throughout. There appears to be little justification for separate calibration except to obtain the value of the temperature coefficient of resistance of the metallic layer. This may be readily measured in a constant temperature bath to a high degree of accuracy. In calculating the theoretical estimate in Fig.16 the value for the density of fused quartz has been taken as 2.20 g cm^{-3} . The ratio $[(\rho ck)_T / (\rho ck)_{30}]^{1/2}$ is also shown in Fig.16 based on the theoretical estimate of (ρck) from TPRC (23). It will be seen that this ratio reaches 1.1 at a temperature of only 70°C and thus heat transfer measurements based on constant thermal properties would be in error by 10% if the rate was 100 W cm^{-2} for 10 ms. The errors which arise from such variation in thermal properties is dealt with in detail in section 2.d(ii).

Pyrex, although widely used as a substrate material, is available in a variety of mixtures although Corning type 7740 appears frequently. Hartunian has reported (24) a series of experiments to determine the variation of the diffusivity α with temperature. The results for α and values of $(\rho ck)^{1/2}$ are tabulated below and it will be seen that the variation in all parameters is much greater than with fused quartz.

Table 6
PYREX, CORNING 7740

Temperature	specific heat c	thermal conductivity k	diffusivity α	$(\rho ck)_T^{1/2}$	$(\rho ck)_T^{1/2}$
$^\circ\text{C}$ K	$\frac{\text{cal}}{\text{g K}}$	$\frac{\text{cal}}{\text{cm s K}}$	$\frac{\text{cm}^2}{\text{s}}$	$\frac{\text{cm}^2 \text{cal}}{\text{K s}^{1/2}}$	$\frac{\text{cm}^2 \text{J}}{\text{K s}^{1/2}}$
24 297	0.185	$3.26 \cdot 10^{-3}$	$7.93 \cdot 10^{-3}$	$3.675 \cdot 10^{-2}$	0.152
50 323	0.193	3.59	8.21	3.93	0.164
82 355	0.203	4.33	9.58	4.44	0.185
100 373	0.208	4.37	9.40	4.51	0.188
120 393	0.215	5.10	10.67	4.96	0.207
129 402	0.218	4.76	9.83	4.82	0.201
147 420	0.223	5.23	10.51	5.11	0.214
174 447	0.231	6.03	11.66	5.59	0.233

Hartunian and Varwig's values for the product (ρck) can be compared with theoretical estimates based on separate determinations of c and k from TPRC (23). The agreement at room temperature is only fair, Fig.17, and a value of between 3.25 and $3.75 \times 10^{-2} \text{ cal cm}^{-2} \text{ K}^{-1} \text{ s}^{-1/2}$, 0.136 and $0.157 \text{ J cm}^{-2} \text{ K}^{-1} \text{ s}^{-1/2}$, would appear to be a realistic estimate.

Despite the greater discrepancy between experimentally observed values for the thermal product $(\rho ck)^{1/2}$ and the theoretical estimate, Pyrex is a cheaper and frequently used substrate material for thin film resistance thermometers. In view of the discrepancy noted above it is probably worthwhile to perform calibrations on each sample to obtain the thermal product if accurate absolute measurements of heat transfer rate are desired. For many applications, however, relative heat transfer rates are all that are required and in these circumstances the value of $(\rho ck)^{1/2}$ is less critical than a knowledge of the temperature coefficient of resistance of the metallic film. Pyrex may be optically polished to the same surface finish as quartz and is perhaps slightly easier to work in the initial stages of substrate preparation.

2.d(ii) Effect of the Variation of Thermal Properties on Calculated Heat Transfer Rates

Non-uniform properties are unlikely to be of importance in metallic substrate gauges since the temperature rises are generally small but with thermally insulating substrates the temperature rise may be in excess of 100°C , even for short flow durations, Fig.6. There is a body of evidence which demonstrates that heat transfer measurements will be subject to errors of about 10%, if uncorrected, when the substrate temperature rises above 150°C . It will be seen from Fig.6 that shock tubes with flow durations less than about $200\ \mu\text{s}$ are unlikely to encounter conditions in which the substrate will exceed 100°C if the heat transfer rate is below $1\ \text{kW}/\text{cm}^2$, but longer running time facilities will meet them even for rates as low as $100\ \text{W}/\text{cm}^2$. Possible methods of correcting for the effects of non uniform properties have been investigated by Reece (26) and Hartunian and Warwig (24). Cook (27) has made a theoretical study of heat transfer phenomena in homogeneous materials and of the effect of variable thermal properties on heat transfer rates deduced from surface temperature measurements. Rearranging Eq (21) as:

$$\dot{q}_s = \frac{T_s \sqrt{\pi}}{2} \sqrt{\frac{\rho c k}{t}}$$

it is seen that the product $(\rho c k)^{1/2}$ is important rather than the separate parameters ρ , c and k and also that for a constant heat transfer rate, in which case T_s rises as $t^{1/2}$, the value of \dot{q}_s deduced will be directly proportional to the value of $(\rho c k)^{1/2}$ used. Values obtained for fused quartz and Corning Pyrex type 7740 have been plotted in Figs.16 and 17 and a compilation of all currently available data on the ratio $[(\rho c k)_T / (\rho c k)_{20}]^{1/2}$ for Pyrex 7740 is shown in Fig.18.

It is clear that there is a large discrepancy between the data obtained by Bogdan, Skinner, Walenta and Hartunian and Varwig who all used essentially the same technique. Hartunian and Varwig's data do not allow for the known decrease in gauge sensitivity dR/dt with temperature but this should not cause the wide differences seen in Fig.18. The corrections to be made to account for this variation in thermal properties are unfortunately not straightforward since because of the rapid variation of the temperature only laminae near the surface experience temperatures high enough to affect their properties. Hartunian and Varwig (24) have obtained an approximate solution noting that the diffusivity, α , is itself only slightly temperature dependent. They obtain a corrected expression for the surface temperature:

$$T_w \left\{ 1 + \frac{b}{k_o} \left[\left(1 + \frac{T_w}{T_o} \right) \left(\frac{T_o}{T_w} \right) \log_{10} \left(1 + \frac{T_w}{T_o} \right) - 0.434 \right] \right\} = \frac{2 \dot{q}_s t^{1/2}}{(\pi \rho c k)^{1/2}} \quad (53)$$

where T_w = corrected surface temperature
 k_o = thermal conductivity at initial temp.
 T_o = initial temperature of substrate, K.

the thermal conductivity k assumed to be of form $(a + b \log_{10} T)$

$b/k_o = 4.73$	Pyrex	} Hartunian and Varwig
1.75	Quartz	
1.81	Plate Glass	

The correction factor: $\left\{ 1 + \frac{b}{k_o} \left[\left(1 + \frac{T_w}{T_o} \right) \left(\frac{T_o}{T_w} \right) \log_{10} \left(1 + \frac{T_w}{T_o} \right) - 0.434 \right] \right\}$

has been evaluated by Hartunian and Varwig for the case in which $\dot{q}_s = \text{constant}$. This factor is plotted versus T_w $^{\circ}\text{C}$ in Fig.19 for substrates of Pyrex (7740) and quartz and it is apparent that Pyrex requires most correction although Reece (26) has pointed out that at 150° the factor should be 1.36 instead of 1.44 and Cook (27) determined $\dot{q}_{act}/\dot{q}_{expt}$, the ratio of the heat transfer rates calculated on the assumption of variable and constant properties (using Hartunian and Varwig's data, Table 6). The errors predicted by Cook are seen from Fig.20 to be somewhat different from those

deduced by Hartunian and Varwig. The present situation is thus somewhat unsatisfactory since no straightforward technique for correcting for variable thermal properties exists in any but the $\dot{q}_s(t) = \text{constant}$ and $\dot{q}_s(t) = K t^{-1/2}$ cases, and even in these simple cases there exist quite large discrepancies between the corrections recommended.

Electronic circuits which compensate for the variable properties have been investigated by Reece (26) and Walenta (28). These are based on the assumption that the variation of (ρc) with temperature is small and that the thermal conductivity k increases linearly, $k = k_0(1 + bT)$. This results in the surface temperature (T_s) ideal based on the assumption of uniform properties being higher than the measured temperature

$$T_{s \text{ ideal}} = T_s + \frac{1}{2} b T_s^2$$

The coefficient b for quartz has been the subject of much research but the discrepancy between different investigators is not reassuring. The electrical correction networks of Reece and Walenta contain proportional plus squaring amplifiers, Fig. 21. The output current i from the squaring amplifier SQ is proportional to the square of the input voltage

$$i = k e_i^2, e_i \geq 0$$

and

$$i = 0, e_i < 0$$

The operational amplifier A has a large open loop gain and the summing junction S is a virtual earth. If the operational amplifier draws negligible current

$$i + \frac{e_i}{R_1} + \frac{e_c}{R_2} = 0$$

$$\text{Thus } e_c = -\frac{R_2}{R_1} \cdot e_i (1 + k e_i)$$

Reece uses $b = 0.25$ to achieve a correction factor of 1.25 for Pyrex substrate temperatures not exceeding 100°C . Walenta has shown that the above form for the correction is at least as good as Hartunian and Varwig's more complex function:

$$k = k_0 \left(1 + a \log_{10} \frac{T_s + T_0}{T_0} \right)$$

where T_0 is the initial surface temperature. Reece has also developed a varistor (voltage-variable resistor) circuit for performing the same correction. Both Reece and Walenta perform the correction to the measured temperature on the assumption that the heat transfer to the surface is constant but the correction is dependent on the boundary conditions as has been shown by Cook (27). Cook's corrections illustrated in Fig. 20 differ depending on whether \dot{q}_s is assumed constant or varying with $t^{-1/2}$ (the shock tube side wall boundary layer case) and this difference is seen to be about 7% at a wall temperature of 200°C . In view of the greater uncertainties surrounding the right form and magnitude of the correction, this discrepancy is acceptable and Walenta has demonstrated that his simple quadratic correction for thermal conductivity gives heat transfer results which are in much better agreement with theoretical predictions than the uncorrected data.

In view of the loss of accuracy which results from the use of substrates such as quartz and Pyrex in tests in which the substrate temperature rises much above 100°C the use of alternative insulating bases would appear to be worth investigating. Firstly to reduce the surface temperature rise and hence delay the onset of the non linearity an insulator with a higher thermal conductivity is required. Such materials will result in reduced overall system sensitivity but this is unlikely to be a disadvantage since the problem only arises at high heat transfer rates or in long duration (0.1 to 1 s) facilities. Ceramics such as alumina (Al_2O_3) and beryllia (BeO) have thermal conductivities of 0.376 and 2.80 $\text{W cm}^{-1} \text{K}^{-1}$ respectively at room temperature in contrast with 0.0142 for quartz. The specific heat of a 96% Al_2O_3 ceramic is

approximately $0.72 \text{ J g}^{-1} \text{ K}^{-1}$ and a 99.5% BeO ceramic (Coors BD-995-2; 600 9th Street, Golden, Colorado 80401) has a value of $0.9 \text{ J g}^{-1} \text{ K}^{-1}$.

The resulting sensitivity of such ceramic based gauges in terms of their surface temperature rise in response to a constant heat flux is shown in Fig.6. It will be seen that the alumina substrate has a 'sensitivity' 18.2% and the beryllia substrate a 'sensitivity' of only 7.8% that of quartz. The variation of $(\rho ck)^{1/2}$ with temperature in alumina and beryllia is shown in Fig.18. Beryllia appears to offer considerable advantages although great care must be taken in machining this material because of its toxicity. Over a range of 160°C the value of $(\rho ck)^{1/2}$ does not depart by more than 1% from its room temperature value and heat transfer measurements to within 2% may thus be made with this material as a substrate up to 1 kW/cm^2 for flow durations of 0.1 s. This may be compared with an error of 5% arising from the use of quartz at heat transfer rates of 100 W/cm^2 for 0.002 s flow duration.

2.e Calibration Techniques

2.e(i) Electrical Discharge Calibration of Thin Film Heat Transfer Gauges

Whether the heat transfer rate to be measured is constant or not the value of $(\rho ck)^{1/2}/\alpha_R$ must be known. This arises because the temperature rise in Eq (21)

$$\Delta T_s = \frac{2\dot{q}_s}{\sqrt{\pi}} \sqrt{\frac{t}{\rho ck}} \quad \text{for a constant heat transfer rate}$$

is generally determined by the change in voltage across the thin film when supplied with a constant current I_0 . Since $R = R_0(1 + \alpha_R \Delta T_s)$

$$\begin{aligned} \frac{R - R_0}{\alpha_R R_0} &= \frac{\Delta R}{\alpha_R R_0} = \Delta T_s \\ \text{Thus } \frac{I_0 \Delta R}{\alpha_R I_0 R} &= \frac{\Delta V}{V_0 \alpha_R} = \Delta T_s \end{aligned} \quad (54)$$

and \dot{q}_s becomes, for the case of constant heat transfer rate:

$$\dot{q}_s = \frac{\Delta V}{V_0} \cdot \frac{\sqrt{\pi \rho ck}}{2 \alpha_R} \cdot \frac{1}{\sqrt{t}}$$

The temperature coefficient α_R may be determined in a separate experiment and care should be taken that the measurement is made spanning the range of expected surface temperatures where this is possible since α_R is not constant. A closer approximation to the variation of R with T is $R = R_0(1 + \alpha_R \Delta T + \beta_R (\Delta T)^2)$ and Bogdan (29) has shown $(dR/dT)_{T_K}$ of the form:

$$\left(1 - \frac{0.15 T}{372}\right) \left(\frac{dR}{dT}\right)_{21^\circ\text{C}} \quad T \text{ in deg K}$$

i.e. β_R is negative.

A convenient calibration technique to obtain $(\rho ck)^{1/2}/\alpha_R$ used by several laboratories consists in passing a constant current through the gauge itself for a short time so that ohmic heating within the film produces a change in resistance (30, 31). A suitable circuit is shown in Fig.22 in which R_0 is the thin film to be calibrated by the discharge of condenser C through the linear resistors R_1 and R_2 . The time constant $C(R_1 + R_2 + R_0)$ is arranged to be about 0.1 s and the testing time is confined to the first 500 μs during which period the current is constant to within 0.5%. The heat generated within the film is transferred to the substrate if the test is conducted in vacuo and hence $q = I_0^2 R_0 / A \text{ W/cm}^2$, where A is film area. The out-of-balance bridge voltage caused by a small increase, ΔR_0 , in the test gauge's resistance is given by:

$$\frac{\Delta V}{I_0} = \frac{\Delta R_0 \cdot R_1}{\Sigma R}, \quad \Sigma R = R_1 + R_2 + R_3 + R_0$$

If the variation of the thin film resistance is approximated by a linear law $R_T = R_0(1 + \alpha_R \Delta T)$ it can be shown that the parameter $\alpha_R (\rho ck)^{-1/2}$ is given by

$$\frac{\alpha_R}{\sqrt{\rho ck}} = \frac{A \sqrt{\pi} \Sigma R}{2 I_0^2 R_0^2 R_1} \frac{\Delta V}{\sqrt{t}} \quad (55)$$

This procedure is relatively simple but has some disadvantages:

- (1) It is necessary to measure the film area which may not be straightforward on curved surfaces.
- (2) Although the bridge may be balanced under D.C. conditions using R_1 as a variable and a galvanometer, this balance may not hold dynamically if there are inductive and/or capacitive elements. An initial transient will then appear at the output although this need not be serious if it is rapidly damped since only the slope $\Delta V/\sqrt{t}$ is required.
- (3) The temperature coefficient α_R is subject to changes with time in some films (see Section 2.f) and a combined coefficient $\alpha_R (\rho ck)^{-1/2}$ does not permit corrections to be made for this variation. If α_R is separately measured, however, $(\rho ck)^{1/2}$ can be evaluated and allowance made if α_R has in fact altered.
- (4) Non-uniformities commonly found in certain types of thin film may produce quite serious errors, up to 15%, in the deduced value of $(\rho ck)^{1/2}$. This source of error is discussed in section 2.e(iii).

The errors introduced by the measurement of the film area may be avoided by a double calibration technique. The film is first pulse calibrated in air and the factor $\Delta R_1/\sqrt{t}$ deduced; in the case of Fig. 22

$$\Delta R = \frac{\Delta V \Sigma R}{I_0 R_1}$$

The film is immersed in a fluid whose thermal properties are well known and stable. Following the analysis given by Maulard (22), if a fraction m , of the heat generated diffuses into the liquid, $\Delta R_1/\sqrt{t}$ is the slope of the curve deduced from an experiment in air and $\Delta R_2/\sqrt{t}$ the slope for a similar experiment conducted in a fluid of known thermal properties $(\rho ck)^{1/2}_{liq}$, we obtain

$$\frac{(\rho ck)^{1/2}_{liq}}{R_0 \alpha_R} = \frac{2 F m R I^2}{\sqrt{\pi} A (\Delta R_2/\sqrt{t})} \quad (56)$$

$$\frac{(\rho ck)^{1/2}}{R_0 \alpha_R} = \frac{2 F (1-m) R I^2}{\sqrt{\pi} A (\Delta R_2/\sqrt{t})} \quad (57)$$

$$\frac{(\rho ck)^{1/2}}{R_0 \alpha_R} = \frac{2 F R I^2}{\sqrt{\pi} A (\Delta R_1/\sqrt{t})} \quad (58)$$

where F is the unknown factor which accounts for the non-uniform film heating. (section 2.e(iii)). From the above equations the correct value of $(\rho ck)^{1/2}$ can be shown to be

$$(\rho ck)^{1/2} = \frac{(\rho ck)^{1/2}_{liq}}{\frac{\Delta R_1/\sqrt{t}}{\Delta R_2/\sqrt{t}} - 1} \quad (59)$$

Thus the effect of non-uniform film thickness on a calibration in air and inaccuracies in the determination of film surface area A are eliminated. This method does not, however, furnish the value of $R_0 \alpha_R$ which is required in data reduction although a separate calibration in a thermostatically controlled bath will give α_R with high accuracy. Maulard has demonstrated that the optimum ratio of the slopes to give the least error in $(\rho ck)^{1/2}$ is $(1+\sqrt{2})$ and thus the liquid should in principle have thermal properties such that:

$$\sqrt{\rho ck}_{liq} = \sqrt{2} \sqrt{\rho ck}_{substr.}$$

Maulard recommends glycerine as a test fluid, whose thermal properties $(\rho ck)^{1/2}$ are $0.0925 \text{ J cm}^{-2} \text{ K}^{-1} \text{ s}^{-1/2} \pm 4\%$, although the ratio of $(\rho ck)^{1/2}$ glycerine to $(\rho ck)^{1/2}$ quartz is only 0.6 instead of the optimum value of 1.414.

2.e(ii) Thermal Radiation Techniques

Maulard has described (32) a radiant flux method for the calibration of thin film gauges although the technique may be used for (almost all) other heat transfer gauges. The equipment consists of a bank of 6 infra-red lamps with a total power of 11 kW housed in an aluminium reflector fitted with a diffusing screen of silica 30 cm x 15 cm, capable of producing a maximum of 25 W/cm^2 . The transducer-to-source distance may be varied to alter the incident heat flux and a high speed water cooled shutter is arranged to expose the transducer for preset time intervals. The calibration unit is illustrated schematically in Fig.23. The infra-red lamps are fed from a three-phase supply with the usual arrangements to reduce current surges during starting, and attain an equilibrium state in about 3 minutes. The power level is controlled by a rheostat and monitored with a wattmeter. Spurious heat flux from the wall is reduced by a coating of lampblack and water cooling to lower the wall temperature. The surface of the transducer and that of a reference (see section 2.e(iv)) are coated with a layer of about $1 \mu\text{m}$ of lampblack (0.25 mg/cm^2) which increases the time constant of the gauge by about 2 to 10 ms.

This additional time constant is of no importance in the case of gauges which are intended for long duration applications (0.1 to 1 s) but it does impose restrictions on the testing of systems intended for shock tubes, shock tunnels and gun tunnels. The depth and width of the substrate in these latter cases are usually based on thermal diffusion times perhaps 5 or 10 times the flow duration and care must therefore be taken in using radiation calibration techniques in which circumstances may cause the simple one-dimensional heat conduction theory to be invalid. Maulard points out, however, that calibrations performed by this radiant flux method are in good agreement with other techniques. This observation is consistent with the data shown in Fig.5 which show that even for a test time of 0.10 s, a substrate thickness of 0.1 cm is adequate to ensure conditions within 1% of one-dimensional. using this calibration technique Maulard has obtained from a series of 78 tests on 24 quartz substrates a mean value of $(\rho ck)^{1/2}$ of $0.155 \text{ J cm}^{-2} \text{ K}^{-1} \text{ s}^{-1/2}$. Although this is 8% above Maulard's own data deduced from the air/glycerine tests, it agrees well with the value obtained by Hartunian and Varwig at room temperature and also with the best estimate based on separate determinations of the three thermal properties, as shown in Fig.16.

A similar radiation calibration system has been described by Schulte, Puronen and Dixon (33) who employed a rotating disc shutter which was contoured to provide a period of constant radiation and a period of variable radiation through the optical aperture. The apparatus, shown schematically in Fig.24, comprises a motor driven disc

which exposes the sensor to be calibrated to a 40 ms interval of constant heat transfer rate in which the height of the aperture remains fixed. The aperture width is fixed and the initial phase of heat transfer is followed by a period during which the contoured edge of the disc imposes a heat transfer rate which varies at $t^{-1/2}$. The second interval results in a surface temperature record on thin film detectors which is of constant amplitude, also of about 40 ms duration. In order to prevent the substrate temperature rising with each pulse a second solenoid shutter is included in the optical path and this is arranged to close after the disc has completed one revolution. The sensor must then be allowed to return to thermal equilibrium before a repeat calibration is performed. The source used was a GE Q100T3/4CL lamp and only the radiation from $\frac{1}{4}$ of the total filament length was used to obtain approximately constant spatial flux densities. As in Maulard's equipment the surface of the sensor to be calibrated was coated with flat black paint whose absorptivity was determined separately to be 0.98 within the wavelength band from 0.25 to 2.7 μm . Absolute calibration of the source may be made with a rapid response gauge such as the Gardon disc radiometer (see section 5).

2.e(iii) Errors Introduced by Non-Uniformity in Thin Film Thickness

It is frequently assumed that a thin film resistance thermometer is homogeneous in structure, uniform in thickness and regular in area. Unfortunately this is far from reality except in the case of evaporated or sputtered gauges. Microscopic examination of films prepared by deposition from liquid bright paints reveals that they are pitted with small holes and have irregular areas. The effect of such irregularities may be reduced by the application of several coats of paint but unless care is taken to achieve a high degree of coincidence of each layer on the previous deposit, the non-uniformity is increased. In addition to this class of non-uniformity there may be a thickness variation of a more regular nature which is caused by surface tension effects in the liquid. Busing (21) has demonstrated that films prepared by hand painting have approximately parabolic thickness variations in the transverse direction. Fig.25 redrawn from Busing's report illustrates this phenomenon. Maulard (22) has pointed out that the effect of such non-uniformities in film thickness may result in serious errors in the value of the thermal product $(\rho ck)^{1/2}$ obtained by electrical discharge calibration. Maulard's analysis, which is followed in the present section, differs in its conclusions from that of Busing who also studied the consequences of film non-uniformity but predicted less severe errors.

Referring to Fig.25, the thin film may be considered as a set of parallel resistances, each having the same terminal voltage V . For an element of width dx ,

$$d\left(\frac{1}{R_o}\right) = \frac{\sigma_R Z(x) dx}{L} \quad (60)$$

The heat generated, $\dot{q}(x)$, in the discharge calibration procedure is thus:

$$\dot{q}(x) = \frac{V^2}{L dx} d\left(\frac{1}{R_o}\right) = \frac{V^2 \sigma_R Z(x) dx}{L^2} \quad (61)$$

Considering a time scale in which lateral conduction within the metallic film is small in comparison with the heat transferred to the substrate, $(Z\ell \ll 1)$, each segment of the substrate is heated only by the film immediately above it. The rise in surface is thus:

$$\begin{aligned} T_s(x) &= \frac{2 \dot{q}(x) \sqrt{t}}{\sqrt{\pi \rho ck}} \quad \text{where } (\rho ck) \text{ refers to the substrate} \\ &= \frac{2 \sqrt{t}}{\sqrt{\pi \rho ck}} \frac{V^2 \sigma_R Z(x) dx}{L^2} \end{aligned} \quad (62)$$

The mean temperature rise of the substrate under the film is given by:

$$\begin{aligned} T_s(\text{mean}) &= \frac{1}{l} \int_l T_s(x) dx \\ &= \frac{2\sqrt{t} V^2 \sigma_R}{\sqrt{\pi \rho c k} L^2 l} \int_l Z(x) dx \end{aligned} \quad (63)$$

However, $T_s(\text{mean})$ cannot be determined and an error arises in assuming that it is equal to $\Delta R / (R_0 \alpha_R)$ where ΔR is the increase in mean film resistance. From Eq (60) the resistance may be found by integration:

$$\frac{1}{R_0} = \frac{\sigma_R}{L} \int_l Z(x) dx \quad (64)$$

Allowing a simple linear variation of conductivity σ_0 with temperature of the form:

$$\sigma = \sigma_{R0} (1 - \alpha_R T_s) \quad (65)$$

we obtain, with ΔR the change in resistance due to a change in temperature T_s

$$\frac{1}{R_0 + \Delta R} = \frac{\sigma_{R0}}{L} \int_l (1 - \alpha_R T_s) Z(x) dx \quad (66)$$

From Eqs (64) and (65) the change in resistance ΔR may be found:

$$\frac{\Delta R}{R_0 \alpha_R} = \frac{\int_l T_s Z(x) dx}{\int_l Z(x) dx} \quad (67)$$

In conjunction with Eq (62), which expresses the space dependent surface temperature in terms of the film thickness, we obtain:

$$\frac{\Delta R}{R_0 \alpha_R} = \frac{2\sqrt{t} V^2 \sigma_R}{\sqrt{\pi \rho c k} L^2} \frac{\int_l Z^2(x) dx}{\int_l Z(x) dx} \quad (68)$$

From Eq (63), which evaluates the mean surface temperature in terms of the film thickness $Z(x)$, the value of $(\rho c k)^{1/2}$ would be deduced to be:

$$\sqrt{\rho c k} = \frac{2\sqrt{t} V^2 \sigma_R \int_l Z(x) dx}{\sqrt{\pi} T_s(\text{mean}) L^2 l} \quad (69)$$

If it is assumed, incorrectly, that:

$$T_s(\text{mean}) = \frac{\Delta R}{R_0 \alpha_R} \quad (70)$$

$$\text{then } \sqrt{\rho c k}_{\text{calc}} = \sqrt{\rho c k} \frac{\left[\int_l Z(x) dx \right]^2}{\int_l Z^2(x) dx} \quad (71)$$

If the form of $Z(x)$ is a parabola, for instance, i.e.:

$$Z(x) = Z_m (1 - 4x^2/l^2)$$

Maulard has shown that:

$$\sqrt{\rho c k}_{\text{calc}} = 5/6 \sqrt{\rho c k}_{\text{actual}}$$

In fact the ratio of the integrals in Eq (71) is always less than unity if Z is variable. There is seen to be an error of about 17% arising in the value of $(\rho c k)^{1/2}$ deduced from electrical pulse calibration if the film is not uniform in the transverse direction, the calculated value being less than the true value. If the non-uniformity is in the

longitudinal sense, a similar analysis by Maulard has shown that the derived thermal product will be:

$$\sqrt{\rho ck} \frac{\int_L \left(\frac{dy}{z}\right)^2}{L \int_L \frac{dy}{z^2}}$$

If the thickness is uniform but the area is not rectangular, the thermal product which will be derived is:

$$\sqrt{\rho ck} \frac{\int_L \left(\frac{dy}{x}\right)^2}{\int_L x dy \int_L \frac{dy}{x^2}}$$

In both the above cases of non-uniformities in the longitudinal direction and in area, the error again results in the derived value of $(\rho ck)^{1/2}$ being less than the true value. If, for instance, a fraction n of the film's length has a thickness $m Z_m$ where Z_m is the thickness of the remainder of the film, it can be shown that the value of the thermal product derived is given by:

$$\sqrt{\rho ck}_{calc} = \sqrt{\rho ck} \left[1 - \frac{n(1-n)(1-m)^2}{n + m^2(1-n)} \right] \quad (72)$$

A film whose thickness over half its length is double the thickness over the remainder would be found to have a thermal product of 0.9 of its true value by electrical discharge calibration, a less serious error than in the case of transverse irregularity, but still above the error levels which should generally be sought in the measurement of heat transfer rates.

Electrical pulse calibration also introduces a further error if the test pulse duration is long in comparison with the characteristic diffusion time of the substrate. In use the thin film is considered to be on the surface of a semi-infinite solid in which one-dimensional heat transfer takes place. In the pulse calibration technique heat is generated within a narrow strip, and then only uniformly if the film is of constant thickness, and diffuses in two dimensions. Spence (34), in an analysis of two-dimensional heat conduction problems related to shock tube measurements, showed that the mean temperature of the substrate beneath the film with \dot{q}_s constant was given by:

$$T_{mean} = \frac{2\dot{q}_s\sqrt{t}}{\sqrt{\pi\rho ck}} \left[1 - \frac{\sqrt{\alpha t}}{2l\sqrt{\pi}} \right] \quad (73)$$

where l is the width of the film. Thus the temperature at a time t is reduced below that which would be observed for strictly one-dimensional heating by a factor $(1 - \delta/(4l\sqrt{\pi}))$ where δ , the penetration depth after a time t , is equal to $2\sqrt{\alpha t}$. Taking, for example, a film of width 1 mm it is seen that an error of -5% in surface temperature occurs after only 39 ms on a quartz substrate.

Care must be taken in the use of the electrical pulse calibration procedure to reduce the errors caused by the following:

- (a) Initial imbalance of the bridge circuit resulting in a step in the bridge output at the origin. If an analogue circuit is also employed with the bridge this transient appears as an infinite heat transfer rate and the time constant of the analogue must be made short in order that the correct analogue output level is rapidly attained.
- (b) The bridge circuit must be made as free of inductance as possible so that oscillatory responses are either avoided or rapidly damped.
- (c) The duration of the test must be neither so long that the substrate heating ceases to be one-dimensional (40 ms for 1 mm wide film on quartz) nor so

short that the film time constant is important ($250 \mu s$ for $0.1 \mu m$ thick film and 1% error level in surface temperature measurement).

- (d) The film area must be measured with as great an accuracy as is required of the final data or a double pulse calibration system must be used, preferably with glycerine and air as working fluids.

2.e(iv) Standard Heat Transfer Gauges

A standard heat flux transducer for the measurement of the heat flux incident on the test gauge is necessary for the regular use of such radiation calibration techniques and Maulard (35) has described a circulating water calorimeter which fulfils most of the requirements. This reference transducer, illustrated in Fig.26, incorporates a lamp-black coated metal disc of area 10 cm^2 inside which water circulates in a spiral groove from centre to periphery. The inlet water temperature is monitored by a thermocouple in the hose 3 and after thorough mixing in the reservoir 7 its temperature is again measured. The tank is insulated with expanded polystyrene and fitted with an overflow. A guard ring 1 is maintained at the temperature of the disc to reduce radial heat conduction. The response time of the system is about 1 minute. The heat transfer rate is obtained directly from the heat balance equation $\dot{q} = \dot{m} c \Delta T / S$; \dot{m} is the mass flow rate of coolant water determined by catching and weighing the cooling water, c its specific heat, S the area of the disc and ΔT the temperature rise. Maulard estimates the total error in $\dot{m} \Delta T$ to be about 2% and allowing a possible error of 1% in effective receiving area considers the final accuracy to be $\pm 3\%$, equal to that of "standard" thermal inertia systems described later in this section. The water calorimeter must be coated with the same lampblack as the transducer to be checked so that the emissivity of the coating does not appear in calibration.

In addition to the use of a standard water-cooled calorimeter there are other reference transducers whose design is based on the "inertial" calorimeter. Although the first type to be described is simply a larger version of the commonly used inertial heat transfer gauge its size does enable more accurate measurement of the heat transfer rate. Fig.27 illustrates a reference gauge described by Maulard (35) and it will be seen that this incorporates features which enable this improved accuracy to be obtained:-

- (a) The area of the active element can be measured to within 1%.
- (b) Improved thermal isolation from the supports is possible.
- (c) The thermocouples may be positioned so that the temperature measured is that of the rear face and the size of the element relative to the thermocouple wires renders the corrections for heat conduction down these wires negligible.

The reference transducer constructed by Maulard has an active surface 25 mm diameter and 4 mm thick in copper held by three 0.5 mm diameter pins providing a 1 mm air gap. The chromel-alumel thermocouples are soldered directly to the rear face of the copper disc and all interior surfaces are highly polished to reduce radiation losses. The lampblack coating may be included in the weight of the copper disc. Sources of error are thus confined to the area of the disc and in temperature measurement. The overall error in \dot{q} ($= \frac{\dot{m} c}{S} dT/dt$) is estimated at $\pm 3\%$. The gauge sensitivity is about $0.00715 \text{ }^\circ\text{C/s per J/cm}^2$ and its time constant about 80 ms before the rate of rise of temperature is within 1% of its final value. Measurements made with this type of reference gauge at heat transfer levels below 40 W/cm^2 give results comparable with the water calorimeter and with an error of about 5% attributed chiefly to the determination of the slope dT/dt . The error is also due to an uncertainty in the value of the specific heat of copper whose value of $0.38 \text{ J g}^{-1} \text{ K}^{-1}$ at 272.18 K is only thought to be accurate to 3% for very pure copper. In order to reduce heat losses the slug temperature should not rise much above ambient; thus dT/dt should be measured within the first stages of heating although a compromise is necessary to achieve an adequate signal level. The thermocouple may be separately calibrated to establish its temperature

sensitivity and this should be carried out over the temperature range expected in practice.

2.f Construction of Thin Film and Thermocouple Gauges

The major requirements of thin film resistance thermometer heat flux meters are (a) a non-zero temperature coefficient of resistance which should remain reasonably constant, (b) strong adhesion to the surface and (c) ease of attachment of electrical leads which should themselves be electrically and thermally inert. One of the most commonly used metals is platinum whose temperature coefficient in bulk form is $3.92 \times 10^{-3}/K$ between 0° and $100^{\circ}C$ and whose stability in oxidising atmospheres makes it widely favoured as a thin film material. In thin film form deposited from liquid bright platinum (Hanovia O5-X) the material has a coefficient around $2.4 \times 10^{-3}/K$. Nickel has a much higher temperature coefficient, $6.63 \times 10^{-3}/K$ between 0° and $100^{\circ}C$ and is frequently used in gauges prepared by vacuum deposition. Platinum films are readily formed on insulating substrates by the use of commercially available preparations such as "Liquid Bright Platinum O5-X" (Englehard Industries Ltd). The deposition technique will be described in some detail since unsatisfactory results will be obtained if care is not taken. The liquid contains fine metallic particles in suspension and chemical agents which lightly attack the surface of the substrate to give a highly adherent film. The liquid should be strongly agitated before use to redisperse the metallic particles and preferably stored away from daylight. The surface of the substrate, whether it be quartz or Pyrex, should be optically polished since the resulting film will be about $0.1 \mu m$ thick and sharp discontinuities in the surface increase the risk of the film itself being irregular. The surface should be thoroughly degreased although excessive attention to this point does not appear to be justified. The liquid, which may be thinned with proprietary thinners may be applied with a fine brush, drawing pen or air brush and allowed to dry, using a lamp if desired. The liquid should be thin enough for brush marks to flow out and dull; poorly adhesive films may result from too thick an application of liquid. The substrate should be inserted in an electric furnace supported on a stainless steel base or refractory brick which has itself been thoroughly pre-baked. The furnace should be clean and not used for the heat treatment of metals or other material. The furnace should be lightly ventilated; this appears to be important in the earlier phases of the baking process when the organic base is evaporated. The temperature is raised to $650^{\circ}C$ in the case of quartz and $680^{\circ}C$ for Pyrex over a period of about 1 hour and maintained at that temperature for a further 30 minutes.

The cooling should be done with substrate in the furnace. Rapid quenching of the substrate is undesirable since this results in internal stresses in the metal film. These stresses appear to be the cause of instability in the electrical properties of the film and its resistance may increase with time due to stress relief. At room temperature this resistance change may amount to 5% over a period of a few weeks and is accelerated at higher temperatures. The variations in resistance do not appear to affect the value of the temperature coefficient but if they are troublesome may be substantially reduced by annealing. A period of 12 hours at $160^{\circ}C$ virtually eliminates this form of instability.

It is preferable to build up a series of coats with separate firing between each coat especially if the substrate is not of high optical finish. It is, however, necessary to ensure that each successive coat is applied exactly over the preceding film. Failure to achieve this degree of coincidence in successive layers of film will result in unsatisfactory calibrations when the electrical discharge method is used since the local joule heating effect will be non uniform. The adhesion obtained with the liquid bright platinum technique is improved by firing at as high a temperature within the ranges quoted above as is consistent with minimum distortion of the substrate.

With care the films may be prepared with consistent temperature coefficients from batch to batch and their abrasion resistance is excellent.

The thickness of films prepared is generally quoted as being between 0.1 and 1.0 micron. Busing (21) has determined the surface profile of painted films and reports a parabolic cross-section with maximum thickness of $0.71 \mu\text{m}$ in films of widths 0.88 mm, the minimum thickness measured being $0.16 \mu\text{m}$ on a film of 0.20 mm width (see also section 2.e(iii) and Fig. 25). It is more difficult to achieve close tolerances on final resistance values although light polishing with jeweller's rouge may be used to increase the resistance.

Electrical leads to the film may be formed by enlarging the width of the deposit although it must be remembered that both leads and film are subjected to the same heat flux. The lead resistance may be substantially reduced by the application of a thicker conducting paint such as Johnson Matthey Silver Paste X351 and X353 or quite simply with solder but care must be taken to ensure that these thicker layers do not affect the boundary layer. A model on which the leads have been prepared using this technique is shown in Fig. 28. If the lead resistance cannot be reduced, care must be taken in using the electrical discharge calibration technique to compensate for the relative areas of leads and active film. In arranging the leads it should be borne in mind that the ends of the active portion of the film must be at least as far from the edge of the substrate as from the rear to preserve the assumptions of the semi-infinite theory.

This may be achieved by increasing the width of the film at the edges of the substrate as shown in Fig. 29 which illustrates a form of thin film heat transfer gauge produced by the DISA Coy.

Further examples of heat transfer models shown in Fig. 30 have substrates inserted into recesses so that their surfaces are continuous with that of the model. In cases in which the substrate is curved it is ground and polished in a supporting mandrel which is the size and shape of the required final model. The polishing process is continued until the surfaces of the substrate are flush with the mandrel; the films are then deposited on the substrate which is cemented into the model with an epoxy resin.

Painted and fired thin films have several advantages: (1) good adhesion, (2) films may be put down on complex curved substrates, (3) a wide range of resistances may be obtained. They do, however, suffer from irregularities in surface area, thickness and to a lesser extent in temperature coefficient. Thin films prepared by vacuum deposition, on the other hand, have controllable thickness and the area may be defined by a masking process. So far the adhesive properties have not equalled those of painted and fired films, which are preferred for stagnation point heat transfer gauges. Two methods of vacuum deposition available at present are capable of producing films with a high standard of geometric uniformity and quite good abrasion resistance. Sputtered thin film gauges have been described by Rabinowicz et al (31), Nicholas (36), and an extensive literature, well surveyed by Holland (37), deals with the method of deposition. Nickel is preferred as the metal with the best all-round electrical and mechanical properties, and films deposited by R.F. bias sputtering have quite good adhesion. Recent advances in electron beam evaporation have enabled films to be made from a wide variety of materials without the complexity and expense of R.F. sputtering equipment. Chromium forms a firm bond on Pyrex and quartz substrates and nickel, when deposited on this sub-layer results in films of good mechanical strength. Abrasion resistance may be greatly improved by the deposition of a final layer of silicon monoxide; this may be done readily by electron beam evaporation. Such layers have been used for the purpose of electrically isolating the film from conducting liquids and ionised gases but the silica has the added advantage of strong adherence to the metal layer and is itself mechanically robust.

Film electrical stability is also improved by the deposition of this further layer which prevents incursion of oxygen. Magnesium fluoride has also been used for the same purpose in the production of abrasion resistant thin film resistors for semiconductor applications. Electron beam evaporation techniques permit the deposition of refractory materials in very thin layers and such normally high melting point substances as zirconium dioxide and cerium dioxide have been used. Current practice for heat transfer gauges appears to be to use quartz as a surface coating; this is entirely satisfactory but in extremely hostile conditions other refractory materials should be considered.

The properties of thin films made by deposition in vacuum cannot be predicted from a knowledge of the bulk properties since quite marked structural changes occur within the range of thicknesses commonly employed for such films. An equally important factor is the pressure of the residual gas in the deposition chamber although it is not proposed to discuss this in great detail. Taking for example a chamber in which the residual pressure is 10^{-5} torr and a vapour source 30 cm from the substrate it is found that less than 5% of the evaporated metal atoms undergo collisions before reaching the surface. At the surface, however, the bombardment by gas atoms is about ten times the rate of arrival of the metal atoms for deposition rates of 1 to 2 Å/s. The probability of gas absorption by the surface is thus very high and the electrical and thermal properties of the metal film will be seriously affected by the trapped gas. It is necessary to reduce the chamber pressure to at least 10^{-7} torr to ensure that the film will not be adversely affected by the residual gas. The substrate temperature is also found to have a marked effect on the film properties. Gas absorption is reduced by elevated substrate temperatures and it is standard practice to heat the material by radiation to between 300 and 400°C; adhesion of the film is thereby improved and the homogeneity increased. The stability of the deposited film may be improved by subsequent annealing, which may conveniently be performed under vacuum after deposition by the use of the same radiant heater.

The resistance of thin films is much higher than that which would be predicted on the basis of the bulk resistivity. The increase depends on both the metal and the film thickness and can be as high as 150 times the bulk value for film thicknesses less than about 100 Å. Silver apparently behaves in a more normal manner and the resistance ratio varies from a value of about 4 at a film thickness of 100 Å to 1.2 at 1000 Å. Fig.31 presents comparisons between observed specific resistances at 20°C and those computed from the resistivities of the bulk metal. The specific resistance in this case is defined as the resistance of a square film measured between opposite edges. The experimental and observed curves, redrawn from Winding, Topper and Baus (38) are nearly parallel when the film thickness exceeds about 200 Å but when the films are thinner the observed specific resistances rise more rapidly than would be predicted on the assumption of a constant resistivity for the material.

The temperature coefficients of resistivity of evaporated films diminish with decreasing film thickness and may, as they do for chromium, pass through zero and become negative for thinner films. Fig.32, again from the data of Winding, Topper and Baus, illustrates this effect for chromium and nickel. Nicholas (36) has reported an extensive study of evaporated, sputtered and painted films specifically for use in heat transfer gauges. It was concluded that evaporated films prepared by the usual techniques were insufficiently adherent and Nicholas recommends the superior properties of sputtered films laid on substrates heated to 300°C. The temperature coefficients of resistance and the specific resistivities were determined for platinum films deposited directly onto quartz and also with sublayers of chromium to improve adhesion. Resistivities of the platinum films with sublayers of chromium were slightly higher than without. From Nicholas' results it is possible to estimate the effect of film thickness on the overall temperature sensitivity. For a square deposit of thickness δ the

resistance between opposite sides is ρ_R/δ and the temperature sensitivity may be expressed as:

$$\frac{\Delta R}{\Delta T} = R_0 \alpha_R = \frac{\rho_R \alpha_R}{\delta}$$

Values of $\rho_R \alpha_R / \delta$ (ohm K^{-1}) for platinum deduced from Nicholas' data are shown in Fig.33 and compared with those for nickel from the data shown in Fig.31 from Winding Topper and Baus. The sensitivity is seen to fall rapidly with increasing thickness and nickel at a thickness of $0.1 \mu m$ is about 2.5 times as sensitive as platinum. This feature, in addition to its greater resistance to abrasion, accounts for its wider use. Chromium is seen to behave in an anomalous manner at thicknesses below about 600 \AA , $0.06 \mu m$, in that its temperature sensitivity changes sign. At thicknesses above 800 \AA its sensitivity is much the same as that of nickel and platinum and the advantages of thin layers, say 500 \AA , as sublayers for either platinum or nickel are apparent.

Table 7
Temperature coefficients of resistance
of vacuum deposited thin films

Metal	Temp. Coeff, K^{-1}		Bulk metal (0 - 100°C)
	Lowest	Highest	
Gold	0.0016 - 0.0028		0.0034
Platinum	0.0015 - 0.0025		0.0039
Rhodium	0.0018 - 0.0020		0.0046
Nickel	0.0003 - 0.0011		0.0064
Pt-Ir(90/10)	0.0007 - 0.0018		0.0012
Chromium	<0.0001 - 0.0006		-
Ni-Cr 80/20	0.0001 - 0.0002		-

from 'Thin Film Microelectronics', Ed Holland (39).

A list of the temperature coefficients of resistance for some of the more useful metals in thin film form is shown in Table 7 and compared with the bulk value for the pure material. It will be seen that platinum and gold have the desirable features of a relatively high temperature coefficient and that the value for chromium, which is useful as a first deposit to increase adhesion, is low so that the sandwich layer formed by the two films (say nickel on chromium) has thermal properties dominated by the nickel film. The adherent properties of chromium are also useful in the formation of electrical leads since the soldering process is less likely to remove the film when a high temperature gradient is established. It is less useful as a thin film thermometer on its own since the temperature coefficient is low, and may even be negative but such films have been used where the sensitivity of the detector was not of importance. Alloy films such as nickel-chromium may also be prepared by electron beam evaporation; the composition of the deposited film, although different from that of the source from which it is prepared, is sufficiently close to retain the very low temperature coefficients found in bulk in this material. Temperature coefficients of $0.01 K^{-1}$ have been reported for 50 \AA nickel-chromium films and this low value can be exploited in the preparation of leads to the sensitive portion of the heat transfer gauge.

In order to avoid lateral heat conduction effects in heat transfer gauge substrates it is highly desirable to confine the active part of the sensor to a region where the heat conduction process is strictly one-dimensional. This may be achieved by

increasing the width of the film to form the leads and the net increase in resistance due to aerodynamic heating in such leads is lower since the initial resistance is lower. Where space considerations are important the use of such low temperature coefficient metal alloys as nickel-chromium or indeed chromium alone may be advantageous. A summary of the important practical requirements for the production of low temperature coefficient leads includes the following:

- (i) The substrate must be held at a temperature above 200°C and preferably as high as 300°C during deposition in order to relieve internal stresses in the film.
- (ii) The deposited film must be annealed for stabilisation; this process may be carried out in atmosphere at a temperature within the range $250\text{--}350^{\circ}\text{C}$.

Soft soldering is adequate for the connection of leads to chromium films or nickel-chromium films although a further layer of gold facilitates this process. The choice of a flux is important in order that the active materials left on the surface do not cause chemical decomposition of the metal films. There is also the problem that many thin films are soluble in soft solder unless precautions are taken to avoid this. A small quantity of silver in the solder prevents the solution of platinum and silver films but in most cases a 60-40 tin-lead resin cored solder will be found satisfactory. If gold films cannot be overlaid on the chromium for soldering a copper deposit, either an electrochemically formed or a vapour deposited film is equally suitable. A low power soldering iron should be used with a small bit although hot gas streams are now available which form excellent connections. Preferably both parts should be tinned before the connection is completed in either case.

The surface condition of the substrate is of greater importance in the preparation of vacuum deposited films than in the case of painted and baked films. Since it is feasible and indeed desirable to restrict the thickness of the film to something less than $0.1\text{ }\mu\text{m}$, 1000 \AA , the surface should be smooth to approximately 100 \AA lest the discontinuities affect the resistance and the film's stability. A film in which the mass per unit area is non-uniform is unlikely to have a uniform resistivity and discharge methods of calibration will then be unreliable. The required smoothness can be attained if the substrate is polished and this should be done wherever possible. Small pit holes in the substrate may be tolerated but in the case of ceramic bases the disadvantage of roughness may be overcome by coating with a suitable glaze. Suitable glazed ceramic substrates are now becoming available for the microcircuitry industry (Corning Glass Works, Corning, N.Y.), and although these are generally in the smaller sizes they can be employed for inserts on heat transfer gauges. In the case of vacuum deposited films the precleaning of the substrate is important and general practice in this respect should be followed. Many instances in which inadequate adhesion has been found are attributable to the precleaning and substrate heating cycle. One of the most effective methods is as follows:

- (i) Rub with a synthetic leather wetted with an ionic detergent.
- (ii) Rinse in de-ionised distilled water.
- (iii) Clean in an ultrasonic bath containing de-ionised water, or a proprietary cleaner.
- (iv) Immerse in alcohol.
- (v) Dry rapidly with hot air jet.

Ion bombardment cleaning in the vacuum chamber prior to metal deposition is also recommended and in most equipment there is a facility for doing this just prior to the deposition itself.

There are several useful reference books which may be consulted for the techniques of vapour deposition and it would be inappropriate in the present context to describe the process in great detail. The current widespread use of the method for the

preparation of thin film microcircuits has resulted in a more thorough understanding of the electrical properties of the films so produced. This was not the case until the last five years or so. The Handbook of Thin Film Technology edited by L. I. Maissel and R. Glang, (40), Vacuum Deposition of Thin Films, (37), and Thin Film Microelectronics, (39), both by L. Holland, contain sufficient detail for the potential user of this technique to acquire the skills involved.

2.9 Analysis of Data from Thin Film Heat Transfer Gauges

The evaluation of the heat transfer rate from the observed surface temperature record may be carried out numerically or by the use of electrical analogues of the heat conduction process. The numerical procedure is convenient if the original surface temperature data is recorded on magnetic tape in either analogue (a voltage proportional to temperature) or digital form. The electrical analogue circuits, which will be described in detail in this section, are widely used. A filter circuit, suggested by Skinner (41), also enables the heat transfer rate to be determined directly from the surface temperature signal in real time. Both the electrical analogue and the Skinner filter circuit may produce high noise levels at their output terminals and practical circuits will be described which enable the signal/noise ratio to be maintained at an acceptable level even for very low heat transfer rates.

2.9(1) Numerical Computation

There are several alternative methods of dealing with the analysis of the surface temperature record. If the heat transfer rate is constant, or very nearly so, direct application of Eq (21) is possible. Small departures from a uniform rate may be taken into account by plotting $(T_s)^{1/2}$ versus t and obtaining the best fit to the resulting straight line. From Eq (20):

$$\dot{q}_s(t) = \frac{\sqrt{\rho c k}}{\sqrt{\pi \alpha_R E_0}} \left[\frac{E(t)}{\sqrt{t}} + \frac{1}{2} \int_0^t \frac{E(t) - E(\tau)}{(t - \tau)^{3/2}} d\tau \right] \quad (74)$$

with $E(t)/\alpha_R E_0$ the rise in the surface temperature $T(t)$.

Numerical integration of the second part of the expression enables $\dot{q}_s(t)$ to be determined when the heat transfer rate is not constant but there is a singularity at $t = \tau$. Cook and Felderman (42), Maulard (19), Henshall and Schultz (30), Vidal (13), and Jones (43) have all recommended numerical procedures for reducing the errors introduced by the uncertainty in the integral term. The effect of this is greatest for small values of t if constant steps of integration are maintained (obviously the most convenient for digital computation). Jones uses a trapezoidal rule to evaluate the integral over the first $(n-1)$ time divisions and the contribution of the last interval is evaluated by assuming a linear voltage-time relation and integrating directly. Vidal also recommends the use of the trapezoidal rule but taking the integrand to be zero at the upper limit. In the case of constant heat flux the integrand vanishes. Whatever technique is employed to avoid the singularity in the integral the errors are reduced with increasing time from the start of the run.

Cook and Felderman assume $E(\tau)$ can be approximated by a piecewise linear function of the form

$$\bar{E}(\tau) = E(t_{i-1}) + \frac{E(t_i) - E(t_{i-1})}{\Delta t} (\tau - t_{i-1}) \quad (75)$$

where $t_{i-1} \leq \tau \leq t_i$ and $i = 1, 2, 3, \dots, n$.

The integral in Eq (74) may be written as:

$$R(t_n) = \frac{1}{2} \int_0^{t_n} \frac{E(t_n) - \bar{E}(\tau)}{(t_n - \tau)^{3/2}} d\tau$$

$$\begin{aligned}
&= \frac{1}{2} \sum_{i=1}^n \int_{t_{i-1}}^{t_i} \frac{E(t_n) - \bar{E}(\tau)}{(t_n - \tau)^{3/2}} d\tau \\
&= \frac{1}{2} \sum_{i=1}^n \int_{t_{i-1}}^{t_i} \left[E(t_n) - E(t_{i-1}) - \frac{E(t_i) - E(t_{i-1})}{\Delta t} (\tau - t_{i-1}) \right] \frac{d\tau}{(t_n - \tau)^{3/2}} \\
&= \frac{1}{2} \sum_{i=1}^n \left\{ [E(t_n) - E(t_{i-1})] \int_{t_{i-1}}^{t_i} \frac{d\tau}{(t_n - \tau)^{3/2}} - \left[\frac{E(t_i) - E(t_{i-1})}{\Delta t} \right] \int_{t_{i-1}}^{t_i} \frac{(\tau - t_{i-1})}{(t_n - \tau)^{3/2}} d\tau \right\} \quad (76)
\end{aligned}$$

Considering the first integral in Eq (76):

$$\int_{t_{i-1}}^{t_i} \frac{d\tau}{(t_n - \tau)^{3/2}} = \left[\frac{2}{(t_n - \tau)^{1/2}} \right]_{t_{i-1}}^{t_i} = 2 \left[\frac{1}{(t_n - t_i)^{1/2}} - \frac{1}{(t_n - t_{i-1})^{1/2}} \right] \quad (77)$$

Considering the last integral in Eq (76) and integrating by parts:

$$\begin{aligned}
\int_{t_{i-1}}^{t_i} \frac{(\tau - t_{i-1})}{(t_n - \tau)^{3/2}} d\tau &= \left[\frac{2(\tau - t_{i-1})}{(t_n - \tau)^{1/2}} \right]_{t_{i-1}}^{t_i} - 2 \int_{t_{i-1}}^{t_i} \frac{d\tau}{(t_n - \tau)^{1/2}} \\
&= \left[\frac{2(t_i - t_{i-1})}{(t_n - t_i)^{1/2}} \right] + \left[4(t_n - \tau)^{1/2} \right]_{t_{i-1}}^{t_i} \\
&= \frac{2\Delta t}{(t_n - t_i)^{1/2}} + 4 \left[(t_n - t_i)^{1/2} - (t_n - t_{i-1})^{1/2} \right] \quad (78)
\end{aligned}$$

Substituting Eqs (77) and (78) into (76):

$$\begin{aligned}
R(t_n) &= \frac{1}{2} \sum_{i=1}^n \left\{ 2[E(t_n) - E(t_{i-1})] \left[\frac{1}{(t_n - t_i)^{1/2}} - \frac{1}{(t_n - t_{i-1})^{1/2}} \right] \right. \\
&\quad \left. - \left[\frac{E(t_i) - E(t_{i-1})}{\Delta t} \right] \left[\frac{2\Delta t}{(t_n - t_i)^{1/2}} + 4((t_n - t_i)^{1/2} - (t_n - t_{i-1})^{1/2}) \right] \right\} \quad (79)
\end{aligned}$$

Now:

$$(t_n - t_i)^{1/2} - (t_n - t_{i-1})^{1/2} = \frac{t_i - t_{i-1}}{(t_n - t_i)^{1/2} + (t_n - t_{i-1})^{1/2}} = \frac{-\Delta t}{(t_n - t_i)^{1/2} + (t_n - t_{i-1})^{1/2}}$$

and substituting into Eq (79) and grouping terms:

$$R(t_n) = \sum_{i=1}^n \frac{E(t_n) - E(t_i)}{(t_n - t_i)^{1/2}} - \sum_{i=1}^n \frac{E(t_n) - E(t_{i-1})}{(t_n - t_{i-1})^{1/2}} + 2 \sum_{i=1}^n \frac{E(t_i) - E(t_{i-1})}{(t_n - t_i)^{1/2} + (t_n - t_{i-1})^{1/2}} \quad (80)$$

At $i = n$, the first term in Eq (80) is indeterminate. Since, however, $E(t)$ was taken as piecewise linear:

$$\lim_{\tau \rightarrow t_n} \left[\frac{K(t_n - \tau)}{(t_n - \tau)^{1/2}} \right] = 0$$

Eq (80) may therefore be written as:

$$\begin{aligned}
R(t_n) &= \sum_{i=1}^{n-1} \left\{ \frac{E(t_n) - E(t_i)}{(t_n - t_i)^{1/2}} - \frac{E(t_n) - E(t_{i-1})}{(t_n - t_{i-1})^{1/2}} \right. \\
&\quad \left. + 2 \frac{E(t_i) - E(t_{i-1})}{(t_n - t_i)^{1/2} + (t_n - t_{i-1})^{1/2}} \right\} + \frac{E(t_n) - E(t_{n-1})}{\sqrt{\Delta t}} \quad (81)
\end{aligned}$$

Eq (74) may now be written as:

$$\dot{q}_n(t) = \frac{\sqrt{\rho c k}}{\sqrt{\pi} \alpha_R E_0} \left[\frac{E(t_n)}{\sqrt{t_n}} + \sum_{i=1}^{n-1} \left\{ \frac{E(t_n) - E(t_i)}{(t_n - t_i)^{1/2}} - \frac{E(t_n) - E(t_{i-1})}{(t_n - t_{i-1})^{1/2}} \right. \right. \\ \left. \left. + 2 \frac{E(t_i) - E(t_{i-1})}{(t_n - t_i)^{1/2} + (t_n - t_{i-1})^{1/2}} \right\} + \frac{E(t_n) - E(t_{n-1})}{\sqrt{\Delta t}} \right] \quad (82)$$

The only approximation involved in the use of this equation is the local linearisation of $E(t)$. The expression in Eq (82) may be further simplified to a form which requires less computation time as follows by noting that when $t_0 = 0$, $E(t_0) = 0$:-

$$\dot{q}_n(t) = \frac{\sqrt{\rho c k}}{\sqrt{\pi} \alpha_R E_0} \left[\sum_{i=1}^n \frac{E(t_i) - E(t_{i-1})}{(t_n - t_i)^{1/2} + (t_n - t_{i-1})^{1/2}} \right] \quad (83)$$

2.g(ii) Analogue Circuits

Although the numerical techniques described in the preceding section are quick and accurate there are many advantages to be gained by the use of electrical analogues for the processing of surface temperature information. The flow of heat into a semi-infinite material with specified thermal properties ρ , c and k is directly analogous to the flow of current into an R-C transmission line. An alternative approach is to design a filter network with the correct transfer function. Both of these methods will be discussed in detail.

The flow of heat into the semi-infinite material is analogous to the current flow into a medium containing distributed capacity and resistance. The analogy may be seen by paralleling the equations governing both cases, Fig.34.

$$\begin{aligned} \frac{\partial \dot{q}}{\partial x} &= \rho c \frac{\partial T}{\partial t} & \frac{\partial i}{\partial t} &= c' \frac{\partial V}{\partial t} \\ -\dot{q} &= k \frac{\partial T}{\partial x} & -i &= \frac{1}{r'} \frac{\partial V}{\partial x} \end{aligned}$$

where c' and r' are the capacity and resistance per unit length. Thus

$$\begin{aligned} \dot{q} &\equiv i & T &\equiv V \\ k &\equiv \frac{1}{r'} & \rho c &\equiv c' \end{aligned}$$

Solving either case we obtain, using Laplace transforms, the equations

$$\begin{aligned} \bar{i} &= \sqrt{\frac{c'}{r'}} \sqrt{p} \bar{V} \\ \bar{q} &= \sqrt{\rho c k} \sqrt{p} \bar{T} \end{aligned} \quad (84)$$

when

$$\begin{aligned} T = V &= 0 & \text{for } t &= 0 \\ T = V &= 0 & \text{for } x &= \infty \end{aligned}$$

In practice an analogue consisting of discrete RC blocks is used to approximate to the electrical case as shown in Fig.35 and the output signal from the thin film heat transfer gauge is applied to its input. The input

$$V_{in} = \alpha_R V_0 T$$

where V_0 is the film set voltage and α_R the temperature coefficient of resistance, gives

an input current

$$\bar{i}_{in} = \sqrt{\frac{\rho c'}{r'}} \alpha_R V_o \bar{T} \quad (85)$$

and hence this current and the heat transfer rate to the insulator are related by

$$\bar{q} = \sqrt{\rho c k} \sqrt{\frac{r'}{c'}} \frac{1}{\alpha_R V_o} \bar{i}_{in} \quad (86)$$

Thus

$$\dot{q} = \sqrt{\rho c k} \sqrt{\frac{r'}{c'}} \frac{1}{\alpha_R V_o} i_{in} \quad (87)$$

i_{in} may be found from the voltage, V_{out} across the input resistor R_i , giving,

$$\dot{q} = \sqrt{\rho c k} \sqrt{\frac{r'}{c'}} \frac{1}{\alpha_R V_o} \frac{V_{out}}{R_i} \quad (88)$$

For correct termination, R_i is related to the chain resistance R , being equal to $R/2$ for a T-section circuit shown by the dotted lines in Fig.35. Such a circuit has been shown by Meyer (44) to have a faster response time than other arrangements. Naturally the value of r'/c' is given by R/C at large times.

The rise time of the T-section analogue is approximately RC and this determines the 'lump' size required. The duration for which this circuit will reproduce a step function in heat transfer rate to within 1.4% has been determined by Meyer as:

$$t = 0.2 n^2 (RC) \quad (89)$$

where n is the number of stages of the analogue. If relatively long times are required Meyer has shown how the circuit may have arithmetically increasing lumps (Fig.36(a)) in order to reduce the number of components used. In this case the number of arithmetic lumps, h , may be regarded as equivalent to a number of uniform lumps, n , given by:

$$n = \frac{h(h+1)}{2} \quad (90)$$

However, it is necessary to have at least 2 uniform sections as input stages to improve the frequency response of the circuit.

The analogue may be calibrated electrically, a gain measurement at a known frequency, ω , within the working range being sufficient. From Eq (84)

$$\frac{V_{out}}{V_{in}} = \frac{R_i i_{in}}{V_{in}} = R_i \sqrt{\frac{c'}{r'}} \sqrt{\omega} \quad (91)$$

and hence the quantity $R_i \sqrt{c'/r'}$ may be found. Furthermore, a check on the working frequency range may be performed by measuring the frequency response of the circuit which should exhibit the $\sqrt{\omega}$ dependence of Eq (91) in this range. An example of this is shown in Fig.37 for the circuit in Fig.36(b). Indeed, such a plot revealed that the arithmetically lumped circuit of Meyer had uniform input lumps of different r', c' from those for the arithmetic section. This required correction to the circuit shown in Fig.36(a) where $r'/c' = R/C$ and a typical analogue used in gun tunnels is shown in Fig.36(b) where its operating time and approximate sensitivity are given.

Skinner (41) has proposed a different form of analogue circuit, in which the network is treated merely as a filter, Fig.38, with the transfer function defined by Eq(91). Analysing this circuit, the output may be derived as follows:

The current through all RC elements is the same, hence:

$$V_{in} - V_{out} = \sum_1^m i \frac{R_n}{1 + pR_nC_n}$$

$$i = \frac{V_{out}}{R_o}$$

From the above two equations

$$\frac{V_{out}}{V_{in}} = \frac{R_o}{R_o + \sum_1^m \frac{R_n}{1 + pR_nC_n}} \quad (92)$$

Skinner shows that this expression may be put in the form:

$$\frac{V_{out}}{V_{in}} = A \frac{(p+a_1) \cdots (p+a_n) \cdots (p+a_m)}{(p+b_1) \cdots (p+b_n) \cdots (p+b_m)} \quad (93)$$

where $a_n = 1/R_nC_n$ and b_n is a rather complicated function of a_n and R_oC_n . By suitable choice of the resistors R_n and R_o and the capacitors C_n it is possible to approximate to a transfer function of the correct form, i.e. $\sim \sqrt{p}$. This may be seen in a Bode diagram shown in Fig.39.

Naturally the values of R_n and C_n required are not easily defined and were computed by Skinner for a certain number of stages. The circuit and frequency response of a 5-stage analogue is given in Fig.40 and for an 8-stage analogue in Fig.41, the value of R_o being equal to 1Ω in both cases. From Eq (92) it can be seen that the parameters R_nC_n affect the frequency scaling whereas in order to change the impedances the values of R_o and R_n may be altered. Therefore the basic analogues of Figs 40,41 may be adapted to any frequency range by changing C_n to C_n/γ and this will make all points at ω in Fig.38 go to $\gamma\omega$, the impedance of the circuit remaining the same. Similarly if it is necessary to change the impedance this may be done by varying R_n and R_o by a constant fraction whilst maintaining R_nC_n constant by changing C_n .

The analogues of both Skinner and Meyer operate well, but the question as to which form is the more efficient in its use of stages requires investigation. Meyer (45) has indeed done a comparison of his uniformly lumped analogue with Skinner's five section analogue and comments that the former gives only a slightly better output than the latter which has considerably fewer components albeit of rather awkward values. The arithmetically lumped circuit was not compared and it is instructive to do this by matching the range of operating frequencies. Of the alternatives the eight section analogue of Skinner covers a frequency range of four decades and a circuit due to Meyer with ten arithmetically lumped sections preceded by two uniform sections was found by experiment to cover the same frequency range. There is therefore little to choose between the analogues although those of Skinner are calculated for set frequency ranges whereas those of Meyer may be extended to cover any range. It is perhaps more convenient to be able to use high tolerance components in multiples as required in the Meyer circuit than to match the exact component values of the Skinner circuit.

A direct comparison between the performance of analogue circuits and digitally reduced data provides a further check on the accuracy of the former if care is taken to use a short sampling time in deriving the heat transfer rate numerically. Two examples of such a comparison are shown in Fig.42. In Fig.42(a) a comparison is shown between the output of a 5-section filter circuit (Skinner) and the data derived numerically at 0.10 ms intervals. The agreement is seen to be well within the natural fluctuation level of the heat transfer signal itself. A second example, shown in Fig.42(b), is the comparison of a 30-section uniformly distributed analogue network designed on Meyer's principles ($C = 0.02 \mu F$, $R = 5 k\Omega$) with digital data derived every milli-second. From a comparison of the analogue network output and the computed data it

was deduced that the analogue 'sensitivity' was $32 \mu\text{V}$ per W/cm^2 while the theoretical value would have been 32.5. From the close agreement commonly found between analogue and digital data there appears to be little advantage to be gained from the use of the more complex digital technique unless of course the signals are recorded in digital form, say on magnetic tape, in the first instance. Provided care is taken in the design of the analogue or filter network, together with its accompanying amplifying and recording units, the accuracy and sensitivity should be entirely satisfactory over a wide range of heat transfer rates. In section 2.h following, practical circuits involving a new type of analogue-amplifier interconnection are illustrated.

2.h Practical Circuits for use with Thin Film Heat Transfer Gauges

A practical circuit is shown in Fig.43(a) and consists of three parts, a constant current supply, an analogue network and an amplifier. These may be separate interconnected units or they may be built as one unit. The current supply utilises the characteristic of a single transistor to provide a constant current, independent of the collector voltage, which may be adjusted by means of the base current. The output voltage V due to a variation $\frac{\Delta R}{R_c}$ in film resistance R is given by:

$$\frac{V}{V_0} = \frac{R_c}{R + R_c} \frac{\Delta R}{R}$$

where R_c is the collector resistance and V_0 the steady film voltage. In practice $R \approx 30 \Omega$ and $R_c \approx 5 \times 10^4 \Omega$ and thus

$$\frac{V}{V_0} = \frac{\Delta R}{R} = \propto_R \Delta T$$

to within 0.1%. The power supply required for the circuit must provide a steady voltage since any voltage ripple from the A.C. mains affects the base voltage via the potential divider which is used to set the base voltage, although this effect may be reduced by placing a large condenser between the base and earth. In operation the current through the thin film is set using the potentiometer in the base potential divider circuit and the current is read on a moving coil meter. Provision is made for monitoring the thin film resistance on the same meter by passing a known small current through the film with the push button shown.

The collector voltage output is then fed to the analogue network described in section 2.g(ii). The analogue is usually connected such that the output across R_1 , Fig.35 section 2.g(ii) is relative to earth, the input being fed to the first capacitance, Fig.43(a). This output may then be amplified in the normal manner. In Fig.43(a) the circuit has been further simplified by using the analogue current monitoring resistor R_1 as the input resistor of a conventional voltage amplifier, the gain being given by the ratio of R_f to R_1 . Conversely this amplifier circuit may be considered as a current-to-voltage converter giving an output voltage proportional to the analogue input current. This mode of interconnection is much superior to that in which the voltage across R_1 is monitored with a high input impedance voltage amplifier because the signal to noise ratio is considerably improved.

Using the circuits shown in Fig.43(a) it is possible to measure heat transfer rates of $10^{-2} \text{ W}/\text{cm}^2$ in flows of 30 ms duration. Typical examples of surface temperatures and corresponding heat transfer rates obtained from the circuits described above are shown in Fig.43(b). The records were obtained in a slow piston isentropic compressor whose flow duration was 210 ms and a shock tube in which the steady flow duration was only 0.5 ms behind the primary shock wave. In the case of the free piston compressor the falling heat transfer rate is associated with the rise in wall temperature.

3 CALORIMETER GAUGES

3.a The Ideal Calorimeter and Limitations of the Simple Theory

All calorimeter gauges, as the name implies, attempt to determine the instantaneous heat transfer rate to a surface by measuring the time rate of change of the thermal energy within an element of the surface. The element concerned is usually in the form of a thin skin and may be either localised (i.e. thermally insulated from the surrounding surface) or continuous with the rest of the surface. The thermal energy is determined from a temperature measurement in or on the surfaces of the 'skin' and it is the rate of change of this temperature that gives the heat flux into the exposed surface. Assuming that no heat is lost from the rear surface, the heat transfer rate per unit area is by definition,

$$\dot{q}_s = \int_0^l \rho c \frac{\partial T}{\partial t} dx \quad (94)$$

For constant ρ and c

$$\dot{q}_s = \rho c l \frac{dT_{\text{mean}}}{dt} \quad (95)$$

for the one-dimensional case, where ρ and c are the density and specific heat respectively of the calorimeter material of thickness l . T is the temperature at a position x within the surface as shown in Fig.44. In all the techniques used Eq (95) is approximated in the form

$$\dot{q}_s = \rho c l \frac{dT_{\text{exp}}}{dt} \quad (96)$$

where T_{exp} is the experimentally observed temperature.

In the next section the manner in which dT_{exp}/dt is related to dT_{mean}/dt is investigated for the ideal one-dimensional case (i.e. no lateral conduction). The presence of a backing material is included in the problem for in certain cases this is necessary and can have a significant effect on the measurement. Typical temperature measuring techniques are sketched in Fig.45. Of all these schemes, the technique illustrated in Fig.45(b), where the total resistance of the calorimeter is measured, has the highest frequency response since it can be shown that the temperature inferred from the change in resistance of the gauge is always close to the mean temperature as shown in sect.3.c. In the cases (a), (c) and (d) there is a finite time required before dT_{exp}/dt corresponds to the mean value, as seen in the example of Fig.47 where the front and back surface temperatures are shown for a constant heat transfer rate. The presence of backing material, necessary for structural purposes, renders Eq (95) approximate as heat is transmitted to the backing material and the order of this error has to be determined.

Further, non-ideal effects such as lateral conduction due to temperature gradients produced by non-uniform heating in the thin skin model, Fig.45(a), or heat loss through the element supports in the case of the local calorimeter, Fig.45(d), need to be considered. Results concerning the effect of connections such as thermocouple wires are discussed and the effect of a non uniform surface temperature on the heat transfer coefficient is considered. Experimental arrangements, their use and calibration are also examined in the following sections.

3.b One-Dimensional Analyses

3.b(1) Equation for Surface Temperature Rise

From section 1, Eq(12) the temperature within the calorimeter for a constant heat transfer rate \dot{q} may be found by substituting, $\bar{q} = \dot{q}_0/\rho$

Thus,

$$\bar{T}_i = \frac{\dot{q}_0 \sqrt{\alpha_1} \left[(1+a) e^{-\sqrt{\frac{p}{\alpha_1}}(x-l)} + (1-a) e^{+\sqrt{\frac{p}{\alpha_1}}(x-l)} \right]}{k_1 p^{3/2} \left[(1+a) e^{+\sqrt{\frac{p}{\alpha_1}} l} - (1-a) e^{-\sqrt{\frac{p}{\alpha_1}} l} \right]} \quad (97)$$

Note also that

$$\frac{\partial \bar{T}_i}{\partial t} = p \bar{T}_i \quad (98)$$

These equations enable the temperature history and the rise time of the gauge to be obtained for the case $a=0$ i.e. no heat loss from the rear face of the gauge in section 3.b(ii) and $a \neq 0$ as shown in section 3.b(iii).

3.b(ii) Calorimeter without Substrate

For the case of $a=0$ i.e. no backing material, Eq (97) reduces to

$$\bar{T}_i = \frac{\dot{q}_0 \sqrt{\alpha_1} \cosh(x-l) \sqrt{\frac{p}{\alpha_1}}}{k_1 p^{3/2} \sinh l \sqrt{\frac{p}{\alpha_1}}} = \frac{\dot{q}_0 \sqrt{\alpha_1} (e^{(x-l) \sqrt{\frac{p}{\alpha_1}}} + e^{-(x-l) \sqrt{\frac{p}{\alpha_1}}})}{k_1 p^{3/2} e^{-l \sqrt{\frac{p}{\alpha_1}}} (1 - e^{-2l \sqrt{\frac{p}{\alpha_1}}})}$$

as given in Carslaw and Jaeger (46). Expanding the term $1/(1 - e^{-2l \sqrt{p/\alpha_1}})$ we obtain:

$$\bar{T}_i = \frac{\dot{q}_0 \sqrt{\alpha_1}}{k_1} \sum_{n=0}^{\infty} \frac{1}{p^{3/2}} e^{[(2n+1)l+x] \sqrt{\frac{p}{\alpha_1}}} + \frac{1}{p^{3/2}} e^{-[(2n+1)l-x] \sqrt{\frac{p}{\alpha_1}}} \quad (99)$$

the terms of which have standard inverse transforms giving

$$T_i = \frac{2 \dot{q}_0 \sqrt{\alpha_1} t}{k_1} \sum_{n=0}^{\infty} \left(\operatorname{ierfc} \frac{(2n+1)l+x}{2\sqrt{\alpha_1 t}} + \operatorname{ierfc} \frac{(2n+1)l-x}{2\sqrt{\alpha_1 t}} \right) \quad (100)$$

The mean temperature is obviously a linear function of time from Eq (95) and the function of Eq (100) is plotted as the difference, $k_1 \Delta T / \dot{q}_0 l$, between the actual and mean temperatures as a function of position for given times in Fig.46. These curves enable particular cases such as Fig.47 to be calculated and allow the temperature within the calorimeter to be determined as a function of time.

From Eq (97) the time derivative of temperature is given by:

$$\frac{\partial \bar{T}_i}{\partial t} = \frac{\dot{q}_0 \sqrt{\alpha_1} (e^{(x-l) \sqrt{\frac{p}{\alpha_1}}} + e^{-(x-l) \sqrt{\frac{p}{\alpha_1}}})}{k_1 p^{3/2} e^{l \sqrt{\frac{p}{\alpha_1}}} (1 - e^{-2l \sqrt{\frac{p}{\alpha_1}}})} \quad (101)$$

Expanding the term in brackets in the denominator again, the following equation is obtained:

$$\frac{\partial \bar{T}_i}{\partial t} = \frac{\dot{q}_0 \sqrt{\alpha_1}}{k_1} \sum_{n=0}^{\infty} \frac{1}{p^{3/2}} e^{-[(2n+1)l-x] \sqrt{\frac{p}{\alpha_1}}} + \frac{1}{p^{3/2}} e^{-[(2n+1)l+x] \sqrt{\frac{p}{\alpha_1}}} \quad (102)$$

These terms have standard inverse transforms and, in particular, give the following series at the front and back faces of the calorimeter:

$$\text{Front} \quad \frac{dT_i}{dt} = \frac{\dot{q}_0 \alpha_1}{k_1 l} \frac{1}{\sqrt{\pi} \sqrt{\alpha_1 t}} \left(1 + 2 \sum_{n=0}^{\infty} e^{-(n+1)^2 \frac{l^2}{\alpha_1 t}} \right) \quad (103)$$

$$\text{Back} \quad \frac{dT}{dt} = \frac{\dot{q}_0 \alpha_1}{k, l} \frac{2}{\sqrt{\pi}} \frac{l}{\sqrt{\alpha_1 t}} \sum_{n=0}^{\infty} e^{-(n+1/2)^2 \frac{l^2}{\alpha_1 t}} \quad (104)$$

Both of these series converge rapidly for the times of interest and may be quickly evaluated to give the difference between the mean temperature derivative $(dT/dt)_{\text{mean}}$ defined by Eq (95), and that in the calorimeter. Graphs of the function:

$$\left[\left(\frac{dT}{dt} \right)_{x=0} - \left(\frac{dT}{dt} \right)_{\text{mean}} \right] / \left(\frac{dT}{dt} \right)_{\text{mean}}$$

are given in Fig.48 plotted against time for the front and back surfaces of the calorimeter. It can be seen that in order to approach the mean value to within 1% it is necessary that $\alpha_1 t / l^2 > 0.5$. The response time will be rather faster at the mid-point of the calorimeter (see Fig.46) but it is safer to assume the rise time of the calorimeter to be the response time of the rear surface. Typical rear surface response times for different materials of various thicknesses are presented graphically in Figs.49, 50 and 51 for convenience along with typical rates of rise of temperature. The limiting temperature differences between the front and rear surfaces can be evaluated from the expression:

$$T_{\text{front}} - T_{\text{rear}} = \tau(\text{rise time}) \times \left(\frac{dT}{dt} \right)_{(\text{rate of rise})}$$

3.b(iii) Calorimeter with Substrate

The analysis in section 3.b(ii) may be repeated for the case of a calorimeter with a substrate using Eqs (97) and (98). In particular, the rate of change of temperature of the front and back surfaces are given by:

$$\text{Front} \quad \frac{dT}{dt} = \frac{\dot{q}_0 \alpha_1}{k, l} \frac{2}{\sqrt{\pi}} \frac{l}{\sqrt{\alpha_1 t}} \frac{1}{(1+a)} \sum_{n=0}^{\infty} \left(\frac{1-a}{1+a} \right)^n e^{-(n+1/2)^2 \frac{l^2}{\alpha_1 t}} \quad (105)$$

$$\text{Back} \quad \frac{dT}{dt} = \frac{\dot{q}_0 \alpha_1}{k, l} \frac{1}{\sqrt{\pi}} \frac{l}{\sqrt{\alpha_1 t}} \left[1 + 2 \sum_{n=0}^{\infty} \left(\frac{1-a}{1+a} \right)^n e^{-(n+1/2)^2 \frac{l^2}{\alpha_1 t}} \right] \quad (106)$$

These functions are easily evaluated and are shown in Fig.48 for the cases $a = 0.33$, $a = 0.10$ and $a = 0.05$, the case $a = 0.1$ corresponding closely with platinum on Pyrex. $(dT/dt)_{\text{mean}}$ in these curves still refers to the rate of rise of temperature without a substrate. It is interesting that even in the case $a = 0.10$, the rate of change of temperature of the rear surface is always in error by at least 10%, the loss of heat to the substrate being substantial within the response time of the calorimeter. In the above case the rise time of the backed calorimeter is approximately that given for the unbacked calorimeter as might be expected. The minimum error in heat transfer rate measured using the rear face temperature is also shown in Fig.48 as a function of a . This enables this quantity to be evaluated for any calorimeter - substrate combination.

The error in inferred heat transfer rate for t large may be estimated by assuming that the error is small such that the calorimeter temperature is given approximately by that in the absence of a substrate. The calorimeter temperature may be considered uniform for t large. Thus the substrate temperature is known and an estimate of the heat lost to this may be found on the assumption that the substrate is semi-infinite. This in turn leads to a correction to the rate of rise of the calorimeter temperature

and the process may be repeated in order to obtain a more accurate correction as shown below.

The heat transfer rate to the substrate in terms of its surface temperature is given by

$$\dot{q}_{\text{substrate}} = \sqrt{\rho_2 c_2 k_2} \sqrt{p} \bar{T}_{\text{substrate}}$$

which may be expressed as

$$\dot{q}_{\text{substrate}} = \sqrt{\frac{\rho_2 c_2 k_2}{p}} \bar{T}_{\text{substrate}} \quad (107)$$

as $T_{\text{substrate}} = 0$ when $t = 0$

Assuming that the substrate surface temperature is equal to the mean temperature in the absence of a substrate,

$$\bar{T}_{\text{substrate}} = \frac{\dot{q}_{\text{surface}}}{\rho, c, l} \frac{1}{p} = \frac{\dot{q}_{\text{surface}} \sqrt{\alpha_1}}{\sqrt{\rho, c, k_1} l p}$$

for constant surface heat transfer rate. Substituting this into Eq (107) gives,

$$\dot{q}_{\text{substrate}} = \dot{q}_{\text{surface}} a \frac{\sqrt{\alpha_1}}{l} \frac{1}{p^{3/2}} \quad (108)$$

Therefore from the energy equation, Eq (94)

$$\dot{T} = \frac{\dot{q}_{\text{surface}} - \dot{q}_{\text{substrate}}}{\rho, c, l} \quad (109)$$

The error in the rate of rise of calorimeter temperature is then obtained by taking the inverse transform of Eq (108):

$$\frac{\dot{T}_{\text{with substrate}} - \dot{T}_{\text{without substrate}}}{\dot{T}_{\text{without substrate}}} = \frac{\dot{q}_{\text{substrate}}}{\dot{q}_{\text{surface}}} = \frac{2}{\sqrt{\pi}} a \sqrt{\frac{\alpha_1 t}{l^2}} \quad (110)$$

A more accurate estimate may be obtained by substituting the corrected rate of rise of surface temperature back into Eq (107) for the heat lost to the substrate. The transformed differential of surface temperature is obtained from Eqs (108) and (109) as:

$$\bar{T} = \frac{\dot{q}_{\text{surface}}}{\rho, c, l} \left(\frac{1}{p} - \frac{a \sqrt{\alpha_1}}{l p^{3/2}} \right)$$

and substitution into Eq (107) gives:

$$\frac{\dot{q}_{\text{substrate}}}{\dot{q}_{\text{surface}}} = \frac{a \sqrt{\alpha_1}}{l} \left(\frac{1}{p^{3/2}} - \frac{a \sqrt{\alpha_1}}{l p^2} \right)$$

The inversion of this equation then gives the desired result:

$$\frac{\dot{q}_{\text{substrate}}}{\dot{q}_{\text{surface}}} = \frac{2a}{\sqrt{\pi}} \left(\frac{\alpha_1 t}{l^2} \right)^{1/2} - a^2 \left(\frac{\alpha_1 t}{l^2} \right) \quad (111)$$

The relationship $\dot{q}_{\text{substrate}}/\dot{q}_{\text{surface}}$ is plotted in Fig.48 from which it will be seen that the approximate solution is quite close to the exact solution for errors in \bar{T} up to 20%. Using the above approximate solution it can be shown, for example, that the heat losses to air as a backing material for a stainless steel calorimeter of 0.25 mm thickness would result in an error of 1% after 2 seconds.

Using the charts, Figs.49, 50 and 51, it is possible to design a calorimeter in most

of the commonly used materials suitable for wind tunnel models and to calculate the signal which would be obtained from a variety of temperature sensors over a wide range of heat transfer rates.

3.c The Rose Calorimeter Gauge

The Rose calorimeter gauge (20) was devised so as to measure high heat transfer rates ($> 1 \text{ kW/cm}^2$) in times of order $100 \mu\text{s}$ and typical sensitivities are $1 \text{ mV/s per W/cm}^2$. The gauge consisted of a strip of metal foil ($\sim 0.003 \text{ cm}$ thick) mounted on an insulating substrate (Fig.55(a)). The heat transferred to the surface is assumed to remain entirely in the foil, negligible heat entering the substrate. The instantaneous heat transfer rate to the surface may be found from Eq (95) where the space-average temperature is deduced from the net resistance of the foil. The temperature in the foil is far from uniform but Rose (20) has shown that for all times the average temperature of the foil is related to the net resistance by the usual relationship,

$$R = R_o \left[1 + \alpha_R (T_{mean} - T_o) \right] \quad (112)$$

to within 1% for typical gauges and heating rates. These gauges are necessarily of low resistance ($\sim 4 \times 10^{-3} \Omega$) and a large constant monitoring current ($\sim 5 \text{ A}$) is passed through the foil giving a voltage of order 0.02 V such that the resistance change may be measured.

The resistance of the foil may be determined by considering this to be a set of elemental laminae connected in parallel, the resistance of each corresponding to the temperature at its position in the foil. The total resistance of the film may be seen with reference to Fig.52 to be:

$$\frac{1}{R} = \sum \frac{1}{\frac{\rho_R(x)L}{w \Delta x}} = \frac{w}{L} \int_0^L \frac{dx}{\rho_R(x)}$$

ρ_R is given by

$$\rho_R(x) = \rho_{R0} (1 + \alpha_R T(x))$$

and hence

$$\frac{1}{R} = \frac{w}{\rho_{R0} L} \int_0^L \frac{dx}{(1 + \alpha_R T(x))}$$

For $\alpha_R T(x) \ll 1$, this may be expanded to give:

$$\frac{1}{R} = \frac{w}{\rho_{R0} L} \int_0^L (1 - \alpha_R T(x) + \alpha_R^2 T^2(x) \dots) dx$$

$$\text{Therefore } \frac{1}{R} = \frac{wL}{\rho_{R0} L} (1 - \alpha_R T_{mean} + \alpha_R^2 T_{mean}^2 \dots) / T_{mean}$$

Inverting and expanding again we obtain:

$$R = \frac{\rho_{R0} L}{wL} \left\{ 1 + \alpha_R T_{mean} - \alpha_R^2 \left[(T^2)_{mean} - (T_{mean})^2 \right] \right\}$$

giving,

$$R = R_o \left\{ 1 + \alpha_R T_{mean} - \alpha_R^2 \left[(T^2)_{mean} - (T_{mean})^2 \right] \right\}$$

Hence the mean temperature measured in this way is given by:

$$\frac{R - R_0}{\alpha_R} = T_{mean} - \alpha_R \left[(T^2)_{mean} - (T_{mean})^2 \right]$$

and the fractional error is therefore:

$$\frac{\alpha_R \left[(T^2)_{mean} - (T_{mean})^2 \right]}{T_{mean}} \quad (113)$$

Rose calculated the error given by Eq (113) by using the function given in Eq (97); the results for various materials on Pyrex are given in Fig.53.

The loss to the substrate and its effect on the inferred heat transfer rate follows from Eq (94). Thus:

$$\dot{q}_{surf} - \dot{q}_{subs} = \rho c l \frac{dT_{mean}}{dt} \quad (114)$$

The quantity $\dot{q}_{subs}/\dot{q}_{surf}$, which gives the fractional error in the measured heat transfer rate, has been evaluated by Rose for various metals on Pyrex and the results may be seen in Fig.54. It may be seen from this figure that the error due to loss to the substrate exceeds 3% for platinum on Pyrex when t (in seconds) is greater than l^2 (in cm^2). Thus a 0.003 cm thick foil is accurate to within 1% for approximately 10^{-5} and after 100 μs the error is approximately 10%. The above estimates are upper limits for this error for in general the thermal contact between the foil and substrate is far from perfect. The errors indicated by Fig.54 may be estimated from the approximate analysis given in the previous section. Eq (111), section 3.b(iii), may be used in a modified form which corrects this for the lag due to the time taken for the heat to diffuse through the calorimeter to the rear surface. The time lag t_0 is given by,

$$\frac{\alpha_l t_0}{l^2} = 0.167$$

which may be seen from Fig.46. The equation giving the heat loss to the substrate is therefore:

$$\frac{\dot{q}_{substrate}}{\dot{q}_{surface}} = \frac{2}{\sqrt{\pi}} a \left[\frac{\alpha_l(t-t_0)}{l^2} \right]^{1/2} - a^2 \left[\frac{\alpha_l(t-t_0)}{l^2} \right] \quad (115)$$

and this is plotted in Fig.54 for platinum on Pyrex and shows fair agreement with the numerical result of Rose. Thus the effect of substrates other than Pyrex may be estimated using Eq (115).

The construction of the gauge and its circuitry may be seen in Fig.55. The chemically pure platinum foil was die-cut to the desired shape which consisted of the main current carrying strip with two narrow side arms for voltage sensing. The leads were soldered onto areas of thin platinum film painted and baked onto a polished Pyrex substrate, the foil also being stretched and soldered between these regions. In use a constant current of approximately 5A is supplied to the film from a battery through dropping resistors and the voltage developed across the potential sensing arms measured on an oscilloscope.

The accuracy of the measurement depends on a knowledge of the geometry of the foil and values of ρ , c and α_R for the platinum. As the gauge is heated appreciably by the monitoring current the initial temperature of the foil is liable to rise considerably above ambient and it was recommended by Rose that this rise should be kept below $50^\circ C$ in order that bulk values of ρ , c and α_R could be used. This temperature rise corresponds approximately to a fractional resistance change of 1.25. The voltage output of

the film is given by:

$$V_{out} = \frac{\alpha_A R_o I}{\rho c L} \dot{q} t \quad (116)$$

The sensitivity of the gauge described above with a monitoring voltage of 0.02 V is 0.60 mV/s per W/cm^2 as may be determined from Fig .49.

Typical results obtained from the use of such platinum calorimeter gauges are also shown in Fig.55. The calorimeter in this instance was located at the stagnation point of a bluff body mounted in a shock tube. After a period of about 10 μs , during which the bow shock wave moved to its equilibrium position, the heat transfer rate fell from a high value of 15 - 20 kW/cm^2 to 5 kW/cm^2 . There followed a period of approximately 40 μs of steady flow, indicated by region (2) in Fig.55(b)) and subsequently the heat transfer rate increased to 10 kW/cm^2 with the arrival of the contact surface.

A different constructional technique has been employed by Aronson (47). An aluminium model was milled to receive an iron calorimeter element. After machining, the recess was anodised to provide an insulating layer which was in turn coated with 'Glyptol' insulating varnish. The model was heated and the calorimeter element pushed into the Glyptol varnish until it was flush with the model surface. Leads were taken through the model and voltage and current connections at the ends of the element were covered with a layer of epoxy cement which was in turn made flush with the model surface. In this instance there would be good thermal contact between the element and its substrate and the estimate of heat losses using the theory presented in this section would be realistic.

The measurement of the average resistance of the calorimeter has been the basis of the 'Morgandyne' gauges (48) developed at A.E.D.C., Tullahoma. In this case, however, the resistance change was measured by making the calorimeter element the secondary of a transformer. The input impedance of the transformer was measured and this reflected the change in resistance in the primary. The calorimeter element was large and its resistance change small but the response of the device could be analysed in a similar manner to the Rose calorimeter gauge.

In order to calibrate his gauges Rose (20) passed a heating current pulse of 700 A amplitude and duration of approximately 100 μs through the gauge. This current pulse was generated by firing a copper clad bullet through two plates to act as a switch but it should now be possible to use high current semiconductor devices such as thyristors to produce this pulse more readily. Sprinks (49) has proposed a method whereby the calorimeter gauge is plunged into a high temperature liquid and has analysed the process which subsequently occurs. Use of the bulk values of ρ , c and k as advocated by Rose appear to be the best procedure at present although the method of radiation calibration proposed by Maulard (32) and Schulte et al (33) and described in section 2.e(ii) is also applicable.

3.d Thin skin calorimeter models

3.d(i) Elementary principles

Thin skin ("thin walled") models are widely used in order to measure heat transfer on complex shapes. The skin may constitute the complete model or be confined to a region of particular interest. Various schemes showing the form of the construction are given in Fig.56; copper and stainless steel are favoured materials for the skin although platinum has been used, for example, in the free flight models.

It is usually the rear face of the skin that is instrumented with thermocouples and the heat transfer rate is inferred from the rate of rise of the temperature thus measured. Typical rates of rise of temperature and response times for a wide range of model materials are given in Figs. 49, 50 and 51, and these combined with the thermo-

couple sensitivities enable the sensitivities of the various systems to be determined. Thus

$$\frac{dV}{dt} = a \frac{dT}{dt} = \frac{a\dot{q}}{\rho c l} \quad (117)$$

where a is thermocouple constant in $\mu\text{V/K}$. Table 1 (section 2.b) shows the value of a for various thermocouples and Table A-1 gives more detail of the variation of a with temperature. The temperature rise and associated thermocouple output for various combinations of calorimeter material and thermocouple are shown in Figs. 49, 50 and 51. Thus it can be seen that a stainless steel skin of 0.17 cm thickness instrumented with a chromel-alumel thermocouple will give a sensitivity of 0.075 mV/s per W/cm^2 .

3.d(ii) The variation of calorimeter properties with temperature

As all the quantities ρ , c and l vary with temperature there is a limit to the maximum allowable temperature before errors are introduced by assuming that these are constant. Curves drawn showing the variation of the quantity

$$\left(\frac{a}{\rho c l}\right)_T / \left(\frac{a}{\rho c l}\right)_{T=0}$$

with temperature for various combinations of thermocouples and calorimeter material are shown in Fig. 57, hence an estimate of the errors in deriving instantaneous heat transfer rates from the observed rates of change of thermocouple output with time may be found. The linear coefficient of expansion of the calorimeter material, γ , was found from ref. (23) and it was assumed that

$$\rho_T l_T = \rho_0 l_0 (1 - 2\gamma T) \quad (118)$$

The variation of specific heat with temperature was also found from ref. (23). The variation of the thermocouple constant a with temperature was obtained by differentiating the data given in ref. (50). It can be seen therefore that there may be considerable errors in the deduced heat transfer rate due to the variation in $a/\rho c l$ although in certain cases the variations due to a and c , which are the main factors involved, sensibly cancel one another (e.g. an iron-constantan thermocouple on a copper calorimeter). The temperature change in the experiment determines the error due to this effect and hence the error is dependent on both the heat transfer rate and thickness of the calorimeter.

In many experiments the flow is reasonably constant and the rate of rise of thermocouple output is taken immediately after the tunnel starting and calorimeter rise time. In this manner it is possible to minimise the effects of the variation of properties with temperature and of conduction along the model surface.

3.d(iii) Conduction effects

In a previous section the calorimeter response time and also the error introduced by a backing material for a constant heat transfer rate were examined. In most experiments, however, it is the heat transfer coefficient that is constant and is to be measured, the heat transfer rate falling as the model surface temperature increases. Thus:

$$\dot{q} = h(T_R - T_f) = \rho c l \left(\frac{dT}{dt}\right)_{\text{mean}} \quad (119)$$

where T_R and T_f are the flow recovery temperature and wall front surface temperature respectively. If the thin skin temperature is monitored on its rear surface then errors are introduced not only in $(dT/dt)_{\text{mean}}$ but also in T_f , even for times much greater

than the response time. The errors incurred by taking T_b , the rear face temperature, to deduce the heat transfer coefficient as:

$$h_b = \rho c l \frac{dT_b/dt}{T_a - T_b} \quad (120)$$

have been examined by Trimpi and Jones (51) and Naysmith (52). The former calculate the ratio h/h_b for specific cases and include the presence of a backing material whereas Naysmith produces an approximate expression which can be used to evaluate h/h_b in the absence of any backing material. The expression is:

$$\frac{h}{h_b} = 1 + \frac{1}{3} \left(\frac{h l}{k} \right) \quad \text{for } t > \frac{l^2}{\alpha}, \quad (121)$$

which gives numerical results in agreement with ref. (51) for the cases calculated. The expression holds good for times greater than the skin response time and is a constant error in the deduced heat transfer coefficient. The error is small for typical systems, amounting to 1.5% when a stainless steel skin of thickness 0.75 mm is subjected to a heat transfer coefficient of $0.1 \text{ W cm}^{-2} \text{ K}^{-1}$. As pointed out by George and Reinecke (53) the criterion that $h l/k \ll 1$ implies that the temperature within the skin is constant and naturally in this case the inferred heat transfer coefficient will be the same as the existing heat transfer rate, a result in agreement with the Eq (121).

Chevallier and Leuchter (54) have considered the case of a thin wall without a substrate for the case of constant h and described the subsequent heating in terms of a characteristic wall time $\tau_1 = \rho c l/h$ and a rise time $\tau_2 = l^2/\alpha$. The first term τ_1 , corresponds to the time taken to reach 1/e of the adiabatic wall temperature and Chevallier and Leuchter assume that $t \ll \tau_1$, whereas τ_2 corresponds to twice the rise time τ previously used here. The ratio of the times τ_2/τ_1 is in fact $h l/k$, which Chevallier and Leuchter refer to as a wall Nusselt number, the dimensionless parameter referred to in the previous paragraph. The authors produce graphs of $dT_{\text{rear}}/dT_{\text{mean}}$ as a function of t/τ which gives the error in the inferred heat transfer rate. For large times, $t \gg l^2/\alpha$, this quantity tends to a constant which is approximately half the error in the heat transfer coefficient given in Eq (121).

It was pointed out in previous sections that heat is lost to any backing substrate employed, and as shown in Fig.48, this can have a marked effect on the inferred heat transfer rate. *(See footnote to this page). Monitoring the calorimeter temperature on the rear surface causes large errors and if the (rear surface) response time is plotted on the curves of those for the instantaneous heat transfer rate from the calorimeter to the substrate for various metals on Pyrex, Fig.54, it can be seen that within this time there is already a significant heat loss to the substrate.

The errors produced by heat lost to backing materials can be deduced in general from Fig.48 which gives

$$\left(\frac{dT}{dt} \right)_{\text{with}} - \left(\frac{dT}{dt} \right)_{\text{without}} \bigg/ \left(\frac{dT}{dt} \right)_{\text{without substrate}}$$

*The heat lost from the rear of the Rose calorimeter, on the other hand, does not affect the results to anything like the same extent. This arises because the time constant itself is short and measurements can be made in the early phases of the flow before any substantial heat loss to the substrate has occurred.

for various values of $(\sqrt{\rho_2 c_2 k_2})/(\sqrt{\rho_1 c_1 k_1}) = a$ and in particular can be seen for a Pyrex backing in Fig. 54. Cooper and Mayo (55) made a rough estimate of the effect for the case of constant heat transfer coefficient h by assuming that the calorimeter temperature was the ideal value and using this as a boundary condition for a balsa wood backing and comment that 'the simplicity of data reduction makes elimination of the insulating fill material (i.e. the substrate) far more preferable than attempting to account for its Presence'. As already mentioned in this section Trimpi and Jones (51) present exact calculations for the effect of losses to balsa and mahogany substrates.

The above conduction effects are termed 'normal' for they are one-dimensional in a direction normal to the skin surface. Conduction may also take place along the skin if there are temperature gradients and this also will produce errors in the inferred heat transfer rate. George and Reinecke (53), have examined this transverse conduction by assuming that the temperature is uniform normal to the skin although varying with position and write the equation for the temperature variation as:

$$\rho c l \frac{\partial T}{\partial t} = \underbrace{\dot{q}_s}_{\text{surf. heat transf.}} + \underbrace{\text{div } l k \text{ grad } T}_{\text{conduction heat transf.}} \quad (122)$$

If the transverse conduction were zero, \dot{q} constant in time and the skin thickness constant, the solution would be:

$$T = \frac{\dot{q}}{\rho c l} t$$

Therefore

$$\frac{\text{conduction heat transf}}{\text{surface heat transf}} = \frac{\alpha t \nabla^2 \dot{q}_s}{\dot{q}_s} \quad (123)$$

and it is required that this be very small depending on the accuracy required in the measured \dot{q}_s . The error increases linearly with time and is independent of the wall thickness and hence it is desirable to measure \dot{q}_s as early as possible in the experimental running time. If the heat transfer rate to a sphere of radius R close to the stagnation point is taken to be:

$$\dot{q}_s = \dot{q}_0 (1 - 0.6 x^2/R^2) \quad (124)$$

where \dot{q}_0 is the stagnation point value and x is the distance from this point to the position considered, then the value of $\nabla^2 \dot{q}_s / \dot{q}_s$ at the stagnation point is:

$$\frac{\nabla^2 \dot{q}_s}{\dot{q}_s} = \frac{2.4}{R} \quad (125)$$

The expression (124) was obtained using a simple fit to the data of Kemp, Rose and Detra (56). Substituting Eq (124) into Eq (123) we obtain the heat lost by conduction as:

$$\frac{\text{conduction loss}}{\text{surface heat transfer rate}} \approx \frac{2.4 \alpha t}{R} \quad (126)$$

Thus the time required for a 5% error in the stagnation point heat transfer rate to a nickel sphere of 1 cm radius may be evaluated as approximately 130 ms.

Further conduction effects may be experienced due to the presence of thermocouple wires attached to the skin. The effect of these wires was first considered by Burnett (57) who represented the wire by a cylindrical heat sink whose value was determined by the heat lost down the wire on the assumption that the temperature at the skin-wire junction was given by the rear face of the skin in the absence of the wire. The

Table 8
Conditions relevant to the measurement of rear surface temperature

Condition	Implication
$t \ll \frac{\rho c l}{h}$	Time is short compared with the time for the wall to reach the adiabatic wall temperature. The heat transfer rate will be sensibly constant.
$\frac{h l}{k} \ll 1$	The temperature difference across the wall required to conduct the heat transfer rate characterised by h is small compared to the driving temperature. The wall is therefore at an approximately uniform temperature, the magnitude of the correction due to the small non-uniformity on the inferred heat transfer coefficient being $h l / (3k)$
$t > \frac{0.8 l^2}{\alpha} (\approx \tau)$	The rise time of the rear surface such that the rate of change of temperature is within 1% of the mean value.
$1 > \frac{\alpha t \nabla^2 \dot{q}_s}{\dot{q}_s}$	The condition that transverse heat conduction is small compared with the incident heat transfer rate.
$\sqrt{\frac{\rho_2 c_2 k_2}{\rho_1 c_1 k_1}} < 0.05$	The rear surface temperature time derivative can come within 5% of the ideal value without a substrate at $t \sim \tau$ although at longer time intervals the error will be greater as shown in Fig.54.

percentage error in the rear surface temperature at the skin-wire junction was evaluated as a function of $\alpha, t / l^2$ for several ratios of skin thickness to wire diameter; the result is shown in Fig.58(a). O.N.E.R.A. (58) have extended these calculations and have also presented the results in the form of the error in the inferred heat transfer rate, shown in Fig.58(b,c). From these results one may see that the effect of a wire mounted on the rear face of the skin produces a great deterioration in the response time of the system, such that a wire diameter to skin thickness ratio of 0.08 produces a 1% response time of $\alpha, t / l^2 = 5$ compared to 0.5 without the wire. Further it is shown in ref (58) that a thermocouple with its junction situated at the mid thickness of the skin would considerably alleviate this situation and the constructional technique to obtain this location is discussed. Conditions relating to the operation of thin wall calorimeter models which have been discussed in this section are summarised in Table 8.

3.d(iv) Construction techniques for thin skin models

The construction of thin skin models may take many forms. Thin sheet may be bent to the desired shape and mounted on an insulating former, (59, 60, 61). Electroformed models have also been used and this technique is especially useful in the construction of models having complex curvature, (62). Harvey (63) gives a detailed description of the construction of a lifting reentry configuration for testing in the NASA Langley Hotshot tunnel. In this case a series of stainless steel panels of 0.4 mm thickness were pressure formed in moulds and then secured to a core which was provided with apertures at the selected measuring points, Fig.56(b). Starner et al (64) used a copper strip bonded

onto a 'Lucite' model with epoxy cement and measured the rear face temperature of the copper strip as shown in Fig.56(d). This latter technique will be subject to substrate losses, which may be calculated using the theory given in section 3.b(iii), a fact recognised by Starner. Thin skin models have also been made from porous materials (61, 65), although the energy balance is somewhat different from the analysis developed in the present volume. The thermocouples are usually attached to the model skin by spot welding, soldering, electron-beam welding or by purely mechanical means. The thermocouple wire may be set into small holes drilled into the skin prior to soldering. Chevallier et al (58) have described in detail techniques whereby the thermocouple wires are installed in the models used at O.N.E.R.A. Self-explanatory diagrams illustrating these techniques are shown in Fig.59. In Fig.59(a) a standard soldering technique is shown whereas the use of an auxiliary plug is illustrated in Fig.59(b); the means whereby wires are pulled into very thin walls is shown in Fig.59(c). The advantage claimed by Chevallier et al for the use of this auxiliary plug is that it permits an accurate determination of the wall thickness at the point at which the temperature is measured. Naysmith (52) describes the method used for spot welding fine thermocouple wires onto stainless steel skins. A simplified circuit suitable for this process is illustrated in Fig.60 although trial and error is required to determine the voltage, current and junction pressure to produce a sound connection. The thermocouple wires should be welded close together in order to define the measuring position. It should be noted that in the case of wires which penetrate the skin, the emf generated corresponds to the lowest temperature of the thermojunction. The connection of the thermocouple circuit may be effected in several different ways which are illustrated in Fig.61. In Fig.61(a) the conventional arrangement using a reference temperature bath at the cold junction is illustrated. A simpler system is shown in Fig.61(b) where the cold junction is at the amplifier terminals and provided that this is at the same constant temperature, the same thermocouple emf will be measured. This circuit may in turn be modified using larger diameter extension leads of the same material which do not affect the circuit and the junctions need not then necessarily be at the same constant temperature, Fig.61(c). Further, copper leads may be attached to the thermocouple wires as shown in Fig.61(d) but in this case this junction becomes the cold junction and must be maintained at a constant temperature. The thermocouple wires need not necessarily be connected at the same point on the skin as shown in Fig.61(e) and Fig.59 and furthermore, a common return line may be used, Fig.61(f). Examples of these arrangements are also shown in Fig.56. In the system employed at O.N.E.R.A., Fig.56(a), the thermocouple-copper junction is located in an oil bath within the tunnel working section. The common return mode of connection is shown in this figure and also in the model used by Varwig, Fig.56(d), where the wall itself constitutes one of the thermocouple materials.

The results from various arrangements were compared by Marvin and Akin (62) on a hemisphere-cylinder model. The following techniques were employed on an electro-deposited copper wall of thickness 0.25 mm: single constantan wires silver soldered into holes drilled in the wall with a common return copper wire silver soldered to the rear of the model; pairs of copper-constantan wires silver soldered in the same manner but without the common return lead; copper-constantan thermocouples spot welded to the rear surface. All systems were reported to give experimental results in close agreement.

Temperature calibration of the thermocouples is possible if the entire model may be submerged in a constant temperature bath. The radiation sources described by Mauiard (32) and discussed in section 2.e(ii) may also be used to calibrate the model directly in terms of the heat transfer rate. Harvey (63) has constructed a hot gas source for the same purpose. Use of the bulk values of ρ , c and k with a temperature calibration of the thermocouple and precise determination of model wall thickness should, however, be sufficient for most purposes.

An example of thin skin model construction technique is shown in Fig. 62. The thin copper skin is supported at nose and base on a Nylon framework and longitudinal slots are left beneath the instrumented section of the surface (66).

3.e. Capsule and 'Slug' Calorimeter Gauges

The capsule gauges are very similar to the thin skin calorimeters discussed in section 3.d differing only in that the skin is limited to a small area and is mounted on an insert which fits into the model. Typical examples of these may be seen in Fig. 63. The temperature of the element is usually sensed by a thermocouple (67) although platinum films (68) and semiconductor resistance thermometers (22) are used.

The response times and sensitivities may be determined in a manner similar to the thin skin calorimeter on the assumption that the element support does not introduce heat losses and thus sensitivities may be obtained from Figs. 49-51. In the original gauge of Ledford, (Fig. 63a), the element was copper and its thickness ranged from 0.051 mm to 0.51 mm; the thermocouple was chromel-constantan. From Fig. 51 this gives a response time of 15 μ s and 1.5 ms and sensitivities of 3 and 0.3 $\text{mV s}^{-1}/\text{watts cm}^{-2}$ respectively. In a later version (68), Fig. 63(b), an aluminium element, 0.25 mm thick, was used and this was anodised on the rear surface providing an insulating surface and thus enabling a thin platinum film of resistance 150Ω to be deposited by sputtering. A bridge circuit was used in order to find the resistance change and hence the temperature rise of the element. For a film voltage of approximately 1 volt the sensitivity of such a film would be $\sim 2 \text{ mV}/^\circ\text{C}$ compared with that for a thermocouple (chromel-alumel) $\sim 0.04 \text{ mV}/^\circ\text{C}$ giving an overall sensitivity of $34 \text{ mV s}^{-1}/\text{watt cm}^{-2}$ whereas the thermocouple would give $0.7 \text{ mV s}^{-1}/\text{watt cm}^{-2}$.

Maulard (35) has described a similar gauge used at O.N.E.R.A. utilising a silicon resistance sensing element, Fig. 63(c), and this device has a high sensitivity by virtue of its much greater resistance. A bridge circuit is used to monitor the resistance change, one arm of the bridge being an identical silicon resistance installed within the gauge and compensating for ambient temperature changes. The resistance thermometer has a temperature coefficient of resistance of $7 \times 10^{-3} \text{ K}^{-1}$ and the sensitivity of the gauge is given by

$$\dot{q} = \left(\frac{\rho c l}{\alpha_R R} \right) \frac{dR}{dt}$$

where R is the sensing element resistance and α_R the temperature coefficient of resistance. In the gauge described by Maulard the silicon resistance thermometer was mounted on an anodised aluminium calorimetric element of thickness 0.3 mm, as was the platinum film of Ledford et al (68), and a typical value of $\rho c l / \alpha_R R$ quoted for these gauges was $10^{-2} \text{ W cm}^{-2}/\Omega \text{ s}^{-1}$. This would imply that the resistance of the silicon element was approximately 1 k Ω . Such silicon resistance sensors are marketed by Kulite of New Jersey, U.S. A. and have a maximum allowed power due to the monitoring current, which would limit the sensitivity of the gauge. A maximum safe current expected for the O.N.E.R.A. gauge described above would be approximately 3 mA and this would give a thermometer sensitivity of $20 \text{ mV}/^\circ\text{C}$ and an overall sensitivity of approximately $0.3 \text{ Vs}^{-1}/\text{watt cm}^{-2}$. A comparison of the three gauges is given in Table 9 where details of a gauge used by Kipke at Braunschweig, (69), are also given.

The construction of the gauges may be seen in Fig. 63 and in all gauges the calorimetric element is mounted in a nylon support. In the A.E.D.C. gauges, Fig. 63(a), (b), the element is bonded around its periphery with adhesive whereas in the O.N.E.R.A. gauge this is held captive at only 3 points within a recess. These different modes of construction influence the heat losses from the element which have been shown to amount to a 50% error in deduced heat transfer rate for the A.E.D.C. gauges under certain

heating conditions (67).

If it is assumed that any heat conduction loss is proportional to the temperature of the calorimetric element, above that of its mounting, the energy equation may be written as:

$$\dot{q}_s = \rho c l \frac{dT}{dt} + K T \quad (127)$$

where K is a "loss" constant. Solving this equation for constant \dot{q}_s and taking $T = T_0$ at $t = 0$ we obtain:

$$T - T_0 e^{-\frac{Kt}{\rho c l}} = \frac{\dot{q}_s}{K} \left(1 - e^{-\frac{Kt}{\rho c l}} \right) \quad (128)$$

substituting Eq(127) into Eq(128) we obtain:

$$\rho c l \frac{dT}{dt} = e^{-\frac{Kt}{\rho c l}} \left(\dot{q}_s - K T_0 \right) \quad (129)$$

As the inferred heat transfer rate is $\rho c l dT/dt$ we obtain from Eq(129)

$$\frac{\dot{q}_{meas}}{\dot{q}_s} = \frac{\frac{dT}{dt}}{\frac{dT}{dt} e^{-\frac{Kt}{\rho c l}} + \frac{K T_0}{\rho c l}} \quad (130)$$

If T_0 is zero Eq(130) reduces to:

$$\frac{\dot{q}_{meas}}{\dot{q}_s} = e^{-\frac{Kt}{\rho c l}} \quad (131)$$

Table 9

gauge	overall diam. mm	overall height mm	calorimetric element material	temperature sensing	temperature sensitivity	overall sensitivity
			diameter mm thickness mm	lead thick- ness mm	mV °C ⁻¹	mV s ⁻¹ / W cm ⁻²
Ledford A.E.D.C. (67,68)	6.35	7.62	copper	chromel constantan	0.04	3 → 0.3
			4.75 0.051 → 0.51	0.051		
Ledford A.E.D.C. (67,68)	6.35	7.62	aluminium (anodised)	platinum resistance	2 34 (1 volt across film)	
			4.75 0.25	0.02 → 0.05 copper		
Maulard O.N.E.R.A. (35)	3.5	9.5	aluminium (anodised)	silicon resistance	20 300 (3 mA sensing current)	
			2.5 0.3	0.05 gold		
Kipke (69) Institut für Strömungsmechanik Braunschweig	3.5	7.0	copper	copper constantan	0.04	0.6
			2.5 0.2	—		

Hence from Eq(130) it may be seen that if the flow starting process produces a high heat transfer rate prior to the establishment of steady flow and there is subsequently a steady heat transfer rate, the net effect will be to produce a high value of T_0 and consequently large errors will occur in the measured heat transfer rate. This was the case in (67) where a value of K was assumed in order to correct the heat transfer data. The value of $K/\rho c$ for the gauges in (67), (Figs. 63(a) and (b)), may be deduced from the data given there as ranging from 1.4×10^{-2} to 0.7×10^{-2} cm sec⁻¹ for gauge thickness from 1.0 mm to 0.05 mm. In the gauge of Maulard (35) the value of $K/\rho c$ may be estimated from oscilloscope traces given as being 1.2×10^{-2} cm s⁻¹ for a gauge of thickness 0.3 mm which is approximately the same as above. In the latter, however, the gauge diameter was 2.5 mm compared to 4.75 mm in (35), indicating that the insulation of the calorimetric element was superior in the O.N.E.R.A. transducer.

Starner (70) has considered the case where the calorimetric element is not insulated but its periphery is held at a constant temperature. For this case Starner has estimated that the time at which the cold boundary affects the temperature in the centre of the element is:

$$t = 0.05 \frac{R^2}{\alpha_1} \quad (132)$$

For an aluminium element of diameter 5 mm this time is approximately 13 ms. This characteristic time may be compared with the response time of the Gardon gauge which is of order 100 times greater and corresponds to the total time for the element to attain a steady state. The gauges of Starner (70) were used in an arc tunnel and were traversed rapidly through the flow to prevent the probe melting under the conditions of high heat transfer rate. Kirchoff, (71), has considered the problem of the melting of calorimeters and has given a criterion for the optimum thickness such that the maximum test time is obtained:

$$l_{optimum} = \frac{k T_{m.p.}}{1.366 \dot{q}_s} \quad (133)$$

where $T_{m.p.}$ is the melting temperature of the calorimeter material. This situation arises because the time taken to reach the melting temperature increases linearly with increasing thickness, while the response time increases as \sqrt{l} , the test duration being the difference between these two times. Starner (70), however, points out that this criterion would be seriously affected due to the deterioration in response time when a thermocouple is fixed to the rear face as considered in section 3.d(iii).

A form of calorimeter used for measuring high heat transfer rates is the 'slug' calorimeter described by Hiester and Clark (72), Vojvodich (73) and Pope (74). Examples of the slug calorimeter are shown in Fig. 64 where it may be seen that the calorimetric elements consist of a thick piece of copper mounted within a stainless steel body, thermally and electrically insulated from the supports by a small air gap. The element is supported on sapphire spheres or thin stainless steel pins and a chromel alumel thermocouple is spot welded onto or 'peened' into the rear face of the sensing element. The heat transfer rate to these gauges may be found from the simple relation,

$$\dot{q}_s = \frac{m c}{A} \frac{dT}{dt} \quad (134)$$

where m is the mass of the calorimeter and A the area exposed to the heat flux. This equation is equivalent to Eq (96) and assumes that there is no heat loss and that the time available for measurement is greater than the response time based on sensor thickness. The "response time" at the rear face of the gauge shown in Fig. 64(d) is approximately 0.3s and its sensitivity approximately $0.02 \text{ mV s}^{-1} \text{ per W cm}^{-2}$.

3.f Thick Wall Calorimeters

This class of calorimeter is used for the measurement of very high heat transfer rates in, for example, rocket thrust chambers (75,76) where rates of the order of $5 \times 10^3 \text{ W cm}^{-2}$ were encountered with test times of order 1 second. Free flight tests (77) have also been carried out with these transducers. In general the sensing element is relatively thick and the response time, $\tau = 0.5L^2/\alpha$, is long, hence within the test time no useful approximation can be made relating the variation of local temperature at some point within the wall to the heat transfer rate at the front surface. Furthermore, large temperature rises often occur in the calorimeter and the variation of the thermal properties and radiative heat losses must be taken into account.

In general the front surface temperature cannot be measured due to the severe external conditions and consequently temperatures must be measured within the calorimeter. Examples of typical calorimeter construction are shown in Fig. 65. The principal difficulty in the analysis of results from such devices is, therefore, the solution of the time-dependent heat conduction equation, Eq (1), for a finite slab, in order to obtain the surface heat flux, the temperature history at certain points within the slab being known. This analysis is usually termed the "inverse" problem of heat conduction.

This "inverse" problem has been approached in numerous ways (75, 78, 79, 80, 81, 82) and these are briefly outlined below. The general one-dimensional solution in transformed coordinates for the temperature distribution in a slab with constant properties in the absence of a substrate and without losses is given by Eq (12) with $(\sqrt{\rho c_2 k_2})/(\sqrt{\rho c_1 k_1})$ set equal to zero. Thus

$$\bar{T}_i = \frac{\bar{q}_s \sqrt{\alpha_1} \cosh(x-l) \sqrt{\frac{\rho_1}{\alpha_1}}}{k_1 \sqrt{\rho_1} \sinh l \sqrt{\frac{\rho_1}{\alpha_1}}} \quad (135)$$

At $x=0$, $\bar{T}_i = \bar{T}_s$ and

$$\bar{T}_s = \frac{\bar{q}_s \sqrt{\alpha_1} \cosh(\sqrt{\frac{\rho_1}{\alpha_1}} - l)}{k_1 \sqrt{\rho_1} \sinh l \sqrt{\frac{\rho_1}{\alpha_1}}} \quad (136)$$

Dividing Eq (136) by Eq (135) yields the surface temperature as a function of the temperature \bar{T}_i at some point, x , within the slab,

$$\frac{\bar{T}_s}{\bar{T}_i} = \frac{\cosh(-l \sqrt{\frac{\rho_1}{\alpha_1}})}{\cosh(\sqrt{\frac{\rho_1}{\alpha_1}}(x-l))} \quad (137)$$

If it were possible to invert Eq (137) then the surface temperature and the temperature at other locations within the slab could be evaluated from a single measured temperature. Further, it would be possible to obtain the surface heat flux by the application of Eq (3) $\bar{q}_s = -k_1 \partial \bar{T}_s / \partial x$. Unfortunately, as stated by Sparrow et al (79), "careful study shows that there is no inverse transform of this equation as written".

A more direct approach is that of Stoltz, (78), who approximates the surface heating by a sum of step functions which start at different times. Thus the first step function at time zero is calculated so as to give the correct temperature at the measuring location after the first time interval. The temperature at this location due to the initial step function is then calculated after the second time interval and this temperature is compared with the observed value. The error found is then corrected by a further step function of surface heat flux which originates after the first time interval. This process is then repeated for all time intervals. Howard (82) describes a similar procedure but in this case a program for computing the temperature within the slab for a given surface heating rate, allowing for surface radiation loss, is used to determine the temperature at a certain location for two input heat transfer rates. These temperatures are then compared with the observed temperature and a corrected surface heat transfer rate found by linear extrapolation of the results. The procedure is repeated

for subsequent time intervals and the resulting constant levels of heat transfer rate are taken to be the actual values in the centres of the time intervals. Howard compares his results with those calculated using an integral method, (83) where the heat transfer rate as defined by the energy equation (Eq(94) section 3.a) is re-written as:

$$\dot{q}_s = \frac{\partial}{\partial t} \int_0^L \rho c T dx \quad (138)$$

Thus

$$\dot{q}_s = \rho \int_0^L c \frac{\partial T}{\partial t} dx \quad (139)$$

where ρ is assumed constant and $\partial T / \partial t$ evaluated by a curve fitting the experimental points at specified positions within the calorimeter element. Stroud (81) also describes an integral method which may be used if at least two experimentally observed temperatures within the calorimeter element are known. The two outer measuring stations should in this case be close to the boundaries of the calorimeter. From the known temperatures the temperature between the measuring stations was found using a finite difference form of Eq (1), and not by simple curve fitting. The temperature between the boundaries and the extreme measuring stations was found by extrapolation. The heat transfer rate was then evaluated from the energy equation, Eq (138), and radiation losses and variable calorimeter properties were also included. A similar technique was employed by Powell and Price (80) to determine the temperature within the calorimeter. In this case, however, the surface heat flux was found from the temperature gradient at the surface of the calorimeter, Eq(3).

The approximation to the semi-infinite solid case has been used by Quentermeyer et al (75) and Howey (84). In (75) the surface heat transfer coefficient, h , and the adiabatic wall temperature, T_{aw} , are assumed to be constant which enables the temperature rise, T_1 , within the calorimeter to be written as,

$$\frac{T_1}{T_{aw} - T_i} = \operatorname{erfc} \left[\frac{\frac{hx}{k_i}}{\frac{2\sqrt{h^2 t}}{\sqrt{\rho_i c_i k_i}}} \right] - e^{\left[\frac{hx}{k_i} + \frac{h^2 t}{\rho_i c_i k_i} \right]} \operatorname{erfc} \left[\frac{\frac{hx}{k_i}}{\frac{2\sqrt{h^2 t}}{\sqrt{\rho_i c_i k_i}}} + \sqrt{\frac{h^2 t}{\rho_i c_i k_i}} \right] \quad (140)$$

The calorimeter properties were determined at a reference temperature

$$T_{ref} = \frac{T_s - T_i}{4} + T_i$$

where T_s and T_i are the surface and initial temperatures respectively. The adiabatic wall temperature was known and at a given time T_1 was evaluated from Eq (140) with an estimated value of h . The result was compared with that observed and the value of h corrected and the process repeated until a value of h consistent with the experimental temperature was found. Howey (84) employed a cylindrical cavity in the calorimeter, within which his thermocouple was mounted, so that the cavity end-wall temperature was approximately equal to the surface temperature of an undisturbed semi-infinite body. This was termed a 'null point calorimeter' and required that the ratio of the cavity radius to its depth from the surface was equal to 1.1. The temperature histories for several calorimeter geometries were computed and an optimum design chosen.

The construction of various thick wall calorimeters may be seen in Fig. 65. Thermocouples are used in all these gauges for the measurement of temperature. In Fig. 65(a) the gauge of Powell and Price (80) is shown. This consists of a calorimetric plug of the same material as the rocket nozzle under test and two insulated thermocouple wires

are swaged into the element. The plug is fitted tightly into the nozzle and finished flush with the wall under examination. The monitoring surface is then electroplated to form the thermocouple junction. In certain instances copper nozzles were instrumented with copper plugs which had a single constantan wire plated with copper (i.e. a common return system as shown in Fig. 61). A thermocouple was also used to measure the rear face temperature as shown in Fig. 65(a). The distance of the thermocouple measuring junction from the surface (i.e. the thickness of plating) is important in that it determines the extrapolation necessary to find the front surface temperature gradient and hence heat transfer rate. An estimate of the error may be found by taking the semi-infinite solution of Eq (26) for the heat flux rate at a position x ,

$$\dot{q}_x = \dot{q}_s \operatorname{erfc} \frac{x}{\sqrt{4\alpha t}}$$

For x small, such that $x^2/(4\alpha t) \ll 1$ the approximation

$$\frac{\dot{q}_x}{\dot{q}_s} = 1 - \frac{x}{\sqrt{\pi\alpha t}}$$

may be made. The error in inferring the surface heat transfer rate when making a measurement 10^{-2} cm from the surface of a copper block is thus 0.5% after 1 s. This estimate may be compared with 1% quoted by Powell and Price (80) for the same geometry in an actual rocket nozzle test. Chin (85) has evaluated the errors in inferred surface heat transfer rate due to thermocouple position error for a slab. The calorimeter used by Stroud (81) to test his numerical procedure is shown in Fig. 65(b). This comprises a nickel cylinder into which grooves were machined allowing the 0.0025 cm diameter thermocouple wires to pass through the cylinder. The thermocouple beads were 'peened' in position and the cylinder fitted into a nickel sleeve. The thermocouple wires were insulated with quartz sleeving and were increased in diameter twice before external connections were made. The rod calorimeter of Quentermeyer et al (75) (Fig. 65(c)), was screwed into the nozzle wall, the thread being oxidised to reduce heat flowing between the rod and the wall. Both wall and calorimeter were of copper, and chromel-alumel thermocouples were installed along the rod, being 'peened' into position. The insulating cavity around the rod was pressurised in order to prevent hot nozzle gas leaking into this cavity.

3.9 Total Calorimeters

Two methods have been used for the measurement of the total heat transferred to a body and although not widely used are of interest. The first method (86) has been used in a ballistic range, the model being retrieved after deceleration down the range and its rise in energy determined. The second method (87) uses a model filled with mercury and monitors the increase in volume of the mercury due to its rise in temperature.

A diagram illustrating the first method is shown in Fig. 66(a). The velocity of the model is determined throughout its flight enabling the instantaneous heating rate to be estimated. At the end of the ballistic range the model is brought to rest by a series of paper barriers, the arrested model falling under gravity into a paper funnel and finally coming to rest in a calorimeter. The temperature in the calorimeter which is in thermal contact with a heat sink is monitored with thermocouples. From the subsequent rise and fall of the calorimeter temperature the total heat addition to the model may be found. Total heat quantities in the range 0.03 - 0.3 J were measured with the system and the results were in fair agreement with predictions.

The model used for the second method is shown in Fig. 66(b). A thin walled nickel or stainless steel model was filled with mercury and supported at its base where any aerodynamic heating could be ignored. A spring loaded piston, located within the sting support system was coupled to a displacement transducer. The displacement of the piston was related to the change in volume of the mercury which was, in turn, given by its

temperature change, effects due to pressure variation being considered negligible. The total heating rate was found from the time rate of change of the volume variation of the mercury:

$$\dot{Q} = \frac{mc}{\left(\frac{\partial V}{\partial T_m}\right)} \frac{dV}{dt}$$

where m is the mass of the mercury and c its specific heat; $\partial V / \partial T_m$ is the rate of change of volume with mean temperature as determined by static calibration. A typical rate of rise of temperature measured for the hemisphere-cylinder was 30°C s^{-1} giving a piston velocity of 0.25 cm s^{-1} corresponding to a heating rate of approximately 30 watts. In practice the model was hydraulically injected into a steady flow and maintained there for some seconds, although the technique could be used in short duration flows.

4. PYROELECTRIC HEAT TRANSFER GAUGES

Pyroelectric transducers depend for their effect on the change of polarisation caused by a rise in the temperature of the dielectric. This may be a serious disadvantage in pressure transducers which rely on the piezoelectric effect for charge production. The pyroelectric effect is not completely understood although Chenoweth (88)

Cooper (89) and Lang and Steckel (90) have investigated the interaction of strain and temperature effects. There is apparently a primary pyroelectric effect, i.e. the polarisation of the dielectric caused by heating is not itself due to a straining within the material.

Pyroelectric heat transfer gauges have not yet achieved wide application in aerodynamic facilities but they have proved to be useful at low heat transfer rates and are widely used in chemical microcalorimeters. The pyroelectric charge production is independent of the temperature distribution and a function of the total energy absorbed by the crystal provided that the maximum temperature does not rise above the Curie point which is about 320°C in barium titanate and 575°C in quartz. The charge δQ generated by an effective temperature δT can be expressed $\delta Q = A\gamma\delta T$ where A is the electrode area and γ the pyroelectric coefficient dP_s/dT , P_s = polarisation coulomb / cm^2 and from Fig. 67 it will be seen that this coefficient is approximately $37.5 \times 10^{-9} \text{ Cb/cm}^2 \text{ }^\circ\text{C}$ in barium titanate. The heat q absorbed by the element is $\rho c l \delta T$ and $\dot{q}(t)$, the heat transfer rate, is $\rho c l dT/dt$ as in all calorimetric devices. Since dQ/dt is the current from the transducer

$$i(t) = \frac{dQ}{dt} = \frac{A\gamma}{\rho c l} \dot{q}(t) \quad (141)$$

The equivalent circuit of a pyroelectric gauge is shown in Fig. 68(a). The electrodes may be either face or edge mounted, Fig. 68(b) and (c). The current generator $i(t)$ with infinite source impedance is in parallel with R_s and C_s , the internal leakage resistance and capacitance of the element. The external load circuit is represented by R_L and C_L resulting in a total load on the element of R_T and C_T . The Laplace transform of the output voltage is given by

$$\bar{V} = \bar{q} \frac{A\gamma}{\rho c l} \frac{\frac{1}{C_T}}{p + \frac{1}{R_T C_T}} \quad (142)$$

and hence by convolution

$$v(t) = \frac{A\gamma}{\rho c l} \frac{1}{C_T} \int_0^t \dot{q}(\tau) e^{-(t-\tau)} d\tau \quad (143)$$

Two regimes of operation may be identified depending on whether $R_T C_T \gg t$ and

taking the case in which $\dot{q}(t)$ is a constant \dot{q}_0 , for $R_T C_T > t$

$$\frac{dV}{dt} = \frac{A\gamma}{\rho c l} \frac{1}{C_T} \dot{q}_0 \quad (144)$$

and when $R_T C_T < t$

$$V(t) = \dot{q}_0 R_T \frac{A\gamma}{\rho c l} \quad (145)$$

The sensitivity is seen to decrease with the time constant $R_T C_T$, i.e. R_T since C_T is largely governed by the element, cable and detector circuit.

An example of the first case is shown in Fig. 69(a) in which $R_T = 20 \times 10^6 \Omega$, $C_T = .00275 \mu F$, i.e. $R_T C_T = 0.055$ secs. The transducer has a calorimeter response in which the rate of rise of voltage is proportional to the heat transfer rate. This approximation is valid to within 1% for \dot{q} constant and $R_T C_T = 50 t$. Reducing the load resistance to 82Ω results in the second type of response in which the instantaneous voltage $V(t)$ is directly proportional to the heat transfer rate, Fig. 69(d) but the signal level is seen to be much lower since the output voltage is directly proportional to R_T and $R_T C_T$. The time constant $R_T C_T$ must be very much less than the resolution required, and with C_T fixed by the transducer element this can only be achieved by reduction of R_T .

The gauge sensitivity in the first case, dV/dt proportional to $\dot{q}(t)$ may be written

$$\frac{dV}{dt} / \dot{q}_0 = \frac{A\gamma}{\rho c l} \frac{1}{C_T}$$

and since the transducer is usually made from lead zirconate or barium titanate, C_T will comprise mainly the element capacitance $C_T = K\epsilon_0 A/l$; hence

$$\frac{dV}{dt} / \dot{q}_0 = \frac{\gamma}{\rho c K \epsilon_0} \quad (146)$$

It will be seen from Eq (146) that the sensitivity is a function of the physical properties of the dielectric only, not of its area or thickness. For barium titanate at $300^\circ C$ the properties have been tabulated by Cooper (89), γ in this case differing slightly from the value shown in Fig. 67:

pyroelectric coefficient	γ	-52×10^{-9} Coulomb $cm^{-2} K^{-1}$
relative permittivity	K	200
density	ρ	$6 \text{ gm } cm^{-3}$
resistivity	ρ_R	10^{10} ohm cm
specific heat	C	$0.502 \text{ J } gm^{-1} K^{-1}$

The sensitivity of the transducer element as a calorimeter is thus $9.77 \text{ V } J^{-1}$ although this would be reduced by cable capacitance. Wood and Andrews (91) have compared thin film and pyroelectric gauges and conclude that a PZT-5A gauge operated as a calorimeter would have a sensitivity about 50 times that of the thin film, but the same gauge in the short time constant mode would have about the same sensitivity as a thin film gauge.

This type of heat transfer gauge is still in an early stage of development and too many effects, such as polarising voltage and mechanical strain, remain to be completely investigated. Chenoweth (88) has investigated the effect of polarising voltage on the sensitivity of such transducers and reports a somewhat complex situation. Spitzer (92) adopted the expedient in his instrument, Fig. 70, of polarising at 150 volts for 5 minutes prior to each experiment to stabilise the sensitivity although he also noted that this was a function of the time of application of the polarizing voltage.

5. MEASUREMENT OF RADIATIVE HEAT TRANSFER

5(a) Instruments Based on Thin Film Gauges

Radiative energy transfer from gases within the shock layer may contribute substantial fractions of the total heat transfer. At stagnation temperatures of 7000°K the total radiation from air lies in the region above $0.2\ \mu\text{m}$ where quartz, lithium fluoride and sapphire windows may be used to isolate the gauge from convection effects. At higher temperatures radiation is also appreciable in the vacuum ultraviolet and no windows of any sort may be used. Many heat transfer gauges may be made to measure radiant as well as convective heat transfer rates by coating the surface with a layer of carbon black or other material whose absorption coefficient can either be measured as a function of wavelength and incidence or is close enough to unity not to require calibration. Such layers have been used on thin and thick film gauges for calibration under pure radiation conditions, see section 2.e(ii), but an increase in time constant due to the thickness of the absorption layer of up to about 2 ms results. If this increase in time constant is unacceptable a form of radiation detector such as that described by Gruszczynski and Rogers (93) may be used. This detector comprises a conventional thin film heat transfer gauge mounted on the inside of a cylindrical cavity, Fig. 71(a), with an entrance slit set off-axis. In this arrangement of slit and detector, which has a highly reflecting internal surface, little energy is re-radiated from the detector slit thereby fulfilling the requirement that its absorptivity be close to unity. The cavity comprises four cylindrical quartz elements whose internal surfaces are coated with thin films, opaque to the incident radiation, connected in series.

At high gas temperatures photoemission from the metallic surface of the gauge may occur unless the unit is filled with a gas with a high electron collision cross section, such as nitrogen. A stagnation point radiation gauge fitted with a sapphire window suitable for wavelengths down to about $0.15\ \mu\text{m}$ is illustrated in Fig. 71(c). The sapphire window is transparent into the near ultraviolet and was used by Gruszczynski and Rogers for radiation measurements at a temperature of $7000\ \text{K}$ where the majority of the radiation is above $0.2\ \mu\text{m}$. At higher temperatures, say above $10,000\ \text{K}$, the total radiation from air approaches that of a black body and there is substantial radiation below $0.15\ \mu\text{m}$ where all window materials absorb so that a windowless system must be employed. A radiation gauge with a fast opening diaphragm has also been described by Gruszczynski and Rogers. The diaphragm of this gauge is made of latex which is ruptured in about $15\ \mu\text{s}$ by a current pulse through a $0.05\ \text{mm}$ wire in contact with the latex sheet across the entrance slit, Fig. 71(d). There was found to be a delay, constant at about $150\ \mu\text{s}$ between the initiation of the fusing pulse and the rupture of the diaphragm, which was short enough to permit triggering via shockwave detectors. Photoelectric emission was avoided in this windowless unit by the use of a mixture of helium and krypton whose stagnation pressure was set equal to that of the free stream to avoid massive efflux of the contained gas. Scagnetti and Crabol, (94), have described a heat flux radiometer based on the thin film resistance thermometer for the measurement of heat transfer rates inside solid propellant rocket motors. Their detector is illustrated in Fig. 72(a) and comprises a conventional thin film resistance thermometer with a matt black front face which is in turn protected with a quartz disc. The absorption coefficient of the surface coating was found experimentally to be 0.9. Similar transducers without the surface absorptive layer were used to determine the convective heat transfer rates which in their experiments were of the order of $400\ \text{W cm}^{-2}$ as compared with $150\ \text{W cm}^{-2}$ for the radiative heat transfer rate. Scagnetti and Crabol employed a conventional equi-sectioned analogue for the reduction of the thin film resistance thermometer signal to heat transfer rate and the number of stages was such that accuracy was retained for the flow duration of the propellant burning of 0.15 secs.

Scagnetti and Crabol have presented an analysis of the operation of their radiometer in the frequency domain. It is equally possible to examine the behaviour of such instruments in the time domain, as was shown in section 1 and then to make the conversion to the frequency domain by the appropriate transformation. The analysis which follows draws on the general solution given in Eq (12) and the transformation from a time to a frequency domain is made by substituting $j\omega$ for p in the Laplace-Transform system.

From Eq (12)(section 1) the temperature within the absorbing layer is:-

$$\bar{T}_l = \frac{\bar{q}_s \sqrt{\alpha_1} \left[(1+a) e^{-(x-l)\sqrt{\frac{p}{\alpha_1}}} + (1-a) e^{(x-l)\sqrt{\frac{p}{\alpha_1}}} \right]}{k_1 \sqrt{p} \left[(1+a) e^{l\sqrt{\frac{p}{\alpha_1}}} - (1-a) e^{-l\sqrt{\frac{p}{\alpha_1}}} \right]}$$

At the rear of the absorbing carbon layer, $x = l$, on the surface of the radiometer:

$$\bar{T}_l = \frac{2 \bar{q}_s \sqrt{\alpha_1}}{k_1 \sqrt{p} \left[(1+a) e^{l\sqrt{\frac{p}{\alpha_1}}} - (1-a) e^{-l\sqrt{\frac{p}{\alpha_1}}} \right]} \quad (147)$$

When illuminated by a modulated light source the heat transfer rate to the gauge may be taken as

$$\dot{q}_s = \dot{q}_0 (1 + \sin \omega t)$$

In practice the steady term \dot{q}_0 will disappear after an interval due to 3-dimensional effects and only the oscillatory term will remain. The solution of Eq (147) may then be obtained by replacing p by $j\omega$:

$$\frac{T_l}{\dot{q}_0} = \frac{2\sqrt{\alpha_1}}{k_1 \sqrt{j\omega} \left[(1+a) e^{l\sqrt{\frac{j\omega}{\alpha_1}}} - (1-a) e^{-l\sqrt{\frac{j\omega}{\alpha_1}}} \right]} \quad (148)$$

which, on rearrangement may be expressed as

$$\frac{T_l}{\dot{q}_0} = \frac{2\sqrt{\alpha_1} e^{-l\sqrt{\frac{j\omega}{\alpha_1}}}}{k_1 \sqrt{j\omega} \left[(1+a) - (1-a) e^{-2l\sqrt{\frac{j\omega}{\alpha_1}}} \right]} \quad (149)$$

Replacing ω by $2\pi f$ where f is the frequency we obtain the modulus of the temperature in the same form as Scagnetti and Crabol (94):

$$|T_l| \sqrt{f} = \frac{\dot{q}_s e^{-l\sqrt{\frac{\pi f}{\alpha_1}}} \frac{a}{\sqrt{2}}}{\sqrt{\pi} \sqrt{\rho_2 c_2 k_2} \left[(1+a) - (1-a) e^{-2l\sqrt{\frac{2\pi f}{\alpha_1}}} \right]} \quad (150)$$

Recognising that

$$a = \sqrt{\frac{\rho_2 c_2 k_2}{\rho_1 c_1 k_1}}$$

and substituting G for the last (square) bracketed term in Eq (150) we obtain:

$$\log \left[|T| \sqrt{f} \right] = \log \frac{\dot{q}_s}{\sqrt{\pi \rho_2 c_2 k_2}} - \ell \sqrt{\frac{\pi}{\alpha_1}} \sqrt{f} + \log G \quad (151)$$

Scagnetti and Crabol have shown that this last term may be approximated by

$$\log G \approx m \ell \sqrt{\frac{\pi}{\alpha_1}} \sqrt{f} \quad (152)$$

where m is a function of α evaluated by them but varying relatively little for different values of α . Thus:

$$\log \left[|T| \sqrt{f} \right] = \log \frac{\dot{q}_s}{\sqrt{\pi \rho_2 c_2 k_2}} - \sqrt{\frac{\pi}{\alpha_1}} \ell \sqrt{f} (1-m) \quad (153)$$

It is possible to check the assumptions on which Eq (153) is based by varying the frequency of the incident radiant heat flux and plotting $\log T \sqrt{f}$ versus \sqrt{f} . Results reported by Scagnetti and Crabol are illustrated in Fig. 72(b), for the case of a heat flux meter without an absorbing layer and with layers of two different thicknesses. It will be seen that the relationship in Eq (153) is valid, the slope of the line giving $(\ell (1-m) \sqrt{f}) = 1.1 \times 10^{-2}$ for a thin layer and 1.6×10^{-2} for a thicker absorbing layer. In practice ℓ in Eq (153) is an 'effective' thickness, shown by Scagnetti and Crabol to be about 0.44 of the total layer. It is necessary to calibrate each instrument for absorption coefficient and Scagnetti and Crabol performed this by an output versus frequency plot as shown in Fig. 72 (b). Extrapolation to the ordinate enables \dot{q}_s to be found since there the relationship in Eq (153) simplifies to

$$\log T \sqrt{f} = \log \frac{\dot{q}_s}{\sqrt{\pi \rho_2 c_2 k_2}} \quad (154)$$

If a value for $\sqrt{\rho_2 c_2 k_2}$ may be assumed either from calibration, as described in section 2.e(i), or from the use of published data, then \dot{q}_s may be found. The incident radiation \dot{q}_i must be obtained from a knowledge of the temperature of the source or from separate calibration utilising one of the 'standard' instruments described in section 2.e(iv). From the knowledge of \dot{q}_s and \dot{q}_i , the absorption coefficient is deduced since $\alpha_s = \dot{q}_s / \dot{q}_i$. The variation with wavelength of the transmission coefficient of the 1 mm quartz disc used on the front face of the transducer is shown in Fig. 72 (c). A further check on the operation of the unit as a radiometer may be made by varying the temperature of the calibrating source and plotting the output at a constant frequency versus T^4 . For the purposes of data analysis from their radiometers, Scagnetti and Crabol have employed conventional equal-section analogue circuits, such as described in section 2.g(ii). In the solid propellant rocket motors in which the tests (94) were conducted the flow duration was approximately 100 to 200 ms with radiative heat transfer rates up to 150 W/cm^2 and convective heat transfer rates up to 400 W/cm^2 , the latter being determined with a heat flux transducer of the same construction but without the carbon film and quartz protection disc.

5.b Circular Disc Radiometers

This instrument, based on an early pyr heliometer of Abbot, was refined by Gardon (95) who investigated its behaviour in detail in 1952. The device is of elegant simplicity and the analysis, reproduced below from Gardon's original paper, illustrates the assumptions which are made. As a radiometer its convenience and small size make it useful as a standard for the direct radiation calibration of many other forms of heat flux transducer. Radiation is absorbed by the blackened surface of a thin circular constantan foil, Fig. 73(a), which is soldered at its circumference to a large copper

block. Energy is absorbed uniformly by the foil but the copper block acts as a heat sink and a radial temperature field is established in the disc. The temperature of the centre of the foil is determined by means of a constantan-copper thermocouple whose cold junction is on the heat sink. Neglecting heat losses from either side of the foil and down the central thermocouple lead and assuming uniform temperature within the thickness of the film the heat balance equation may be written:

$$2\pi r \delta r S \frac{\partial T}{\partial t} = 2\pi r \delta r \dot{q}_s - \frac{\partial T}{\partial r} k 2\pi r S + \left(\frac{\partial T}{\partial r} + \frac{\partial^2 T}{\partial r^2} \right) \delta r k 2\pi (r + \delta r) S \quad (155)$$

Thus

$$\frac{1}{\alpha} \frac{\partial T}{\partial t} = \frac{\dot{q}_s}{Sk} + \frac{1}{r} \frac{\partial T}{\partial r} + \frac{\partial^2 T}{\partial r^2} \quad (156)$$

with boundary conditions:

$$\begin{aligned} T &= 0 \text{ at } t = 0 \text{ for } 0 < r < R \\ T &= 0 \text{ at } 0 < t < \infty \text{ for } r = R \\ \alpha &= \text{diffusivity } k/\rho c. \end{aligned}$$

The temperature distribution in the steady state ($\partial T / \partial t = 0$) is obtained from the equation

$$\frac{\dot{q}_s}{Sk} + \frac{1}{r} \frac{\partial T}{\partial r} + \frac{\partial^2 T}{\partial r^2} = 0 \quad (157)$$

whose solution with boundary conditions $T = 0$ at $0 < t < \infty$ and $r = R$, allowing k to be temperature dependent according to a simple law $k = k_0 (1 + \beta T)$, is:

$$T \left(1 + \frac{\beta}{2} T \right) = \dot{q}_s \frac{R^2 - r^2}{4k_0 S} \quad (158)$$

The temperature difference ΔT between T_R and the centre is thus obtained from

$$\Delta T \left(1 + \frac{\beta}{2} \Delta T \right) = \dot{q}_s \frac{R^2}{4k_0 S} \quad (159)$$

Thus if β were zero, the sensitivity $\Delta T / \dot{q}_s$ would be constant. The thermocouple sensitivity is not constant and Gardon selected copper-constantan junctions for which the output voltage could be expressed as

$$E \text{ (mV)} = 0.0381 \Delta T + \frac{0.444}{10^4} (\Delta T)^2 - \frac{28.7}{10^9} (\Delta T)^3 \quad (160)$$

Neglecting the third term the expression simplifies to

$$E \text{ (mV)} = 0.0381 \Delta T (1 + 0.00117 \Delta T)$$

which has an error of 2.5% at 190°C and 5% at 300°C (soft and hard solder melting points respectively). By this choice of junction Gardon matched the variation of thermal conductivity of constantan, which up to 100°C may be expressed as $k_0 \text{ (J cm}^{-1} \text{ K}^{-1} \text{ s}^{-1}) = 0.02175 (1 + .00115 \Delta T)$. The resulting error is thus only 2% due to the closely similar behaviour of k and E with temperature. The sensitivity of the gauge may therefore be expressed as

$$\frac{E}{\dot{q}_s} = 0.0437 \frac{R^2}{S} \text{ mV/ W cm}^{-2} \quad (161)$$

The response time of the transducer would be derived from a solution of Eq (156) with \dot{q}_s a step function which has not yet been reported although Baines (96) has made a frequency response analysis. Gardon argues that the response time, τ , should be of order $R^2 / (4\alpha)$ but this estimate is based on a one-dimensional conduction process which is certainly not the case in the disc radiometer. Nevertheless there is fair agreement between Gardon's estimates of $\tau = 3.7R^2$ where R is the foil radius in cm, for

constantan at a mean temperature of 70°C and a series of measurements in three radiometers (see Table 10). Sheppard (97) has shown that the transient response of the transducer can be described by a single time constant at least over a time interval of several times τ . The value of Sheppard's constant is $\tau_c R^2 / (5.65\alpha)$, rather less than the value suggested by Gardon. In fact as will be seen from Table 10 there is reasonable agreement between Gardon's estimates and his actual measurements with errors in both the positive and negative sense but it is interesting to note that the response is capable of description by a simple exponential function because the user then has the capability of assessing the errors which will arise in making observations at any particular point of the rise time.

The simplicity of Eq (161) governing the sensitivity, and the estimate of the 'response time' of the disc radiometer enable a design chart to be drawn which has as axes foil diameter and foil thickness and enables the sensitivity and time constant to be read off. Fig. 73(c), reproduced from Gardon (95), illustrates the wide ranges of sensitivities and response times which are available. For instance a small transducer with foil diameter 0.2 cm and thickness 0.002 cm will have a sensitivity of 0.24 mV per W/cm^2 and a time constant of about 40 ms. Gardon presented a series of design studies for radiometers with sensitivities between 0.043 and 0.43 mV per W/cm^2 . The results are summarised in Table 11 below and emphasise the importance of the correct choice of sensitivity to avoid radiation effects from the rear face of the disc. Conduction losses in the central thermocouple wire have been neglected in the analysis given above. Malone (98) has investigated corrections which could be applied to measurements made with such disc radiometers to allow for this loss under convective heating conditions. For a 0.0076 cm diameter central wire 0.128 cm long the sensitivity was found to be 97.5% and the response time 115% of the theoretical values. In fact Gardon's measurements in actual transducers showed that departures of up to 65% on ideal for sensitivity and 27% for response time so that there appears to be little advantage in attempting complex corrections. The transducers must be calibrated against some reference source, such as a water calorimeter, but their great advantage lies in the fact that they are essentially steady state instruments which have a comparatively short response time. Malone has also investigated the foil temperature distribution in the presence of convective heat transfer and concluded that it was possible to assign an effective temperature of $T_{\text{edge}} + 0.75 (T_{\text{centre}} - T_{\text{edge}})$ to the foil as a whole.

Baines (96) has analysed the frequency response of thin disc heat transfer gauges. It was concluded that the quasi-steady value deduced for the heat transfer rate, i.e.

$$\dot{q}_s = \frac{4\ell k (T_0 - T_R)}{R^2}$$

is valid for $\omega < 0.04\alpha/R^2$ and here the phase error will be less than 1 degree. For $\omega < 4.0\alpha/R^2$ a better approximation is given by

$$\dot{q}_s = \rho c \ell \left[\frac{4\alpha}{R^2} (T_0 - T_R) + \frac{1}{4} \frac{dT_R}{dt} + \frac{3}{4} \frac{dT_0}{dt} \right] \quad (162)$$

and again the phase error will be less than 1 degree. For example a disc sensor with diameter of 0.3 cm will be satisfactory to the above quoted phase limits up to about 7 Hz, this frequency increasing as the inverse square of the disc radius.

bution of heat transfer rates before designing a model, instrumented with localised transducers, to obtain more detailed and accurate information. This research has gained impetus from heat transfer studies on possible space-shuttle configurations (99) and the use of optical techniques for mapping heat flux distributions is finding increasingly wide application.

The underlying principle is similar to many of those previously discussed in the present monograph. Under transient heating conditions the surface temperature of a model increases and the temperature is determined in the present case by the dependence of radiation, either reflected or emitted by the surface, on the body temperature. The radiation may be detected and analysed by special wavelength-sensitive electro-optical transducers or the model may simply be photographed at a known time interval after the onset of the transient flow. In most cases it will be seen that the model surface is coated with special paints or other preparations which enhance the emission or reflection process and the surface finish of these preparations must be carefully controlled so that unexpected phenomena, such as tripping of the boundary layer, do not occur. Models are frequently made of good thermal insulators to increase the temperature rise of the model and hence the overall detection sensitivity.

Temperature sensitive paints have been widely used in the gas turbine industry for the location of 'hot spots' in combustion chambers and blading and were adapted to the examination of heat transfer rate in transient wind tunnels by Stainback (100) who investigated heat flux distributions on X-15 models. The various techniques which enable the change in surface temperature to be measured are described in sections 6.b(i) - (v) and the determination of heat transfer from them in section 6.c.

6.b Surface Temperature Measurements

6.b(i) Temperature sensitive colour-change paints

This category of temperature sensitive surface treatment consists of a paint which contains metallic salts which liberate a variety of substances, such as carbon dioxide, at specific temperatures and the resulting colour change is irreversible. The paints are marketed under various names such as "Thermocolor" or "Detectotemp". The temperature at which the paints change colour can range from room temperature to 1600°C and they may undergo multiple colour changes at a set of temperatures. Jones and Hunt (101, 102) report that these preparations exhibit an undesirable sensitivity to pressure and rate of rise of surface temperature, a higher colour-change-temperature resulting from a greater rate of rise of temperature. Some so called 'temperature sensitive' paints are sensitive to pressure and exhibit colour changes at constant temperature when the ambient pressure is changed. Sensitivity to pressure and humidity were not, however, observed by Sartell and Lorenz (103) in their experiments although the dependence on heating rate was recognised and a reference technique, to be described below, was used to eliminate this effect. The 'paint' is usually available in powder form ("Thermocolor", Faber-Castell, Stein bei Nürnberg; "Detectotemp", Hardman Coy, Belleville, N.J., U.S.A.) and may be dissolved in alcohol, then sprayed or painted onto the model. Stainback (100) used a high temperature silicon lacquer, sprayed over the paint in order to bond the paint to the model. In practice the paint is illuminated by white light and photographed with a cine camera.

6.b(ii) Phase-change coatings

These coatings consist of materials having calibrated melting points suspended in an inert volatile liquid and are marketed under the name "Tempilag," (Tempil, 132 West 22nd St., N.Y. 10011). The coatings are supplied as liquids which may be mixed with thinners and sprayed or painted onto models to produce a dull finish, opaque film. Upon heating to the phase-change temperature the film melts and becomes a glossy transparent liquid, which if allowed to cool, solidifies but remains glossy. Jones and Hunt, (102), tested these coatings to examine their sensitivity to both pressure changes and heating

rates and observed that the temperatures at which they changed phase were independent of these effects and were in agreement with that quoted by the manufacturers for pressures between atmospheric and 3 mm Hg. Heating rates were varied from 0.2 to 100 K s⁻¹. Coatings with phase-changes occurring at virtually any temperature between 38°C and 1371°C are currently available. The model is illuminated and photographed with a cine camera. If the model is dark, this underlying colour is revealed as the paint melts, enabling the phase change to be clearly defined. Throckmorton, (104), avoided the effect of light reflections from windows and other surfaces by the use of polarised light with filters so arranged that the model was most clearly visible.

6.b(iii) Liquid crystals

One of the first aerodynamic applications of liquid crystals is that reported by Klein (105) who used the technique to identify regions of high temperature and transition on a model of complex shape. There appears to have been little development of the technique for aerodynamic purposes although it has wide application in non-destructive thermal testing (106). Fergason (107) has given a detailed review of their properties. The crystals used for thermal mapping are compounds of cholesteryl, normally liquid at room temperature, which nevertheless have an internal order resulting in the preferential reflection or transmission of light of certain wavelengths. Small changes in temperature alter this internal molecular structure and hence cause the preferred wavelength for reflection or transmission to be altered. When illuminated by white light and viewed by eye the liquid will therefore pass from a colourless liquid through a range of colours to colourless again as its temperature is varied. The primary disadvantage of the substance for use in aerodynamic tests is its sensitivity, not unexpected in view of its structure, to mechanical shear such as that existing on a model surface in a wind tunnel (105). Further, most of these substances have an inherent response time of order 0.1 s (106). A more "robust" form is the encapsulated liquid crystal (106) where the material is enclosed in spheres of diameter 40-50 μm and this form would appear to have more promise for aerodynamic applications.

6.b(iv) Thermographic phosphors

As the name suggests, these phosphors form a class in which the intensity of emitted radiation is temperature dependent. In use the phosphor material is illuminated by ultra-violet light which results in excitation of the electrons, and these, during their subsequent relaxation to lower energy levels, emit visible radiation. The probability that the relaxation, and subsequent visible radiation emission, will occur is temperature dependent and the amount of radiation may thus be used to determine local temperatures. The process is similar to the excitation of electrons in semiconductors and may be characterised by the transitions shown in Fig. 74. There are two energy bands which may normally be occupied by the electrons, the valence band and the conduction band, separated by a forbidden energy band. At sites of impurities in the crystal, some intermediate energy levels, forbidden in the pure crystal, may exist and it is these impurity centres which play an important role in the de-excitation process. The energy acquired by the electron in reaching the conduction band may be released by several mechanisms but impurities, for example, allow the de-excitation to proceed to the intermediate levels. The intensity of the light is temperature-dependent because the stages in de-excitation are themselves temperature-dependent. A decrease in the phosphorescent intensity with increasing temperature, above a threshold level, is characteristic of the phosphors used for heat transfer investigations. The relaxation time for a strongly emitting phosphor is characteristically short and may be less than 1 ms.

The phosphors most widely used at present are prepared by the U.S. Radium Corporation and sold under the name of 'Radelin' phosphors. These may be incorporated in a lacquer which may be sprayed onto the surface to form a coating between 10 and 25 μm thick.

Dixon and Czysz (108) have reported the first use of these phosphors for the measurement of surface temperatures in wind tunnels ; they used an acetate lacquer to transfer the $9\text{ }\mu\text{m}$ powder to the model.

The variation of surface brightness with temperature for a range of phosphors is shown in Fig. 75, where it will be seen that each phosphor is useful over a range of temperatures and its response within this useful range is approximately logarithmic. In use the model is illuminated with ultraviolet light and the visible radiation is recorded photographically. Very high speed film is required in short duration tests and Polaroid ASA 3000 positive film, ASA 400 Royal X Pan or 2485 Estar-AH (Kodak) are used. In order to 'calibrate' the overall system it is customary to fit the model with conventional surface temperature sensors so that contours of equal surface temperature may be drawn through these points along lines of constant photographic density. The photographic density depends on the angles of illumination and observation of the model and this factor must be taken into account in the data reduction. Dixon and Czysz employed a General Electric BH-6 high intensity lamp fed from a D.C. power source and filtered with a water cooled filter (Corning Glass Coy 5970) to produce maximum radiation at $0.356\text{ }\mu\text{m}$. With this high intensity source and Polaroid recording film it is possible to resolve about 0.2°C changes in surface temperature, which corresponds to a minimum heat transfer rate resolution of approximately 0.05 W/cm^2 in a 0.1 s duration facility when epoxy models are used. This resolution is reduced by a factor of ten if the model material is a good thermal conductor such as steel. An example of heat transfer results obtained by this method is given in section 6.c.

6.b(v) Infra-red emission

The surface temperature of a heated body may also be obtained from observations of its radiation at infra-red wavelengths. This technique has been embodied in two commercially available infra-red scanning cameras (AB Bofors and AB Aga) which have been used for the measurement of wind tunnel model temperatures whence heat transfer rates were deduced (109, 110). The operation of the scanning camera may be seen in Fig. 76 and a calibration curve for one field point obtained by Compton (110) is also shown. The object is scanned optically by an oscillating mirror which provides vertical scanning and a prism which rotates about a vertical axis. In the system used by Thomann and Frisk (109) and Compton (110) the vertical oscillation is at a frequency of 16 Hz (to give flicker-free images in normal usage) and the prism is rotated at a constant speed of 1600 rev/s . The liquid-nitrogen-cooled indium-antimonide detector has a rise time less than $1\text{ }\mu\text{s}$ and it is sensitive in the region between 2 and $5.4\text{ }\mu\text{m}$. The rise time is more than adequate for picture resolution which is generally limited only by the aperture required to attain an acceptable signal-to-noise ratio at the output of the detector. The overall resolution is at present approximately 100 picture elements per line scan. The detector noise level corresponds to about 0.2°C in temperature resolution at 20°C ambient although this incremental sensitivity improves at higher source temperatures. Because of the losses in the optical path it is necessary to calibrate the model in place in the tunnel working section, and the overall sensitivity depends on the position of the scanning beam. Compton (110) employed a calibrating source coated with the same flat-black paint ('3M', Nextel) as the model, which produced a slightly grainy coating, approximately 0.05 mm thick, resistant to abrasion in hypersonic tunnels. The model will also reflect infrared radiation arriving from other parts of the tunnel in addition to radiating itself and Compton reported difficulty in using the technique in a shock tunnel because of radiation, believed to be from hot dust particles in the flow. No such background radiation was apparent in either the NASA Ames 1.07 m hypersonic tunnel or the F.F.A. $M = 7$ blowdown tunnel in which Thomann and Frisk carried out the first experiments. The latter authors used a thin plastic foil (Cryovac XL, 0.025 mm thick) supported by a perforated force-carrying metal sheet since the normal windows of the tunnel absorbed the wavelengths ($2 - 6\text{ }\mu\text{m}$) over which the detector was

sensitive.

6.c The determination of heat transfer rates from optically recorded surface temperatures

Of the several methods currently available for the optical determination of surface temperature described above, thermographic phosphors, phase change paints and infrared detection have enjoyed a continued application as may be seen from the many papers in (99) which are based on these three techniques. Having obtained the surface temperature, the heat transfer rate may be determined in the same manner as that described in sections 2.a and 3 depending on whether the model may be considered a semi-infinite medium or whether its skin is of finite thickness. In many instances the surface temperature rise is significant compared with the adiabatic wall temperature and the previous solutions obtained for constant heat transfer rates are no longer applicable. If the heat transfer rate is not constant the surface temperature may still be expressed in the form given by Eq (16);

$$\bar{q}_s = \sqrt{\rho_2 c_2 k_2} \sqrt{p} \bar{T}_s \quad (163)$$

The heat transfer rate may also be expressed in terms of the heat transfer coefficient, h ;

$$\dot{q}_s = h (T_{aw} - T_s) \quad (164)$$

where T_{aw} is the adiabatic wall temperature. Transforming this equation with T_{aw} constant

$$\bar{q}_s = \frac{h T_{aw}}{p} - h \bar{T}_s \quad (165)$$

Eliminating \bar{q}_s between Eqs (163) and (165) enables the surface temperature \bar{T}_s to be obtained in terms of the heat transfer coefficient h :

$$\bar{T}_s = \frac{h T_{aw}}{p(\sqrt{\rho_2 c_2 k_2} \sqrt{p} + h)} \quad (166)$$

This equation may be inverted to give

$$\frac{T_s - T_i}{T_{aw} - T_i} = 1 - e^{-\frac{h^2 \alpha_2 t}{k_2}} \operatorname{erfc} \frac{h \sqrt{\alpha_2 t}}{k_2} \quad (167)$$

where T_i is the initial model temperature. Curves of this expression as a function of $\beta = h \sqrt{\alpha_2 t} / k_2$ are plotted in Fig. 77 for a range of β from 10^{-5} to 10 and the equation itself may be obtained from Eq (140) by setting $\infty = 0$. The graph may be used directly to determine the heat transfer coefficient h if the model temperature T_s after a time interval t is known. Sartell and Lorenz (103), Kafka et al (112), Cérésuela et al (113) have all used colour change paints to determine heat transfer rates to complex shapes. The paints are sensitive to rate of rise of temperature as well as the actual temperature, as mentioned previously, and all the authors quoted have employed reference spheres, made from the same material as the model to overcome this difficulty. The reference sphere is heated in the same flow as the test model. Cérésuela et al use the Fay and Riddell (114) theory for the prediction of the stagnation point heat transfer rate and the results of Smith (115) for the angular distribution. From the frame by frame examination of pictures such as shown in Fig. 78 a curve, Fig. 79(a) is drawn, tracing the movement of colour boundaries with increasing test time. By the use of the known spatial distribution of heat transfer coefficient Fig. 79(b), it is possible to eliminate the angular position θ and obtain a calibration curve for the colour change such as shown in

Fig. 79(c). Such a family of curves enables a heat transfer coefficient h to be assigned to any point on a model, however complex in shape, where an identifiable colour change occurs at a known time. Cérésuela et al used models cast in RTV silicon rubber, the very low thermal conductivity of this material (see Table A-2) allowing thin coatings to behave in a strictly one-dimensional manner for the test times available (10 s). Fig. 5 includes a curve which enables the requisite thickness of RTV rubber to be determined and Fig. 6 has curves which enable the surface temperature rise for a wide range of heat transfer rates to be determined.

The phase change coatings discussed in section 6.b(ii) have been used on semi-infinite bodies by Jones and Hunt (102) and Throckmorton (104). The heat transfer rate may be found in the latter case from Eq (167) and Throckmorton has examined the errors which arise from the assumption of a constant adiabatic wall temperature and constant substrate thermal properties (See also section 2.d(i)). An example of the change in the appearance of the model after the phase change has occurred is shown in Fig. 80. The phase change coating used in this instance was 'Tempilaq'. The model consisted of a simple conical shape flown in an N.O.L. ballistic range. The model was photographed using a high resolution front-lighted laser system. In Fig. 80(a) the appearance of the model prior to flight can be seen. The light coloured areas are those sections of the model which have been coated with the phase change paint while the dark areas show the surface of the model itself. Fig. 80(b) is a photograph taken at $3,353 \text{ m s}^{-1}$ in an ambient pressure of $10,000 \text{ N m}^{-2}$ and the phase change, which appears at 1889 K , has not yet occurred. Fig. 80(c) is a third photograph, taken at $3,444 \text{ m s}^{-1}$, again in an ambient pressure of $10,000 \text{ N m}^{-2}$ and the entire surface of the model is above the phase change temperature. The surface of the model is seen through the now transparent, glossy surface coating.

As in all optical methods of surface temperature registration, the thermographic phosphor technique requires the use of elaborate data analysis equipment. The heat transfer rate to optical density calibration must first be established. This may be done by reference to heat transfer rate sensors set into the model or by a separate experiment but it is necessary to allow for the differing angles of illumination which may occur and some form of source monitoring by an ultraviolet sensitive light meter is desirable. The resulting film, which must be in negative form, is then scanned by an 'isodensitracer' which produces contours of constant photographic density. From the calibration curves it is then possible to assign a heat transfer rate to each contour. An example which shows the high resolution attainable with this technique is shown in Fig. 81.

The infrared technique described in section 6.b(v) may be used in a similar manner to the thermographic phosphors to obtain heat transfer rates. A calibration curve is first taken from a test plate coated with the same flat black paint, Fig. 76(b), and a selected point is matched to the shape expected of the curve from a knowledge of the detector spectral response and a black body source. Compton has pointed out that this calibration procedure is valid only for a single position of the scan point in the field of view. The calibration curve will be of the same shape at all points of the scan but a further calibration must be carried out to allow for the image spot location and both of these factors must be used in data reduction to obtain correct temperature information over the entire field of view. Fig. 82 illustrates the close agreement which may be achieved between thermocouple measurements of heat transfer rate and those derived from the infrared scanning system. In this instance the vertical scan was dispensed with and a scan was made along one generator of a thin skin model. The short period fluctuations are reportedly due to the introduction of noise in the data reduction process during which the information, in analogue form on magnetic tape, is digitised. The points labelled 'hand data reduction' in Fig. 82 were obtained directly from oscillograms of the camera output.

7. THE ERRORS IN DEDUCED HEAT TRANSFER RATE ARISING FROM A SURFACE TEMPERATURE DISCONTINUITY DUE TO THE PRESENCE OF AN ISOLATED HEAT TRANSFER GAUGE

Many of the heat transfer gauges described in the previous sections, when set into a wind tunnel model, assume a temperature different from the surrounding model surface and this may introduce errors in the measurement. For example a slug calorimeter, when inserted in an insulating model, could assume a temperature lower than its neighbouring surface and the opposite would be true when a thin film heat transfer gauge on a Pyrex insert is mounted in a metal model (Fig. 83). It is to be expected that this would influence the measured heat transfer rate in two ways. Firstly the heat transfer rate to the gauge as defined by the equation

$$\dot{q}_s = h(T_{aw} - T_w)$$

would be influenced by a change in h , the heat transfer coefficient, due to the effect on the boundary layer of the surface temperature discontinuity. Secondly, heat losses from the transducer to the surrounding model will also occur. Naturally, any change in the wall temperature, T_w , will cause the heat transfer rate to vary and this has already been considered in section 6.c for the case of a constant heat transfer coefficient.

Heat loss to the supporting structure in the case of a slug calorimeter has already been discussed in section 3.e. Experimental work on the magnitude of this error is described by Hornbaker and Rall (116) who subjected slug calorimeters to both radiant and convective heating. Matching the thermal response of the surrounding surface with that of the calorimeter may possibly alleviate this problem although the conduction effects due to an electrical insulator which necessarily surrounds the calorimeter produces further disturbances (116). The Gardon gauge (sec. 5) relies on conduction to its surrounding structure and hence will not be subject to these losses and this type of transducer is therefore well suited to examining the effect on the heat transfer coefficient alone.

A similar heat loss phenomenon to that of the slug calorimeter occurs when a thin film resistance thermometer mounted on an insulating substrate is inset in a metal model, Fig. 83 (b). So long as the element is further from the metal boundary than the x_T values shown in Fig. 5 the accuracy of the overall measurement would not, however, be affected.

The effect of a surface temperature discontinuity on the heat transfer coefficient has been considered by many authors, including Rubesin (117) and Kays (118), for the case of a flat plate with an incompressible, constant property, boundary layer. This particular problem is solved by Kays in both the cases of a laminar and a turbulent boundary layer. The solutions obtained by Kays will be used in this section to obtain an estimate of the error in the heat transfer rate and heat transfer coefficient produced by such surface temperature discontinuities caused by the presence of the heat transfer gauge. It is expected that a reasonable estimate of the error in compressible flows will also be given by the same analysis.

The notation used in the analysis is illustrated in Fig. 83(a), x being the distance from the leading edge of the flat plate which has an initial length, L , with wall temperature, T_{w1} , followed by a wall temperature T_{w2} for $x > L$. The temperature T_{w2} would therefore be the surface temperature of a semi-infinite medium in the thin film heat transfer gauge or the calorimetric element temperature in the calorimeter gauge, Fig. 83(b).

From (118) the heat transfer coefficient on a constant temperature flat plate for an incompressible constant property boundary layer is given by:

$$St Pr^{2/3} = 0.332 Re_x^{-1/2}$$

(laminar boundary layer)

and

$$St Pr^{0.4} = 0.0295 Re_x^{-1/5}$$

(turbulent boundary layer)

where the Stanton Number, $St = h/(\rho U c_p)$, h being the heat transfer coefficient, ρ the density and c_p the specific heat at constant pressure. Pr and Re_x are the Prandtl number and Reynolds numbers based on distance from the plate leading edge respectively. The heat transfer rate, \dot{q}_s , to the surface downstream of the discontinuity may be evaluated, following Kays (118) as:

$$\begin{aligned} \frac{\dot{q}_s}{\dot{q}_o} &= 1 + \frac{T_{w1} - T_{w2}}{T_o - T_{w1}} \left[1 - \left(\frac{L}{x} \right)^{3/4} \right]^{-1/3} \\ &= 1 + \frac{T_{w1} - T_{w2}}{T_o - T_{w1}} J \left(\frac{L}{x} \right) \quad (\text{laminar}) \end{aligned} \quad (168)$$

$$\begin{aligned} \frac{\dot{q}_s}{\dot{q}_o} &= 1 + \frac{T_{w1} - T_{w2}}{T_o - T_{w1}} \left[1 - \left(\frac{L}{x} \right)^{9/10} \right]^{-1/9} \\ &= 1 + \frac{T_{w1} - T_{w2}}{T_o - T_{w1}} K \left(\frac{L}{x} \right) \quad (\text{turbulent}) \end{aligned} \quad (169)$$

where \dot{q}_o in both cases is the heat transfer rate that would exist at a position x ($x > L$) if the wall were at a uniform temperature T_{w1} . The functions J and K have been evaluated and are plotted in Fig. 84. The heat transfer coefficient in the two cases is given by:

$$\frac{h}{h_o} = \frac{T_o - T_{w1}}{T_o - T_{w2}} + \frac{T_{w1} - T_{w2}}{T_o - T_{w2}} J \left(\frac{L}{x} \right) \quad (\text{laminar}) \quad (170)$$

$$\frac{h}{h_o} = \frac{T_o - T_{w1}}{T_o - T_{w2}} + \frac{T_{w1} - T_{w2}}{T_o - T_{w2}} K \left(\frac{L}{x} \right) \quad (\text{turbulent}) \quad (171)$$

The above equations enable the surface temperature effect to be estimated in the case of thin film heat transfer gauges where the measurement is located at a specific position on a Pyrex or quartz insert. However in the case of a calorimeter gauge the finite size of the calorimetric element requires that an average heat transfer rate be taken. The above equations, Eqs (168) and (169), are therefore integrated over the surface of the gauge and the following expressions for the average heat transfer coefficient, relative to that at the centre of the gauge in the absence of the temperature discontinuity, are obtained:

$$\frac{h_m(L, x)}{h_o \left(\frac{L+x}{2} \right)} = 1 + I \left(\frac{L}{x} \right) \frac{T_{w1} - T_{w2}}{T_o - T_{w2}}, \quad \frac{L}{x} > 0.5 \quad (\text{laminar}) \quad (172)$$

$$\frac{h_m(L, x)}{h_o \left(\frac{L+x}{2} \right)} = F \left(\frac{L}{x} \right) + H \left(\frac{L}{x} \right) \frac{T_{w1} - T_{w2}}{T_o - T_{w2}} \quad (\text{turbulent}) \quad (173)$$

The functions F and H have been evaluated by Westkaemper (119) and he proposes the approximation

$$\frac{h_m(L, x)}{h_o \left(\frac{L+x}{2} \right)} = 1 + H \left(\frac{L}{x} \right) \frac{T_{w1} - T_{w2}}{T_o - T_{w2}} \quad (174)$$

for $(L/x) > 0.5$. The functions I, H are plotted in Fig. 84. The average heat transfer rate is readily found from the average heat transfer coefficients using the relationship:

$$\dot{q}_m = h_m (T_o - T_{w2})$$

The case of the laminar boundary layer with a temperature discontinuity has been examined by Chapman and Rubesin (120) and with reference to the measurement of heat transfer rates using Rose calorimeter gauges by Sprinks (121). Sprinks uses the analysis of Lighthill (122) and arrives at the same result as that deduced from Kays (118) given in Eq (168). The turbulent boundary layer with the surface temperature discontinuity has been studied by Rubesin (117) and Reynolds, Kays and Kline (123). The latter conclude that Eq (169) is a relationship which is valid for a wider Reynolds number range than that originally proposed by Rubesin (117). Rubesin integrated his relationship to give the error in the slug calorimeter situation whereas Westkaemper (119) integrated the relationship of Reynold et al (Eq(169)) to give Eqs (173) and (174). The equation obtained by Rubesin is similar to Eq (173), the values of $F(L/x)$ and $H(L/x)$ being greater than those given here although Westkaemper (119) notes an error in the value of $F(L/x)$ deduced by Rubesin. Experimental verification of the relationship expressed in Eq (174) and that for the turbulent boundary layer case proposed by Rubesin was performed by Bachmann, Chambers and Giedt (124) who used a Gardon gauge placed in both an isothermal and non isothermal structure. The results indicated that the change in heat transfer coefficient may be estimated using the equations given in this section.

The effect described above may be quite large and has been evaluated for the following situations: (a) A thin film heat transfer gauge and

(b) A copper capsule calorimeter, both mounted in metallic flat plate models.

We consider first case (a) in which a thin film is mounted 2 mm from the leading edge of a Pyrex substrate which itself is 5 cm from the leading edge of a flat plate model. Assuming a flow stagnation temperature of 1000 K and heat transfer rate of 100 W cm^{-2} , the rate of rise of substrate surface temperature will be 100°C in approximately 20 ms (Fig. 6). Assuming further that the rise in temperature of the metal is small, the wall temperature T_{w1} may be taken as 300 K. With $T_o = 1000 \text{ K}$, $T_{w2} = 400 \text{ K}$ and $L/x = 0.96$, the ratio h/h_o may be calculated from Eqs (170, 171) and Fig. 84 to be 0.63 for a laminar and 0.92 for a turbulent boundary layer respectively. As an example of the case (b) above we may consider a copper capsule calorimeter gauge, similar to those illustrated in Table 9, section 3, set into a thick aluminium plate and located 5 cm from the leading edge. Assuming the same flow conditions as in case (a), i.e. $T_o = 1000 \text{ K}$, $\dot{q} = 100 \text{ W cm}^{-2}$, the model surface temperature will rise 10 K in 50 ms (Fig. 7). Taking, for the purposes of this example a calorimeter of diameter 2.5 mm and thickness 0.2 mm, it will be seen from Fig. 51 that the element will rise 75 K in temperature in 50 ms. The quantities T_o , T_{w1} , and T_{w2} are thus 1000 K, 310 K and 375 K with $L/x = 0.952$ respectively. The resulting average heat transfer coefficient over the surface of the calorimeter compared with its value at the centre in the absence of a temperature mismatch may be expressed by the ratio $h_m/h_{(L+x)/2} = 0.63$ and 0.92 for laminar and turbulent boundary layers.

In view of the effects of such temperature discontinuities on measured heat transfer coefficients it is desirable to attempt to match the thermal conductivities of heat transfer gauges and model. If this is not possible the measurements should be made as far downstream as possible from any material mismatches in the model surface.

References

1. Hertzberg A. A shock tube method of generating hypersonic flows. J. Aero Sci. 18, 12, 1951, p.803.
2. Woodley J.G. Performance estimates for a reflected-shock tunnel with a modified driver to produce high test-section Reynolds numbers. A.R.C. C.P. 1057, 1969.
3. Cox R.N.
Winter D.F.T. The light gas hypersonic gun tunnel at ARDE, Fort Halstead, Kent. Agard Rept. 139, July 1957.
4. Needham D.A.
Elfstrom G.M.
Stollery J.L. Design and operation of the Imperial College No. 2 gun tunnel. A.R.C. 32569, 1970.
5. East R.A. Performance and operation of the University of Southampton hypersonic gun tunnel. University of Southampton, Rept AASU268, April 1967.
6. Leuchter O. Soufflerie pilote R"O. ONERA TP No.296, 1965.
7. Perry R. The Longshot type of high Reynolds number tunnel. Proc. 3rd Hypervelocity Techniques Symp. Denver, March 1964.
8. Lukasiewicz J.
Whitfield J.D.
Jackson R. Aerodynamic testing at Mach numbers 15 to 20. Hypersonic Flow Research. Vol 7, New York, Academic Press, 1962, p.473.
9. Richards B.E.
Enkenhus K.R. Hypersonic testing in the VKI Longshot free piston tunnel. AIAA J., 8, 6, 1969, p.1020.
10. Ludwig H. Der Rohrwindkanal. Z. für Flugwissenschaften. 3, 7, July 1955, p.206.
11. Davis J.W.
Gwin H.S. Feasibility studies of a short duration high Reynolds number wind tunnel. NASA TM X-53571, 1967.
12. Glowacki W.J.
Harris E.L.
Lobb R.K.
Schlesinger M.I. The NOL hypervelocity wind tunnel. AIAA paper No. 71-253, 6th Aerodynamic Testing Conference, Albuquerque, March 1971.
13. Vidal R.J. Model instrumentation techniques for heat transfer and force measurements in a hypersonic shock tunnel. C.A.L. Report AD-917-A-1, 1956.
14. Cresci R.J.
Libby P.A. Some heat conduction solutions involved in transient heat transfer measurements. Polytechnic Institute of Brooklyn, PIBAL No.384, 1957.
15. Metcalfe S.C.
Dumbrell S.G. Private communication.
16. Dixon W.P.
Kendall D.N.
Schulte E.H. Semiconductor surface thermocouples for determining heat transfer rates. Proc. 2nd Int. Congr. Instr. in Aerosp. Simul. Facilities, IEEE/G-AES, 1966, 12-1.
17. Kendall D.N.
Dixon W.P. Heat transfer measurements in a hotshot wind tunnel. IEEE Aerospace Systems Conf. Seattle, 1966.
18. Czysz P.A.
Kendall D.N. Testing technology advances associated with development of an arc heated impulse tunnel. AIAA paper No 66-759, Aerodynamic Testing Conf., 1966.
19. Maulard J. Etude du fluxmètre à température superficielle pour mesures dans les tubes à choc. ONERA NT 139, 1969.

20. Rose P.H. Development of the calorimeter heat transfer gauge for use in shock tubes. Rev. Sci. Instr. 29, 7, 1958 (p.557).
21. Busing J.R. On the Joule heating method of calibrating thin film resistance thermometers. Cranfield Coll. of Aeronautics, Rept CoA Aero., 183, 1965.
22. Maulard J. Les fluxmètres thermique à température superficielle pour tubes à choc. Réch.Aér., No.126, Sept 1968, p.39.
23. Touloukian Y.S.(Ed) Thermophysical properties of high temperature solid materials, Vol.4. Thermphys. Prop. Res. Center (TPRC).New York,MacMillan,1967.
24. Hartunian R.A.
Varwig R.L. On thin film heat transfer measurements in shock tubes and shock tunnels. Phys. Fluids, 5, 2, 1962, p.169.
25. Bogdan L. Measurement of the thermal parameter $(q_{ck})^{\frac{1}{2}}$ for clear fused quartz. AIAA J., 4, 8, 1966, p.1477.
26. Reece J.W. Non linear effects due to high heat flux in thin film thermometry and means for their compensation. Proc. 2nd Int. Congr. Instr. Aerosp. Simul. Facilities. IEEE/G-AES. 1966. 10-1.
27. Cook W.J. Determination of heat transfer rates from transient surface temperature measurements. AIAA J., 8, 7, 1970, p.1366.
28. Walenta Z.A. Analogue networks for high heat transfer rate measurements. UTIAS Tech.N. No.84, 1964.
29. Bogdan L. High temperature, thin film resistance thermometers for heat transfer measurements. NASA CR-26, 1964.
30. Henshall B.D.
Schultz D.L. Some notes on the use of resistance thermometers for the measurement of heat transfer rates in shock tubes. ARC CP No 408, 1959.
31. Rabinowicz J.
Jessey M.E.
Bartsch C.A. Resistance thermometer for heat transfer measurement in a shock tube. GALCIT Memo 33, 1956.
32. Maulard J. Mesure des flux thermique élevés. Moyens d'étalonnage. Rech. Aér. No.93, March 1963.
33. Schulte E.H.
Puronen E.O.
Dixon W.P. Calibration Apparatus for Surface Thermocouples. Proc. 3rd Int. Congr. Instr. Aerosp. Facilities, IEEE/G-AES. May 1969, p.92.
34. Spence D.A. Two heat diffusion problems with shock tube applications. RAE Tech. Note Aero 2637, 1959.
35. Maulard J. Calibration method used at ONERA for hotshot and shock tube heat transfer transducers. Proc. 3rd Int. Congr. Instr. Aerosp. Simul. Facilities, IEEE/G-AES. May 1969, p.95.
36. Nicholas M. Etude électrique des couches minces de platine pulvérisé avec application aux fluxmètres thermique. ONERA NT 168, 1970.
37. Holland L. Vacuum deposition of thin films. London, Chapman and Hall, 1970.
38. Winding C.C.
Topper L.
Baus B.V. Metal film resistance thermometers for measuring surface temperatures. Industr. and Eng. Chemistry. 47, 3, 1955, p.386.
39. Holland L.(Ed) Thin film microelectronics. London, Chapman & Hall, 1965.
40. Maissel L.I.
Glang R. (Ed) Handbook of thin film technology. New York, McGraw-Hill, 1970.

41. Skinner, G.T. Analogue network to convert surface temperature to heat flux. ARS J., 30, 6, 1960, p.569.
42. Cook W.J.
Felderman E.J. Reduction of data from thin film heat transfer gauges. A concise numerical technique. AIAA J. 4, 3, 1966, p.561.
43. Jones J.J. Shock tube heat transfer measurements on inner surface of a cylinder (simulating a flat plate) for stagnation temperature range 4100 to 8300°R. NASA TN-D-54, 1959.
44. Meyer R.F. A heat flux meter for use with thin film surface thermometers. NRC Canada, Aero. Rep. LR-279, 1960.
45. Meyer R.F. Further comments on analogue networks to obtain heat flux from surface temperature measurements. NRC Canada, Aero. Rep. LR-375, 1963.
46. Carslaw H.S.
Jaeger J.C. Conduction of heat in solids. 2nd Ed. Oxford, University Press, 1959.
47. Aronson P.M. Pressure and heat transfer instrumentation used in the NOL hypersonic shock tunnels. Proc. 4th Int. Shock Tube Symp., AD 274039, 1961.
48. Morgan C.C.
Andrews J.C. "Morgandyne" heat transfer transducer and flame-torch calibration technique for hypervelocity wind tunnels. AEDC TR-60-1, 1960.
49. Sprinks T. On the calibration of calorimeter heat transfer gauges. AIAA J., 1, 2, 1962, p.464.
50. Weast R.C. (Ed) Handbook of chemistry and physics, 52nd edn. Cleveland, Chemical Rubber Coy, 1971.
51. Trimpi R.L.
Jones R.A. Transient temperature distribution in a two component semi-infinite composite slab of arbitrary materials subjected to aerodynamic heating with a discontinuous change in equilibrium temperature or heat transfer coefficient. NACA Tech Note. 4308, 1958.
52. Naysmith A. Measurement of aerodynamic heat transfer in intermittent wind tunnels. R.A.E. Tech. Note. Aero. 2942, 1964.
53. George A.R.
Reinecke W.G. Conduction in thin skinned heat transfer and recovery temperature models. AIAA J., 1, 8, 1963, p.1956.
54. Chevallier J.-P.
Leuchter O. Mesures dans les souffleries hypersoniques à rafales brèves. ONERA T.P. No. 823, 1970.
55. Cooper M.
Mayo E.E. Normal conduction effects on heat transfer during transient heating of thin skin models. J. Aero. Sci., 24, 1957, p.461.
56. Kemp N.H.
Rose P.H.
Detra R.W. Laminar heat transfer around blunt bodies in dissociated air. J. Aero. Sci., 26, 1959, p.421.
57. Burnett D.R. Transient temperature measurement errors in heated slabs for thermocouples located at the insulated surface. J. Heat Transf., Nov. 1961, p.505.
58. Chevallier J.-P.
Pontézière J.
Bétremlieux A. Méthode calorimétrique de mesure des flux de chaleur en soufflerie. ONERA NT 159, 1970.
59. Brown R.D. A comparison of the theoretical and experimental stagnation point heat transfer in an arc heated subsonic stream. NASA TN D-1927, 1964.

60. Hillsamer M.E.
Rhudy J.P. Heat transfer and shadowgraph tests of several elliptical lifting bodies at Mach 10. AEDC TDR-64-19, 1964.
61. Stalmach C.J.
Bertin J.J.
Pope T.C.
McCloskey M.H. A study of boundary layer transition on outgassing cones in hypersonic flow. NASA CR-1908, 1971.
62. Marvin J.G.
Akin C.M. Pressure and convective heat transfer measurements in a shock tunnel using several test gases. NASA TD-3017, 1965.
63. Harvey W.D. Instrumenting models for aerodynamic heat transfer studies involving transient heating rates. ISA Trans., 6, 1, 1967, p.42.
64. Starner K.E.
Varwig R.L. Thick film thermocouple gauges for roughened model heat flux measurements. ISA Trans. 9, 2, 1970, p.113.
65. Scott C.J. Transient temperature response of a thin walled, transpiration cooled porous surface. A.S.M.E. paper 67-HT-27, 1967.
66. Wood N.B. Hypersonic laminar heat transfer and boundary layer transition on sharp and blunted cones. RARDE Memo. 40/68, 1968.
67. Ledford R.L. A device for measuring heat transfer rates in arc discharge hypervelocity wind tunnels. AEDC TDR-62-64, 1962.
68. Ledford R.L.
Smotherman W.E.
Kidd C.T. Recent developments in heat transfer rate, pressure and force measurement for hotshot tunnels. Proc. 2nd Int. Congr. Instr. Aerosp. Simul. Facilities, IEEE/G-AES Aug. 1966, 2-1.
69. Kipke H.P. Private communication.
70. Starner K.E. Use of thin skinned calorimeters for high heat flux arc-jet measurements. ISA Trans., 7, 3, 1968, p.181.
71. Kirchhoff R.H. Calorimetric heating-rate probe for maximum time response interval. AIAA J., 2, 5, 1964, p.966.
72. Hiester N.K.
Clark C.F. Feasibility of standard evaluation procedures for ablating materials. NASA CR-379, 1966.
73. Vojvodich N.S. Performance of ablative materials in a high energy, partially dissociated frozen nitrogen stream. NASA TN D-1205, 1962.
74. Pope R.B. Stagnation point convective heat transfer in a frozen boundary layer. AIAA J., 6, 4, 1968, p.619.
75. Quentmeyer R.L.
Schacht R.L.
Jones W.L. Hot gas-side heat transfer with and without film cooling on a simulated nuclear rocket thrust chamber using H_2-O_2 . NASA TND-6638, 1972.
76. Witte A.B.
Harper E.Y. Experimental investigation of heat transfer rates in rocket thrust chambers. AIAA J., 1, 2, 1963, p.443.
77. Cornette E.S. Forebody temperatures and calorimeter heating rates measured during Project Fire II Reentry at 11.35 Km s^{-1} . NASA TM-X-1305, 1965.
78. Stoltz G. Numerical solutions to an inverse problem of heat conduction for simple shapes. ASME Trans. Ser.C., J. Heat Transfer, 82, 1, 1960, p.20.
79. Sparrow E.M.
Haji-Sheikh A.
Lundgren T. The inverse problem in transient heat conduction. ASME Trans. Ser. E, J. App. Mech., 31, 3, 1964, p.369.

80. Powell W.B.
Price T.W. A method for the determination of local heat flux from transient temperature measurements. ISA Trans., 3, 3, 1964, p.246.
81. Stroud C.W. A numerical method for determining heating rates from thick calorimeter data. NASA TN D-3846, 1967.
82. Howard F.G. Single thermocouple method for determining heat flux to a thermally thick wall. TN D-4737, 1968.
83. Cornette E.S. Forebody temperatures and total heating rates measured during Project Fire II reentry at 11.35 km s^{-1} . NASA TMX-1120, 1966.
84. Howey, D.C. A 2-dimensional study of miniaturised calorimetric techniques for extreme stagnation heating rates (3,000-10,000 BTU/ft² sec). ISA Trans., 7, 1, 1968, p.52.
85. Chin J.H. Effect of uncertainties in thermocouple locations on computing surface heat fluxes. ARS J., Feb. 1962, p.273.
86. Chapman G.T.
Jackson C.T. Measurement of the heat transfer to bodies of revolution in free flight by the use of a catcher calorimeter. NASA TN D-1890, 1963.
87. Hunt L.R.
Howell R.R. Experimental technique for measuring total aerodynamic heating rates to bodies of arbitrary shape with results for Mach 7. NASA TN D-2446, 1964.
88. Chenoweth A.G. Dynamic method for measuring the pyroelectric effect with special reference to Barium Titanate. J. App. Phys., 27, 1, 1956, p.78.
89. Cooper J. Minimum detectable power of a pyroelectric thermal detector. Rev. Sci. Instr., 33, 1, 1962, p.92.
90. Lang S.B.
Steckel F. Study of the ultra-sensitive pyroelectric thermometer. Rev. Sci. Instr., 36, 12, 1965, p.1817.
91. Wood A.D.
Andrews J.C. Fast response total thermal radiation detectors. Proc. 2nd Int. Congr. Instr. Aerosp. Simul. Facilities, IEEE/G-AES, Aug. 1966, 13-1.
92. Spitzer C. A comparative performance analysis of pyroelectric heat transfer sensors for use in hypersonic impulse facilities. Proc. 2nd Int. Cong. Instr. Aerosp. Simul. Facilities, IEEE/G-AES, Aug. 1966, 11-1.
93. Gruszczynski J.
Rogers D.A. Vacuum ultraviolet sensitive total radiation gauge system. Proc. 2nd Int. Congr. Instr. Aerosp. Simul. Facilities, IEEE/G-AES, Aug. 1966, 17-1.
94. Scagnetti M.
Crabot J. Mesure des fluxes de chaleur pendant la phase d'allumage d'un propergol solide. Réch. Aér. No 123, 1968, p.45.
95. Gardon R. An instrument for the direct measurement of intense thermal radiation. Rev. Sci. Instr., 24, 1953, p.366.
96. Baines D.J. A comparative theoretical evaluation of five commonly used types of unsteady heat flux sensor. Australian Dept. Supply, W.R.E. Salisbury, Report HSA 27, 1970.
97. Sheppard T.D. The determination of the time constant of an asymptotic calorimeter when the heat flux variation across the surface is small. Lockheed Missile and Space Coy, Report LMSC 672154, 1962.
98. Malone E.W. Design and calibration of thin-foil heat flux sensors. ISA Trans., 7, 3, 1968, p.175.

99. Space Shuttle Aerothermodynamics Technology Conference Vol II. Heating. NASA TM X-2507, 1972.
100. Stainback P.C. A visual technique for determining qualitative aerodynamic heating rates on complex configurations. NASA TN D-385, 1960.
101. Jones R.A.
Hunt J.L. Use of fusible temperature indicators for obtaining quantitative aerodynamic heat transfer data. NASA TR-R-230, 1960.
102. Jones R.A.
Hunt J.L. Use of temperature sensitive coatings for obtaining quantitative aerodynamic heat transfer data. AIAA J., 2, 7, 1964, p.1354.
103. Sartell R.J.
Lorenz G.C. A new technique for measurement of aerodynamic heating distributions on models of hypersonic vehicles. Proc. 1964 Heat Transfer and Fluid Mech. Institute, Stanford Univ. Press, 1964, p.130.
104. Throckmorton D.A. Heat transfer testing in phase B shuttle studies with emphasis on phase change improvement. NASA TM X-2507, 1972, p.661.
105. Klein E.J. Liquid crystals in aerodynamic testing. Aeronautics and Astronautics, July 1968, p.70.
106. Fergason J.L. Liquid crystals in non-destructive testing. Appl. Optics, 7, 9, 1968, p.1729.
107. Fergason J.L. Liquid crystals. Scientific American, 211, 1964, p.77.
108. Dixon W.P.
Czys P.A. The use of thermographic phosphors for heat transfer measurement in a hypersonic impulse tunnel. Soc. Photog. Instr. Eng. 11th Annual Tech. Symp., Aug 1966.
109. Thomann H.
Frisk B. Measurement of heat transfer with an infrared camera. Int. J. Heat Mass Transfer, 11, 1968, p.819.
110. Compton D.L. Convective heating measurement by means of an infra-red camera. NASA TM X-2507, 1972, p.645.
111. Borg S.-B. Thermal imaging with real time picture presentation. Applied Optics, 7, 9, 1968, p.1697.
112. Kafka P.G.
Gaz J.
Yee W.T. Measurement of aerodynamic heating of wind tunnel models by means of temperature sensitive paints. J. Spacecraft Rockets, 2, 3, 1965, p.475.
113. Cérésuela R.
Bétremaux A
Cadars J. Mesures de l'échauffement cinétique dans les souffleries hypersonique au moyen de peintures thermosensibles. Réch. Aér. No 109, Nov.-Dec. 1965.
114. Fay J.A.
Riddell F.R. Theory of stagnation point heat transfer in dissociated air. J.Aero. Sci., 25, 2, 1958, p.73.
115. Smith C.G. Heat flux distribution over hemispherical nosed bodies in hypersonic flight. J. Aero. Sci., 28, 1961, p.69.
116. Hornbaker D.R.
Rall D.L. Thermal perturbations caused by heat-flux transducers and their effect on the accuracy of heating rate measurement. I.S.A. Trans., 3, 1964, p.123.
117. Rubesin M.W. The effect of an arbitrary surface-temperature variation along a flat plate on the convective heat transfer in an incompressible turbulent boundary layer. NACA TN 2345, 1951.
118. Kays W.M. Convective Heat and Mass Transfer. New York, McGraw-Hill, 1966.
119. Westkaemper J.C. On the error in plug-type calorimeters caused by surface-temperature mismatch. J. Aero. Sci., 28, 1961, p.907.

120. Chapman D.R.
Rubesin M.W. Temperature and velocity profiles in the compressible laminar boundary layer with arbitrary distribution of surface temperature. J. Aero. Sci., 16, 9, 1949, p.547.
121. Sprinks T. Influence of calorimeter heat transfer gauges on aerodynamic heating. AIAA J., 1, 2, 1963, p.497.
122. Lighthill M.J. Contributions to the theory of heat transfer through a laminar boundary layer. Proc. Roy. Soc., (London) 202A, 1950, p. 359.
123. Reynolds W.C.
Kays W.M.
Kline S.J. Heat transfer in the turbulent incompressible boundary layer, II. Step wall-temperature distribution. NASA Memo 12-2-58W, Dec. 1958.
124. Bachmann R.C.
Chambers J.T.
Giedt W.H. Investigation of surface heat flux measurements with calorimeters. ISA Trans., 4, 1965, p.143.
125. Offenhartz E.
Weisblatt H. Determination of the time history of the flow field about various blunt body shapes and sizes during experiments in 1.5 inch diameter shock tube. AVCO RAD-TR-2-58-10, 1958.
126. Schultz D.L. Thin film resistance thermometers and calorimeters. I. Mech. Eng., London, Symp., "Developments in Techniques for Temperature Measurement". April 1962.
127. Czysz P.A.
Kendall D.N. Improved methods in wind tunnel technology. McDonnell Coy. Report, F 938, 1968.

A-1

Characteristics of thermocouples 0-800°C

Extracted from B.S. 1041: Part 4: 1966.

Copper-Constantan

	0°C	100°C	400°C	800°C
approximate EMF (mV)	0	4.2	20.6	-
sensitivity (μ V/k)	38	46	21	-

Iron-Constantan

	0°C	100°C	400°C	800°C
approximate EMF (mV)	0	5.3	21.8	45.5
Sensitivity (μ V/k)	50	50	50	50

Nickel/10% Chromium-Constantan

	0°C	100°C	400°C	800°C
approximate EMF (mV)	0	6.3	29	61.1
sensitivity (μ V/k)	59	68	80	78

Nickel/Chromium - Nickel/Aluminium

	0°C	100°C	400°C	800°C
approximate EMF (mV)	0	4.1	16.4	33.3
sensitivity (μ V/k)	40	40	40	40

Platinum/10% Rhodium - Platinum

	0°C	100°C	400°C	800°C
approximate EMF (mV)	0	0.64	3.25	7.34
sensitivity (μ V/k)	5	7	9	11

Platinum/13% Rhodium - Platinum

	0°C	100°C	400°C	800°C
approximate EMF (mV)	0	0.64	3.40	7.95
sensitivity (μ V/k)	5	7	10	12

Platinum/5% Rhodium - Platinum/20% Rhodium

	0°C	100°C	400°C	800°C
approximate EMF (mV)	0	-	1.4	3.3
sensitivity (μ V/k)	0.15	-	6	8

Rhodium/Iridium - Iridium

	0°C	100°C	400°C	800°C
approximate EMF (mV)	0	-	1.9	4.2
sensitivity (μ V/k)	3	-	5.5	5.5

A-2

Thermal Properties of Electrical Insulators at 300 K

Insulator	Density ρ g cm^{-3}	Specific Heat c $\text{J g}^{-1} \text{K}^{-1}$	Thermal Cond k $\text{J cm}^{-1} \text{s}^{-1} \text{K}^{-1}$	Diffusivity $k/\rho c$ $\text{cm}^2 \text{s}^{-1}$	Thermal Product $(\rho ck)^{1/2}$ $\text{J cm}^{-2} \text{K}^{-1} \text{s}^{-1/2}$
Pyrex** Corning 7740	2.22	0.775	0.0136	0.00791	0.153
Fused Silicon SiO_2	2.21	0.755	0.014	0.0084	0.153
Alumina+ 99.5% Al_2O_3	3.89	0.71	0.376	0.136	1.02
Alumina+ 96% Al_2O_3	3.72	0.86	0.247	0.0755	0.90
Beryllia+ 99.5% BeO	2.85	1.01	1.59	0.55	2.14
Epoxy* (casting)	1.15	1.7 + 2.1	0.002 + 0.005	0.001 + .0021	0.063 + 0.11
RTV*	1.2	1.55	0.0026	0.0014	0.07
Air (N.T.P.)	0.00129	1.005	0.000253	0.195	0.000574

* Materials Engineering

Materials selector issue, Vol. 70, No. 9, 1969. Reinhold Publ. Corp..

+ Coors Ceramics Bulletin 952; 600 9th St., Golden, Colorado.

** Experimental values from Harturian and Varwig (24).

A-3

Thermal Properties of Metals at 300 K
(from TPRC (23))

Metal	Melting Point, $^{\circ}\text{C}$	density ρ g cm^{-3}	specific heat c $\text{J g}^{-1} \text{K}^{-1}$	conductivity k $\text{J cm}^{-1} \text{K}^{-1} \text{s}^{-1}$	diffusivity α $\text{cm}^2 \text{s}^{-1}$	thermal product $(\rho ck)^{1/2}$ $\text{J cm}^{-2} \text{K}^{-1} \text{s}^{-1/2}$
Platinum	2047	21.5	0.13	0.70	0.25	1.40
Steel (AISI 430)	1683	7.9	0.46	0.18	0.05	0.809
Copper	1356	8.9	0.38	3.97	1.17	3.66
Gold	1337	19.3	0.13	3.14	1.25	2.81
Aluminium	933	2.71	0.86	2.37	1.02	2.35
Lead	327	11.3	0.13	0.35	0.24	0.717
Nickel	1728	8.90	0.45	0.84	0.21	1.83
Inconel	1683	8.47	0.43	0.14	0.04	0.714
Chromium	2123	7.16	0.45	0.94	0.29	1.74
Iron	1535	7.874	0.108	0.803	0.94	0.826

NOMENCLATURE

$a = (\rho_2 c_2 k_2 / \rho_1 c_1 k_1)^{1/2}$	\dot{q}_{meas} = measured heat transfer rate
a = thermocouple sensitivity	\dot{q}_0 = constant surface heat transfer rate
a_n = value of a zero, Eq (93)	\dot{q}_0 = amplitude of radiative surface heat transfer rate
A = arbitrary function of p	$\dot{q}_{\text{surf}}, \dot{q}_s$ = surface heat transfer rate
A = area	\dot{q}_{subst} = heat transfer rate to substrate
b_n = value of a pole, Eq (93)	\dot{q}_x = heat transfer rate at depth x
B = arbitrary function of p	r = radial coordinate of disc foil radiometer
c = specific heat	r' = distributed electrical resistance per unit length
c' = distributed electrical capacitance per unit length	R = model nose radius
C = electrical capacitance	R = electrical resistance
C = arbitrary function of p	R = radius of disc foil radiometer or capsule calorimeter
D = arbitrary function of p	R_c, R_f = collector and feedback resistors
E, E_o, E_n = thin film output voltage	R_e = Reynolds number
f = frequency, Hertz	R_n = stage resistance in analogue circuit
$F(L/x)$ = function of L/x , Fig.84	R_o = output resistance in Skinner analogue circuit
h = heat transfer coefficient	R_o = initial resistance of Rose calorimeter gauge
h = number of stages in analogue circuit, arithmetic increase	R_l = output resistance in Meyer analogue circuit
h_b = heat transfer coefficient inferred from T_R	ΔR = resistance change
h_m = mean heat transfer coefficient	s = thickness of disc foil radiometer
$H(L/x)$ = function of L/x , Fig.84	S = area
i = electrical current	S_t = Stanton number
i_{in} = input current	t = time
$I(L/x)$ = function of L/x , Fig.84	Δt = time difference
$J(L/x)$ = function of L/x , Fig.84	T = temperature or temperature change
k = thermal conductivity	T_{av} = spatial average temperature
k_o = thermal conductivity at ref.temp.	T_R, T_{aw} = recovery or adiabatic wall temp.
K = "loss" constant, Eq(127)	T_{exp} = experimentally observed temp.
K = relative permittivity	T_i = initial temperature
$K(L/x)$ = function of L/x , Fig.84	T_m = spatial mean temperature
l = width of film, Fig.25(d)	$T_{\text{m.p.}}$ = melting temperature
l = calorimeter or thin film thickness, Fig.3	T_R, T_f = rear and front surface temp. of calorimeter
L = distance, Fig.83(a)	T_s = surface temperature
L = length of thin film, Fig.25(d)	T_{subst} = substrate surface temperature
L = length of calorimeter gauge, Fig.52	T_w = corrected surface temperature, Eq(53)
m = mass	T_w = wall surface temperature
m = fraction of heat diffusing into liquid, Eq(56)	T_{w1}, T_{w2} = wall surface temperature, Fig.83
\dot{m} = mass flow rate of coolant water	T_x = temperature at depth x
M = flow Mach number	T_o = starting temperature of calorimeter
n = summation integer	T_o = substrate surface temperature in absence of metallic film
n = number of identical stages in Meyer analogue circuit	T_o, T_R = centre and edge temperature of disc foil radiometer
p = Laplace variable	
P_r = Prandtl number	
P_s = dielectric polarisation	
\dot{q} = heat transfer rate, specifically that per unit area	
\dot{q}_1 = incident radiative heat transfer rate	

T_1, T_2 = temperature in regions 1 and 2, Fig.3	ϵ_0 = dielectric constant of free space
ΔT = temperature difference or error	θ = angular position
$\dot{T} = dT/dt$	λ = variable of integration
U = velocity	ρ = density
V = voltage	ρ_R = electrical resistivity
V_{in} = input voltage	ρ_{RO} = initial electrical resistivity
V_{out} = output voltage	ρ_T = density at temperature T
V_0 = initial voltage across thin film	$\sqrt{(\rho ck)}$ = thermal product
W = width of Rose calorimeter gauge	$\sqrt{(\rho ck)_T}$ = thermal product at temperature T
x = distance	$\sqrt{(\rho ck)}_{liq}$ = thermal product of calibrating liquid, Eq(56)
$x^* = x/\sqrt{(4\alpha t)}$	$\sqrt{(\rho ck)}_{subst}$ = thermal product of substrate
y = coordinate, Fig.25(d)	$\sigma = (1 - a)/(1 + a)$
$\dot{y} = (\dot{q}_0 - \dot{q})/\dot{q}_0$, fractional error in measured heat transfer rate, \dot{q}	σ_R = electrical conductivity
$Z = \sqrt{(\alpha_1 t)}/l$	τ = variable of integration
$Z(x)$ = film thickness, Fig.25(d)	τ = rise time of calorimeter gauge
Z_m = maximum film thickness	ω = circular frequency, radians s^{-1}
$\alpha = k/\rho c$ thermal diffusivity	$\bar{U}, U(p) = \int_0^\infty U(t)e^{-pt}dt$, Laplace transform of $U(t)$
α_R = temperature coefficient of resistance	
α_s = surface absorption coefficient	
α_1, α_2 = thermal diffusivity in regions 1 and 2, Fig.3	In general suffices 1 and 2 refer to regions 1 and 2 in Fig.3
β = temperature coefficient of thermal conductivity	
$\beta = h\sqrt{(\alpha_2 t)}/k_2$, non-dimensional parameter	
γ = scaling factor for Skinner analogue circuit	
γ = pyroelectric coefficient, Eq(141)	
δ = thermal penetration depth	
δ = thickness of evaporated film	
η = coefficient of linear expansion	

Conversion Factors to SI Units

Quantity	British unit	SI unit	Factor
Heat transfer rate per unit area (\dot{q})	Btu ft ⁻² sec ⁻¹	W m ⁻²	1.1349 x 10 ⁴
Heat transfer coefficient (h)	Btu ft ⁻² sec ⁻¹ °F ⁻¹	W m ⁻² K ⁻¹	2.0428 x 10 ⁴
Density (ρ)	lb ft ⁻³	kg m ⁻³	1.60185 x 10
Specific heat (c)	Btu lb ⁻¹ °F ⁻¹	J kg ⁻¹ K ⁻¹	4.184 x 10 ³
Thermal conductivity (k)	Btu ft ⁻¹ sec ⁻¹ °F ⁻¹	J m ⁻¹ s ⁻¹ K ⁻¹	6.2265 x 10 ³
Thermal diffusivity (α)	ft ² sec ⁻¹	m ² s ⁻¹	9.2903 x 10 ⁻²
Thermal product (ρck) ^{1/2}	Btu ft ⁻² °F ⁻¹ sec ^{-1/2}	J m ⁻² K ⁻¹ s ^{-1/2}	2.0428 x 10 ⁴

In order to convert British units to SI units, multiply by the factor shown.

Calculated from data given in NASA SP-7012 with 1 (thermophysical) calorie = 4.18400 J

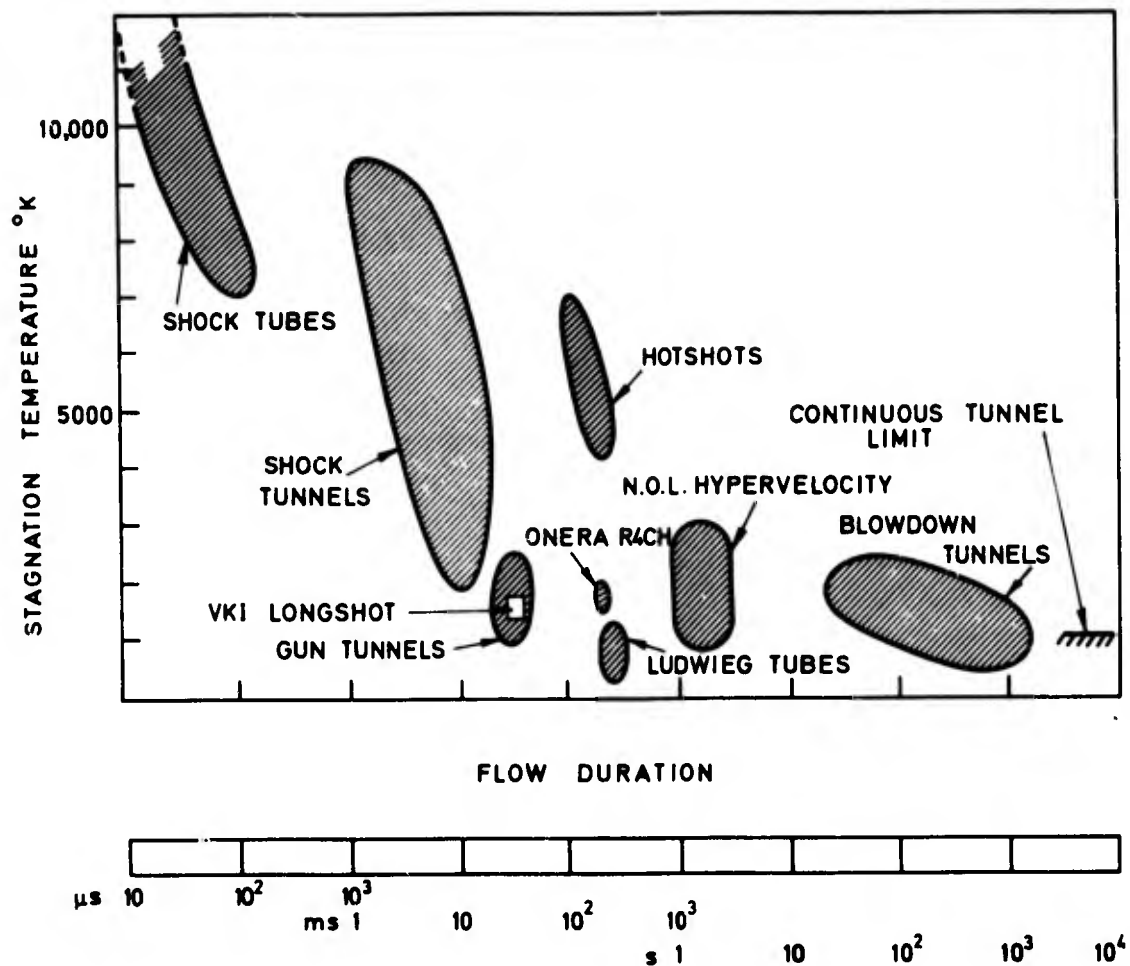


Fig.1

Stagnation temperature and flow duration of intermittent hypersonic facilities compared with temperature limit for continuous tunnels. Information from NASA CR - 1874 and RAE Tech. Memo Aero 1308.

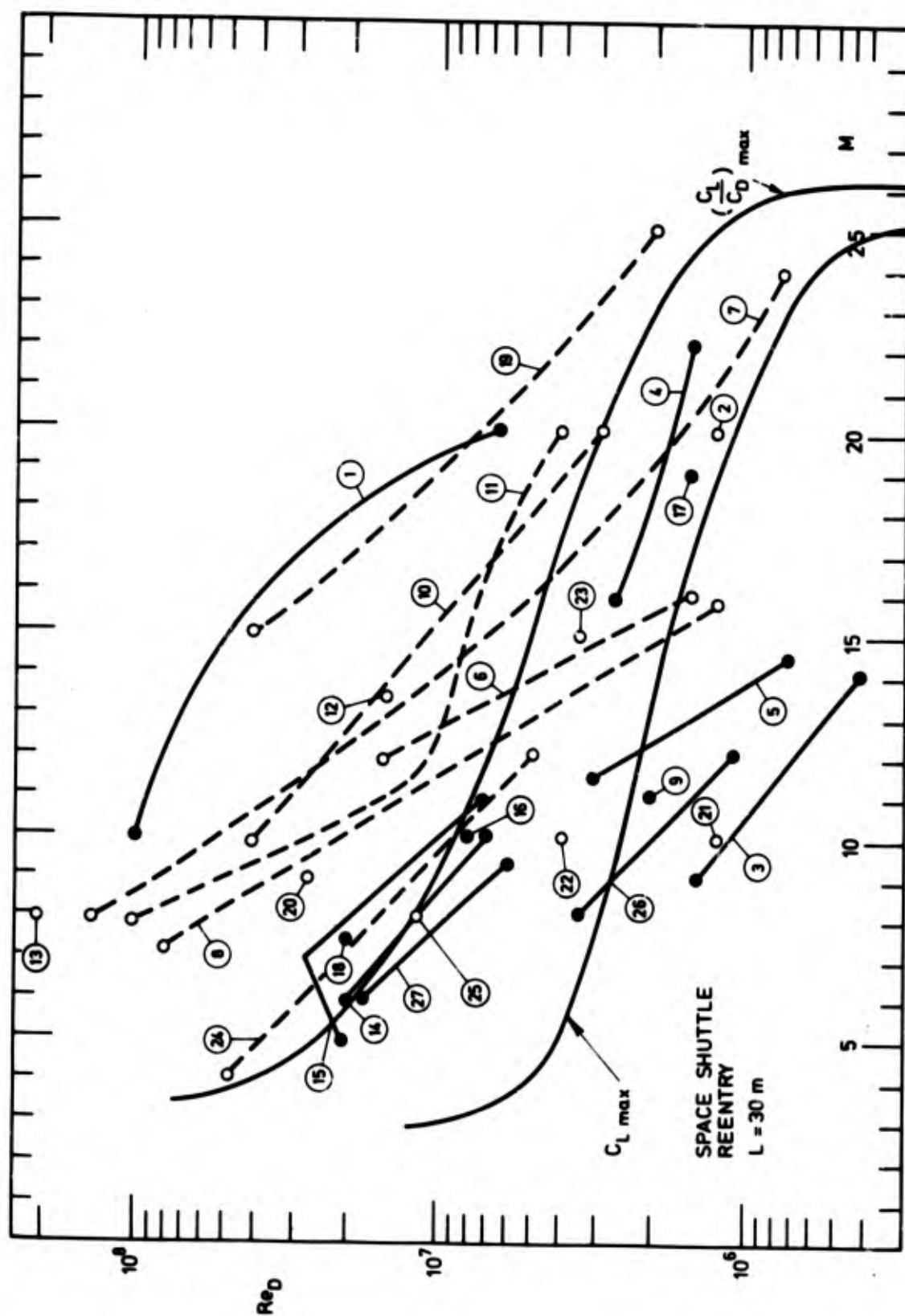


Fig.2

Performance characteristics of intermittent and continuous hypersonic facilities compared on the basis of Re_D , the Reynolds number based on the nozzle exit diameter and Mach number. Information from NASA CR-1874 and RAE Tech. Memo Aero 1308. Where available Re_D is shown over the operating range of the facility. O and O - - - O intermittent facilities. ● and ● - - - ● blowdown and continuous facilities. Tunnels are identified on the accompanying table, p. 88.

No	Type	Location	Flow Duration s	Mach number	T stag K	Re/m maximum conditions	Nozzle Exit Diam., m
1	Blowdown	N.O.L.	1-4	10-20	1030-2800	$7.5 \times 10^7 - 4.27 \times 10^6$	1.52
2	Shock tunnel	Aerosp. Corp.	0.01-0.012	14-20	2800	$3 \times 10^5 - 3.96 \times 10^6$	1.19 (M=20)
3	Blowdown	Wright-Patterson	180-240	8.5-11.5	1389-2333	$5 \times 10^4 - 2 \times 10^6$	0.61-0.81
4	Blowdown	Wright-Patterson	30-120	16-22	1667-2444	$3 \times 10^5 - 3 \times 10^6$	0.76
5	Blowdown	Wright-Patterson	20-300	12-14	277-1389	$7 \times 10^5 - 2.6 \times 10^6$	0.51
6	Shock tunnel	Boeing	0.002-0.01	12-16	556-8000	$2 \times 10^6 - 2 \times 10^7$	0.76
7	Shock tunnel	C.A.L.	0.002-0.006	6.5-24	722-6389	$3 \times 10^3 - 2.3 \times 10^8$	2.45
8	Shock tunnel	C.A.L.	0.004-0.013	5.5-20	611-3222	$1.5 \times 10^4 - 1.3 \times 10^8$	1.22
9	Blowdown	Fluidyne	60	7-18	667-2222	$6 \times 10^4 - 6 \times 10^7$	0.51
10	Gun tunnel	G.E.C.	0.015-0.040	10-20	1389	$3 \times 10^3 - 6.6 \times 10^7$	0.56
11	Hotshot	L.T.V.	0.03-0.30	8-20	1500-4500	$3.2 \times 10^5 - 2.3 \times 10^7$	0.33
12	Hotshot	McDonnell-Douglas	0.140	11.5-24	4340	$5.4 \times 10^5 - 4.6 \times 10^7$	1.02
13	Shock tunnel	McDonnell-Douglas	0.007	7-20	1111-3333	$2.7 \times 10^6 - 1.4 \times 10^9$	0.76
14	Blowdown	McDonnell-Douglas	1800	6-10	472-1372	$4 \times 10^6 - 4 \times 10^7$	0.61
15	Blowdown	NASA Ames	15-240	5-14	1922	$2.0 \times 10^5 - 2.6 \times 10^7$	1.07
16	Continuous	NASA Langley	7200	10	1006-1089	$1 \times 10^6 - 7.4 \times 10^6$	0.79 x 0.79
17	Continuous	NASA Langley	90-600	19	1555-1944	$6 \times 10^5 - 3 \times 10^6$	0.48
18	Blowdown	NASA Langley	0.001-0.040	7.5	644-839	$3 \times 10^5 - 4 \times 10^7$	0.46
19	'Longshot'	VKI Belgium	0.02	15-25	2600	$1 \times 10^7 - 2.4 \times 10^7$	0.61
20	Gun tunnel	I.C. London	0.003-0.005	9-18	1500	8×10^7	0.31-0.46
21	Shock tunnel	Sud Aviation	0.20	10-18	7000	$1.3 \times 10^6 - 1.2 \times 10^7$	0.12-0.40
22	R'O'CH	O.N.E.R.A.	0.10	10 - 15	1700	5×10^6	0.135-0.20
23	Hotshot	O.N.E.R.A.	0.30	15-20	2000-7000	$10^7 - 10^8$	0.70
24	Ludwig tube	D.F.V.L.R. Gött.	0.02-0.10	3-12	300-1100	7×10^7	0.50
25	Gun tunnel	Braunschweig	120	8-16	2000	$2.2 \times 10^5 - 6.9 \times 10^5$	0.16
26	Blowdown	Comvair		8-12	733-811	$1.2 \times 10^5 - 4.6 \times 10^6$	0.46
27	Continuous	B.R.L.		6-9.2	478-1089		0.48

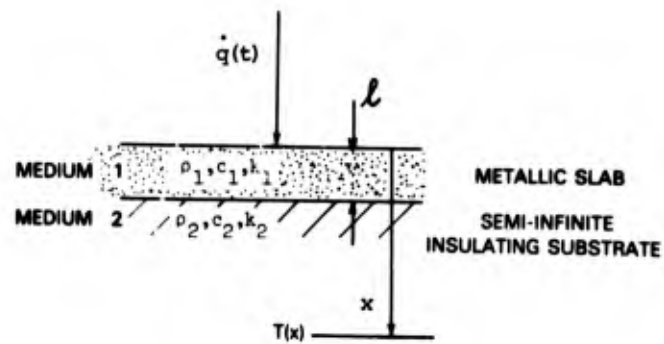


Fig.3

Coordinate system for heat conduction in metallic slab on semi-infinite insulating substrate.

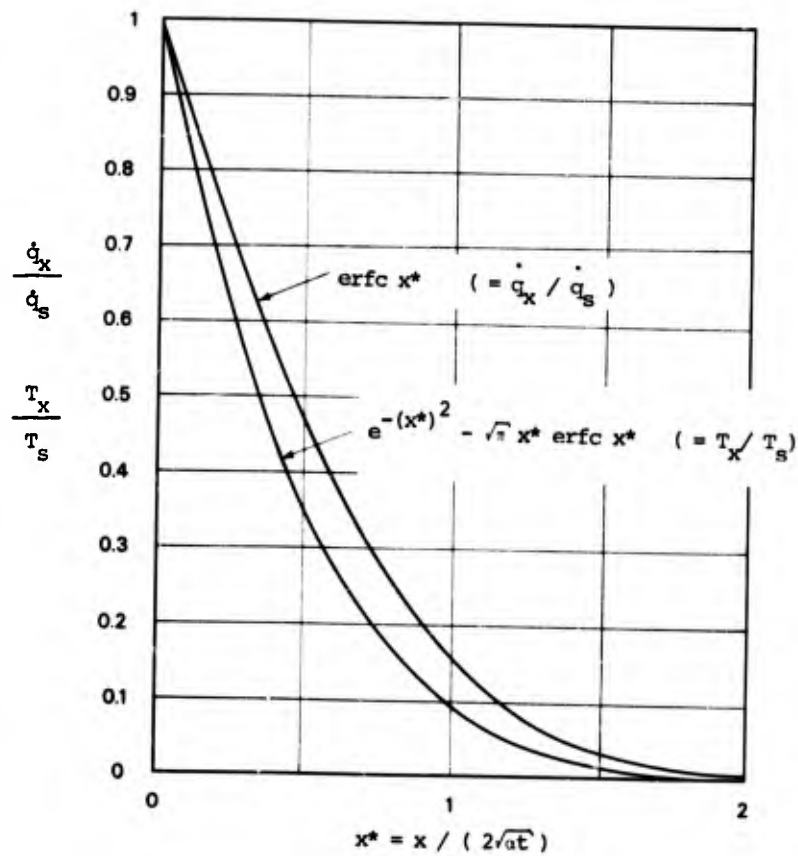


Fig.4

Penetration of thermal pulse into substrate due to step function heat flux (\dot{q}_s) at surface. Redrawn from Maulard (19).

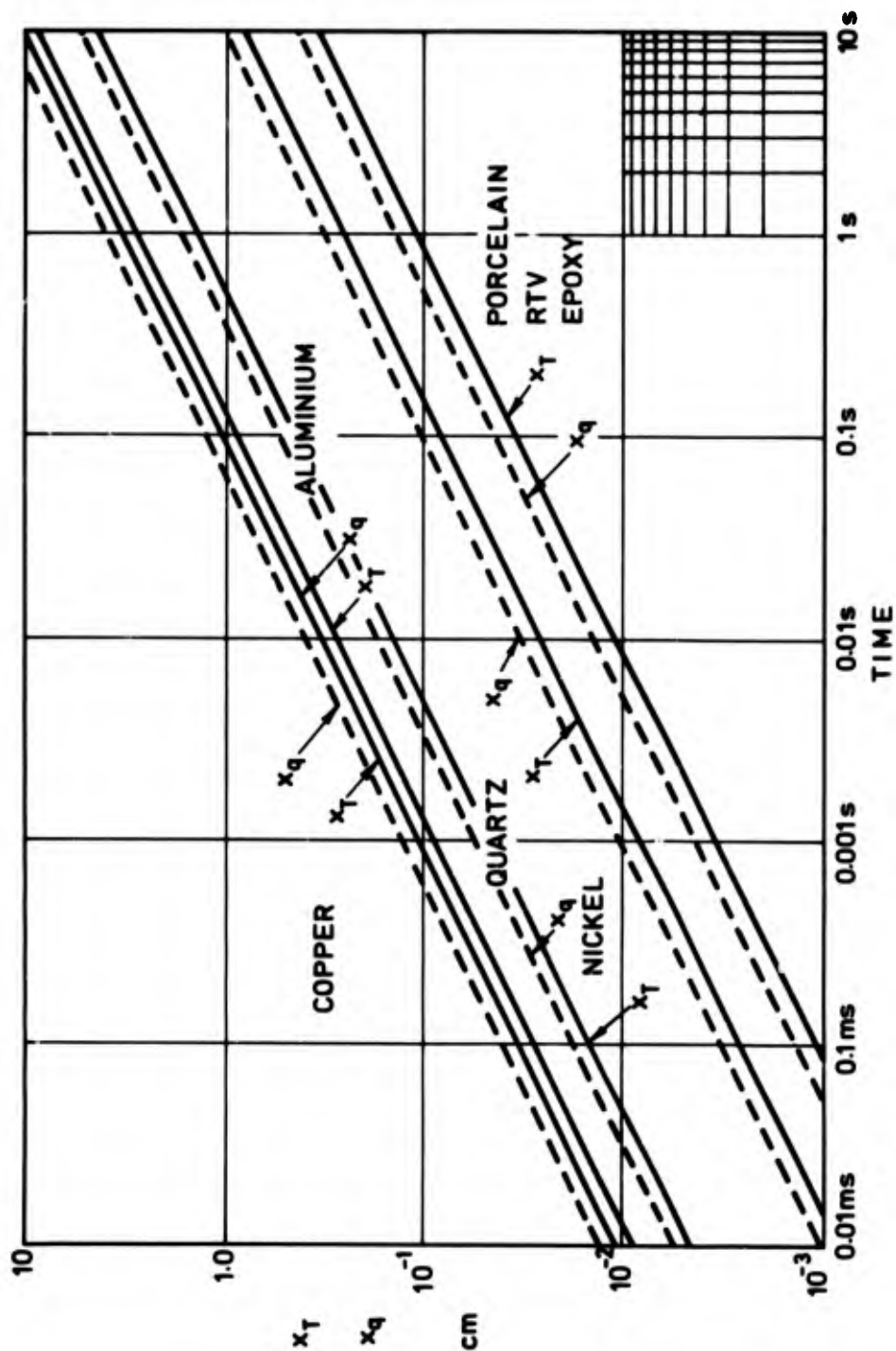


Fig.5

Depths x_T at which temperature T_x is 1% of surface value and x_q at which heat transfer rate \dot{q}_x is 1% of surface value T_s and \dot{q}_s respectively. Calculated from Eqs (25,26). Thermal properties, assumed constant, from Tables A-2, A-3.

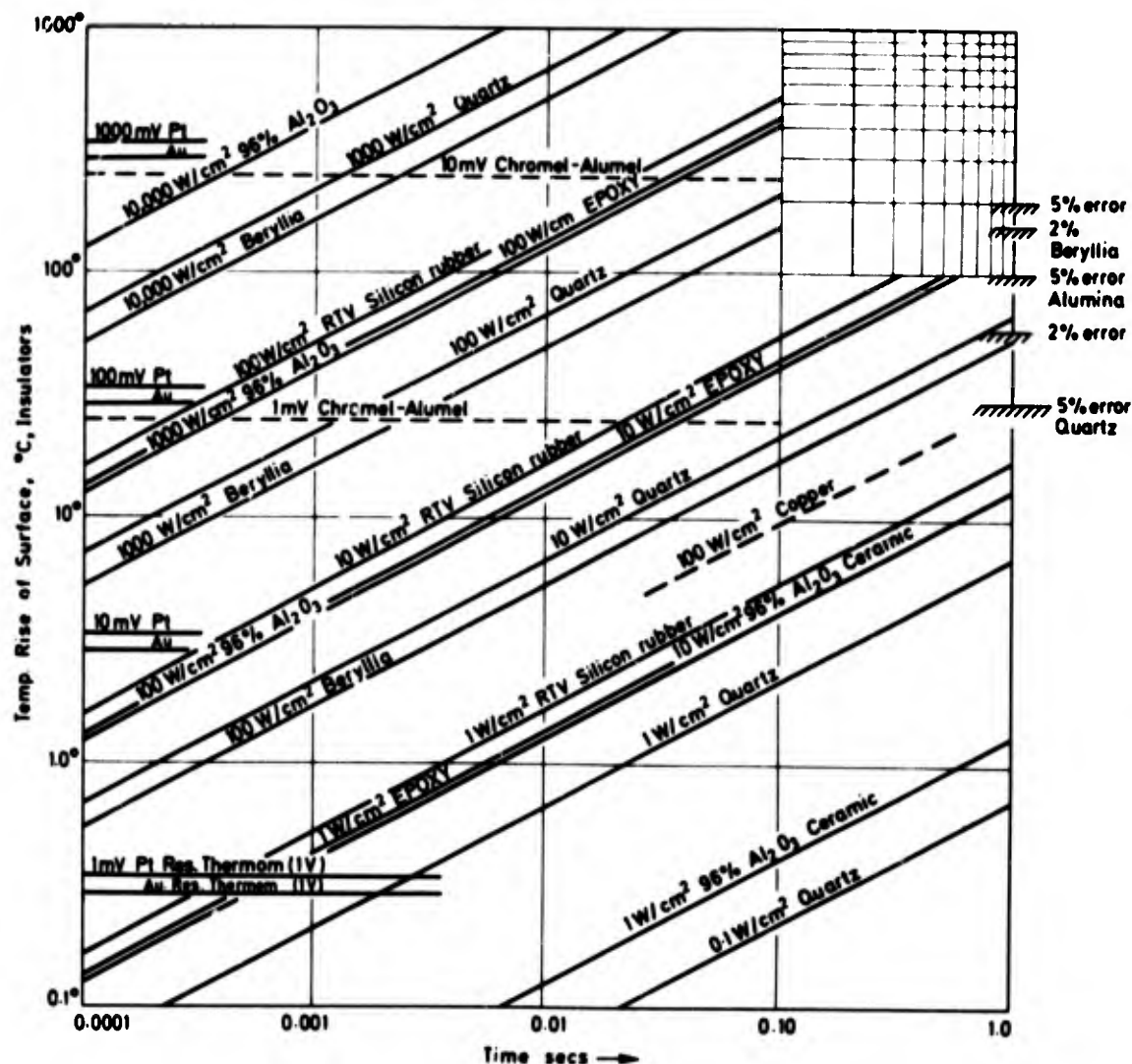


Fig.6

Surface temperature of semi-infinite insulators as function of time for heat transfer rates, assumed constant, between 1 W/cm^2 and 10 kW/cm^2 . Expected signal levels from platinum and gold resistance thermometers (energised with 1 volt) and from chromel-alumel thermocouples (Table A-1). Error levels on right refer to limits of surface temperature increase permitted before non-uniform thermal properties reduce accuracy to value shown.

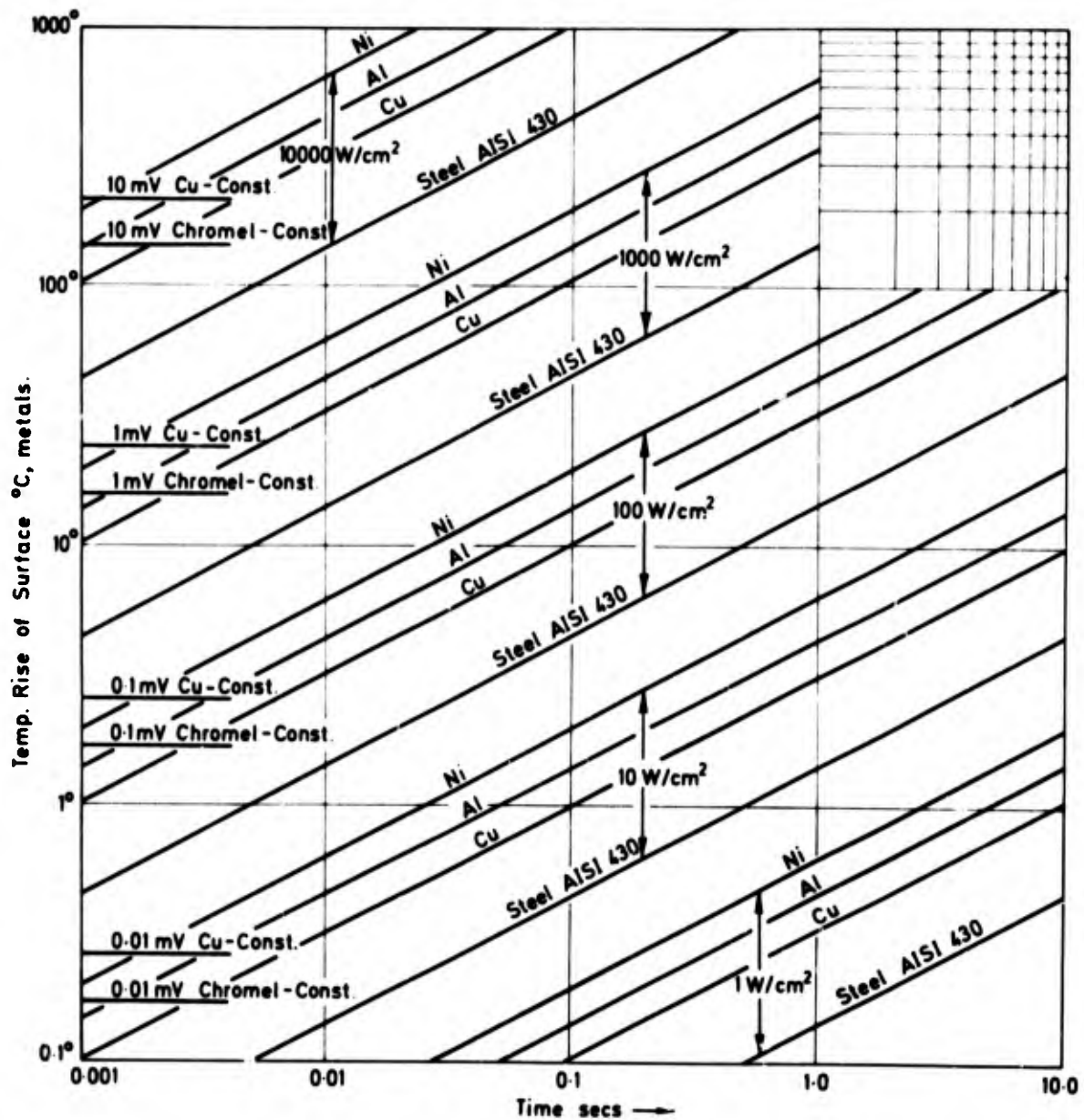
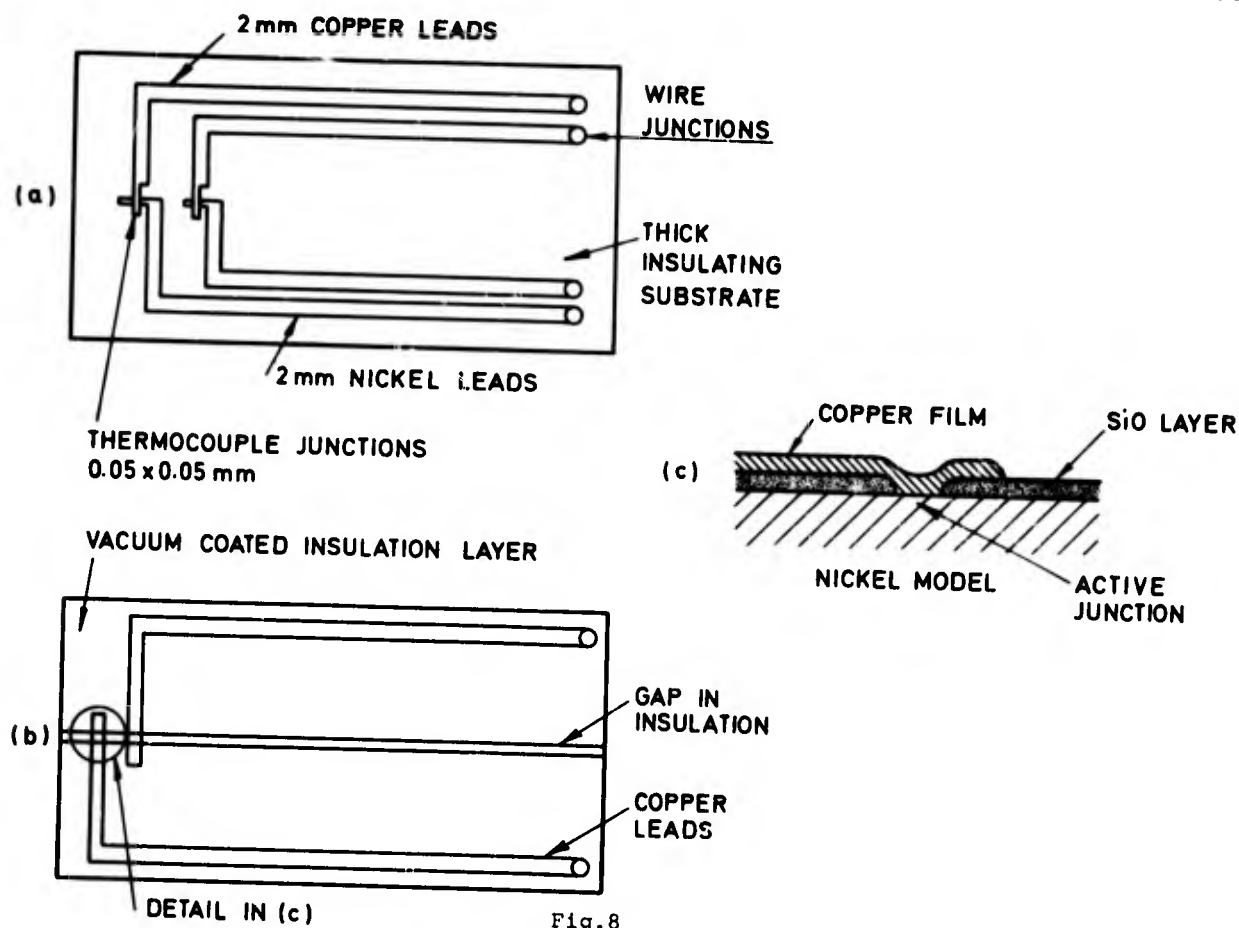
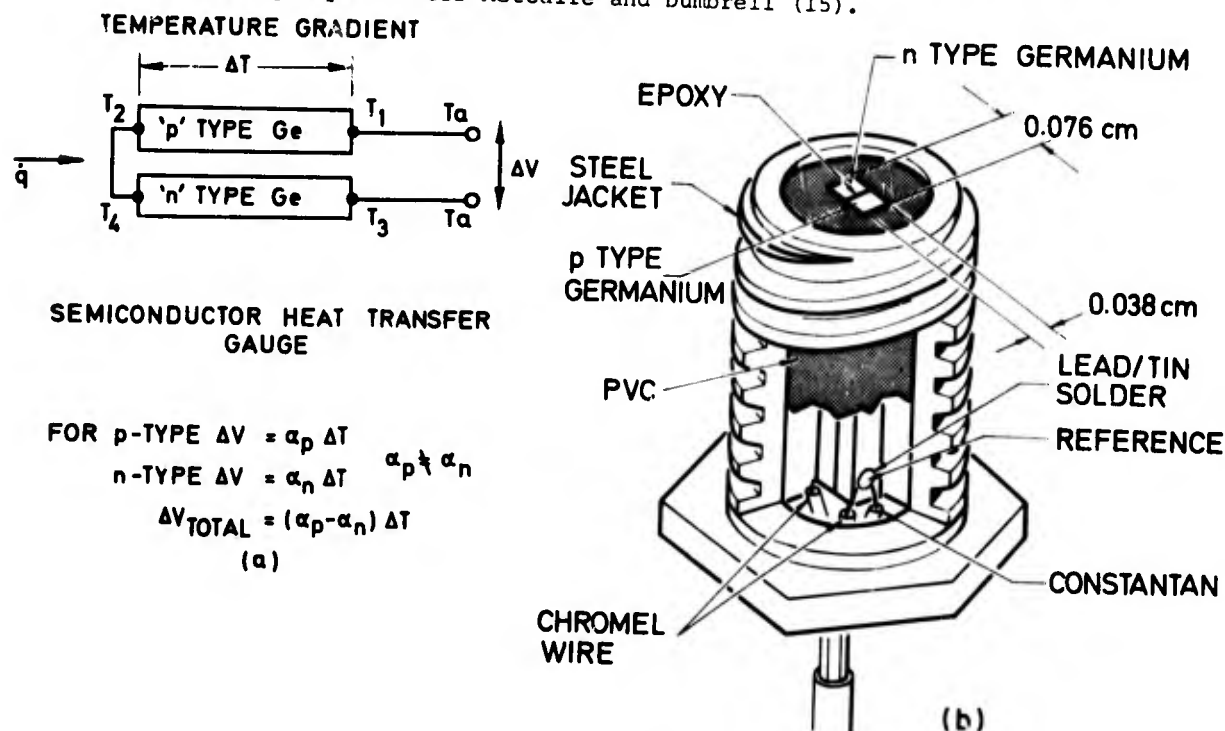


Fig.7

Surface temperature of semi-infinite conductors as function of time for a range of heat transfer rates, assumed constant, calculated from Eq(21). Expected signals from copper-constantan and chromel-constantan thermocouples calculated from temperature sensitivities in B.S.1041. Thermal properties of metals from Table A-3.



Construction technique for evaporated thin film thermocouples. (a) Technique for use with insulating substrate and evaporated copper - nickel junction. (b) Use of nickel model surface as one leg of the thermojunction with evaporated silicon oxide insulating layer. After Metcalfe and Dumbrell (15).



Semiconductor thermocouple heat transfer gauge in which the semiconductor bars form a semi-infinite substrate. (a) Bar interconnections. (b) Construction details, Redrawn from Dixon, Kendall and Schulte (16).

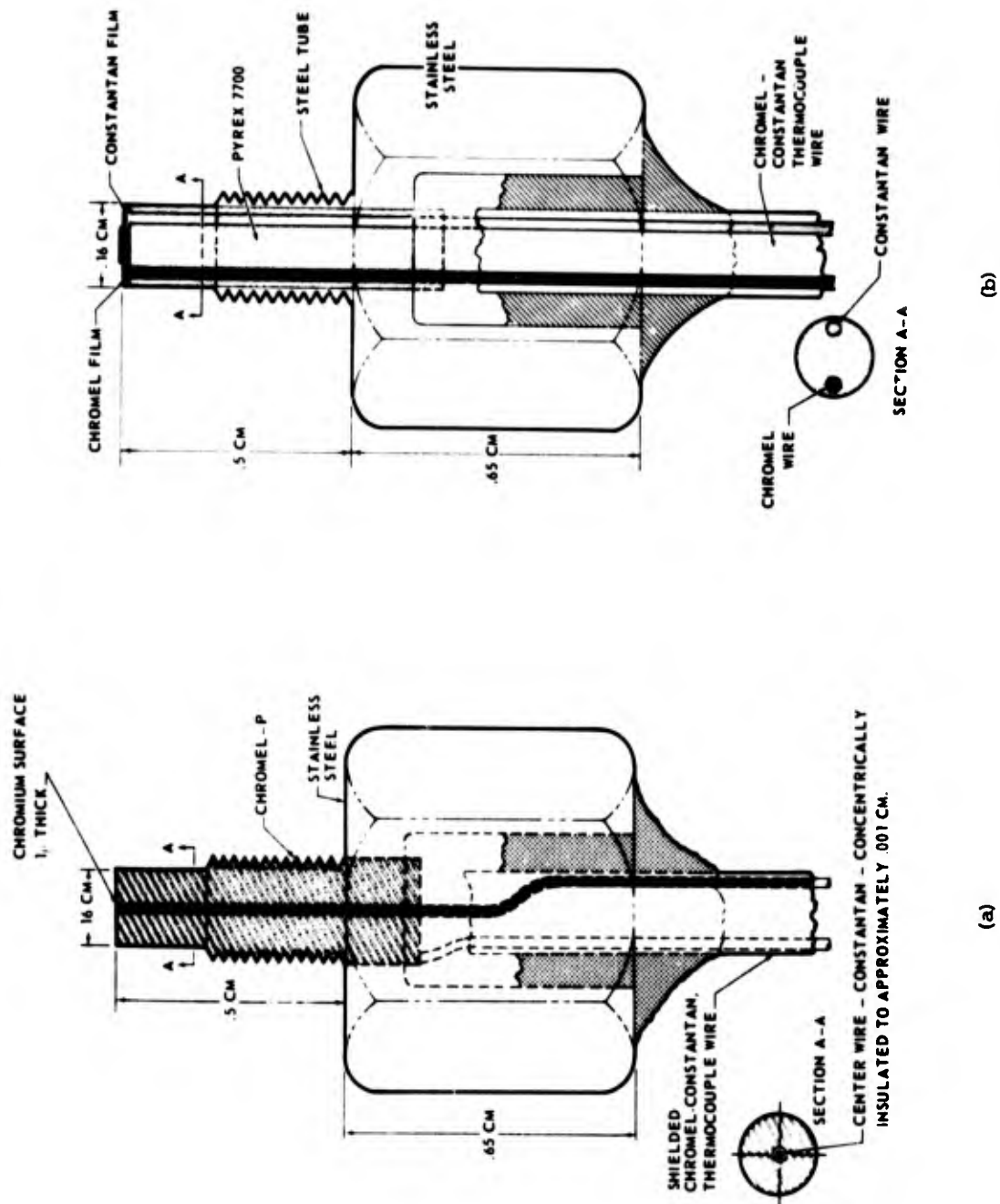


Fig. 10

Thin film heat transfer gauges mounted on metallic and insulating substrates.

(a) Chromel constantan thermocouple on Chromel-P substrate. (b) Chromel constantan thermocouple on Pyrex 7740 substrate. Reproduced with permission from Kendall and Dixon (17) and (18).

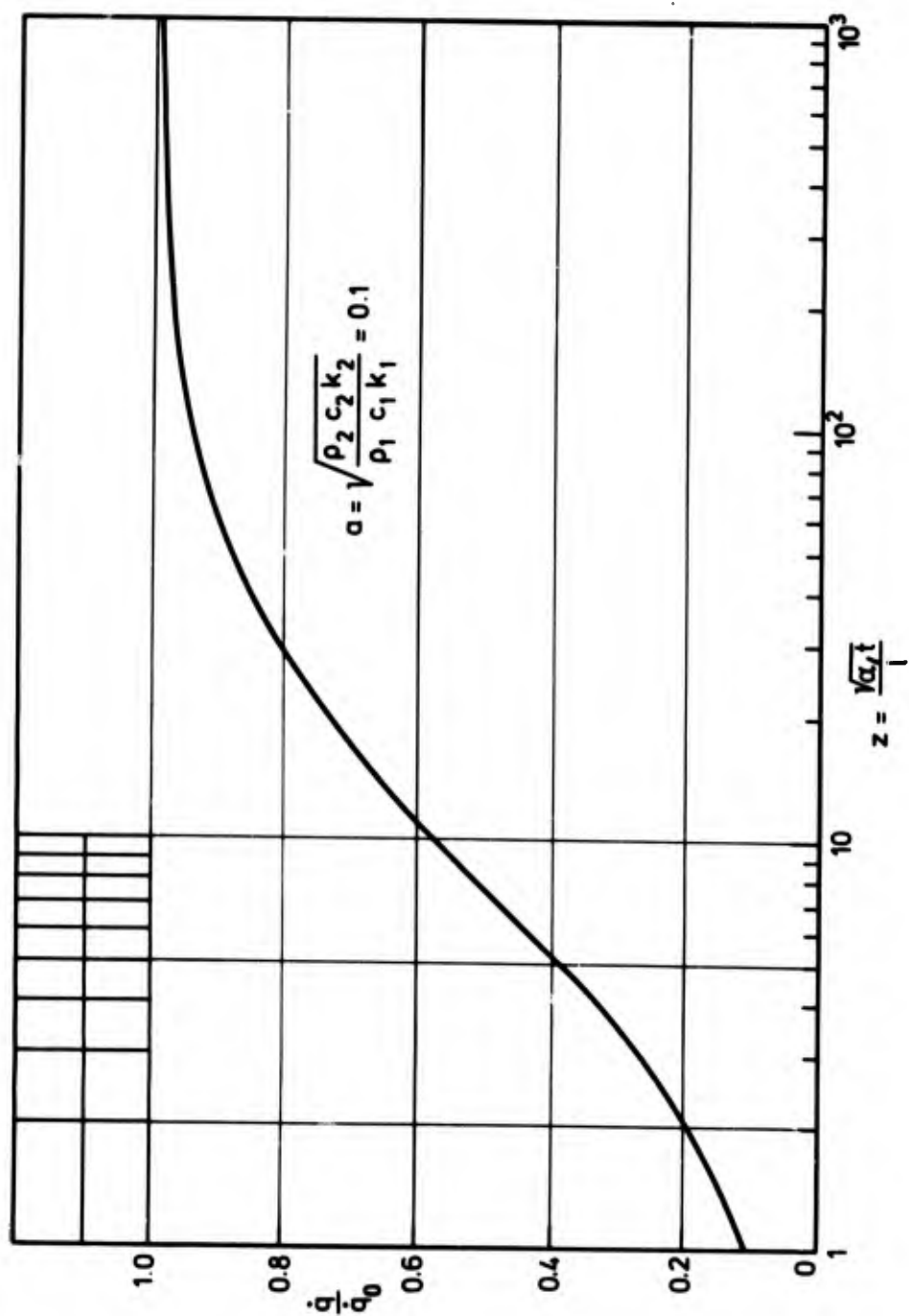


Fig.11

Effect of surface metallic film on calculated heat transfer rate as deduced from Eqs (34) and (35). \dot{q}/\dot{q}_0 expressed in terms of the dimensionless parameter $z = \sqrt{\alpha_f t}/l$ for any film material for the case $a = 0.1$. \dot{q} = heat transfer rate deduced from the observed temperature rise assuming an homogeneous solid, Eq(20). \dot{q}_0 = amplitude of actual step function in heat transfer rate.

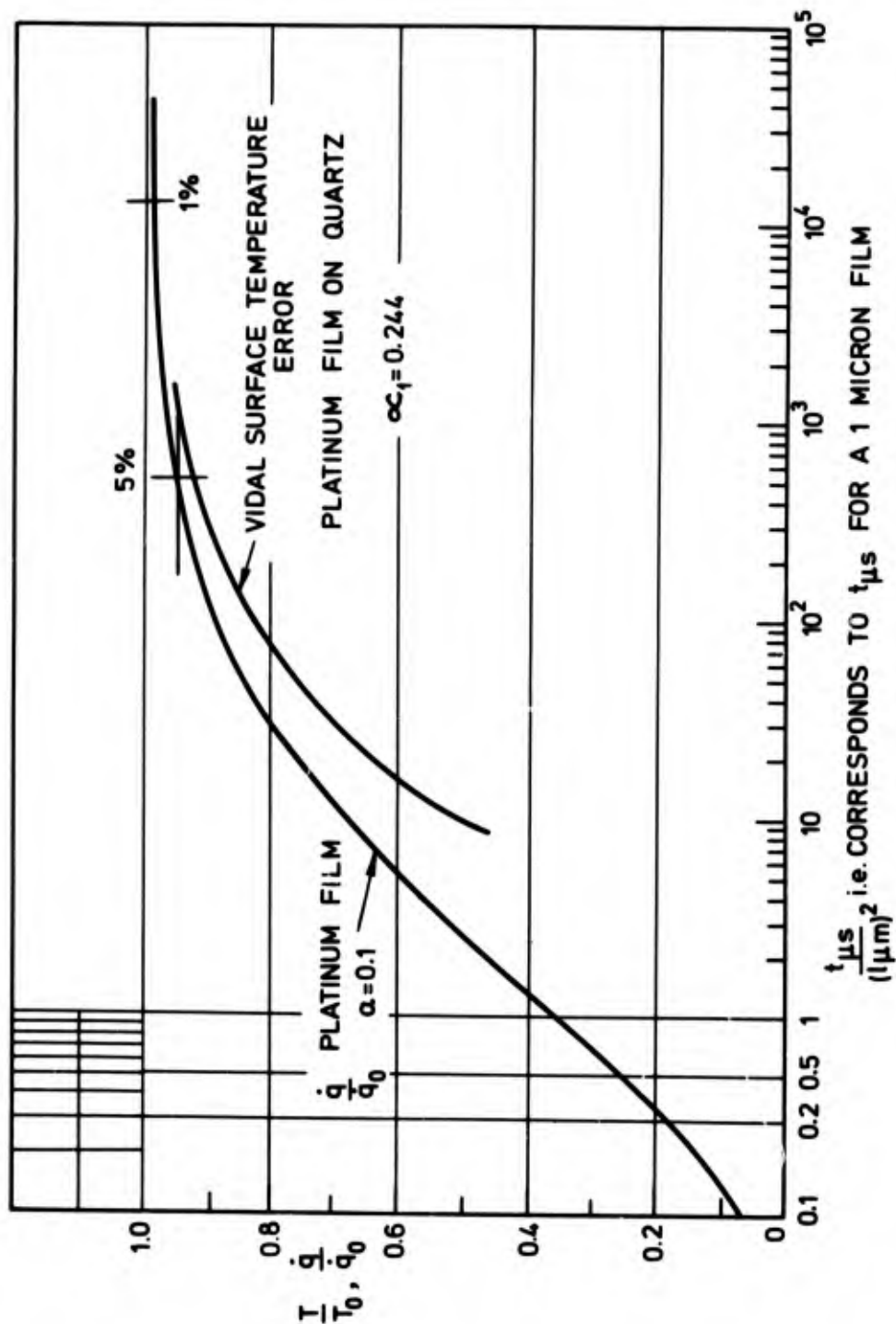


Fig.12

Effect of surface metallic film on heat transfer rate and surface temperature for a platinum film on quartz. \dot{q}/\dot{q}_0 and T/T_0 expressed in terms of the parameter $(t_{\mu s})/(l_{\mu m})^2$. \dot{q} = heat transfer rate deduced from the observed temperature rise assuming an homogeneous solid, Eq(20). \dot{q}_0 = amplitude of actual step function in heat transfer rate. T = observed temperature rise in presence of film. T_0 = temperature which would occur in absence of the surface film when solid is subjected to the same heat transfer rate, as calculated in section 2c. Vidal surface temperature error from (13).

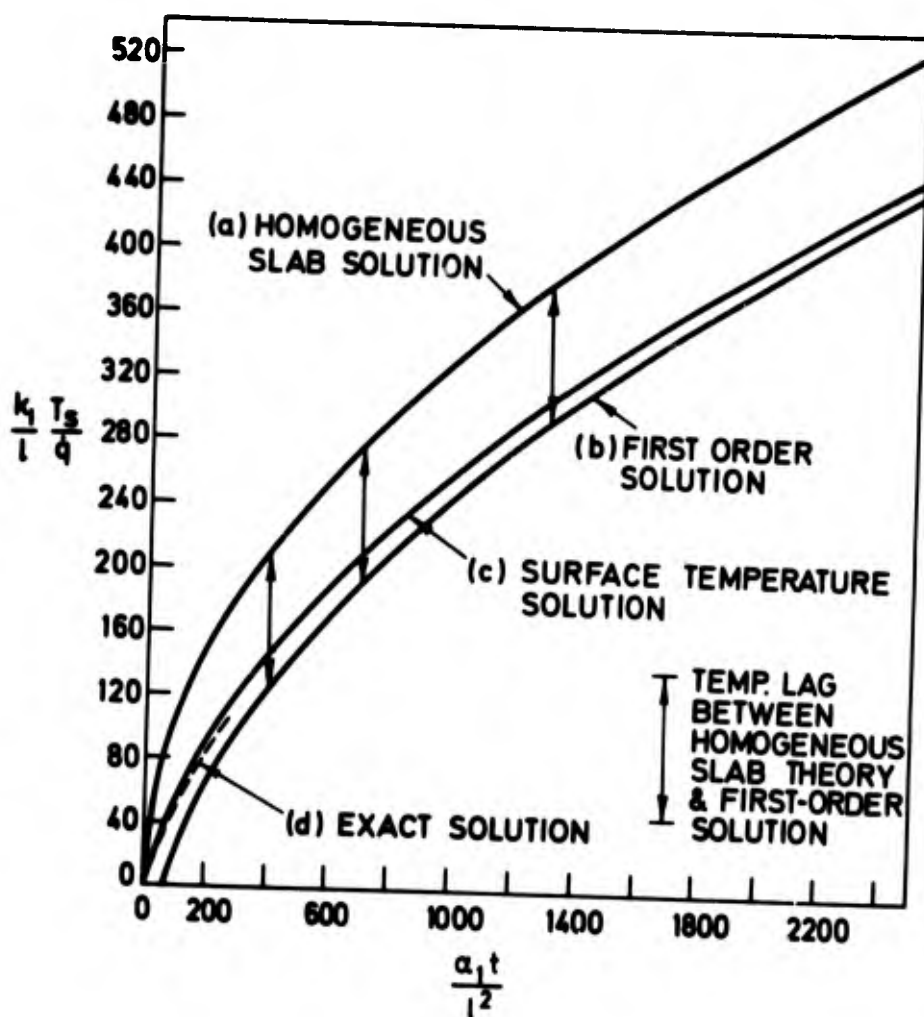


Fig.13

Transient temperatures in semi-infinite solids subjected to constant heat transfer rates. (a) Homogeneous solution calculated from Eq (21) for quartz substrate. (b) First order solution calculated from Eq(51) for platinum film on quartz substrate. (c) Surface temperature solution from Eq(48). (d) Exact solution calculated from Eq (49) with $x = l/2$ Redrawn from Vidal (13).

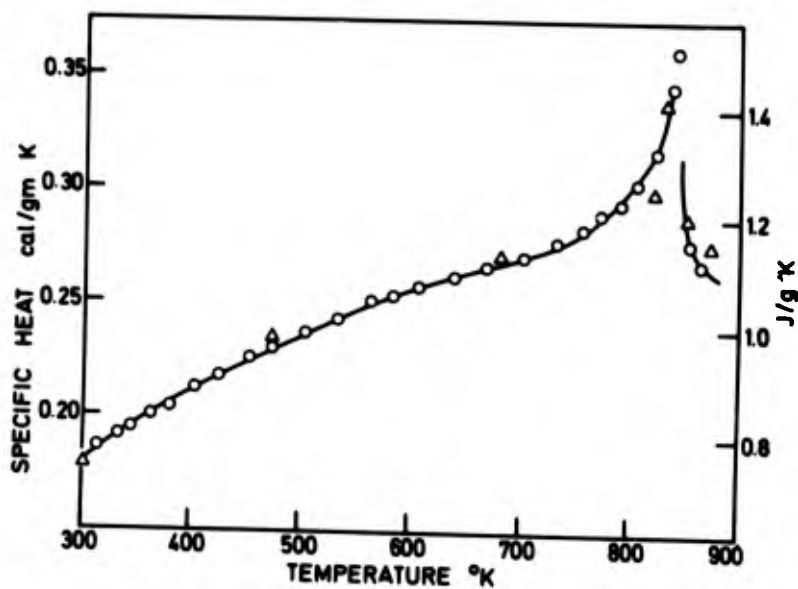


Fig.14

Specific heat of quartz between 300 and 900 K. Data selected as representative from TPRC (23). Increase at 850 corresponds to phase transformation.

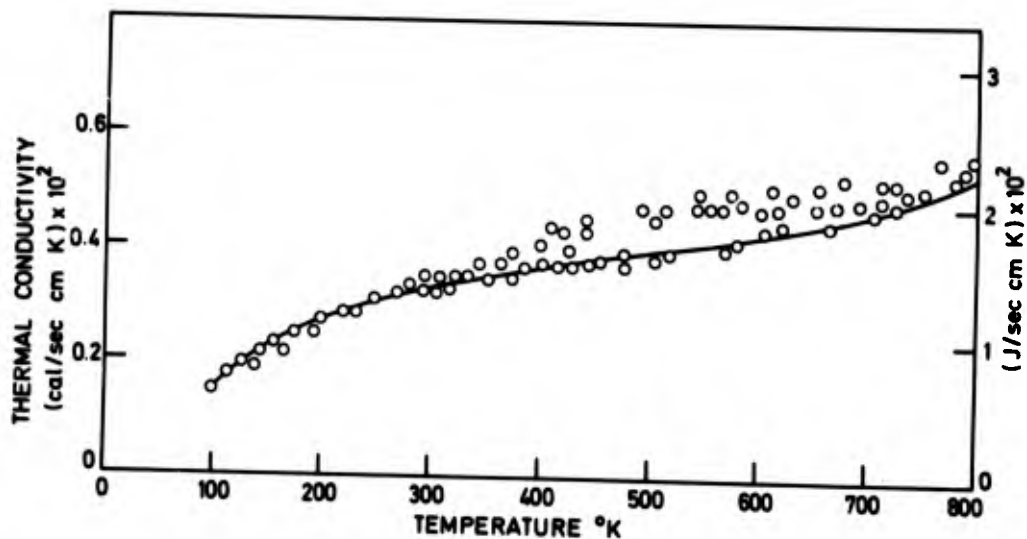


Fig.15

Thermal conductivity of quartz between 100 and 800 K. Data selected as representative from TPRC (23). Curve indicates current recommended values above 400 K.

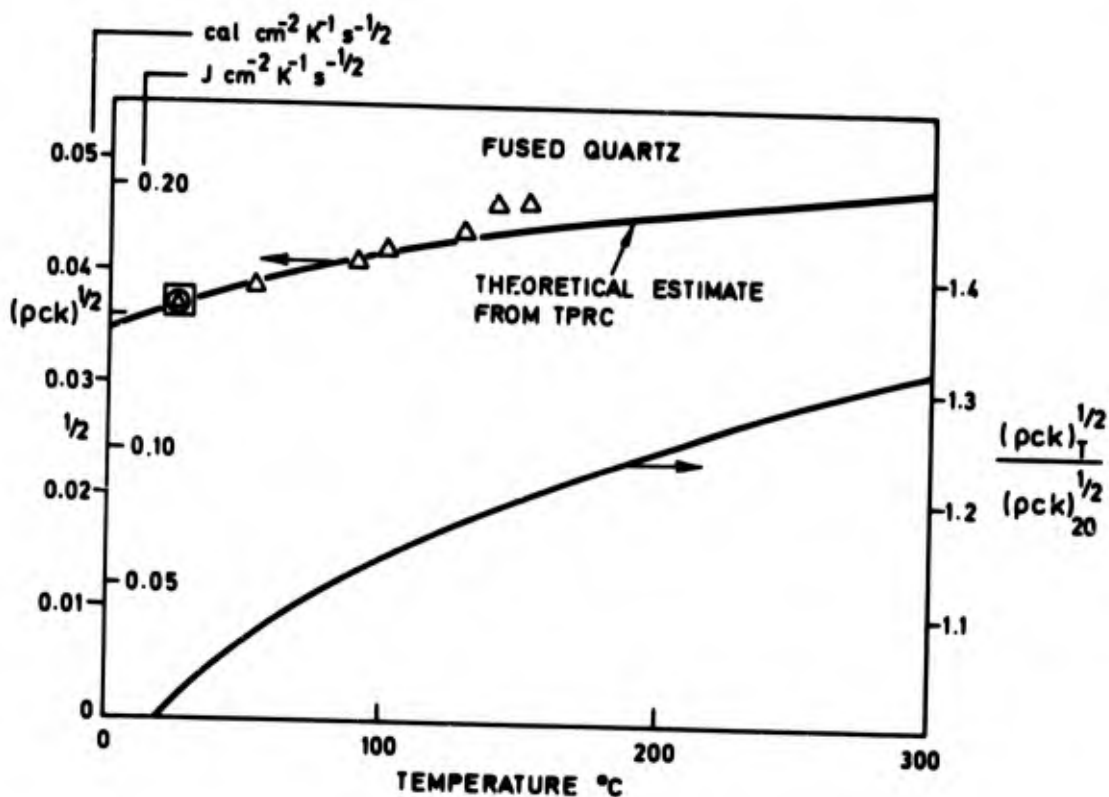


Fig.16

Variation with temperature of thermal product $\sqrt{(\rho ck)}$ for fused quartz. Theoretical estimate based on $\rho = 2.20 \text{ g cm}^{-3}$ and thermal properties from TPRC (23). Δ Hartunian and Varwig (24), \square Bogdan (25), \square Maulard (22).

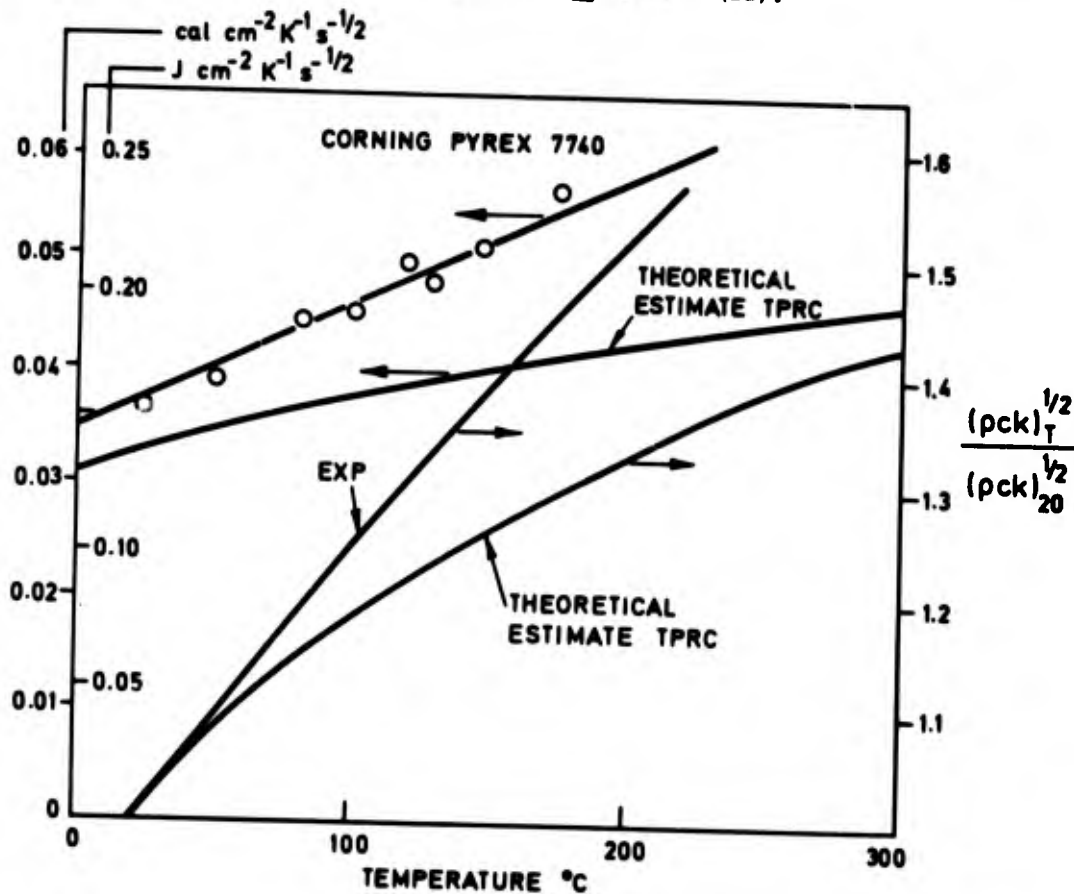


Fig.17

Variation with temperature of thermal product $\sqrt{(\rho ck)}$ for Corning Pyrex 7740. \circ Hartunian and Varwig (24). Theoretical estimates derived from thermal properties in TPRC (23).

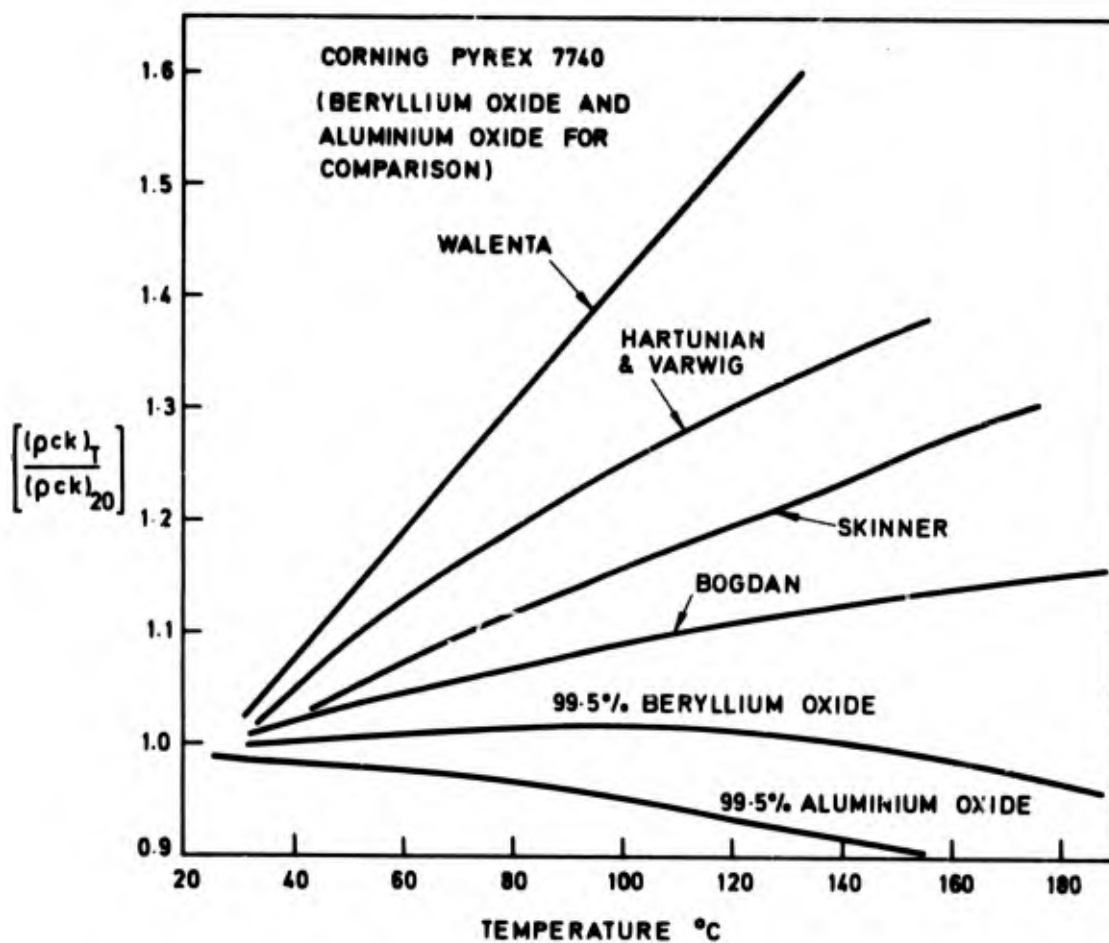


Fig.18

Variation of thermal product $(pck)^{1/2}$ of Pyrex with temperature. Data from Walenta (28), Hartunian and Varwig (24), Skinner (41) and Bogdan (29). Thermal product of BeO and Al_2O_3 calculated from manufacturer's information for 99.5% sample purity (Coors Ceramics).

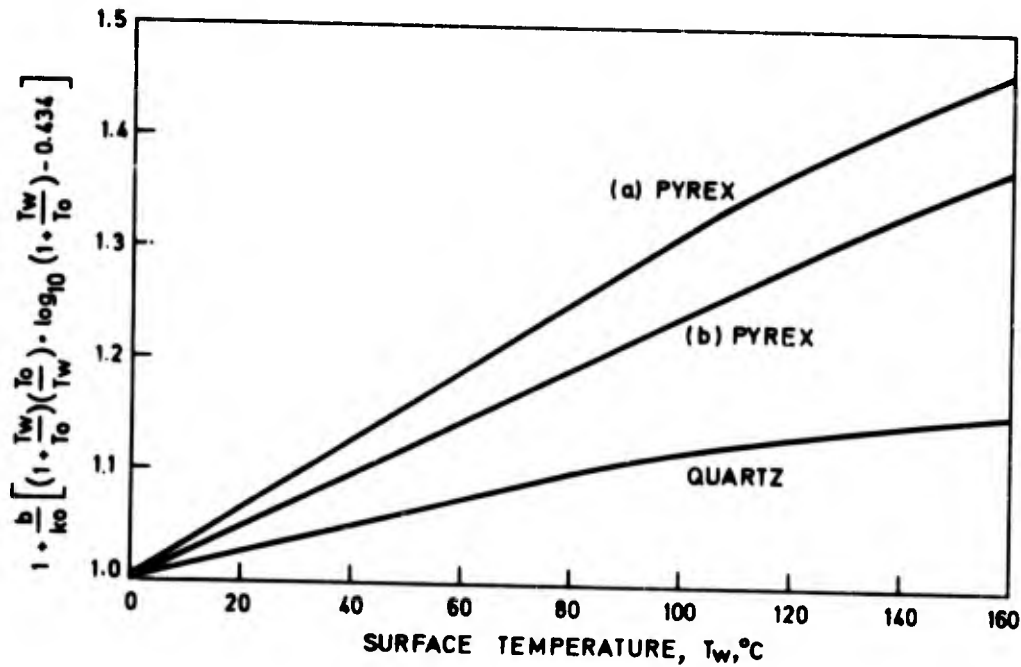


Fig.19

Correction factor for heat transfer rate as function of surface temperature proposed by Hartunian and Varwig (24) for Pyrex and quartz.

T_0 = initial temperature of substrate assumed to be 300 K,

T_w = wall temperature,

b = nonlinear factor in thermal conductivity equation of type $k = a + b \log_{10} T$

$b/k_0 = 4.73$ for Pyrex, 1.75 for quartz. k_0 is thermal conductivity at 300 K.

Curve (a) for Pyrex is that calculated by Hartunian and Varwig (24), curve (b) is a correction suggested by Reece (26), for constant heat transfer rate.

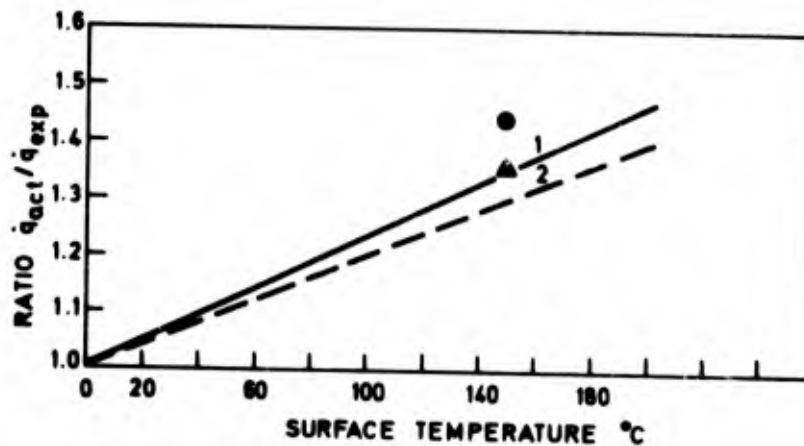
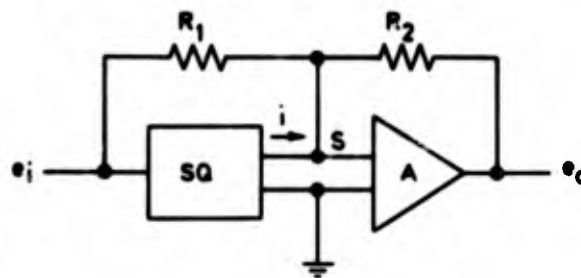


Fig.20

Correction factors $\dot{q}_{\text{actual}}/\dot{q}_{\text{exptl}}$ for heat transfer rates calculated by Cook (27) for Pyrex 7740. Initial conditions assumed are for $T_0 = 21^\circ\text{C}$. Curve (1) based on heat transfer rate varying as $t^{-1/2}$; curve (2) for constant heat transfer rate.

● = data point from Hartunian and Varwig (24) for Pyrex (see also Fig.19), ▲ = same data point corrected by Reece (26), both for $\dot{q} = \text{constant}$.



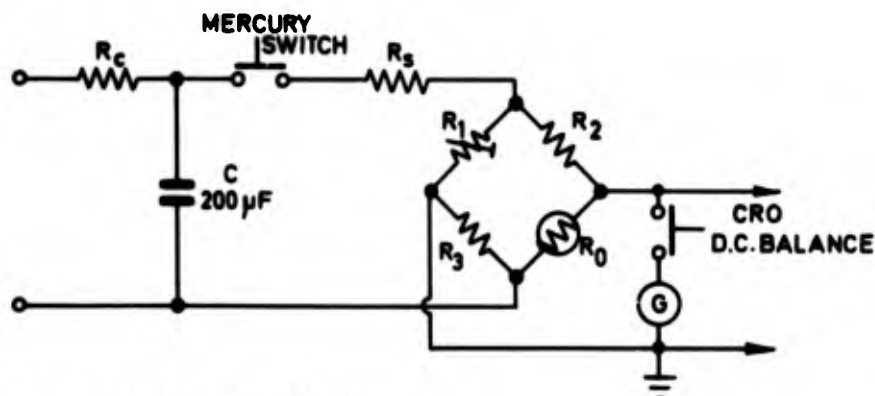
SQ SQUARING AMPLIFIER $i = k e_i^2$

A OPERATIONAL AMPLIFIER

S SUMMING JUNCTION

Fig.21

Compensation circuit proposed by Reece (26) for correction of effect of nonlinear thermal properties of thin film substrates.



$$C(R_s + R_2 + R_0) \sim 0.1 \text{ sec}$$

R_0 = FILM RESISTANCE

R_2, R_3 = FIXED BRIDGE RESISTANCES

R_1 = 4 DECADE VARIABLE RESISTANCE

R_s = SERIES RESISTANCE

IF BRIDGE IS INITIALLY BALANCED $R_1 R_0 = R_3 R_2$

$$\frac{\Delta V}{I_0} = \frac{\Delta R_0 R_1}{(R_1 + R_2 + R_3 + R_0) + \Delta R_0} \quad \frac{\Delta R_0}{R_0} = \alpha \Delta T$$

$$\dot{q} = \frac{I_0^2 R_0}{A} = \frac{\sqrt{\pi}}{2} \frac{\sqrt{p_{ck}}}{\sqrt{t}} \Delta T$$

$$\text{Thus } \frac{\alpha}{\sqrt{p_{ck}}} = \left[\frac{A \sqrt{\pi} I R}{2 I_0^3 R_0^2 R_1} \right] \frac{\Delta V}{\sqrt{t}} \quad \frac{\text{cm}^2 \text{ sec}^{1/2}}{\text{J}}$$

Fig.22

Circuit for the electrical discharge calibration of thin film resistance thermometer heat transfer gauges.

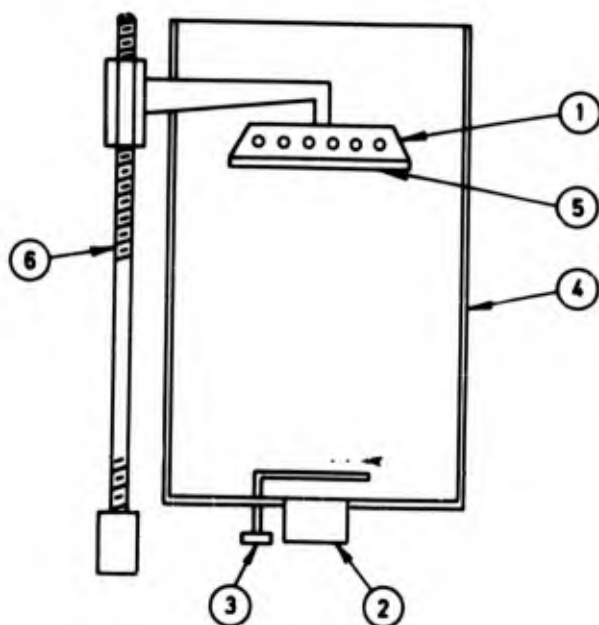


Fig.23

Schematic diagram of ONERA radiation calibration system for calorimeter gauges. (1) 2 kW quartz envelope tungsten filament lamps. (2) Transducer to be calibrated. (3) Fast acting shutter. (4) Non-reflecting water cooled enclosure. (5) Diffusing screen. (6) Height control. Redrawn from Maulard (32).

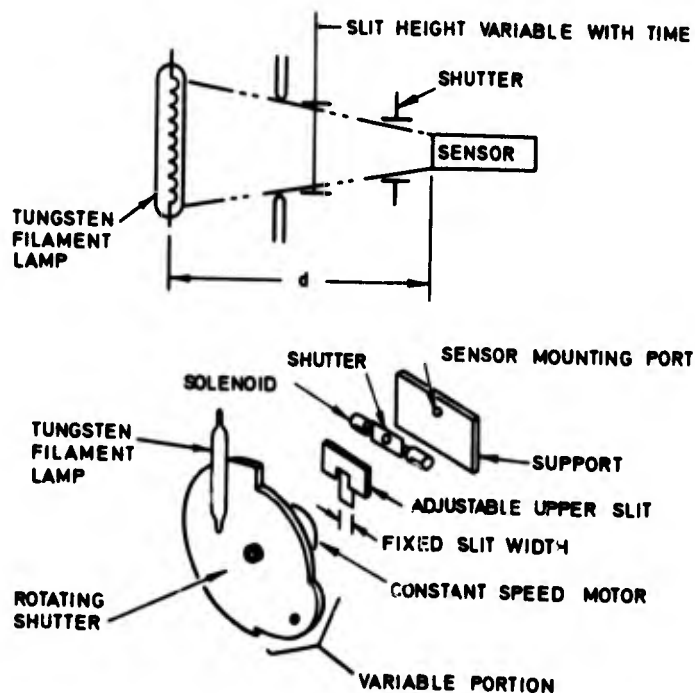


Fig.24

Radiation calibration method with rotating shutter of variable amplitude giving constant radiation flux or flux varying at $t^{-1/2}$. Redrawn from Schulte, Puronen and Dixon (33).

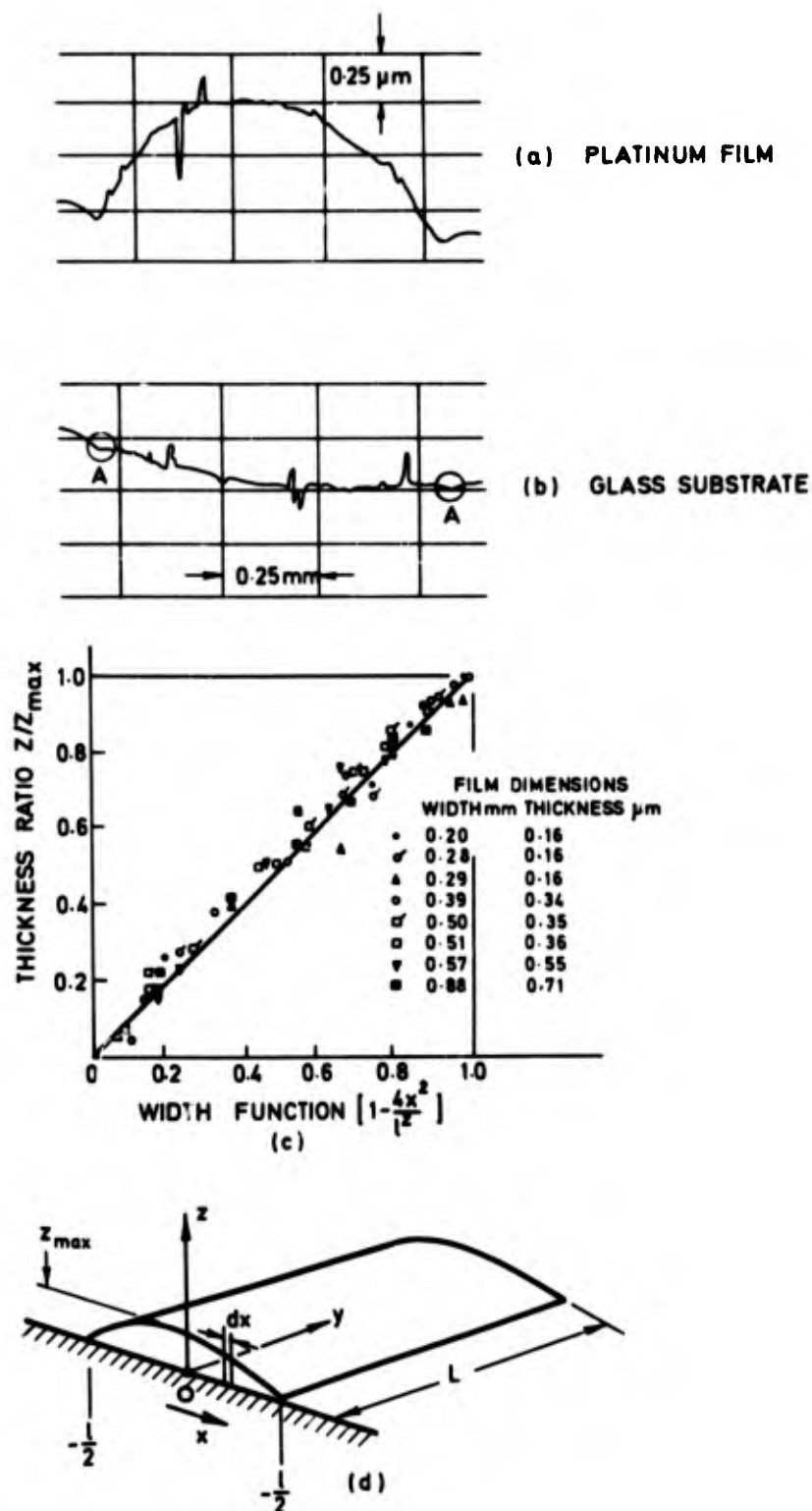


Fig.25

Thickness variation of metallic films deposited by the liquid bright platinum process. (a) Surface profile of substrate and film. (b) Profile of glass substrate after etch removal of film. (c) Thickness ratio Z/Z_{\max} , as function of $(1 - 4x^2/l^2)$ demonstrating parabolic profile sketched in coordinate system (d) for analysis of effect of non-uniformity on accuracy of electrical discharge calibration. Redrawn from Busing (21).

1. Cooled guard ring
2. Metal calorimeter disc
3. Water inlet hose
4. Thermocouple cold junction
5. Water outlet
6. Thermocouple hot junction
7. Insulated Perspex tank
8. Stirrer
9. Stirrer motor

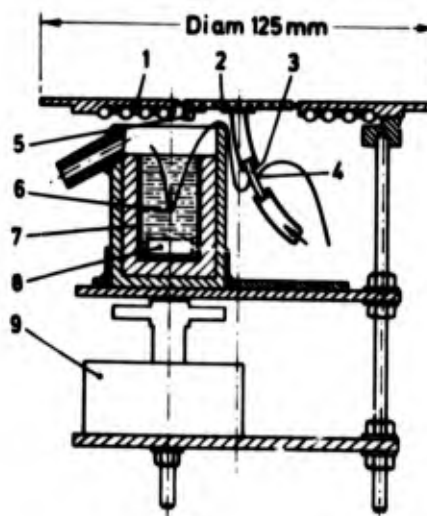


Fig.26

Reference water calorimeter for use as 'standard' in radiation calibration of thin film resistance thermometers and calorimeter heat transfer gauges. Redrawn from Maulard (35).

1. Rhodium plated platinum support pins
2. Copper calorimetric disc
3. Chromel-alumel thermocouple wires 0.3 mm diam.
4. Internally polished brass sleeve
5. Terminals

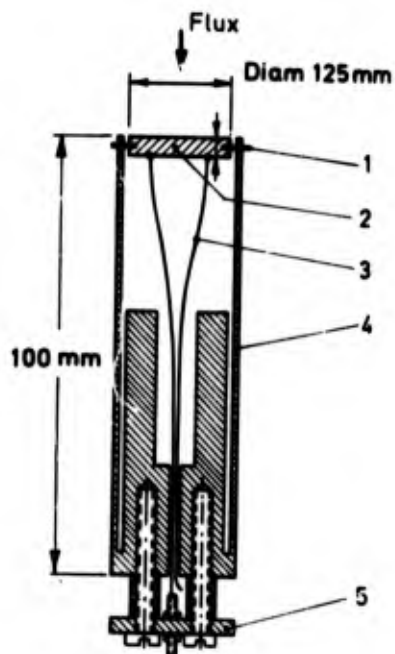


Fig.27

'Standard' thermal inertia calorimeter for radiation calibration of thin film resistance thermometer and other calorimeter transducers. Redrawn from Maulard (35).

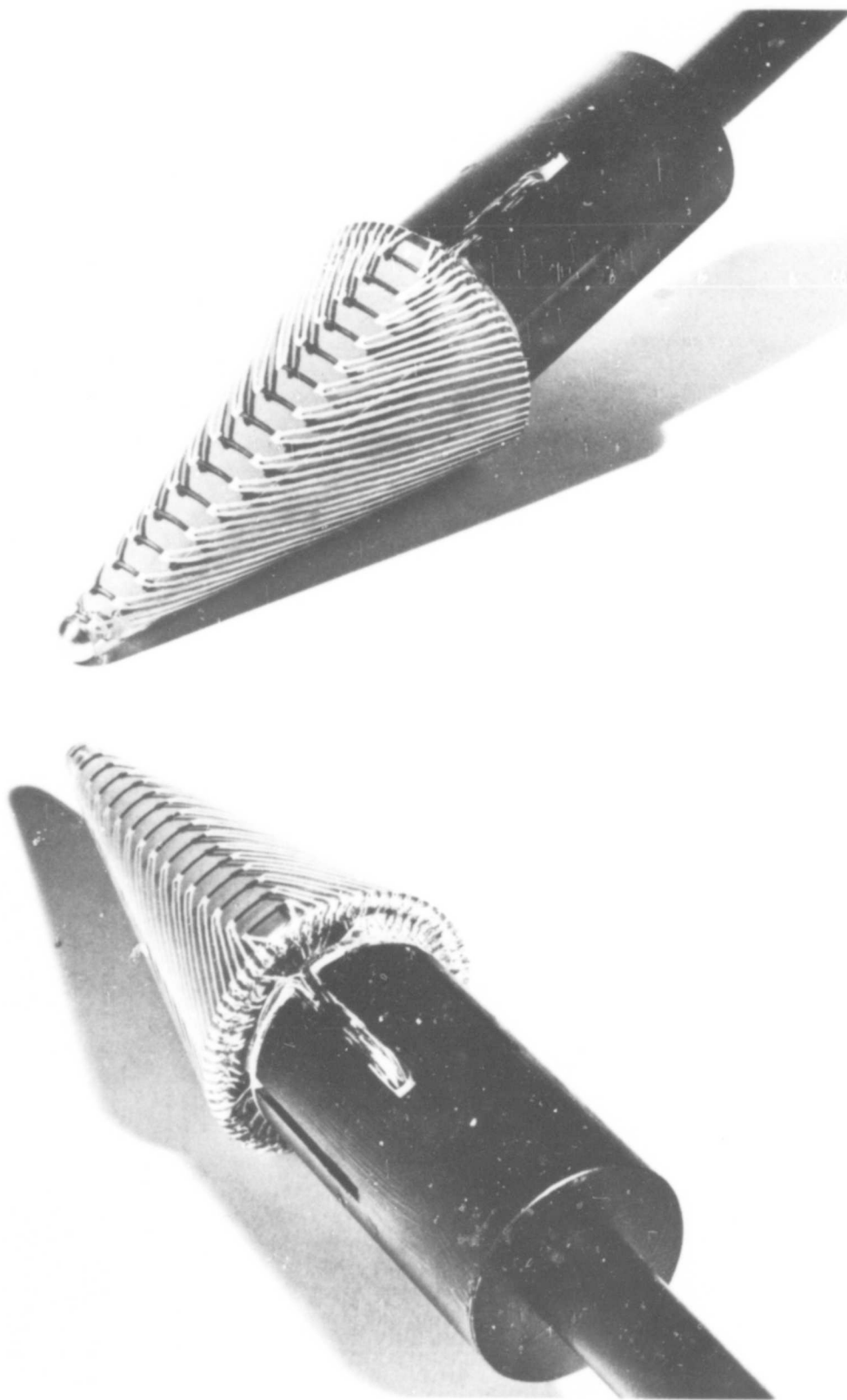


Fig. 26

Model construction for thin film resistance thermometer gauges illustrating use of separate current and voltage leads. Thin films in liquid bright platinum and leads in thick conducting silver paste with external connections (lower) at rear of model. Franco-German Research Institute, Saint Louis.

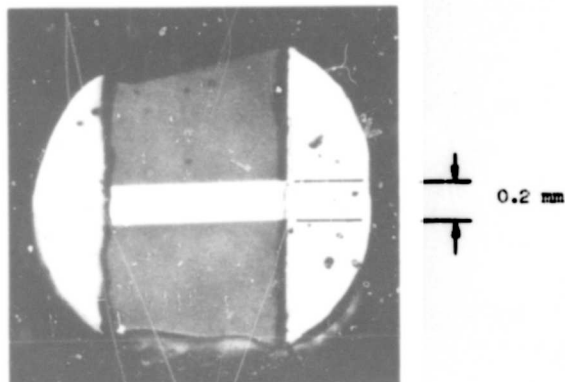


Fig.29

Nickel film deposited on quartz substrate by R.F. sputtering with SiO insulating layer. The active portion of the film is isolated from the edge of the substrate by a low resistance lead, DISA Coy, Herlev, Denmark.

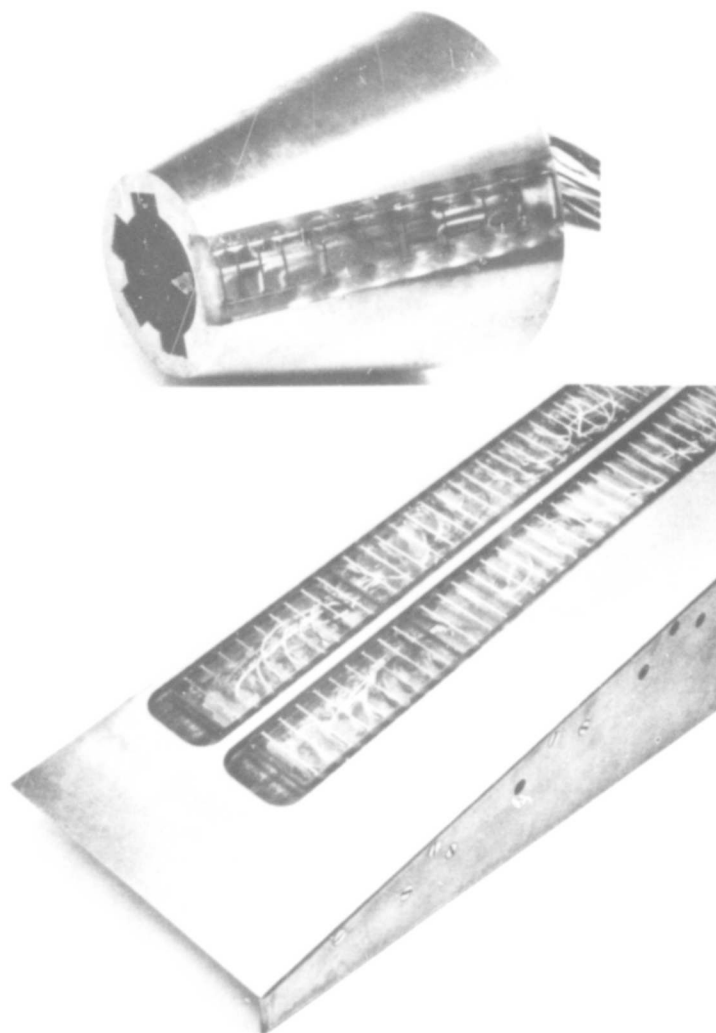
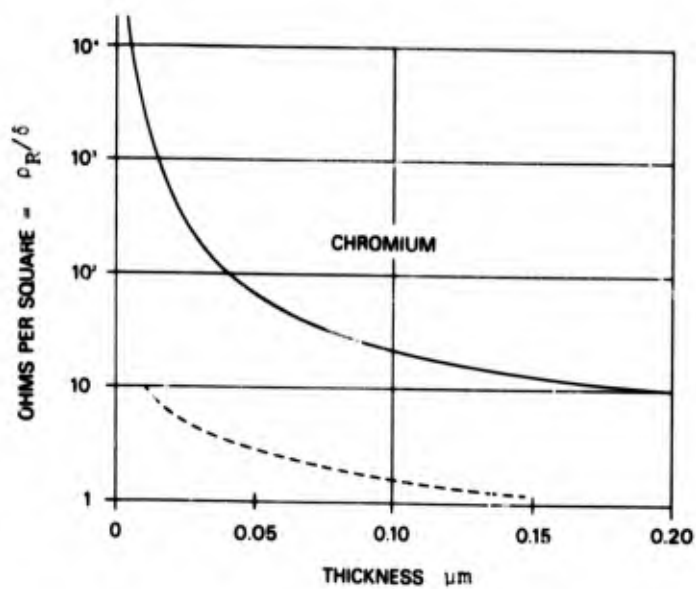
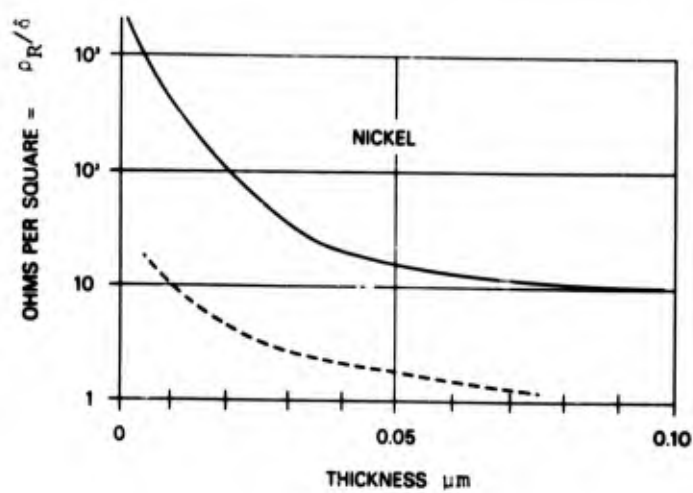


Fig.30

(a) Thin film gauges produced by the liquid bright platinum process mounted on quartz substrate which has been optically polished to model contour. The insert is set into the model with Epoxy resin.
(b) Flat plate instrumented with thin films on quartz substrate. In both cases (a) and (b) the active section of the thin film gauge is isolated from the 'cold' model by a poor thermal conductor.



(a)



(b)

Fig.31

Effect of film thickness on electrical resistance per square.
 - - - - Computed values based on resistivity of bulk material.
 Redrawn from Winding, Topper and Baus (38) with mean curve
 shown for all substrates tested.

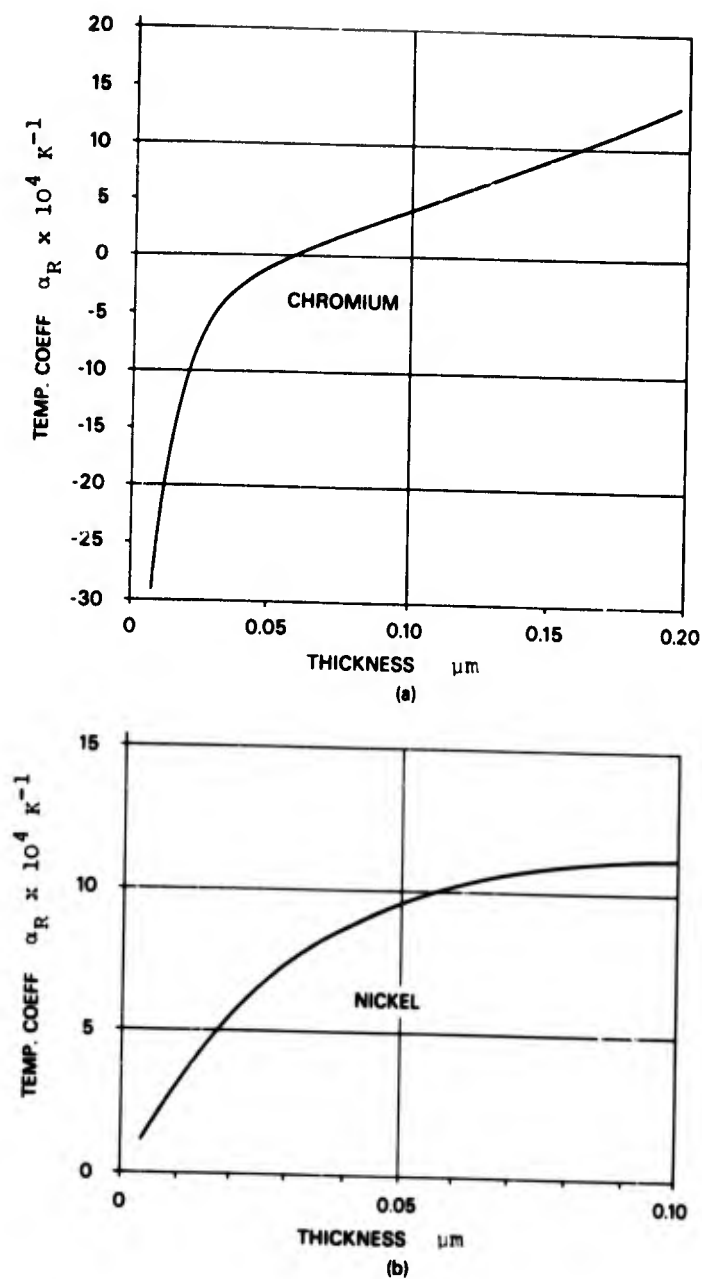


Fig.32

Effect of film thickness on temperature coefficient of resistance of chromium and nickel films at 20°C. Mean curves drawn through data of Winding, Topper and Baus (38)

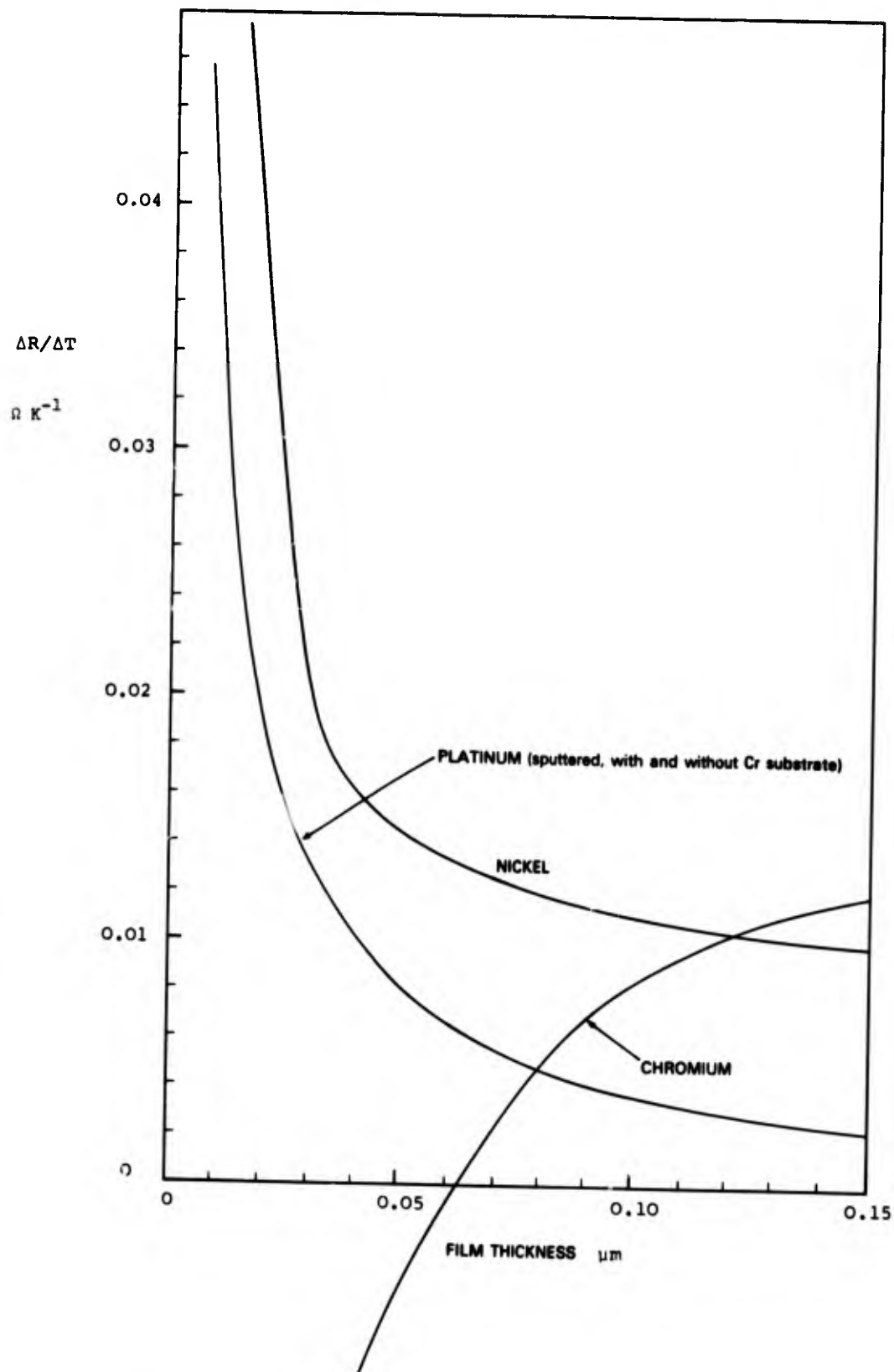
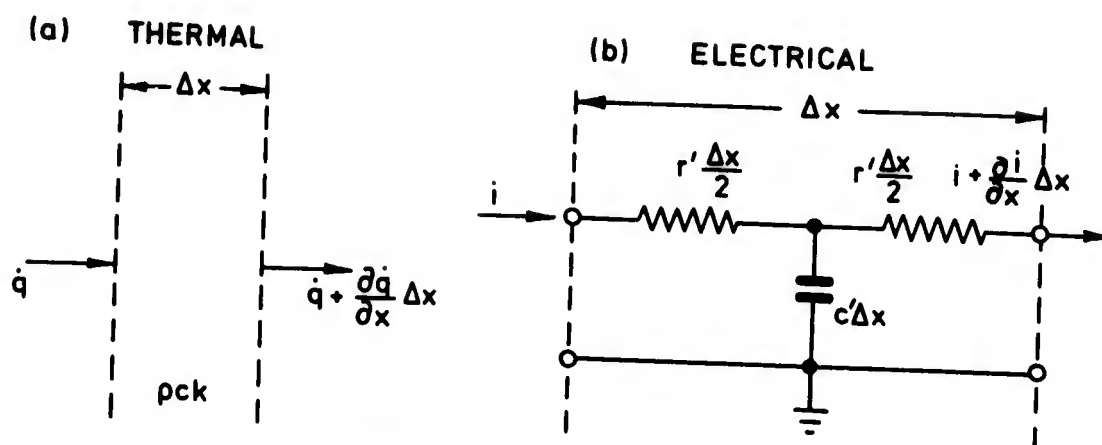


Fig.33

Effect of film thickness δ on temperature sensitivity $\Delta R/\Delta T$, ΩK^{-1} , for sputtered platinum, evaporated nickel and evaporated chromium. Calculated for a square deposit in which $\Delta R/\Delta T = \rho_R \alpha_R / \delta$.



Rate of gain of energy in element Δx

$$= -\frac{\partial \dot{q}}{\partial x} \Delta x$$

which by conservation of energy

$$= \rho c \Delta x \frac{\partial T}{\partial t}$$

Thus

$$\frac{\partial \dot{q}}{\partial x} = -\rho c \frac{\partial T}{\partial t}$$

The conduction equation is:

$$\dot{q} = -k \frac{\partial T}{\partial x}$$

Combining the above Eqs the diffusion equation is obtained:

$$\frac{\partial^2 T}{\partial x^2} = \frac{\rho c}{k} \frac{\partial T}{\partial t}$$

Rate of gain of charge in element Δx

$$= -\frac{\partial i}{\partial x} \Delta x$$

which by conservation of charge

$$= c' \Delta x \frac{\partial V}{\partial t}$$

Thus

$$\frac{\partial i}{\partial x} = -c' \frac{\partial V}{\partial t}$$

Ohm's law is:

$$i = -\frac{1}{r' \Delta x} \frac{\partial V}{\partial x} \Delta x = -\frac{1}{r'} \frac{\partial V}{\partial x}$$

Combining the above Eqs the transmission line equation is obtained

$$\frac{\partial^2 V}{\partial x^2} = r' c' \frac{\partial V}{\partial t}$$

Fig. 34

Derivation of the electrical analogue of heat conduction.

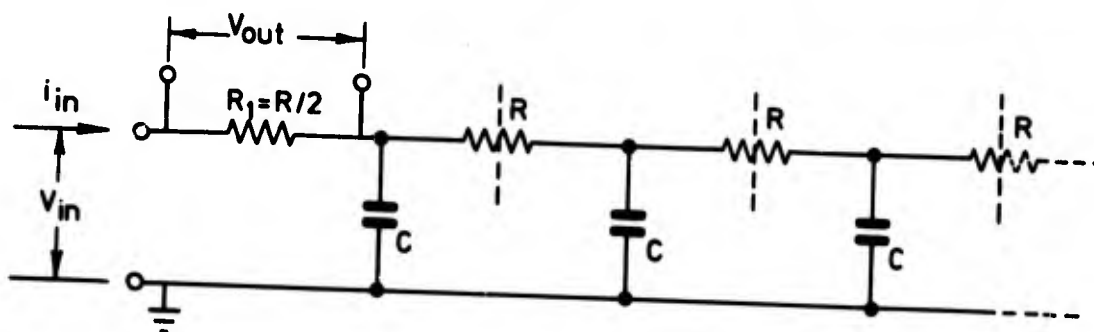


Fig. 35

Electrical analogue using equal sections representing an homogeneous heat conductor.

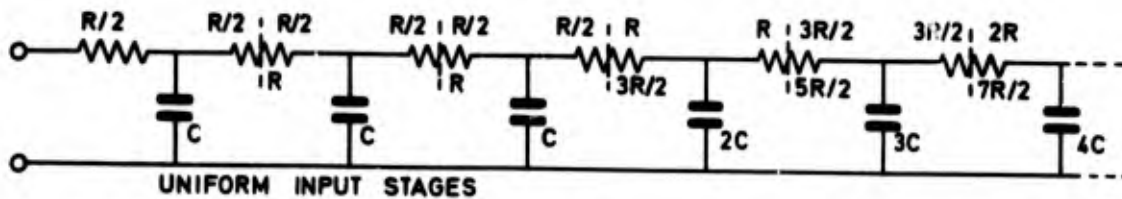


Fig.36(a) Analogue circuit proposed by Meyer (44,45) with component values increasing arithmetically.

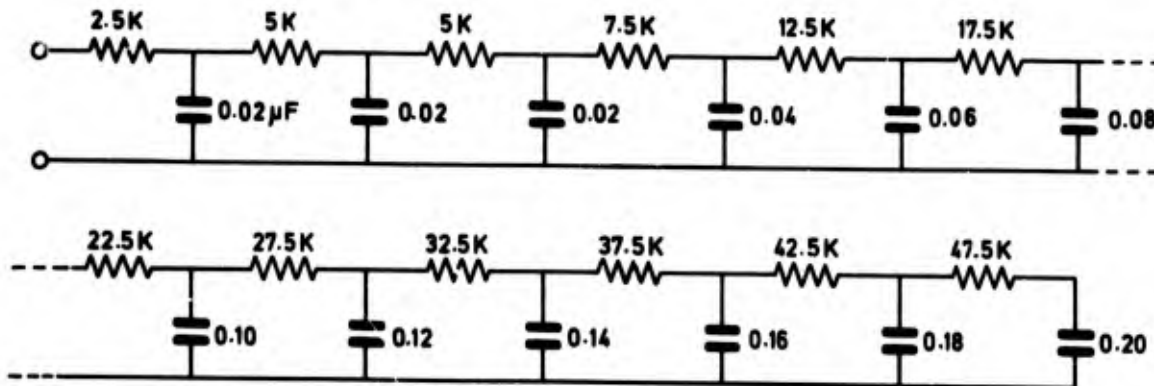


Fig.36(b) Practical analogue circuit for use with gun tunnel. Operating time 100 μ s to 50 ms. Sensitivity when used with platinum films on Pyrex 65 μ V per W/cm^2 .

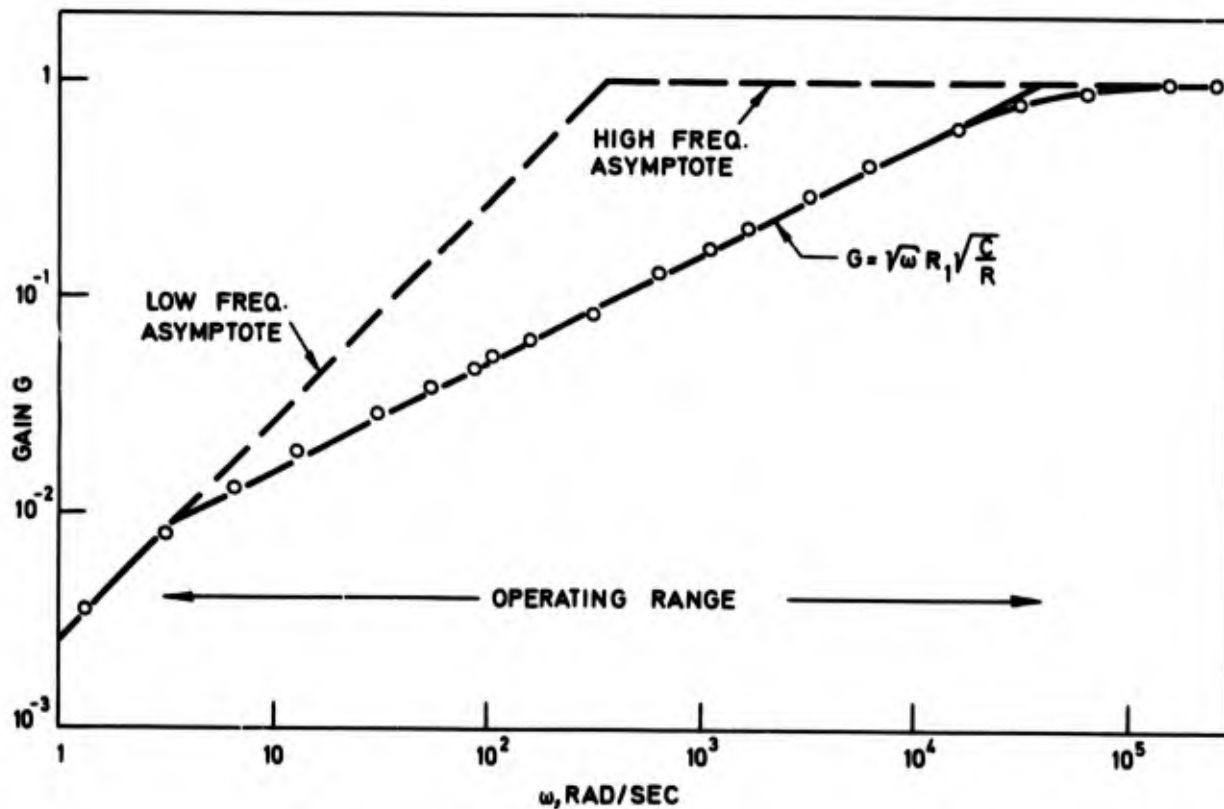


Fig.37 Frequency response of Meyer analogue circuit with sections increasing arithmetically, Fig.36(b). Useful frequency range $5 - 2 \times 10^4$ R/s.

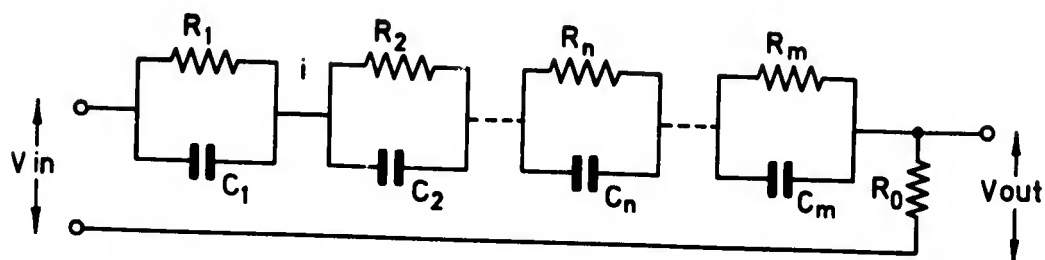


Fig.38

Schematic diagram of filter network proposed by Skinner (41) for data reduction of signals from thin film surface temperature gauges.

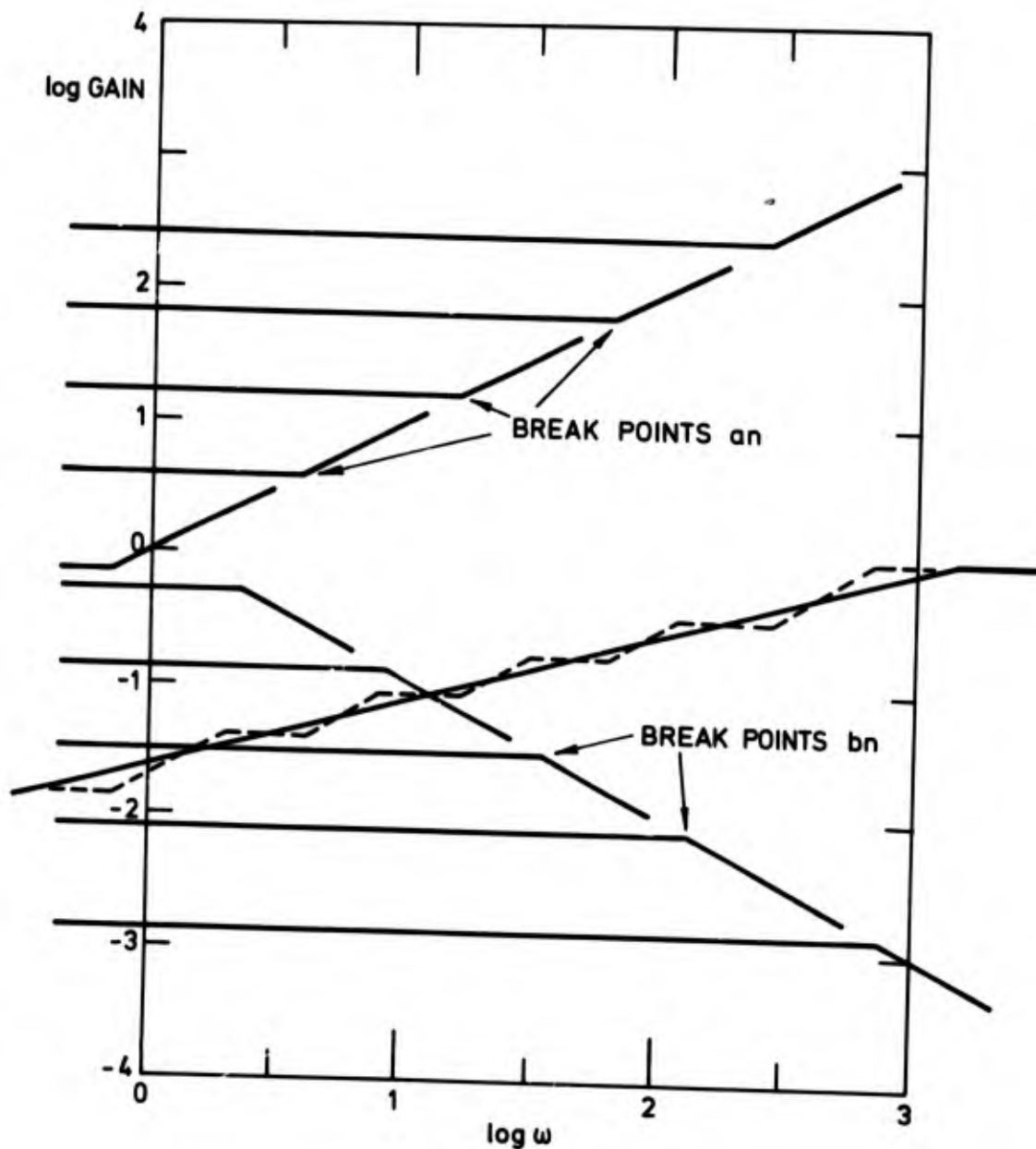
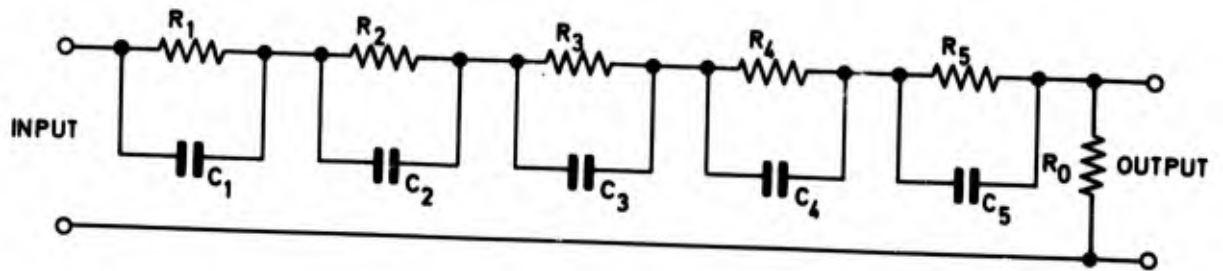


Fig.39

Bode diagram illustrating frequency response of 5 - section filter network. Break points a_n arise from zeroes and break points b_n arise from poles of transfer function, Eq(93). The dotted line represents the summation of the asymptotic lines a_n and b_n which have resultant slope, shown by the solid line, of +10 dB/decade.



5 section network

R_1 (ohms)	4.966401×10	C_1 (microfarads)	2.909726×10^{-2}
R_2 "	8.503515	C_2 "	2.939961×10^{-2}
R_3 "	4.285704	C_3 "	1.458337×10^{-2}
R_4 "	2.142304	C_4 "	7.293549×10^{-3}
R_5 "	1.149405	C_5 "	3.398497×10^{-3}

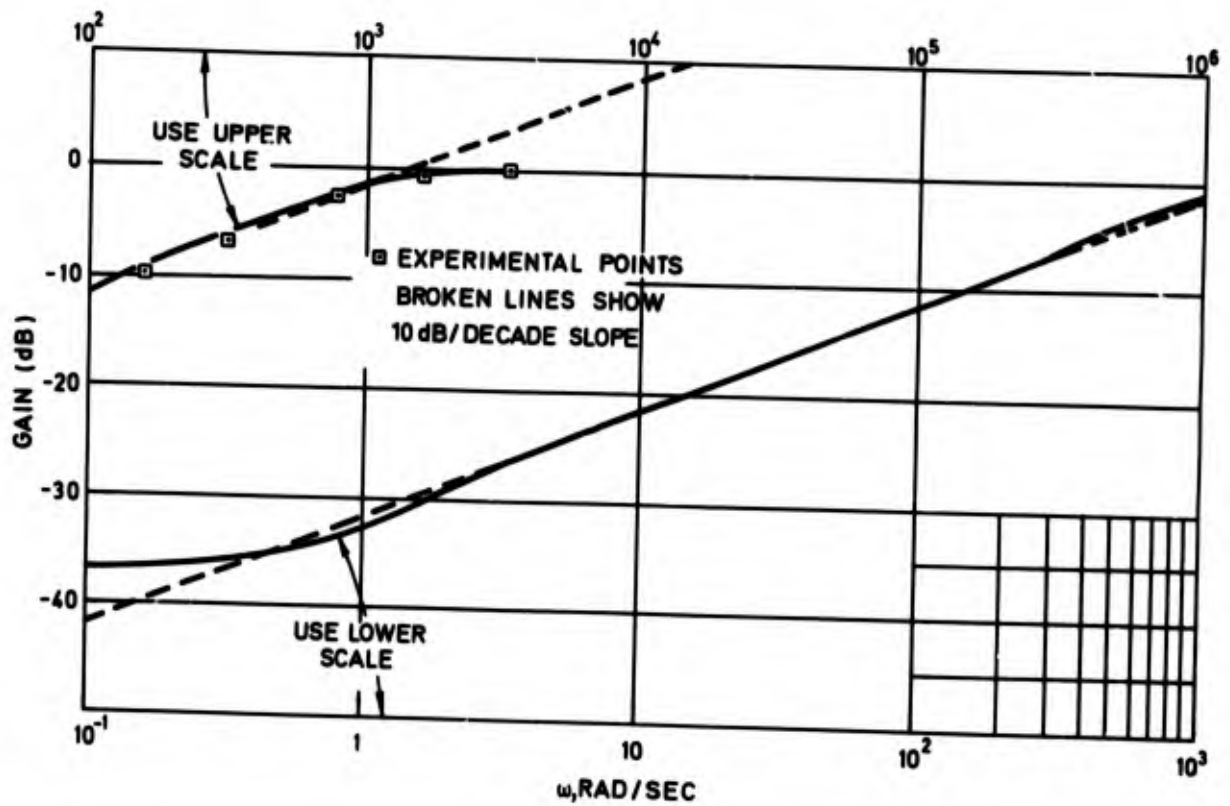
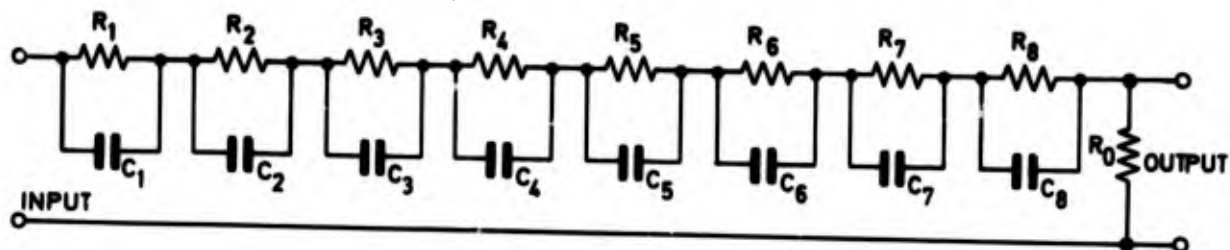


Fig.40

Component design and amplitude response of 5 - section filter network. Useful bandwidth 1 to 10^3 Rad/s. Redrawn from Skinner (41).



8 - section network

R_1 (ohms)	3.870281×10^2	C_1 (microfarads)	3.691131×10^{-3}
R_2 "	6.750660×10	C_2 "	3.703341×10^{-3}
R_3 "	3.397350×10	C_3 "	1.839669×10^{-3}
R_4 "	1.696983×10	C_4 "	9.207518×10^{-4}
R_5 "	8.480326	C_5 "	4.606250×10^{-4}
R_6 "	4.237072	C_6 "	2.304805×10^{-4}
R_7 "	2.117516	C_7 "	1.152957×10^{-4}
R_8 "	1.131264	C_8 "	5.395305×10^{-5}

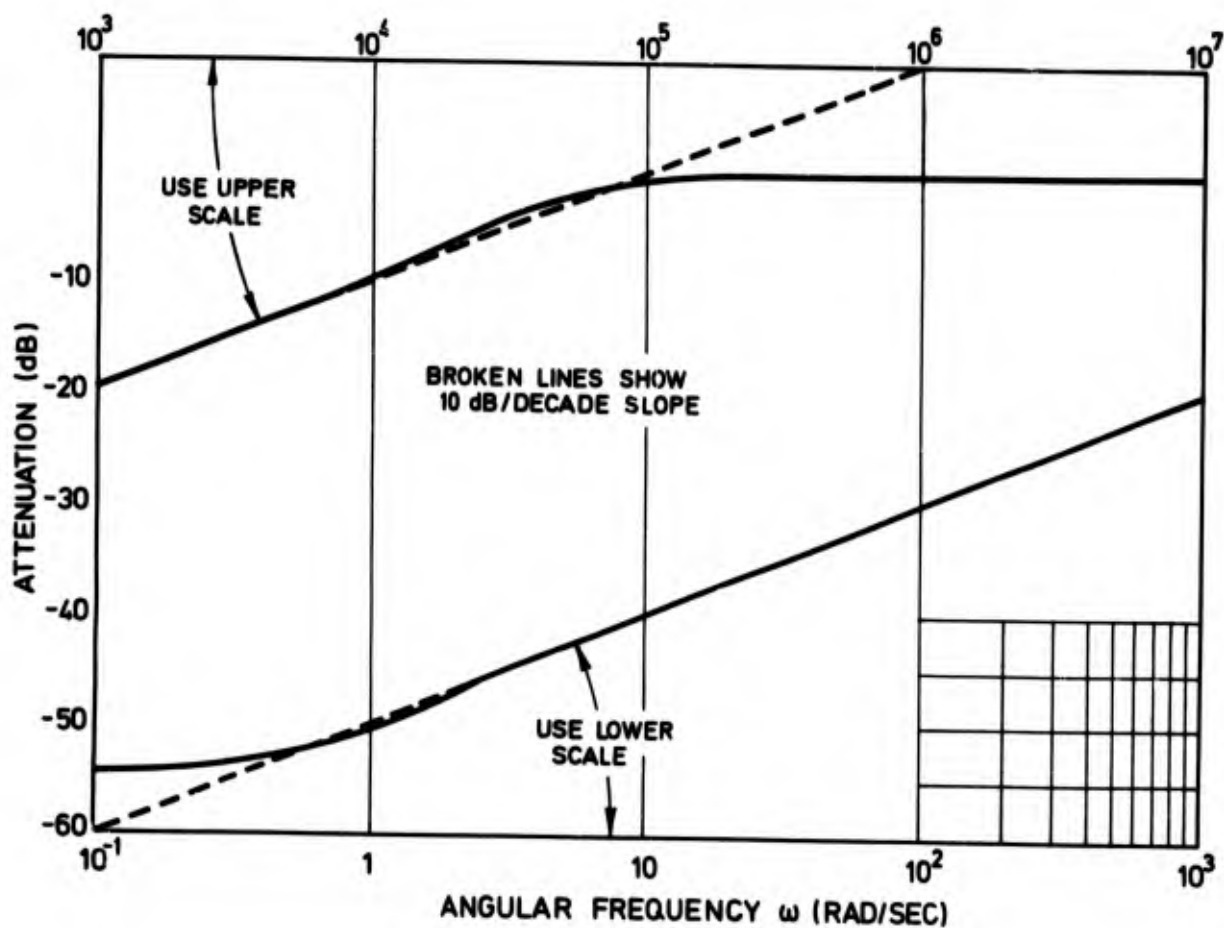
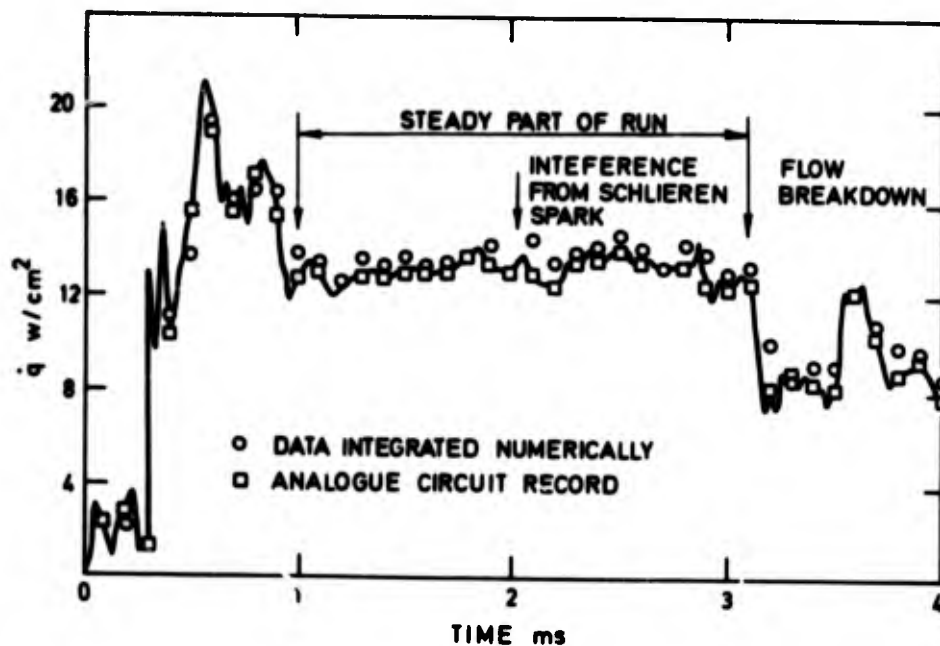
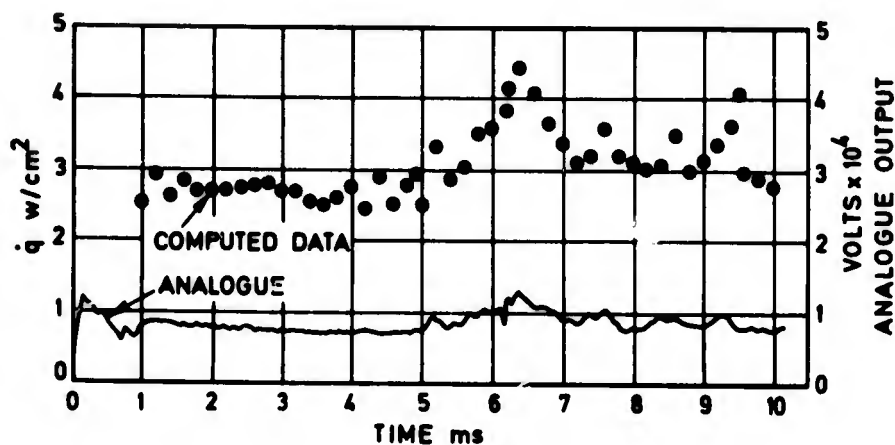


Fig. 41

Component design and amplitude response of 8 - section filter network with useful bandwidth from 1 to 10^5 Rad/s. Redrawn from Skinner (41).



(a)

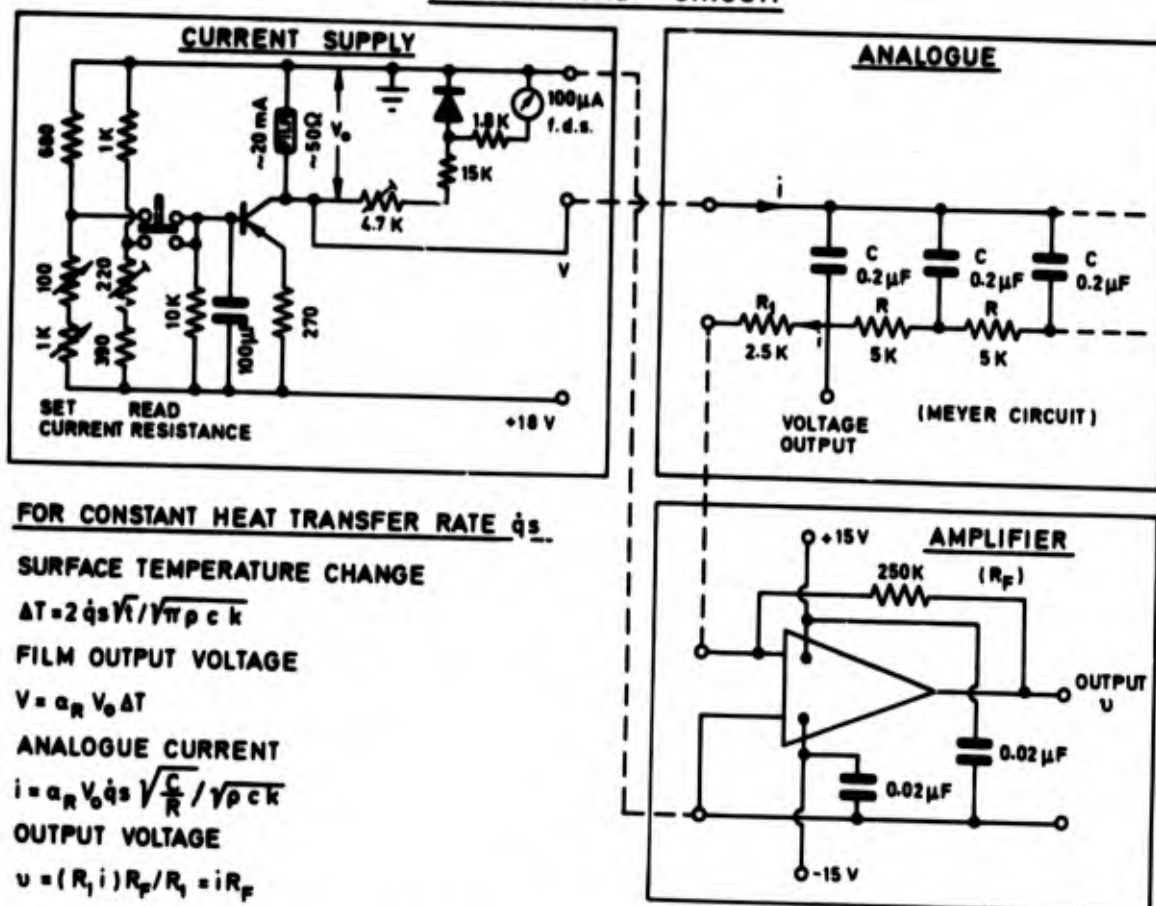


(b)

Fig.42

(a) Comparison of heat transfer rate data derived by numerical integration of Eq(74) and record from 8 - section filter network. Heat transfer to model in CAL shock tunnel. Redrawn from Skinner (41). (b) Computed heat transfer data compared with output of 32 - section equal element analogue circuit. Analogue sensitivity $32.5 \mu\text{V}$ per W cm^{-2} . Record from flat plate in NPL shock tunnel, $M = 7$. Redrawn from Schultz (126) with permission of the Institution of Mechanical Engineers, London.

(a) PRACTICAL CIRCUIT



FOR CONSTANT HEAT TRANSFER RATE \dot{q}_s

SURFACE TEMPERATURE CHANGE

$$\Delta T = 2 \dot{q}_s \sqrt{t} / \sqrt{\pi \rho c k}$$

FILM OUTPUT VOLTAGE

$$V = \alpha_R V_0 \Delta T$$

ANALOGUE CURRENT

$$i = \alpha_R V_0 \dot{q}_s \sqrt{\frac{C}{R}} / \sqrt{\pi \rho c k}$$

OUTPUT VOLTAGE

$$u = (R_1 i) R_F / R_1 = i R_F$$

(b) TYPICAL OUTPUTS

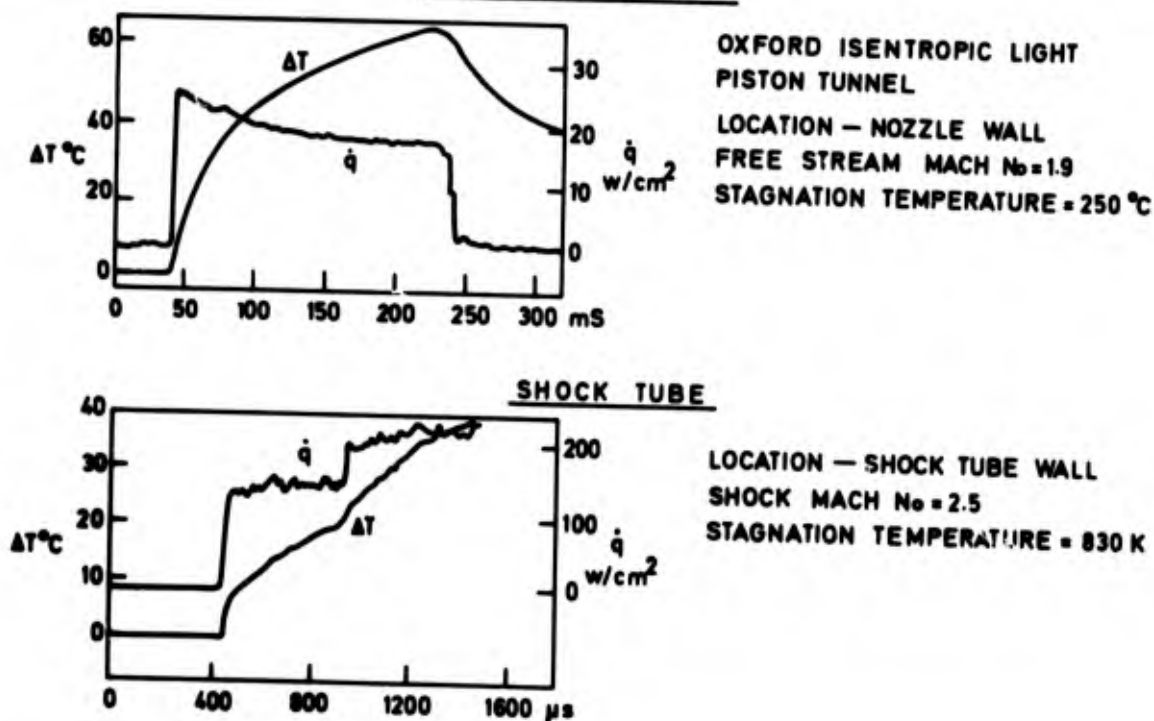
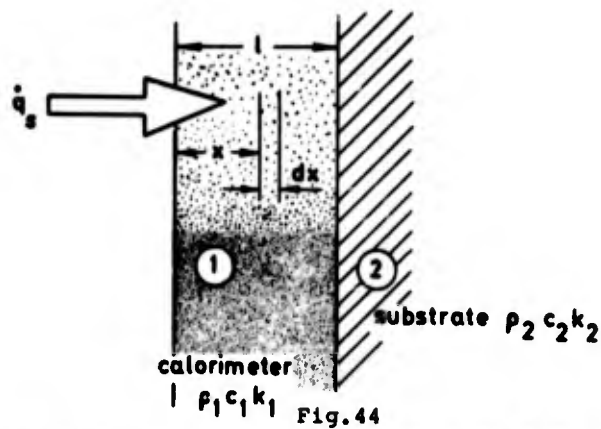


Fig.43

- (a) Transistor constant current supply for thin film resistance thermometers, analogue circuit and current-to-voltage converter.
- (b) Typical signals from thin film gauges in long run time facility and shock tube together with analogue heat transfer outputs.



Model for heat conduction in calorimeters


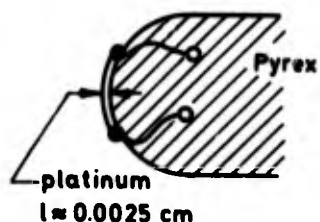
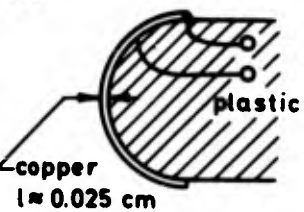
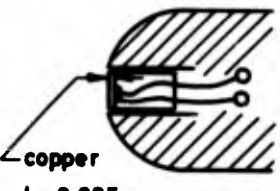
<p>(a)</p>  <p>stainless steel $l \approx 0.0254 \text{ cm}$</p>	<p>continuous 'thin skin' with air backing.</p>	<p>local temperature measured by a thermocouple within the wall, Chevallier (58), or at rear surface, Harvey (63).</p>
<p>(b)</p>  <p>Pyrex platinum $l \approx 0.0025 \text{ cm}$</p>	<p>localised calorimeter on Pyrex support.</p>	<p>mean temperature determined by measuring film resistance, Rose (20).</p>
<p>(c)</p>  <p>plastic copper $l \approx 0.025 \text{ cm}$</p>	<p>continuous skin on plastic backing</p>	<p>local temperature measured by thermocouple at rear surface, Starner and Varwig (64).</p>
<p>(d)</p>  <p>copper $l \approx 0.025 \text{ cm}$</p>	<p>isolated calorimeter with air backing.</p>	<p>local temperature measured by thermo- couple, thin film or semiconductor resistance thermometer on rear surface, Ledford (67, 68) Maulard (35), Kipke (69).</p>

Fig. 45

Typical calorimeters and methods of temperature measurement.

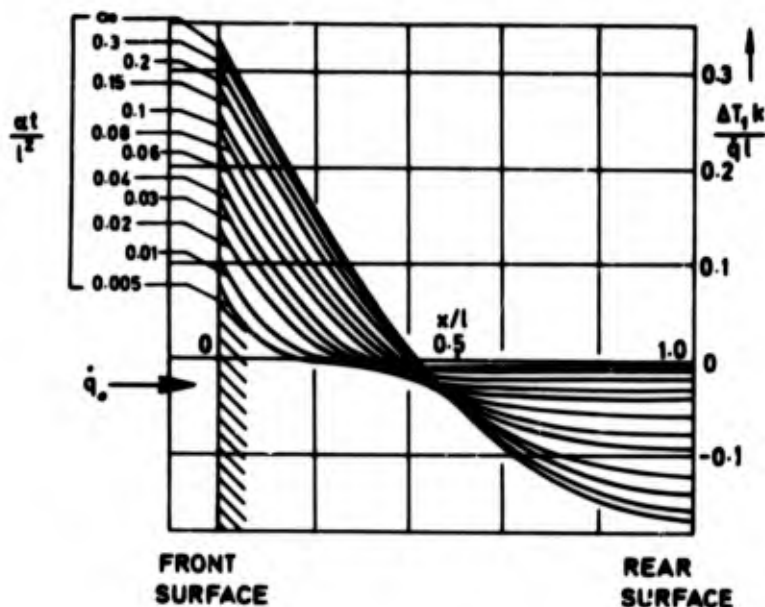


Fig. 46

The difference, ΔT_1 , between the temperature at a position x and the mean temperature in a slab when subjected to a constant heat transfer rate \dot{q}_0 there being no loss from the rear of the slab. Shown in non-dimensional form, $\Delta T_1 k / (\dot{q}_0 l)$, as a function of position, x/l , for given times at/l^2 . Thus $T_1 = T_{\text{mean}} + \Delta T_1$ where T_{mean} is given by $T_{\text{mean}} = \dot{q}_0 t / (\rho c l)$. After Carslaw and Jaeger (46).

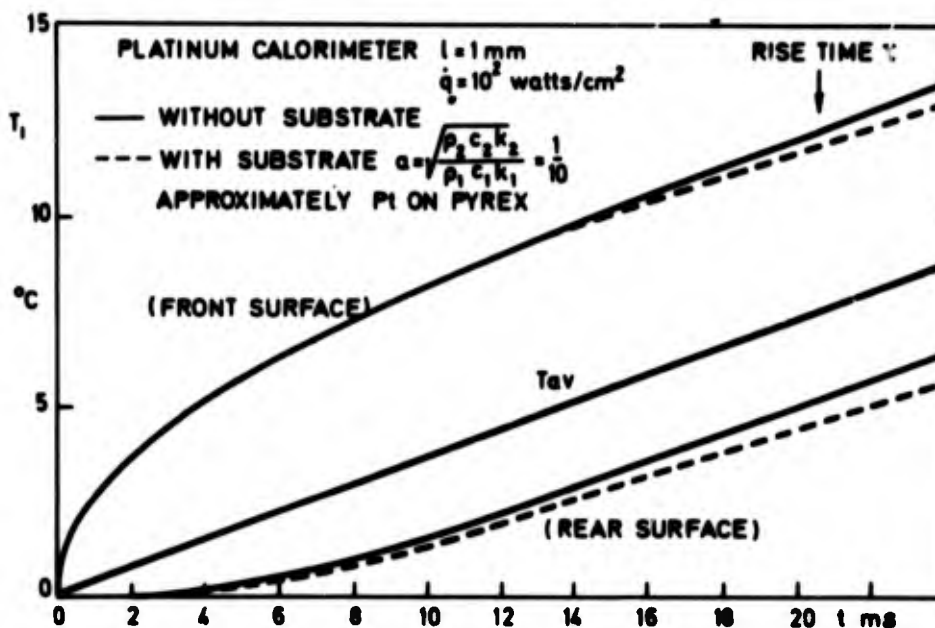
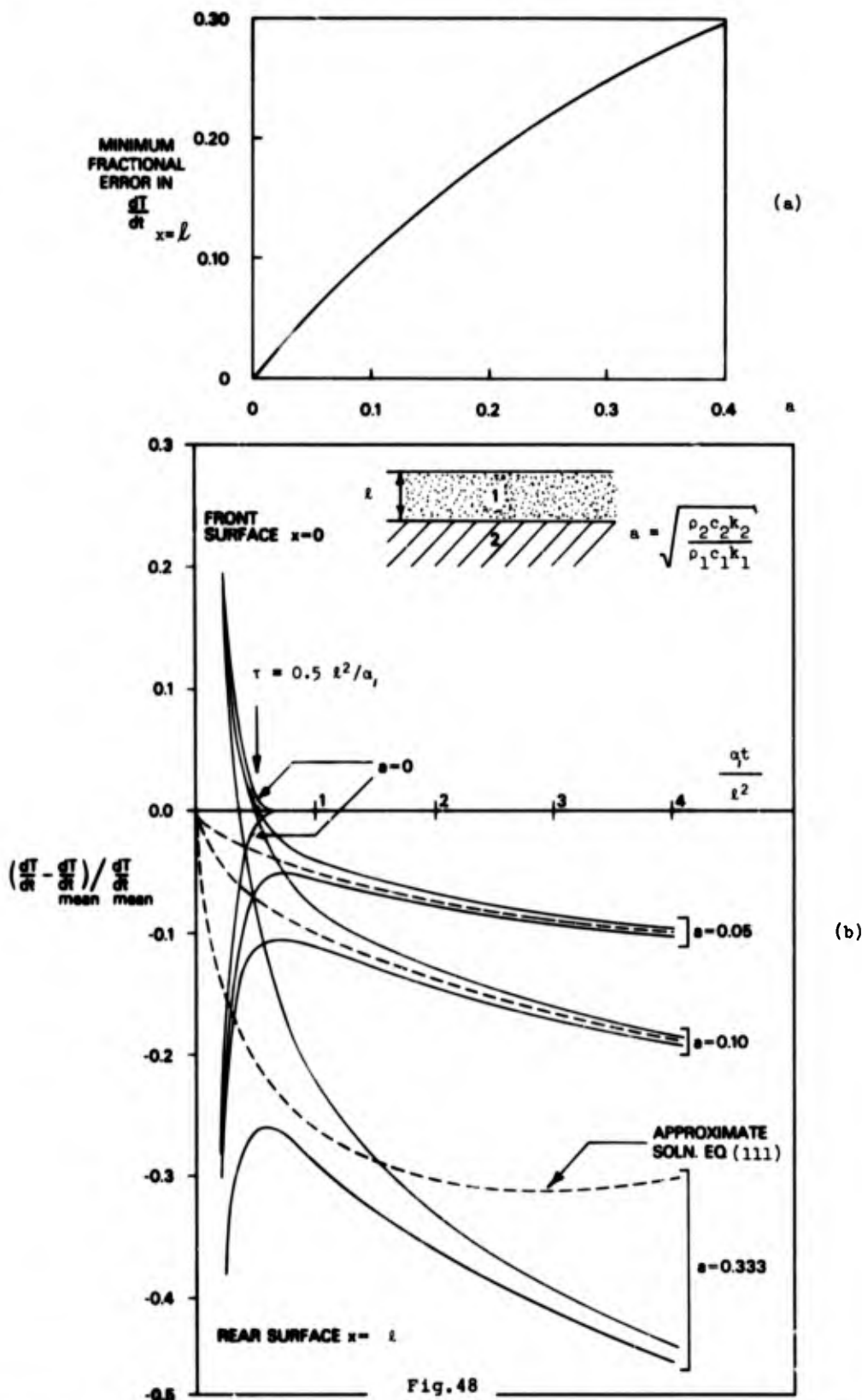


Fig. 47

The front surface, rear surface and average temperature in a calorimeter gauge without substrate as calculated from Fig. 46 for a platinum calorimeter. $l = 1 \text{ mm}$ and $\dot{q}_0 = 10 \text{ W cm}^{-2}$. The average temperature increases linearly with time whereas the rear surface lags in time. The effect of a substrate on the front and rear surface temperatures is shown and it is apparent that the rear surface is influenced from the initiation of the flow.



The rate of rise of the front and rear surface temperatures of a calorimeter gauge, $(dT/dt)_{x=0, x=l}$, in the presence of a substrate compared with that for the mean temperature in the absence of a substrate, $(dT/dt)_{\text{mean}}$. (a) Minimum fractional error in the rate of rise of rear surface temperature, $\left[\frac{(dT/dt)_{x=l} - (dT/dt)_{\text{mean}}}{(dT/dt)_{\text{mean}}}\right]$, as a function of $a = \left[\frac{\rho_2 c_2 k_2}{\rho_1 c_1 k_1}\right]^{1/2}$ found from Fig.48(b) below. (b) Fractional error in the rate of rise of front and rear surface temperature for $a = 0.0$ (no substrate), 0.05, 0.10 and 0.33 as a function of non-dimensional time $(a_1 t/l^2)$, determined from Eq(106). Also shown as a dotted line is the approximate solution, Eq(111). The rise time of the gauge $\tau = 0.5 l^2/a_1$ is also shown.

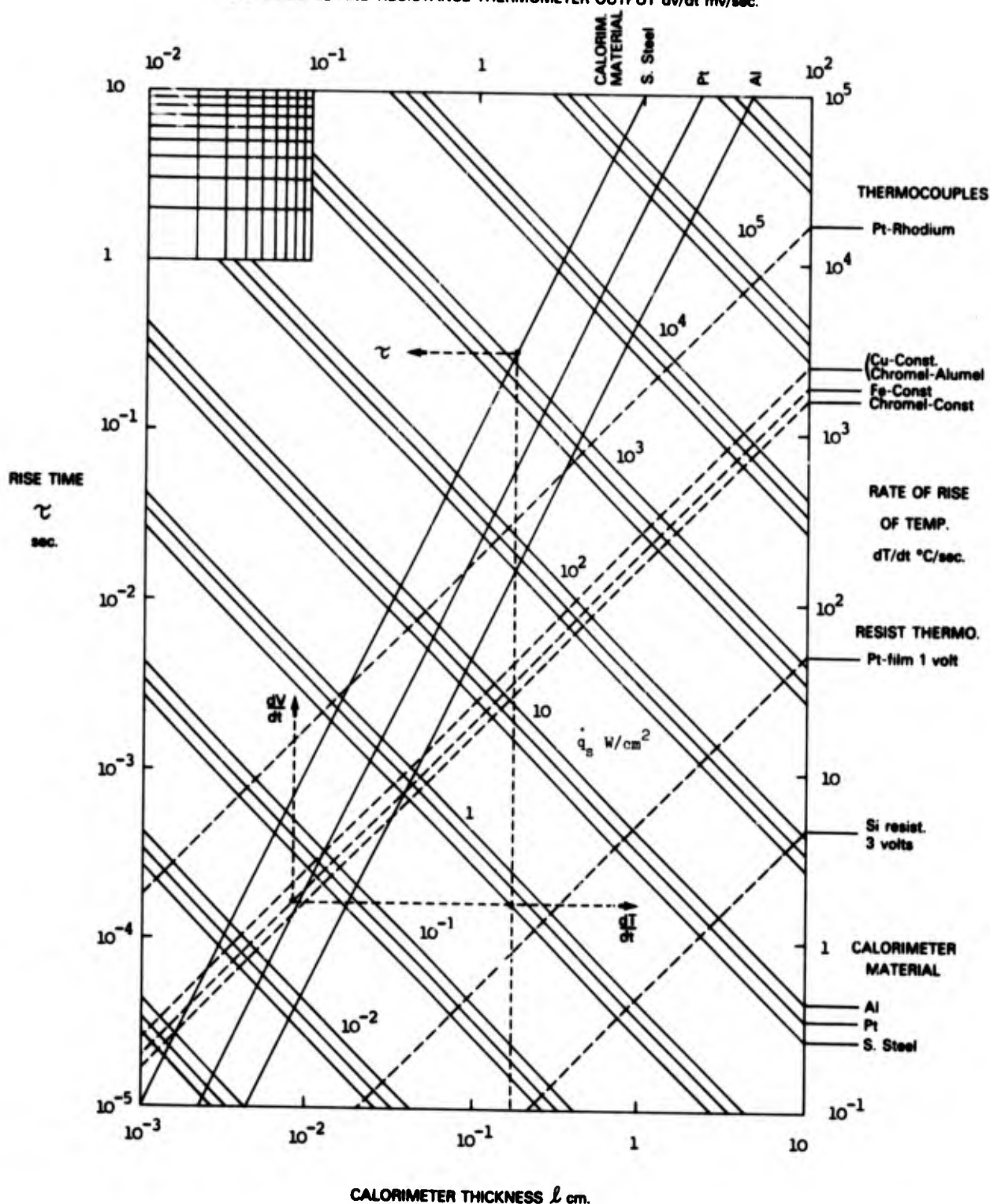
THERMOCOUPLE AND RESISTANCE THERMOMETER OUTPUT dV/dt mv/sec.

Fig.49

Calorimeter design chart for aluminium, platinum and stainless steel. For a given calorimeter thickness, l cm, the rise time, τ seconds, may be found. Also for a given l and a particular heat transfer rate, q_s W cm⁻², the rate of rise of calorimeter temperature, dT/dt (K s⁻¹) is shown which enables the voltage output, dV/dt (mV s⁻¹) for various temperature sensors to be found. This procedure is indicated by the dotted lines.

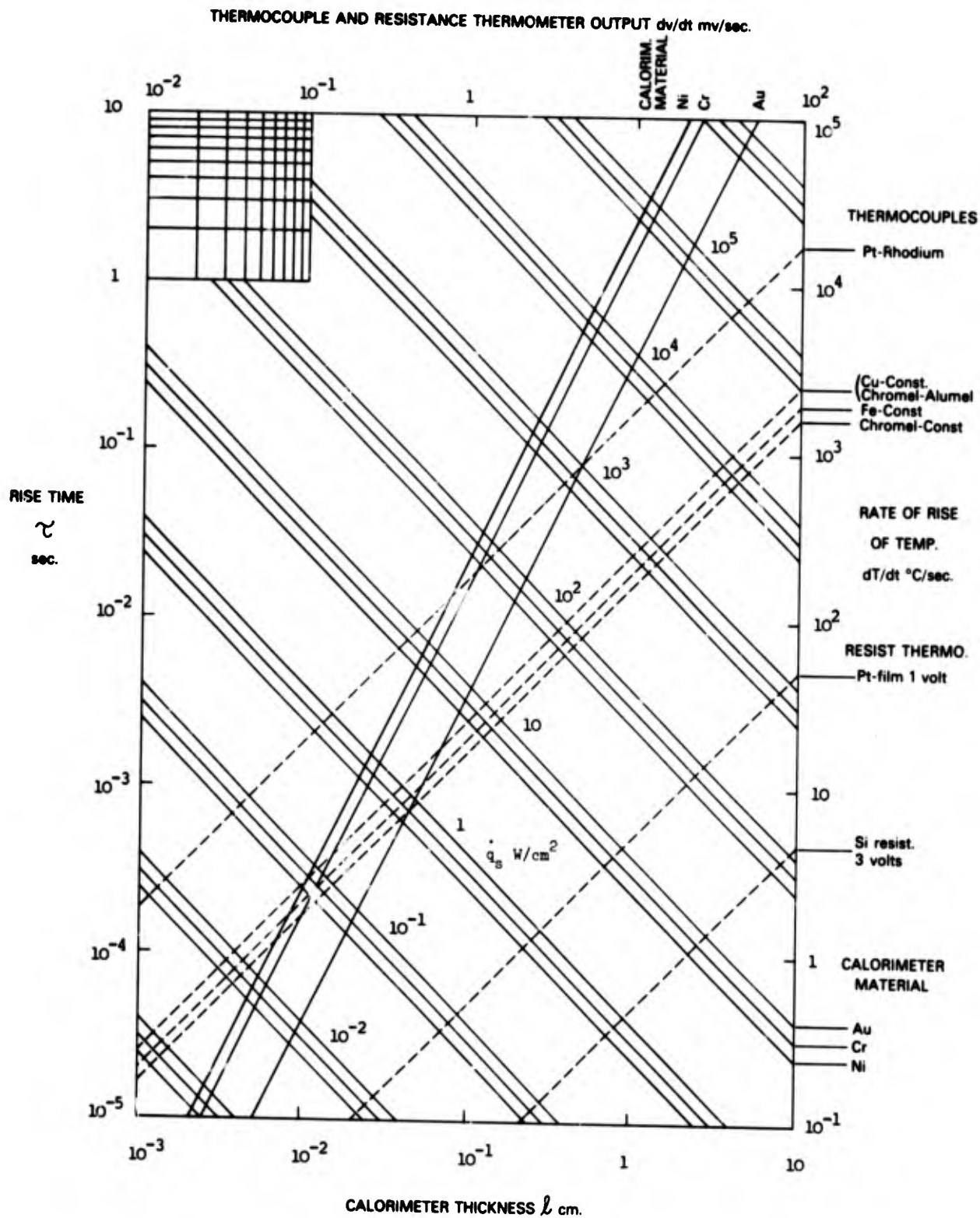


Fig.50

Calorimeter design chart for gold, chromium and nickel. Refer to Fig.49 for details of use.

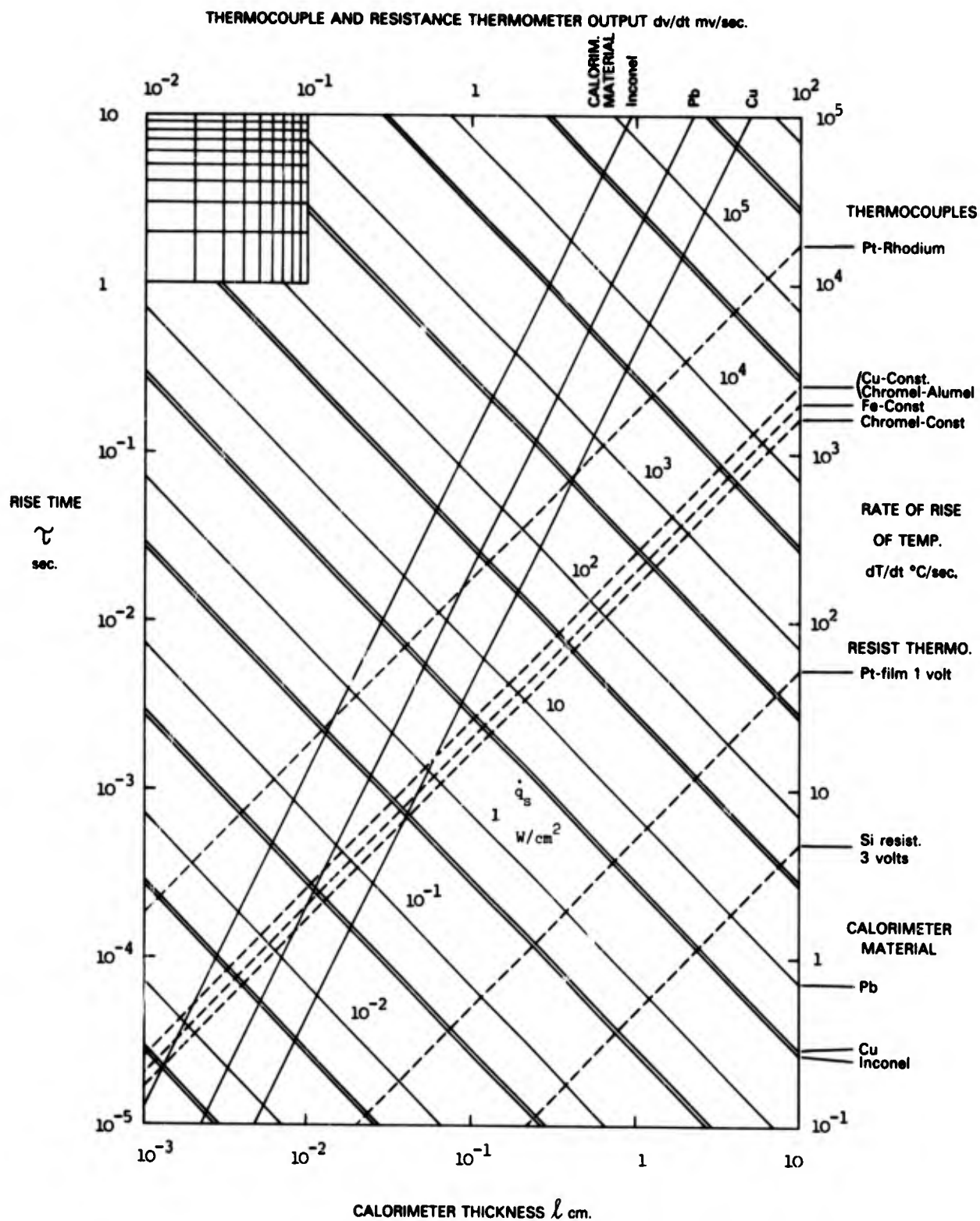


Fig. 51

Calorimeter design chart for lead, copper and Inconel. Refer to Fig.49 for details of use.

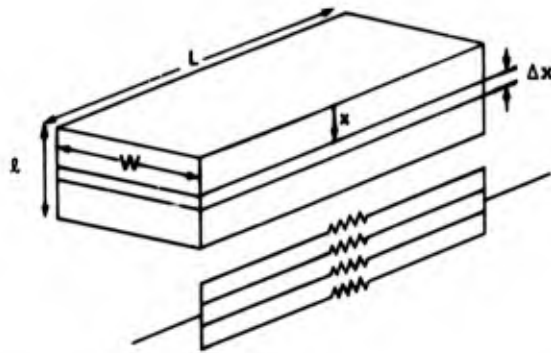


Fig.52

Coordinate system and equivalent electrical circuit for the analysis of the Rose calorimeter.

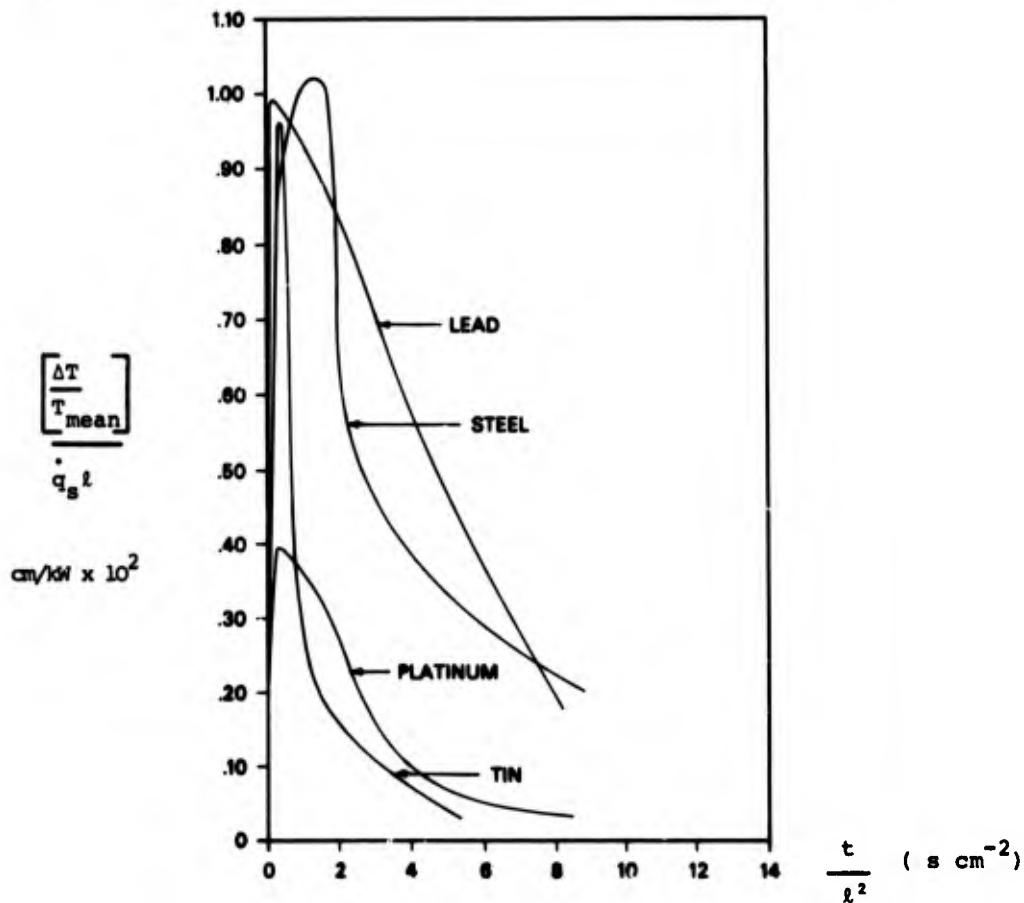


Fig.53

Error in the determination of the mean temperature of a Rose calorimeter mounted on a Pyrex substrate. Temperature is evaluated from the variation of the electrical resistance:

$$R = R_0 [1 + \alpha_R (T_{\text{mean}} - T_0)]$$

A step function in surface heat transfer rate, \dot{q}_s , is assumed and the error, ΔT , is normalised in the form, (Eq(113)):

$$\frac{\Delta T / T_{\text{mean}}}{\dot{q}_s l} = \frac{\alpha_R [(T^2)_{\text{mean}} - (T_{\text{mean}})^2]}{\dot{q}_s l T_{\text{mean}}}$$

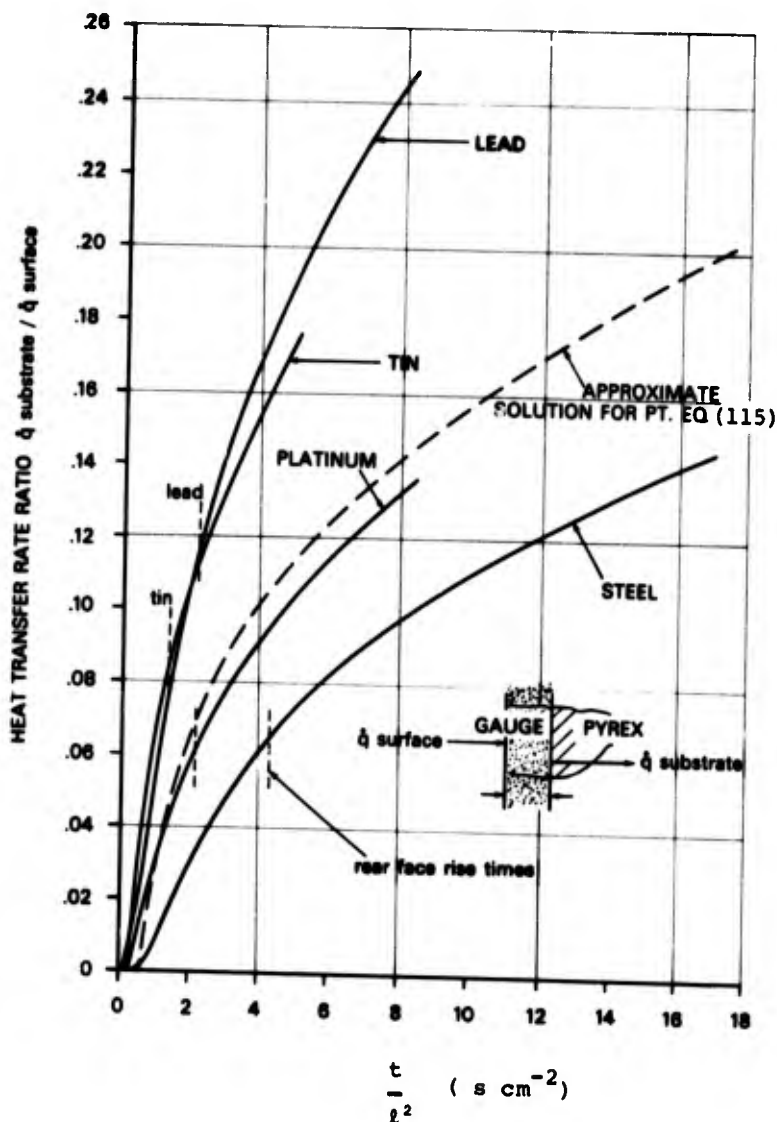


Fig.54

Rate of loss of heat to the substrate, $\dot{q}_{\text{substrate}}$, as a fraction of the incident heat transfer rate, \dot{q}_{surface} , for calorimeters on Pyrex substrates. Curves for lead, tin, platinum and steel are redrawn from Rose (20). Approximate solution shown for comparison with platinum is calculated from Eq(115). This equation may be used to evaluate $\dot{q}_{\text{substrate}} / \dot{q}_{\text{surface}}$ for substrates other than Pyrex. Vertical dashed lines indicate the rear surface rise time as defined by $\tau = 0.5l^2/\alpha$

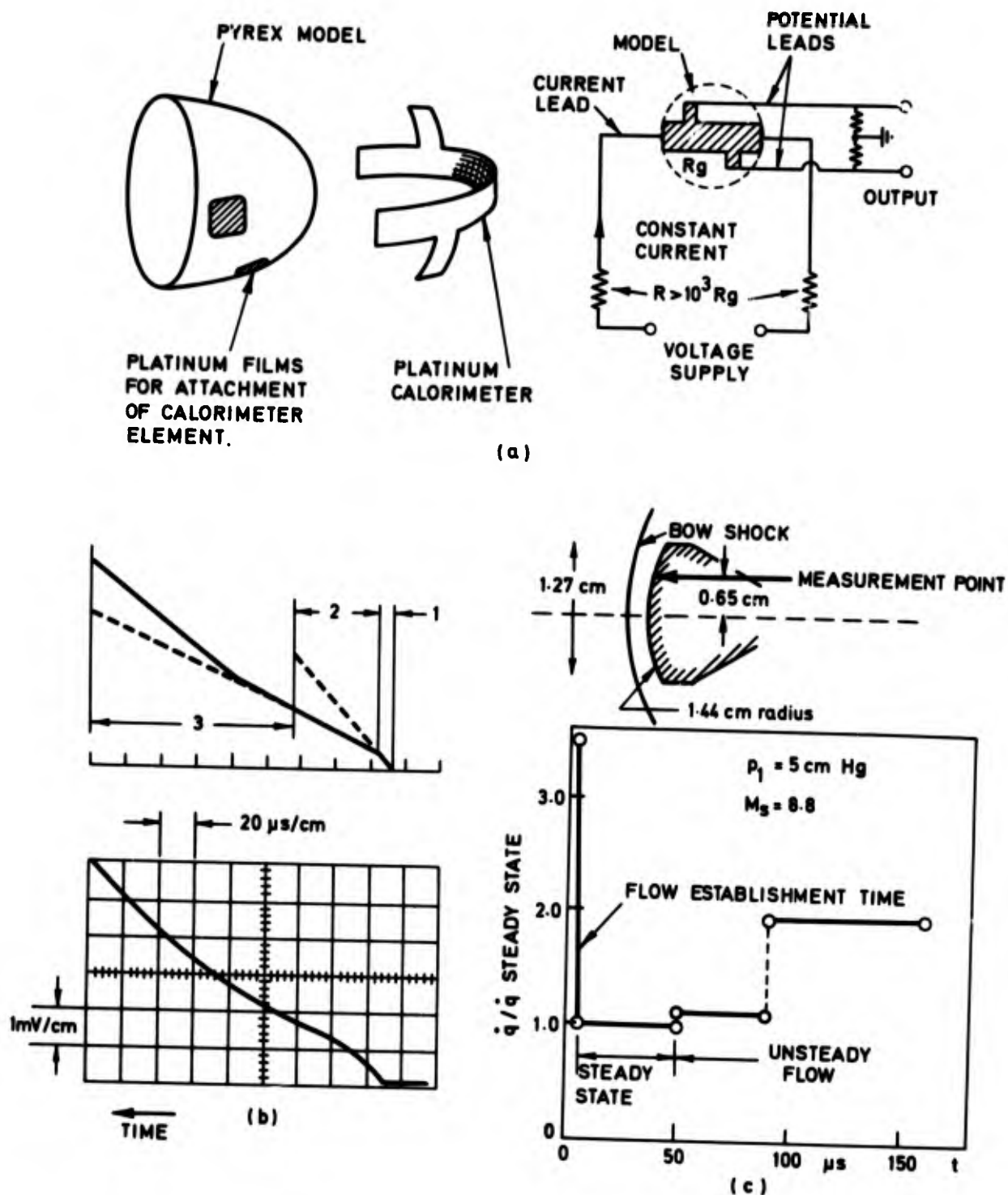


Fig.55

Schematic diagram illustrating construction of Rose calorimeter gauge and current feed system. Note that the calorimeter element is in good thermal contact with the substrate only at points beyond the active section of the sensor element. (b) Voltage output of Rose calorimeter near stagnation point of bluff body in a shock tube; 1 - flow establishment time, 2 - steady state, 3 - unsteady flow. (c) Heat transfer rates deduced from oscillogram in (b), $\dot{q}_{s.s.} = 5 \text{ kW cm}^{-2}$. Redrawn from Offenhartz and Weisblatt (125).

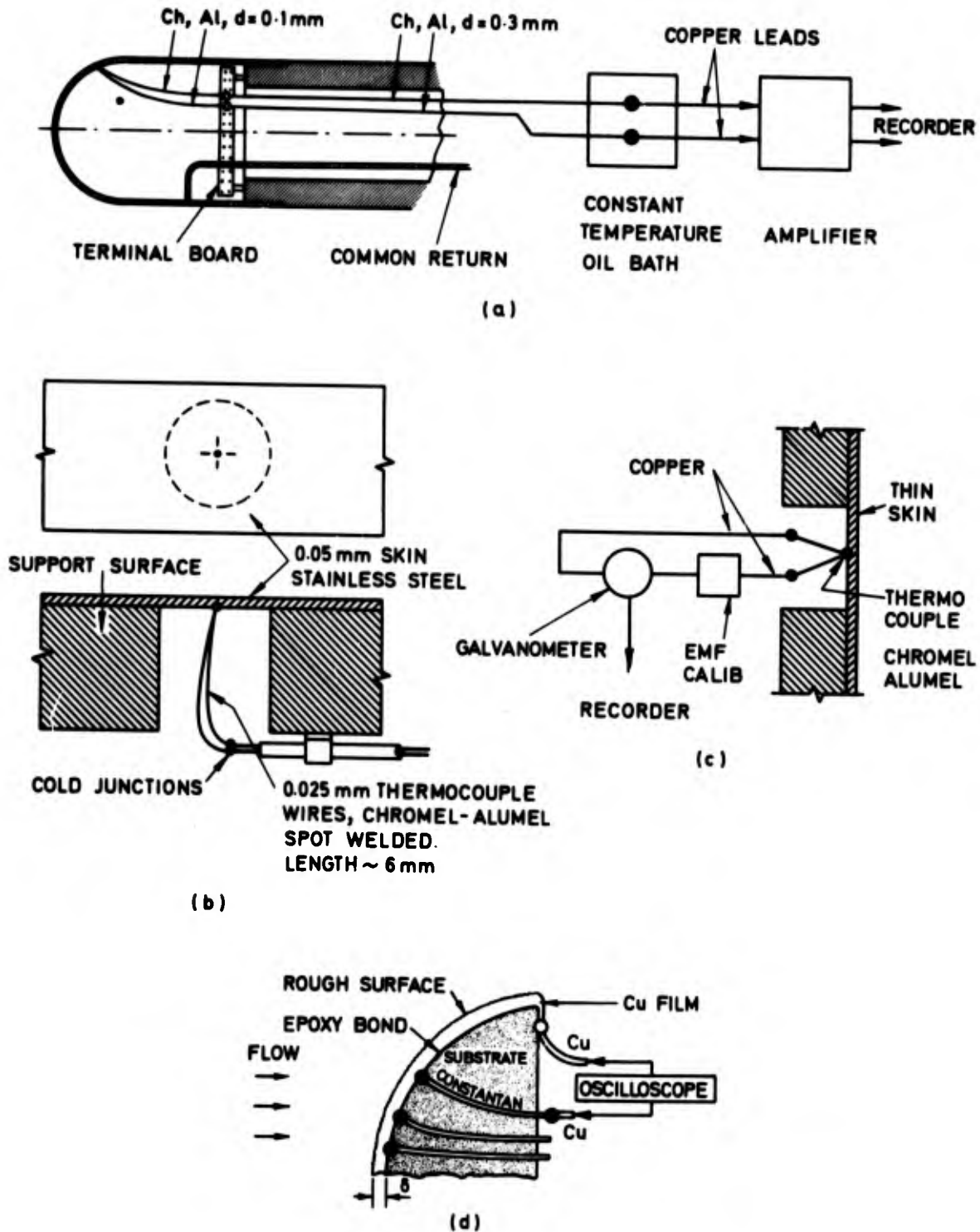


Fig.56

Constructional techniques and thermocouple connections used in thin skin calorimeter models. (a) ONERA technique employing chromel-alumel thermocouples and external cold junctions at controlled temperature. After Chevallier et al (58). (b) Constructional technique and circuit (c) used by Harvey (63) in which localised areas of complex model shapes are instrumented. (d) Technique used by Starner and Varwig (64) to measure heat transfer rates to rough surfaces. The skin is bonded onto the substrate surface and a common return is used.

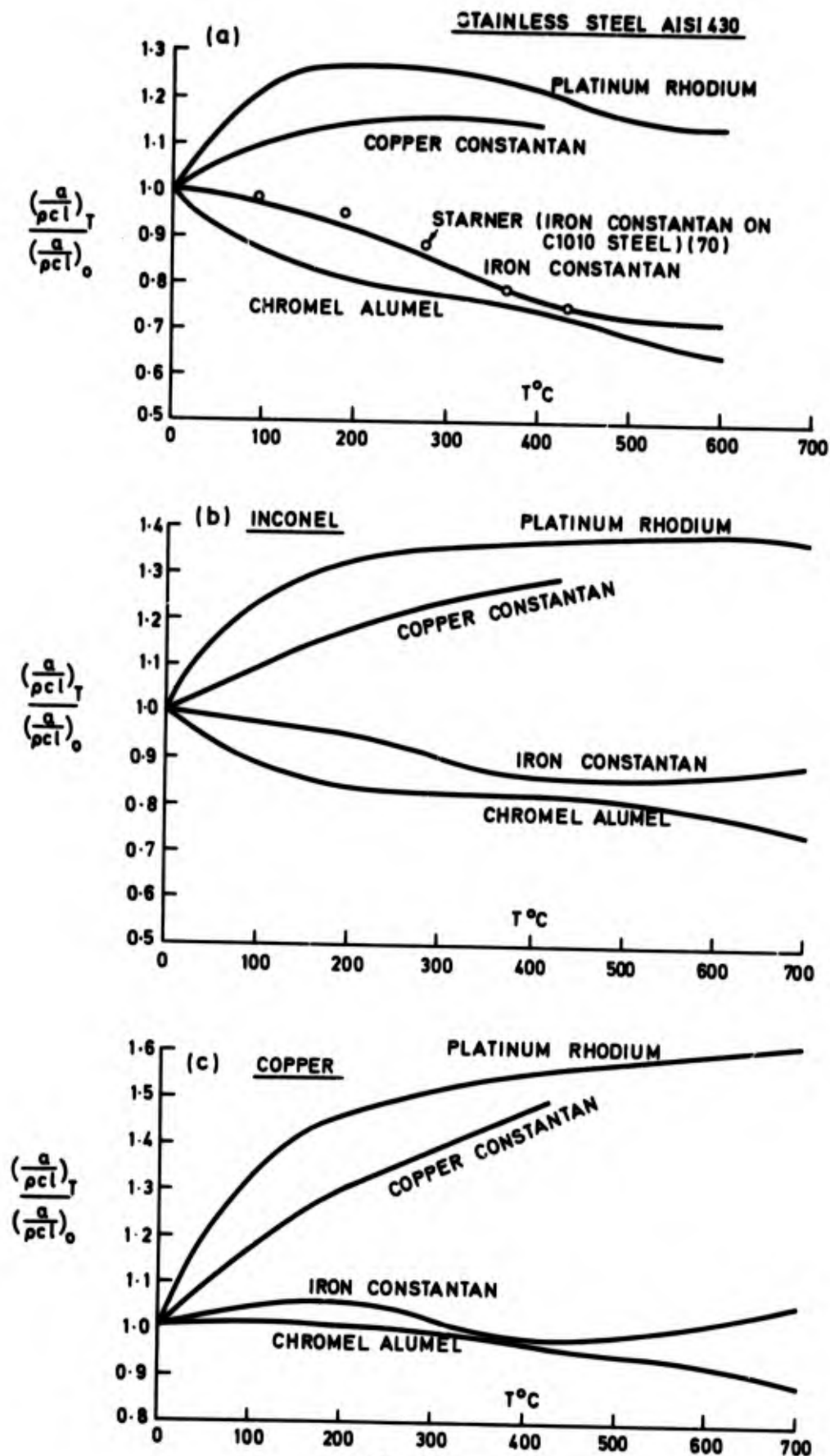
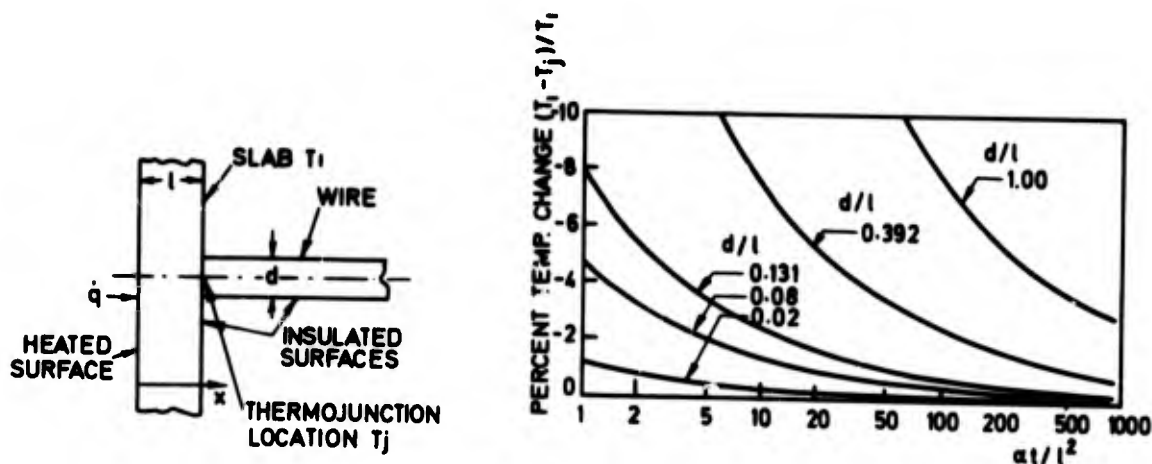


Fig. 57

The effect of the variation of calorimeter thermal properties and thermocouple sensitivity on the overall sensitivity of thin skin models. (a) Stainless steel AISI 430. (b) Inconel. (c) Copper. Thermal properties from Table A - 3 and thermocouple sensitivities from (50).



(a) RELATIVE TEMPERATURE ERRORS

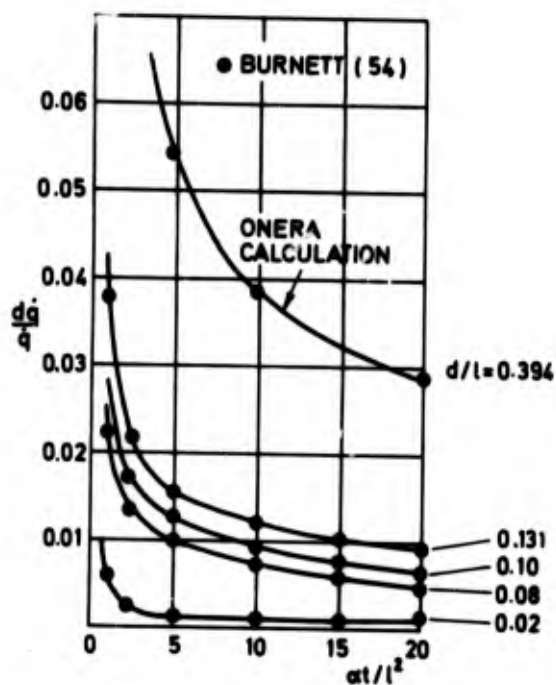
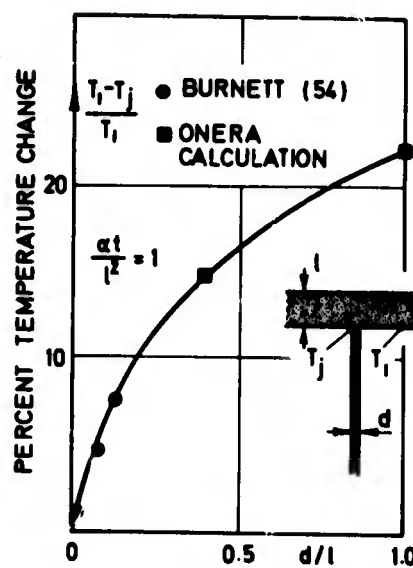
(b) RELATIVE ERRORS IN
HEAT TRANSFER RATE(c) INFLUENCE OF WIRE DIAM.
ON TEMPERATURE
MEASUREMENT

Fig.58

- (a) Errors in rear face temperature measurement due to presence of finite thermocouple wire for constant heat transfer rate. Redrawn from Burnett (57).
- (b) Errors in inferred heat transfer rate due to heat conduction in thermocouple leads.
- (c) Errors in rear face temperature measurement due to finite thermocouple wire dimensions. Curves extended by ONERA from cases treated by Burnett, see (a) above, $\alpha t / l^2 = 1$. Redrawn from Chevallier et al (58)

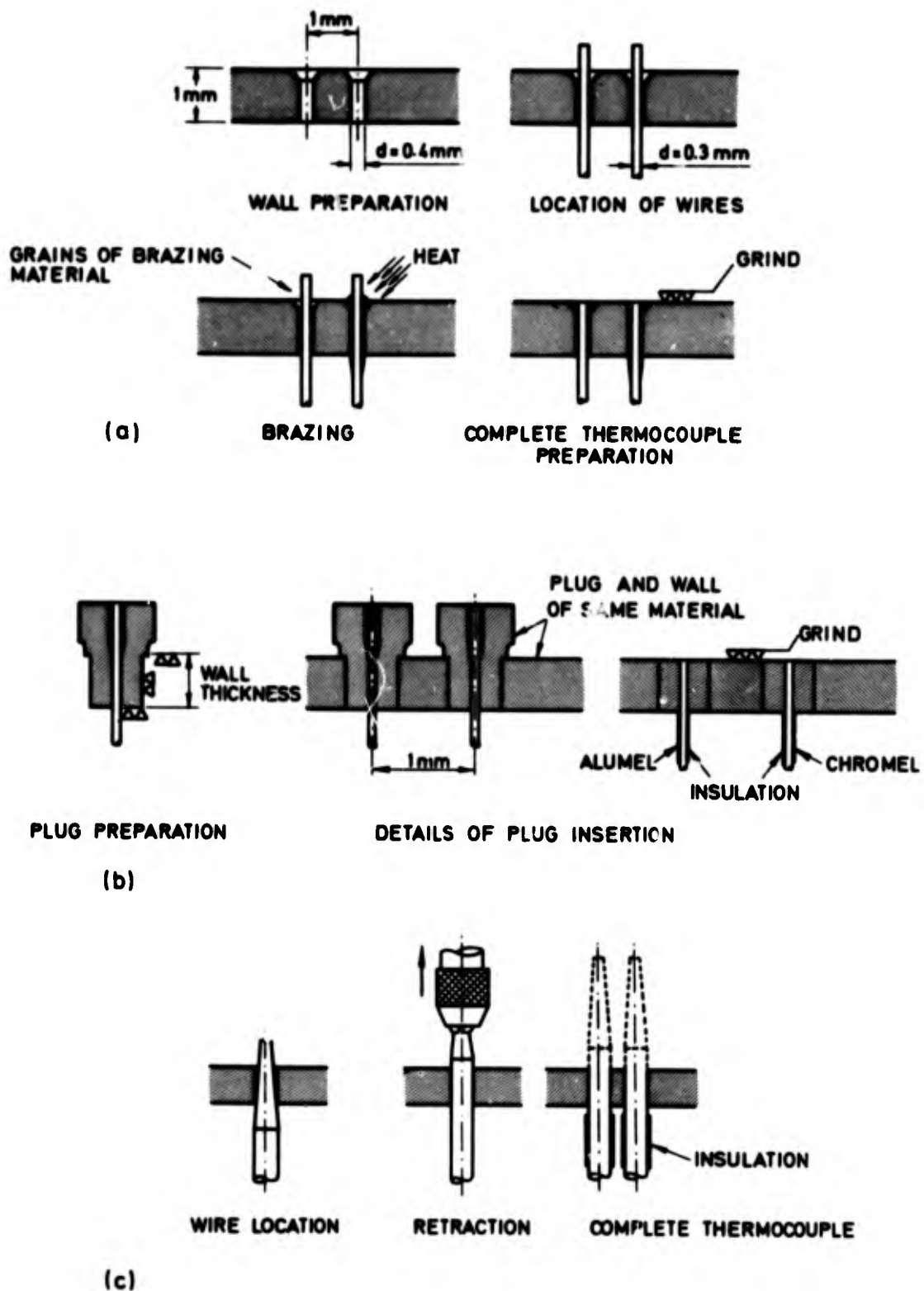


Fig.59

Techniques for construction of thin wall thermocouples employed at ONERA.
 (a) Simple brazing method. (b) Preparation and insertion of thermocouple plug insert with precise control of wall thickness at point of temperature measurement.
 (c) Technique suitable for very thin walls. Redrawn from Chevallier et al (58).

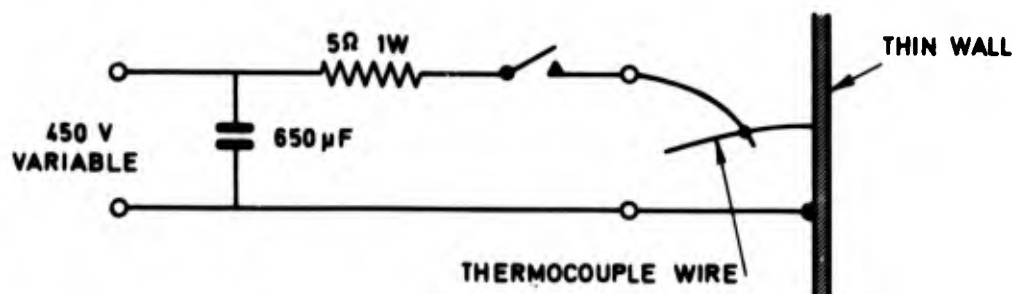


Fig. 60

Technique for spot welding fine thermocouple wires to thin wall models. The junction of the lead and thermocouple may be made with a spring clip. The complete junction is made by welding two wires close together on the surface.

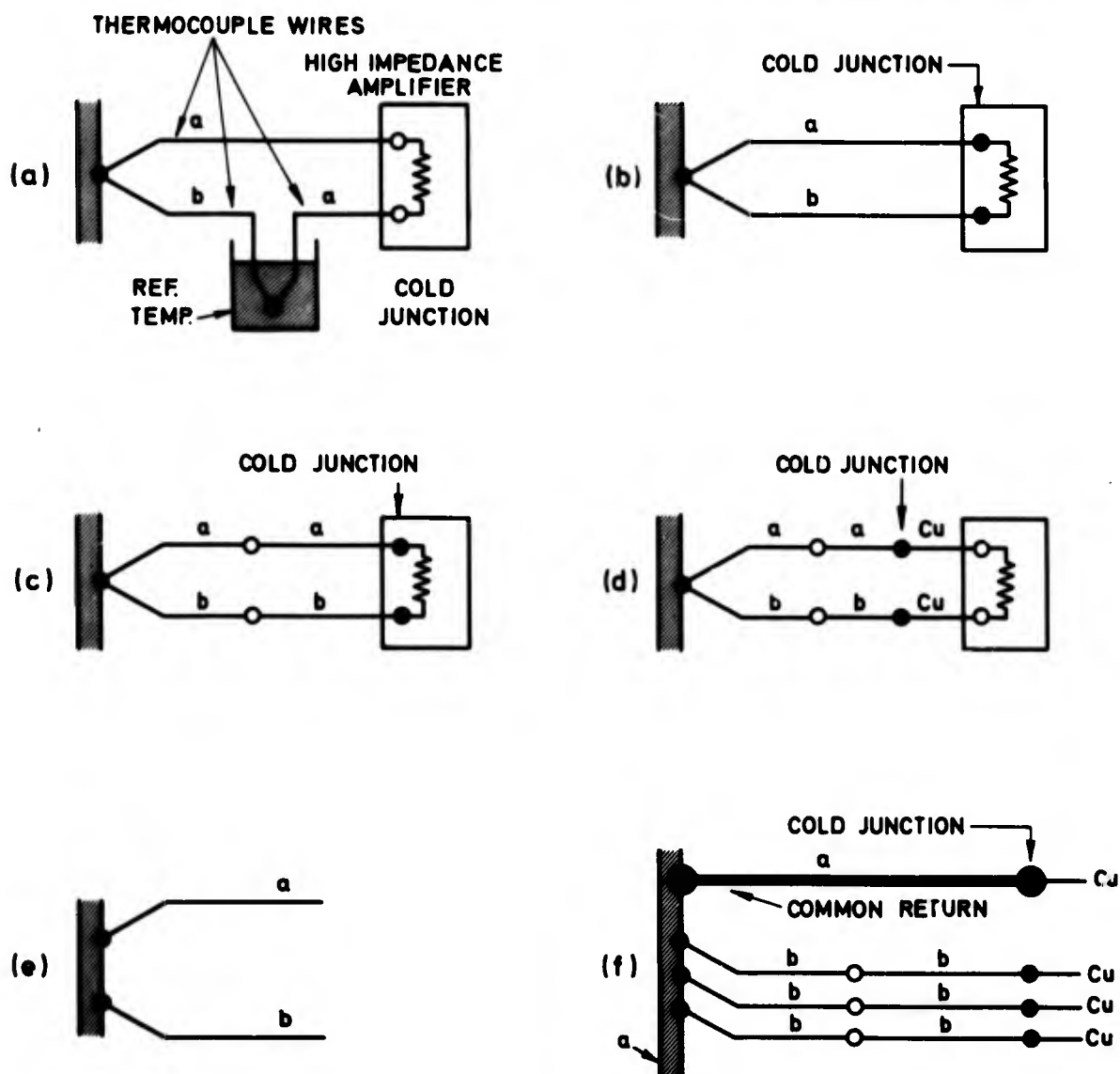
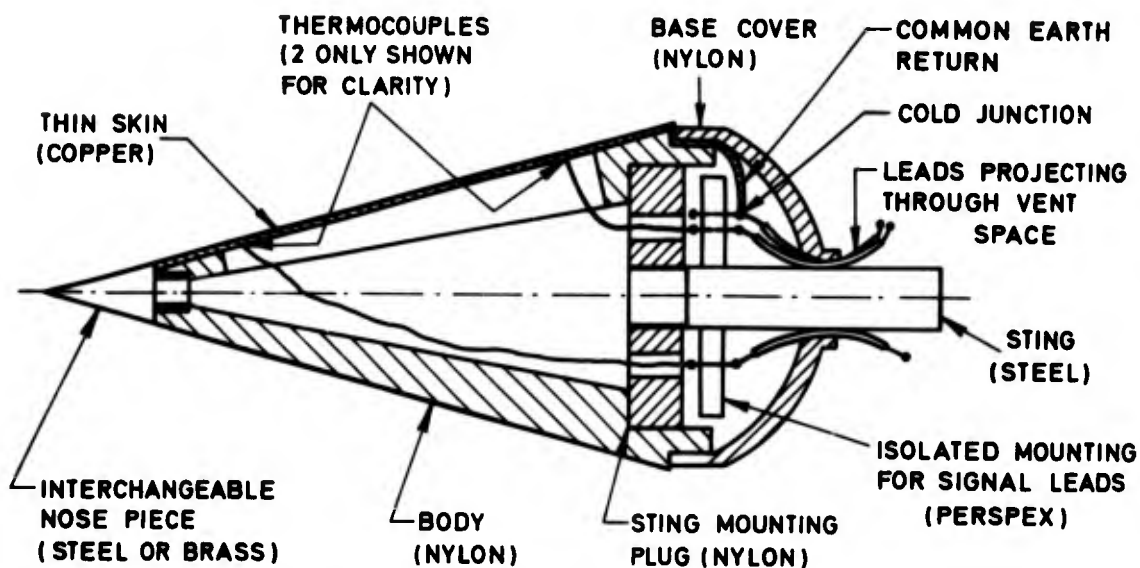


Fig. 61

Alternative connections for the attachment of thermocouple wires to thin skin calorimeter models. The thermocouple wires are 'a' and 'b' and possible locations for the 'cold' junctions are shown.



(a)



(b)

Fig.62

(a) Thin skin heat transfer model with part of skin raised to show slot beneath.
 (b) Construction details of the model. The skin is supported by the Nylon body except in the region in which the thermocouples are mounted. Total model length 15.24 cm, slot width 0.51 cm, copper skin thickness 0.022 cm, thermocouple wire diameter 5.08×10^{-3} cm constantan, cold junction at inside rear of model assumed to remain at laboratory ambient temperature. Reproduced from Wood (66), by permission of the Controller, H.M. Stationery Office.

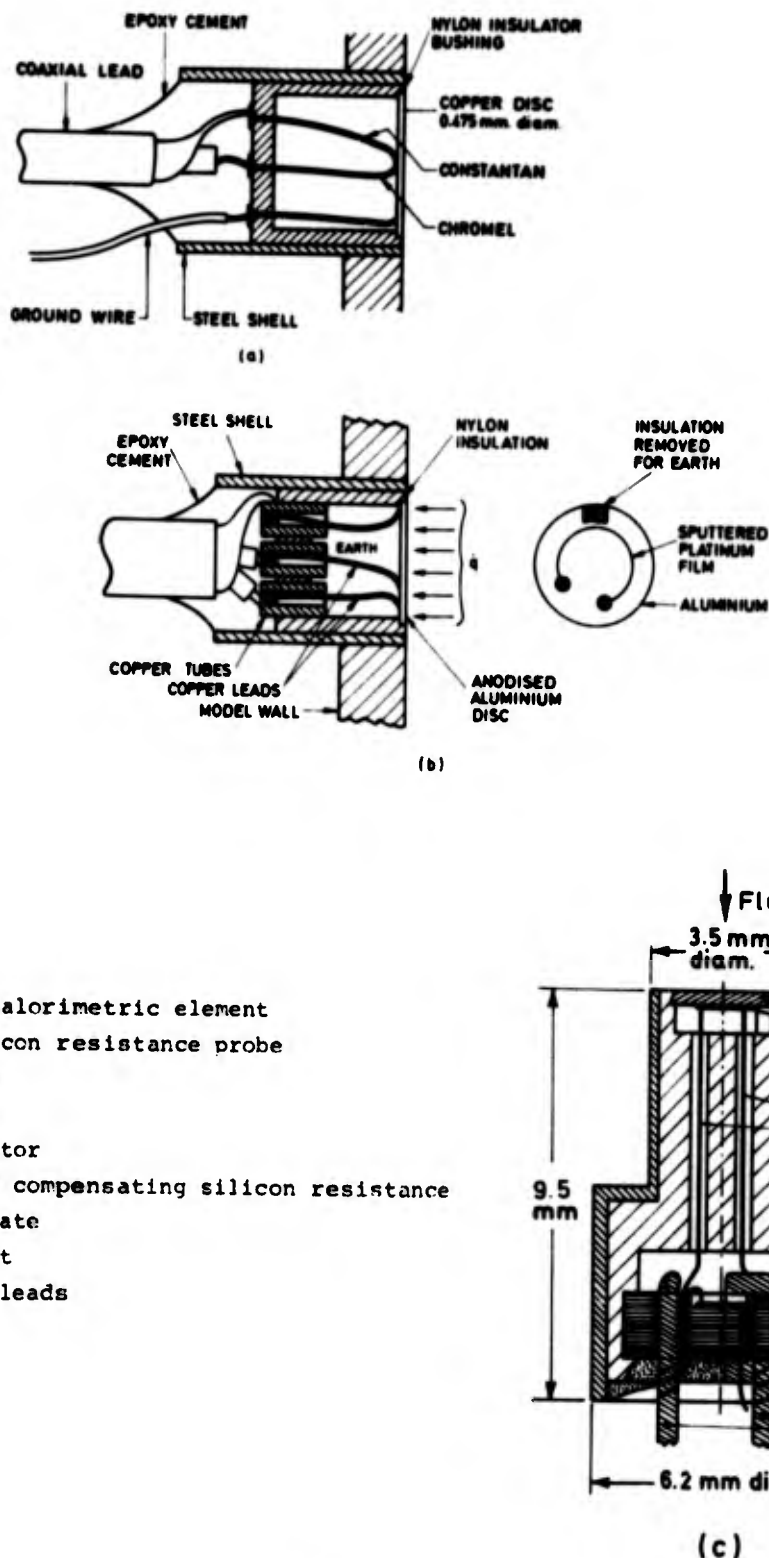


Fig.63

'Capsule' calorimeters for insertion in metallic or insulating models. (a) Copper disc calorimeter of Ledford (67) with chromel constantan thermocouple. (b) Aluminium disc calorimeter with thin platinum film sputtered on anodised surface, Ledford (68). (c) Aluminium disc calorimeter of Maulard (35) using silicon resistance as temperature sensor.

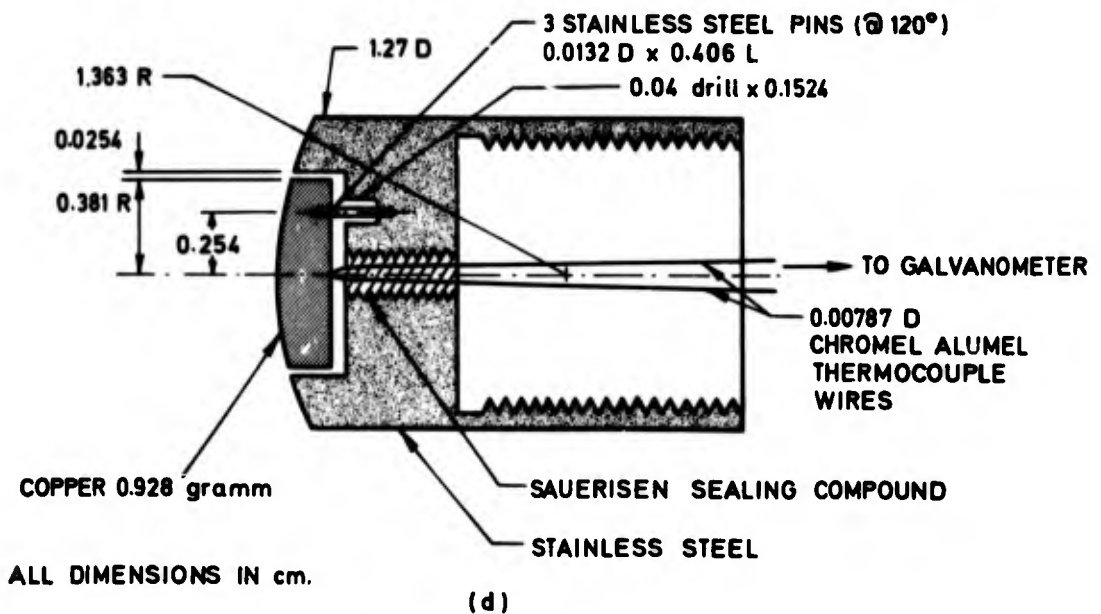
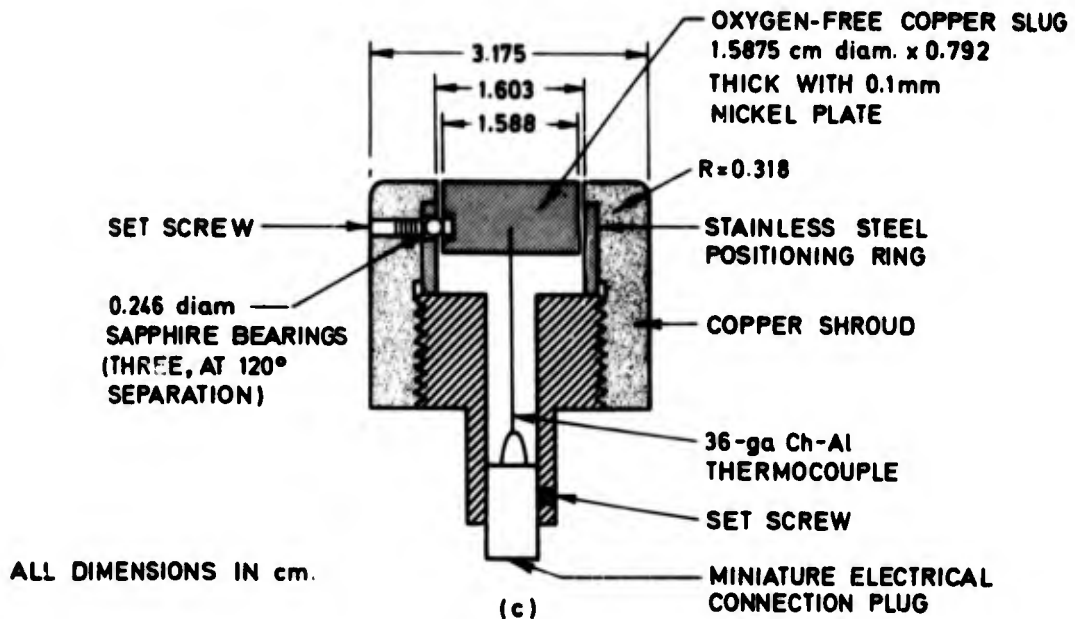
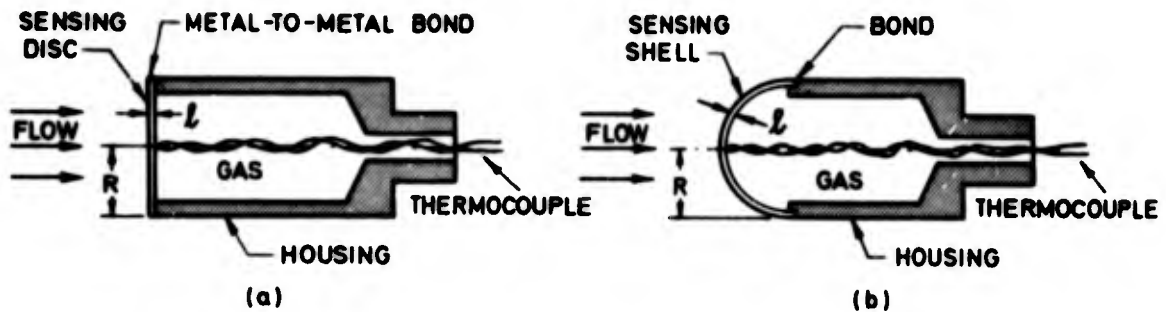


Fig.64

Typical capsule and slug calorimeters. (a) Stagnation point probes developed by Starnier (70). (b) Slug calorimeter of Heister and Clark (72). (c) Slug calorimeter of Vojvodich (73).

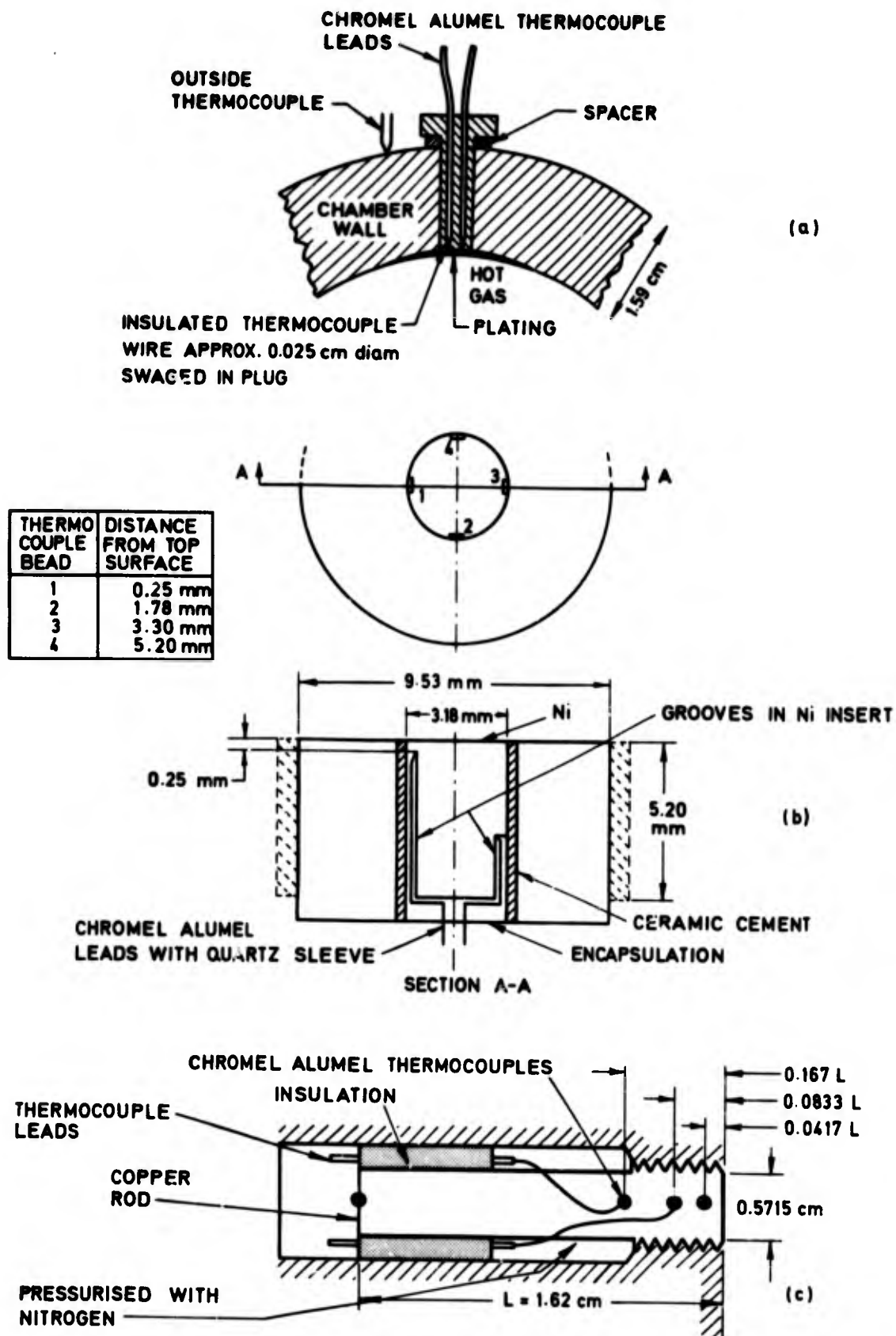
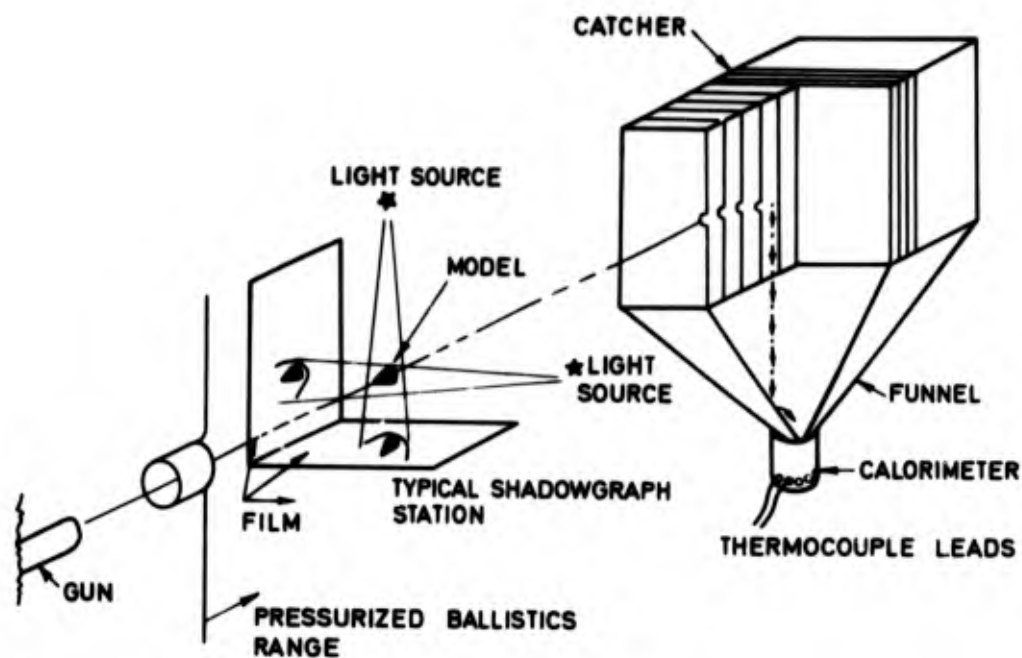
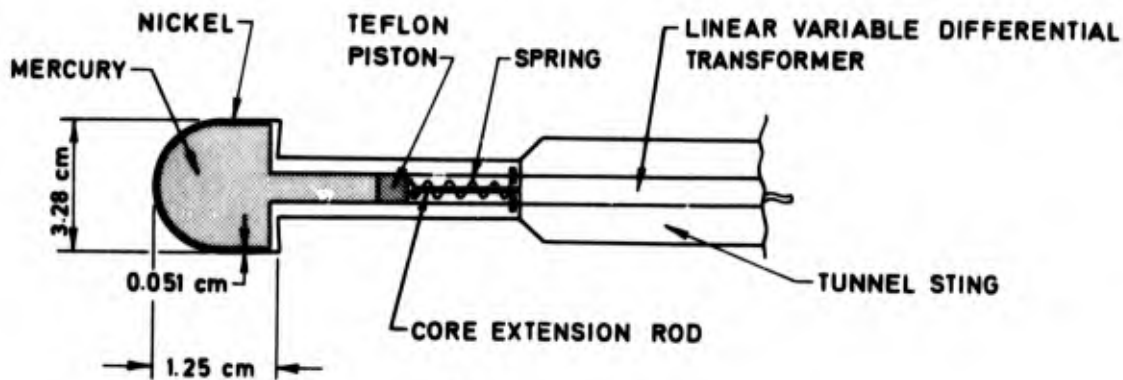


Fig.65

Examples of thick wall calorimeters. (a) Calorimeter due to Powell and Price (80) for use in rocket nozzles. (b) Calorimeter of Stroud (81) for use at stagnation point. (c) Nozzle wall calorimeter of Quentermeyer, Schacht and Jones (75).



(a)



(b)

Fig.66

(a) "Catcher" calorimeter technique of Chapman and Jackson (86) for use in ballistic ranges. The model is decelerated by a series of paper sheets and delivered to a calorimeter in which its total energy increase is measured. (b) Mercury expansion calorimeter of Hunt and Howell (87). The device is similar to a mercury-in-glass thermometer in which the mercury column is the calorimetric element. The increase in volume is found by measuring the movement of the piston.

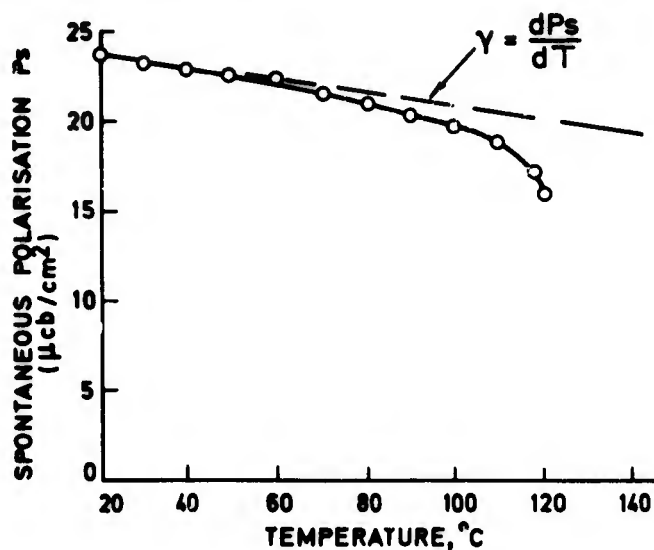


Fig.67

Spontaneous polarisation in single crystal barium titanate as function of temperature. Redrawn from Chenoweth (88).

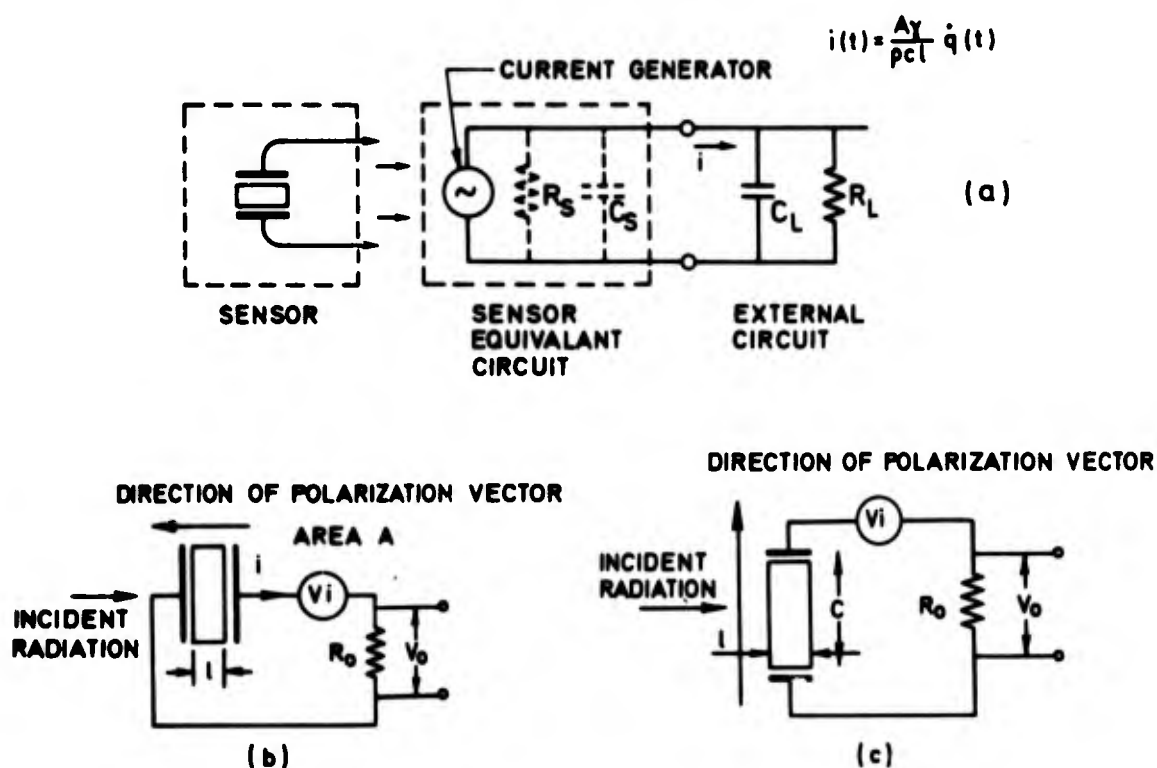


Fig.68

(a) Equivalent circuit of pyroelectric heat transfer gauge. R_s, C_s represent leakage resistance and self capacitance of transducer element. R_L, C_L represent lumped parameters of the external circuit. (b) Electrode arrangement for face-electrode transducer. (c) Electrode arrangement for edge-electrode transducer.

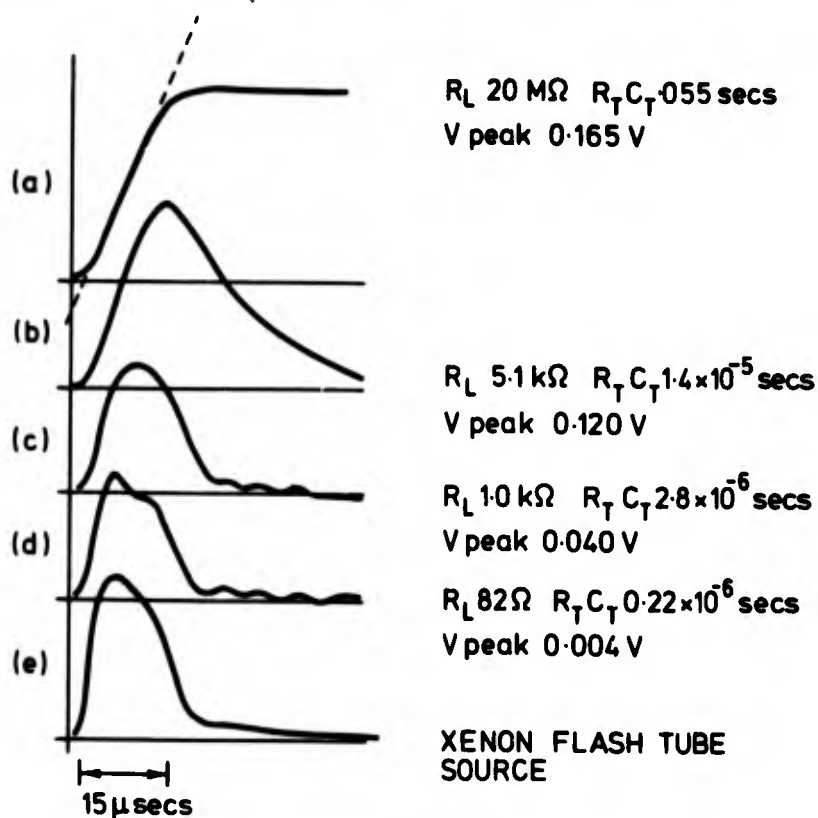


Fig.69

Examples of pyroelectric gauge signals with calorimeter type response in (a) $V_t = \int \dot{q}(t) dt$. Response in (b), (c) and (d) obtained with diminishing time constant. At (c) time constant is 2.8 μ s and ringing of transducer due to thermal distortion is evident. Calibration pulse from Xenon flash tube source shown in (e) monitored by photomultiplier. Redrawn from Wood and Andrews (91).

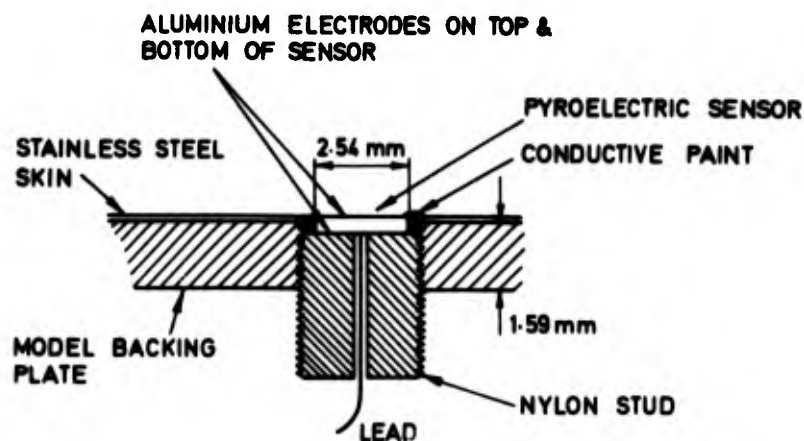


Fig.70

Cross section of pyroelectric heat transfer gauge. Redrawn from Spitzer (92).

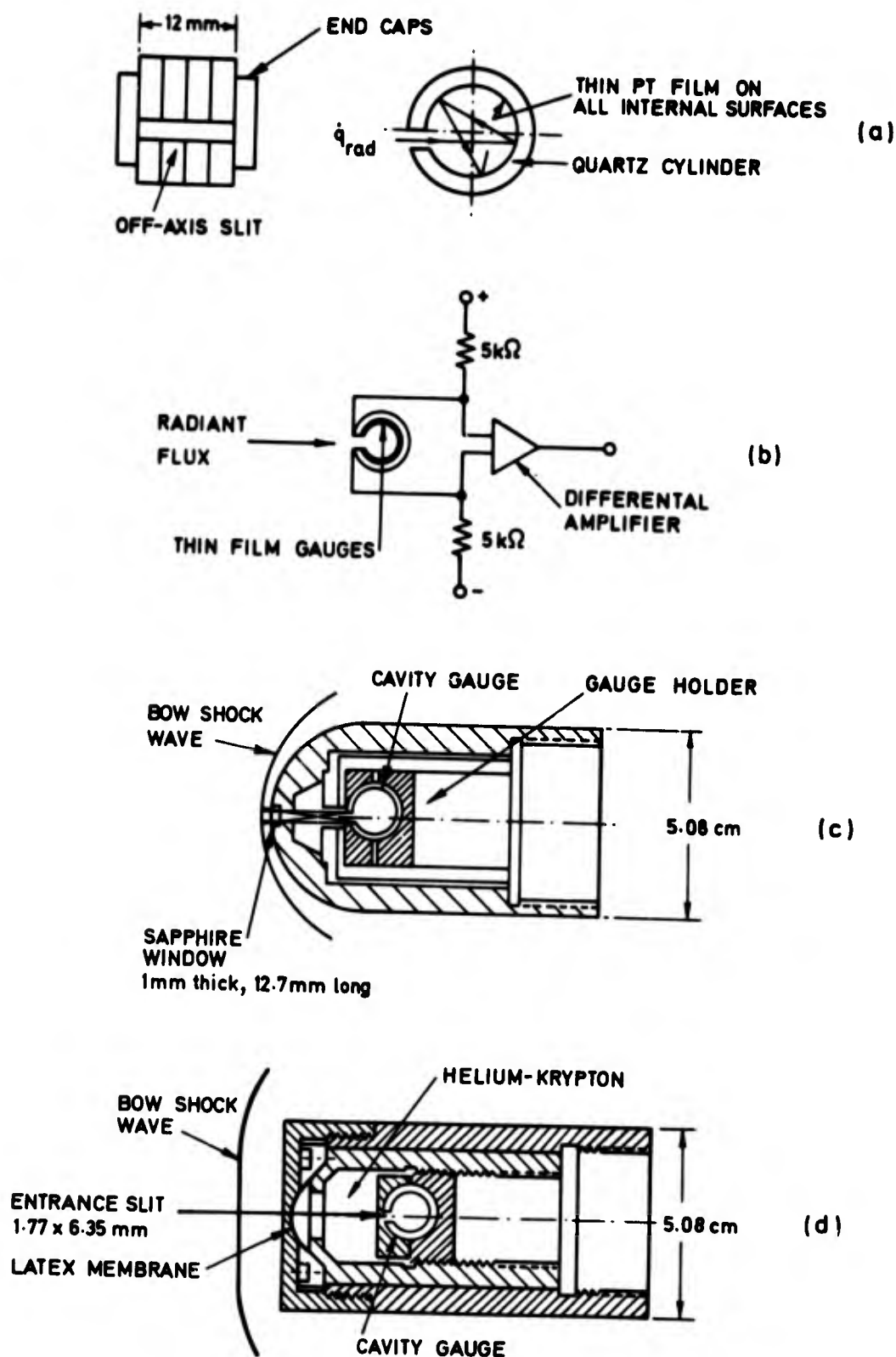


Fig. 71

Radiation heat transfer gauges based on thin film sensors. (a) Total internal reflection system with off-axis slit. (b) External connections to radiometer, all internal thin film sensors connected in series. (c) Location of cavity radiometer in model with sapphire window. (d) Windowless installation with latex rubber diaphragm. Redrawn from Gruszczynski and Rogers (93).

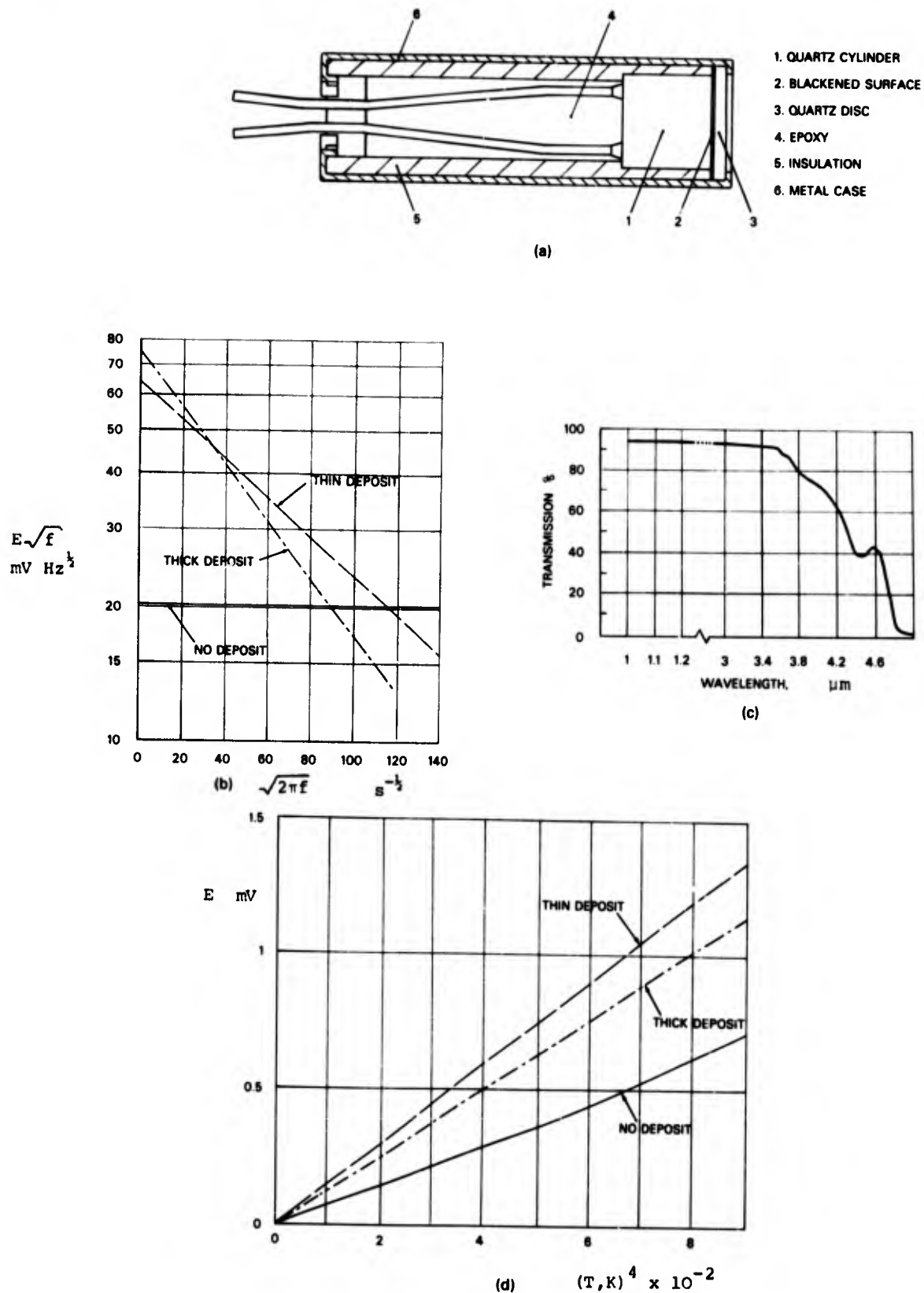


Fig.72

Thin film radiometer developed by Scagnetti and Crabol (94). (a) Construction. (b) A.C. calibration, $\log E\sqrt{f}$ as function of $\sqrt{2\pi f}$ exhibiting linear relationship in agreement with Eq(153). E is film output voltage proportional to substrate surface temperature, f the frequency of incident radiation. (c) Transmission characteristics of isolating quartz disc. (d) A.C. calibration, E as function of T^4 at a fixed frequency. T is calibration source temperature. From Eq(148) the film temperature and hence E is proportional to the absorbed heat flux and a linear relationship is expected.

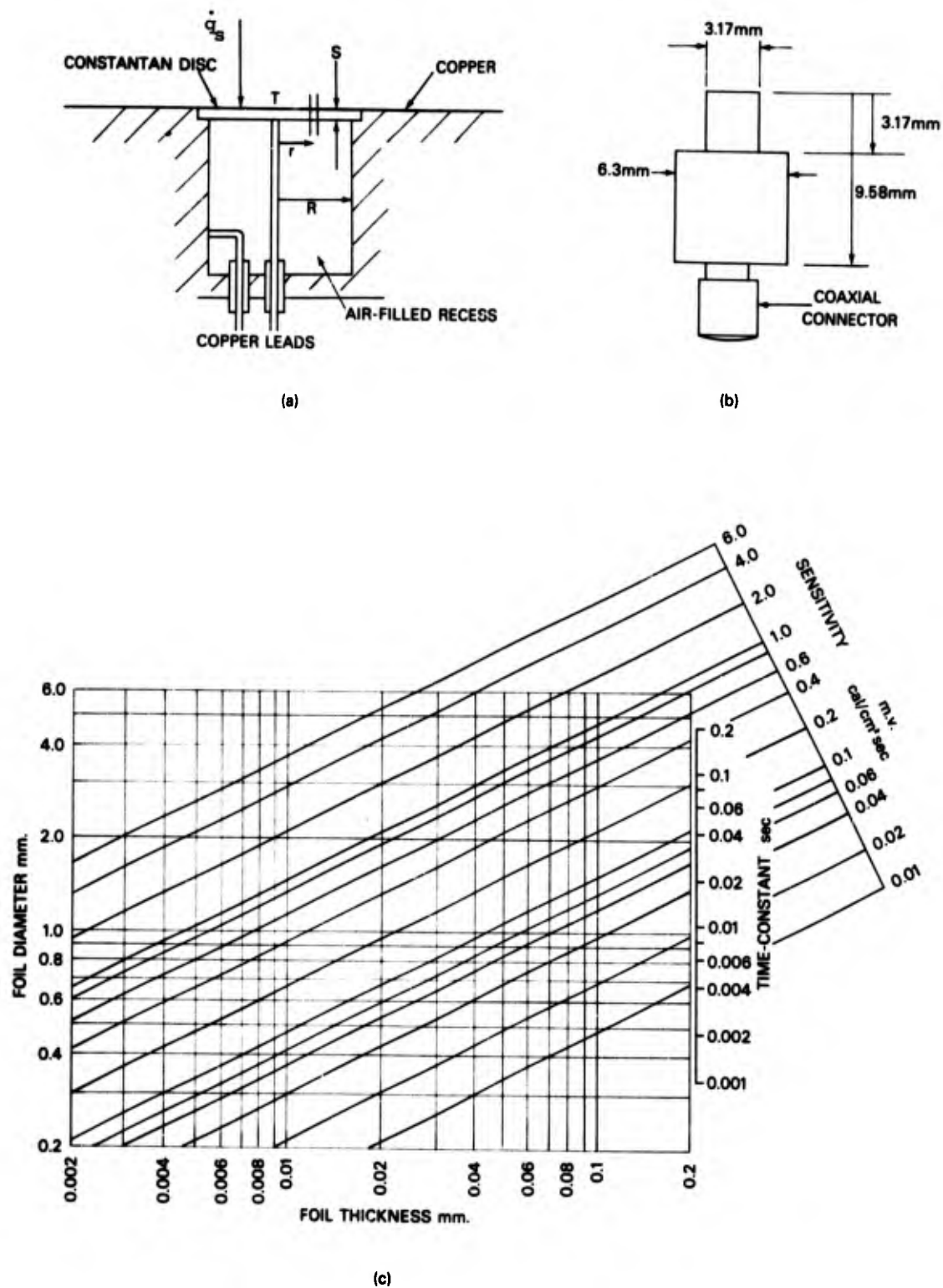


Fig.73

(a) Construction of Gardon thin foil radiometer and coordinate system for analysis of sensitivity and time constant. (b) Dimensions of typical miniature radiometer. (c) Design chart for thin foil radiometers. Redrawn from Gardon (95).

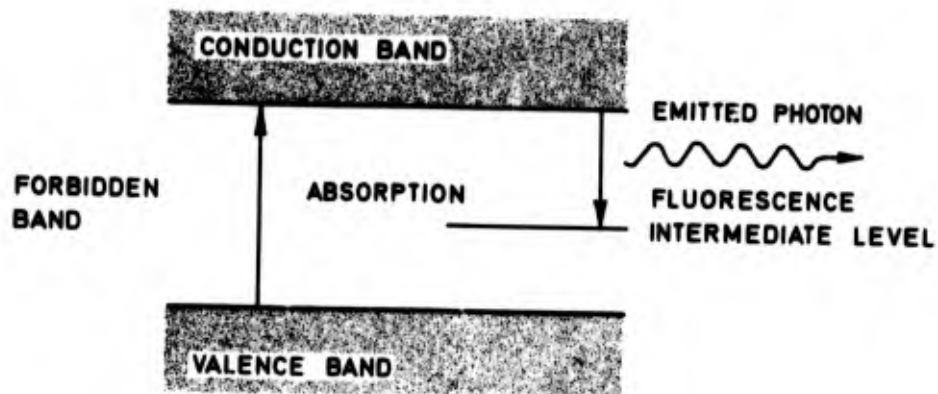


Fig.74

Simplified electronic energy level diagram for a phosphorescent solid.

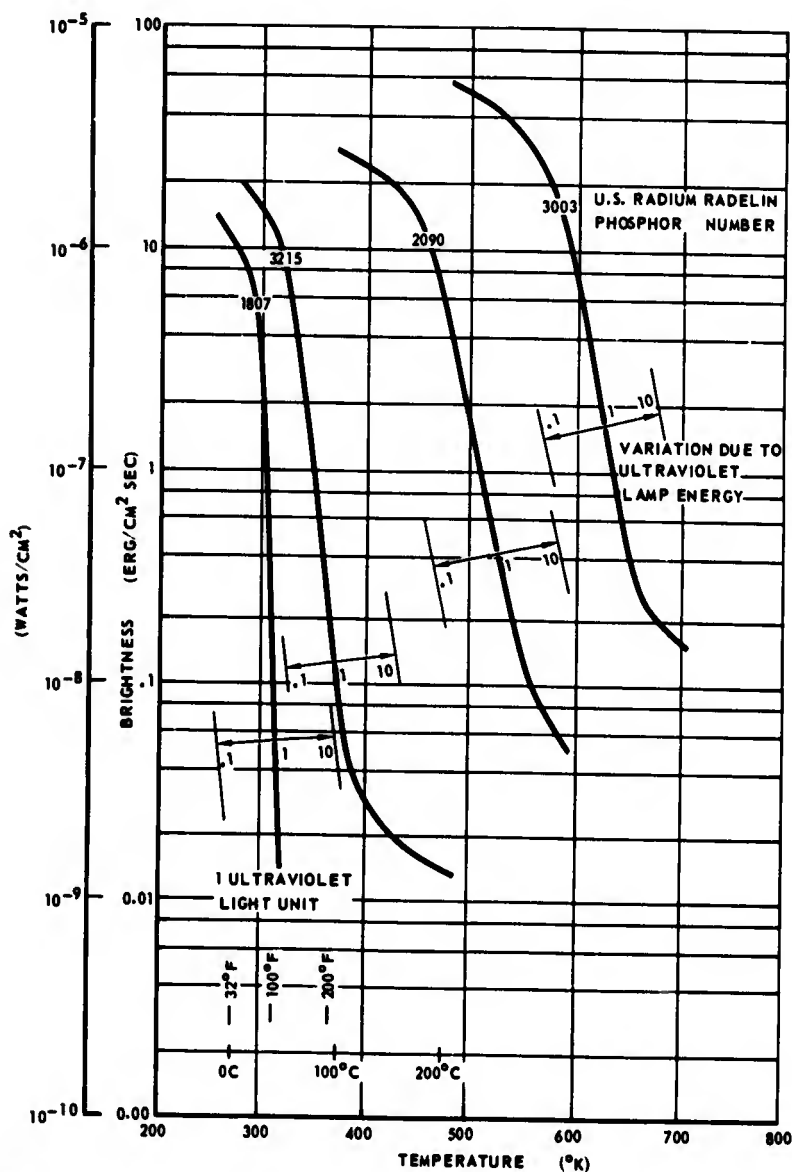


Fig.75 Brightness of four types of 'Radelin' phosphors as a function of the temperature and ultraviolet illuminating intensity. Curves relate to 1 ultraviolet light unit; this corresponds to a single 100 W mercury lamp with ultraviolet filter 134.62 cm from the model or two 15 W fluorescent 'blacklite' lamps 76.2 cm from the model and is approximately $100 \mu\text{W cm}^{-2}$. From Czyst and Kendall (127).

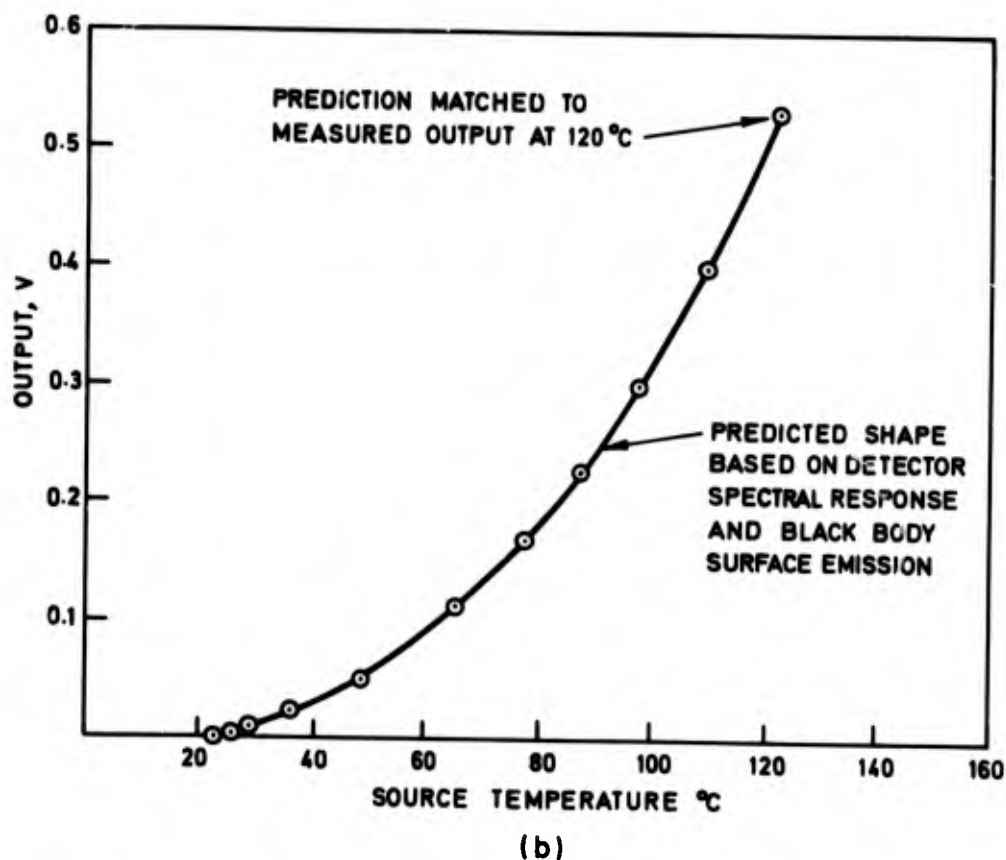
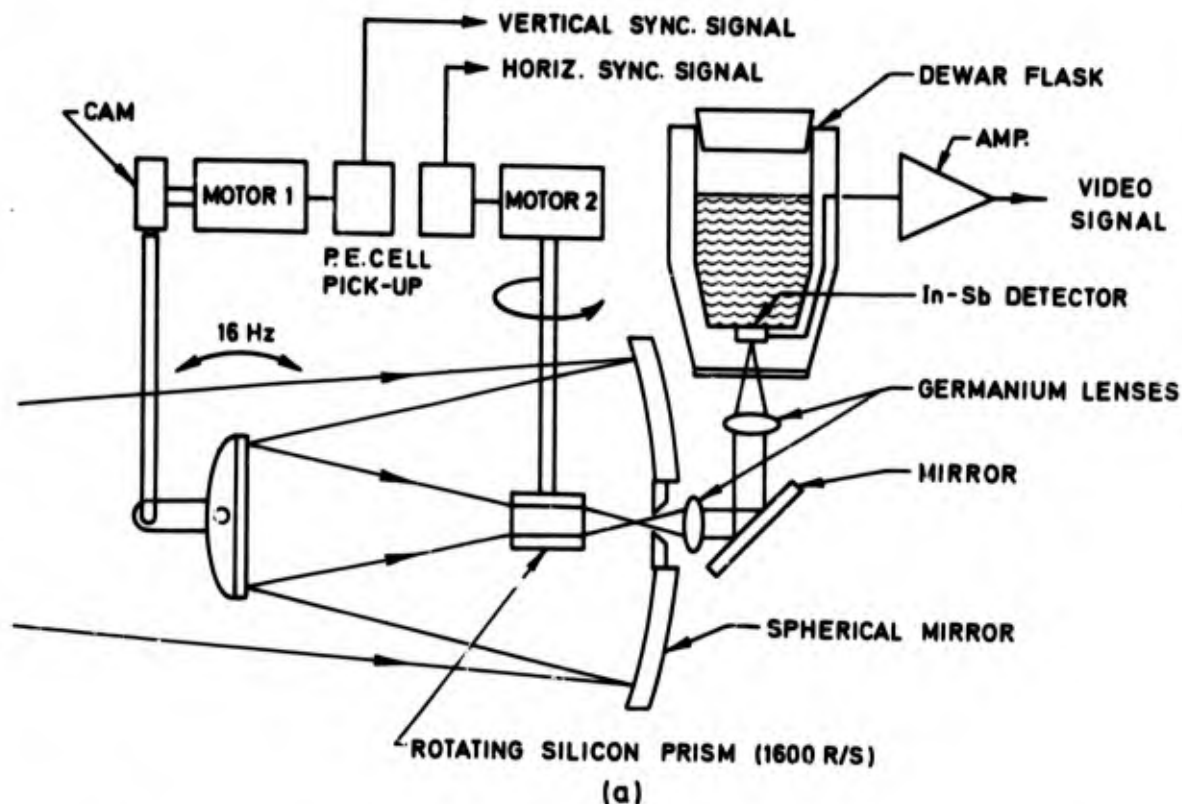


Fig.76

(a) Scanning infrared camera for surface temperature measurements. After Thomann and Frisk (109). (b) Calibration curve for the infrared camera output as a function of surface temperature. The form of the curve is predicted on the assumption that the emitted radiation is black body and this is fitted to the observed value at one temperature. Redrawn from Compton (110).

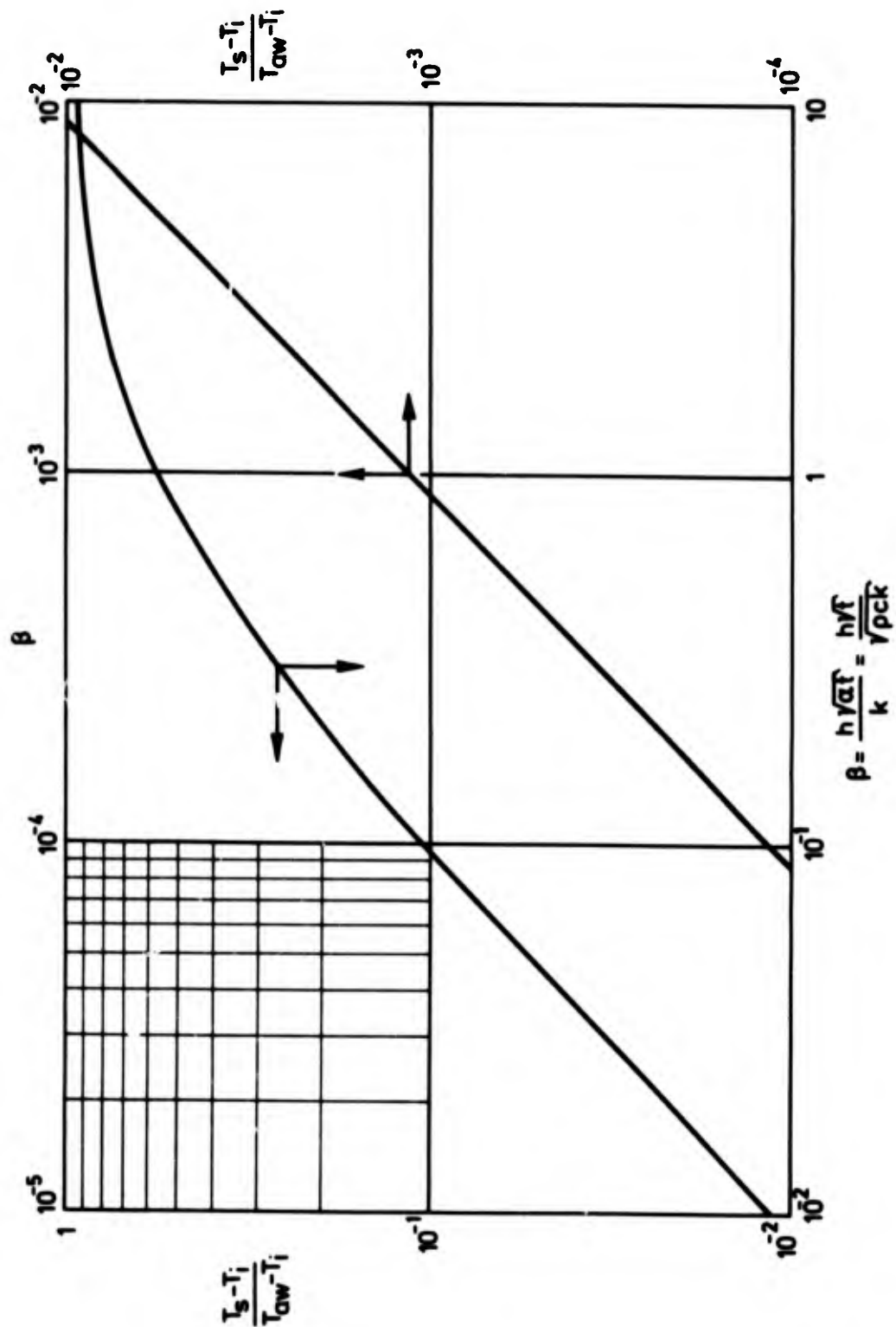


Fig.77

The ratio of the surface temperature rise ($T_s - T_i$) to the temperature difference ($T_{aw} - T_i$), where T_i is the initial model temperature, as a function of the dimensionless parameter $\beta = h \sqrt{at}/k$. Curves calculated for the case $h = \text{constant}$ and a semi-infinite solid.

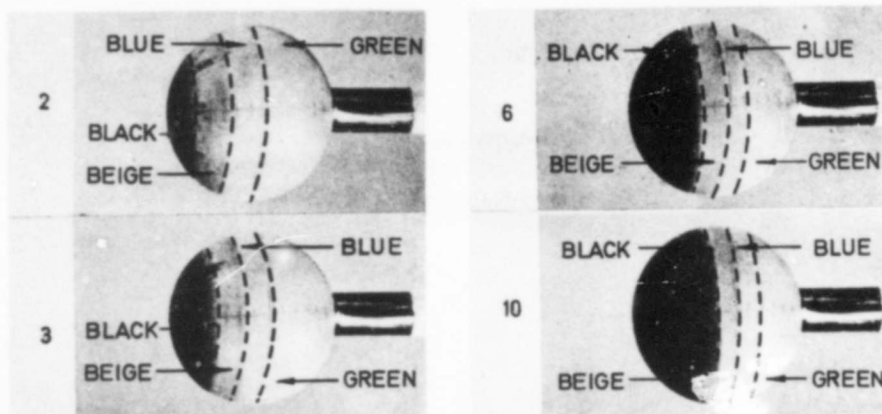


Fig.78

Colour changes observed on sphere of 6 cm diam. in hypersonic tunnel (ONERA R3). RTV insulation 5 mm thickness on wooden core. Times in seconds after initiation of flow.

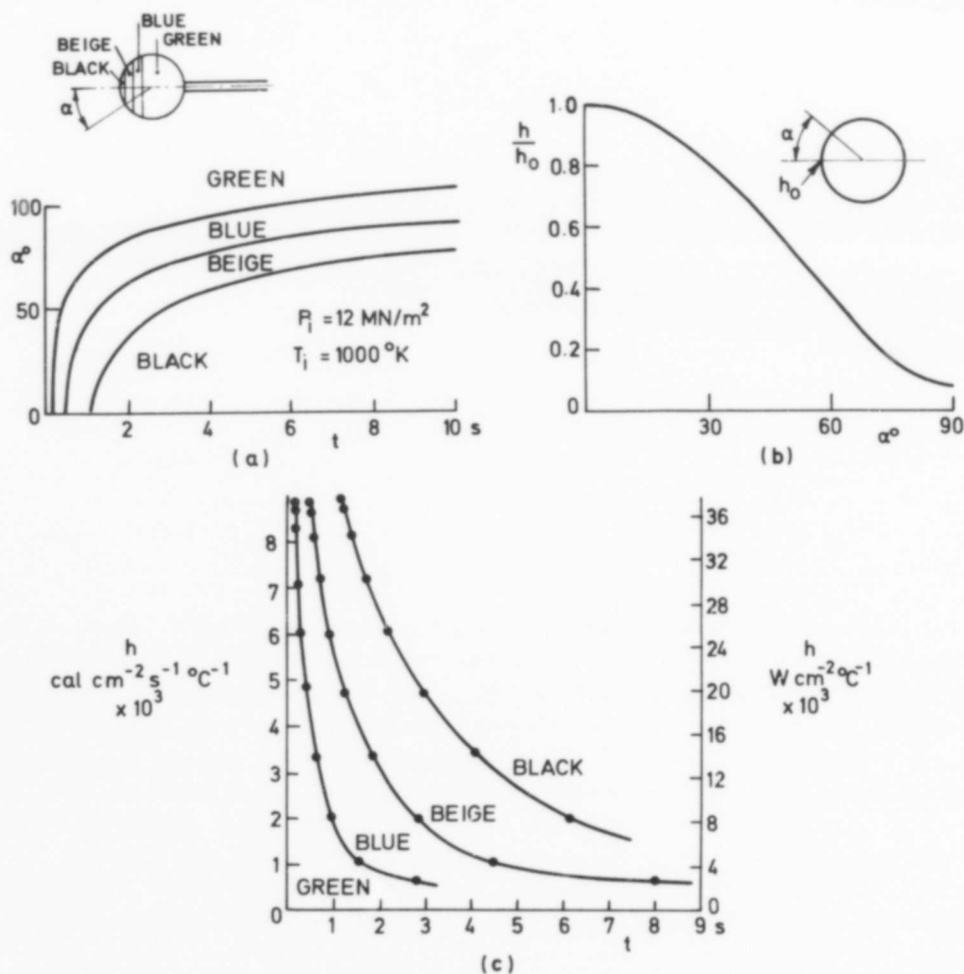


Fig.79

(a) Movement of colour change boundaries with increasing time. (b) Theoretical distribution of heat transfer coefficient (h/h_0) on sphere based on Smith (115). h_0 is stagnation point heat transfer coefficient deduced from Fay and Riddell (114). (c) Final calibration curves of colour change, time and heat transfer coefficient. Redrawn from Ceresuela et al (113).

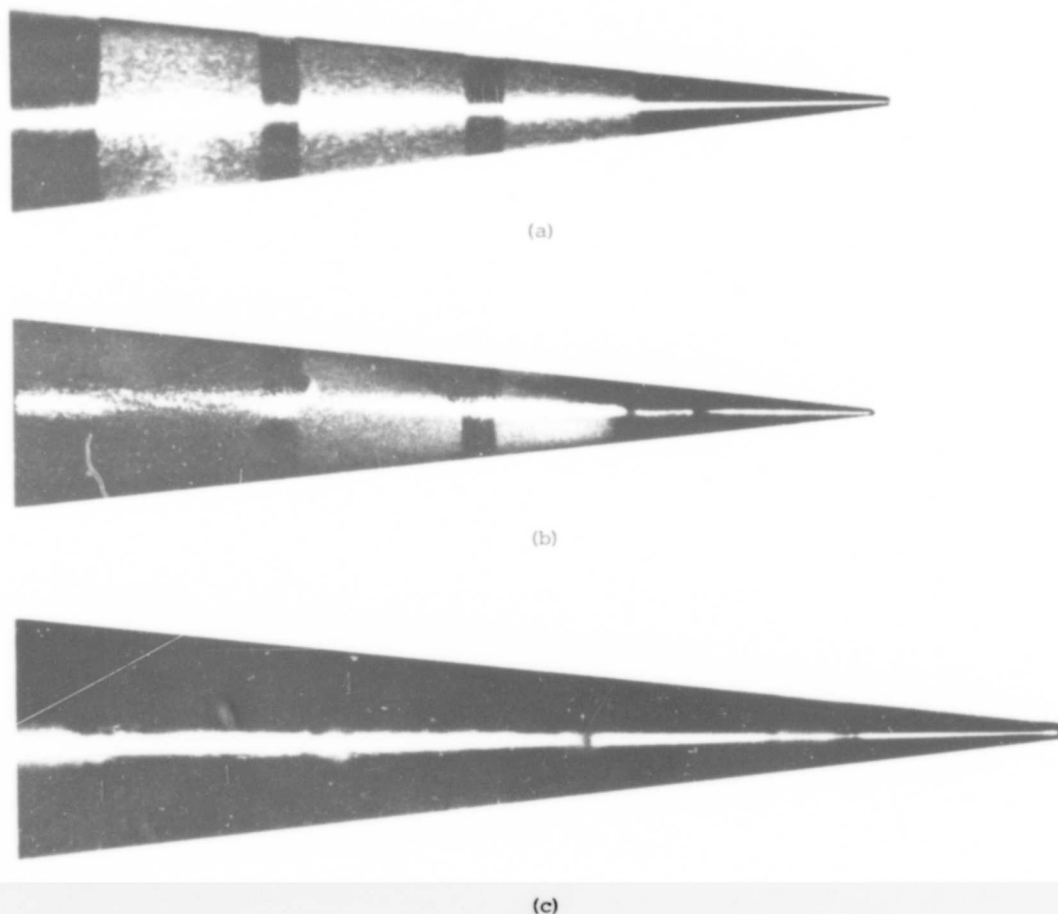
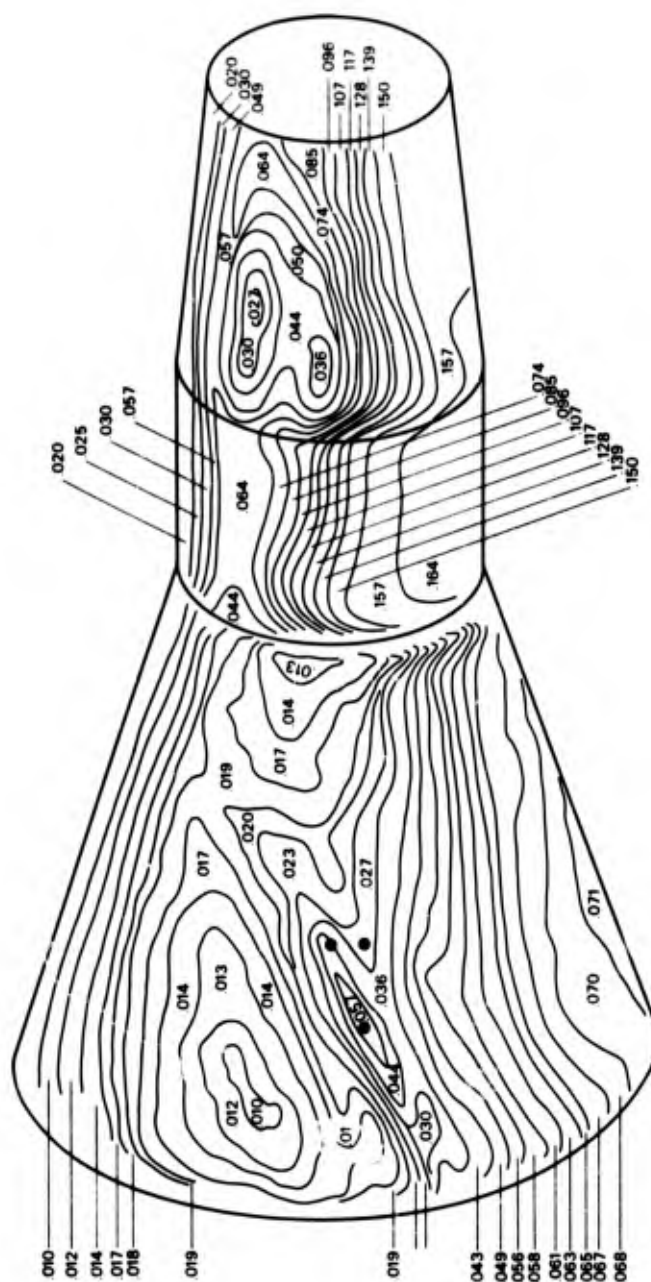


Fig.80

Surface temperature measurements in a ballistic range by means of phase change surface coatings. (a) Model before launch. The three broad grey bands define the area coated. Black areas caused by specular reflection from uncoated surface of model. (b) Front lighted laser photograph of model in flight at 3353 m s^{-1} in ambient pressure of $10,000 \text{ N m}^{-2}$. Model temperature below 1889 K , the critical phase change point for the coating. (c) Photograph of model in flight at 3444 m s^{-1} in ambient pressure of $10,000 \text{ N m}^{-2}$. Entire model surface is seen through the coating whose temperature is in this case above the critical of 380 K . Temperature sensitive phase change coating of 'Tempilaq', the Tempil Corporation, 132 West 22nd St, New York, N.Y. NOL Ballistics Range.



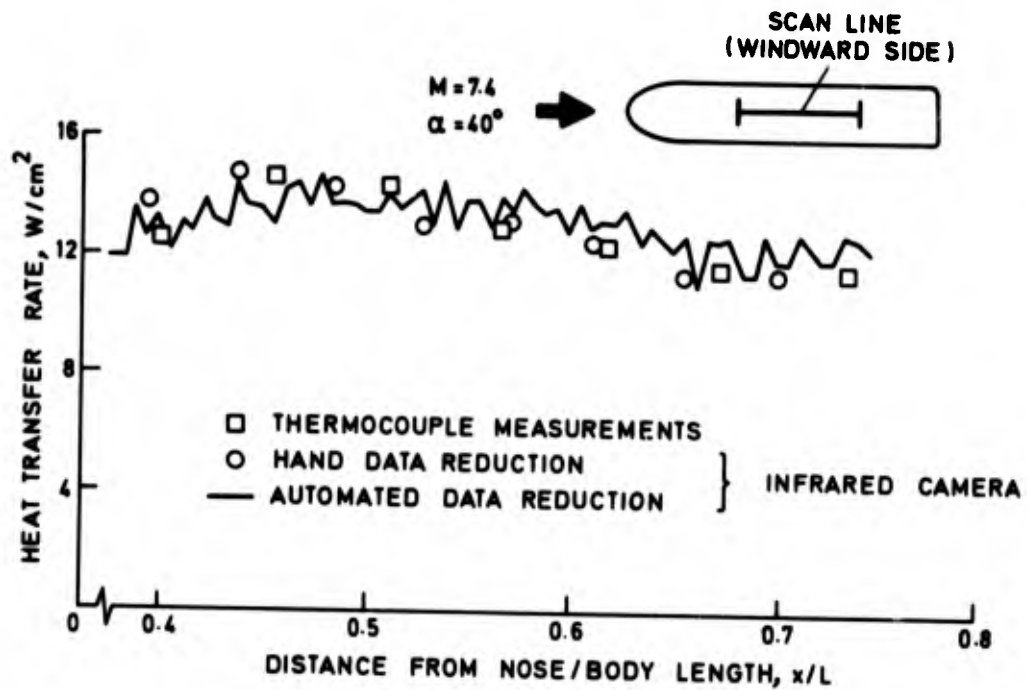


Fig.82

Comparison of heat transfer rates measured by infrared camera and surface thermocouples. Redrawn from Compton (110).

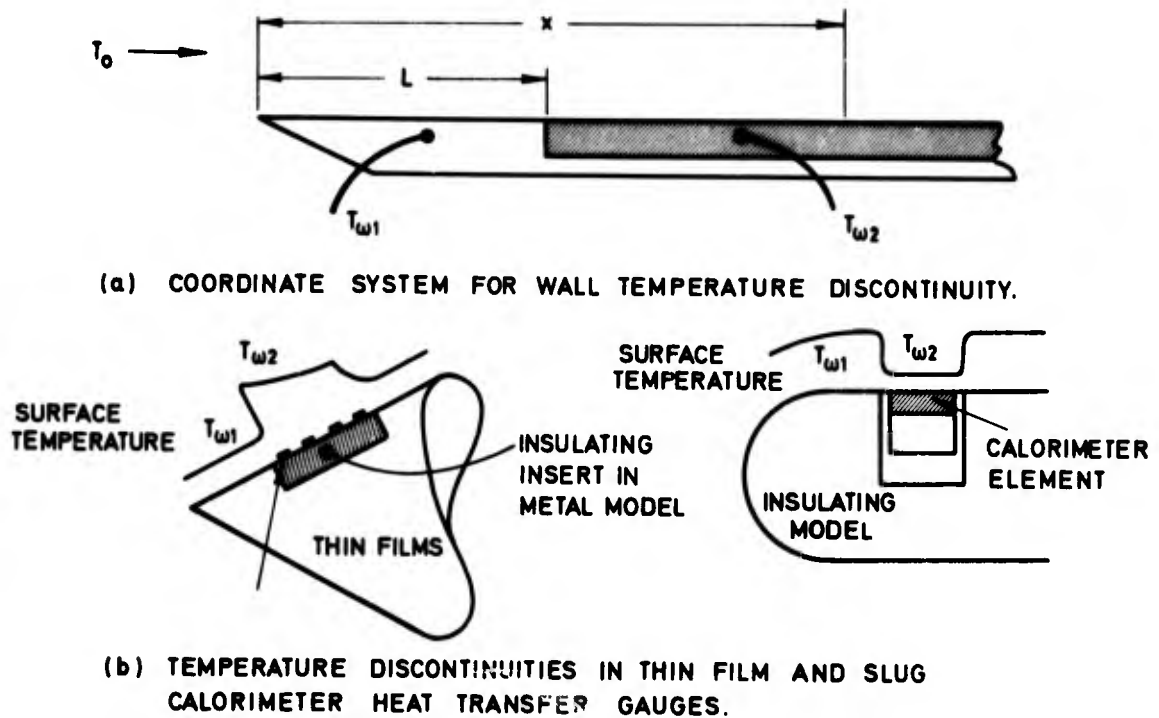


Fig.83

The effect of the presence of the heat transfer gauge on the distribution of surface temperature.

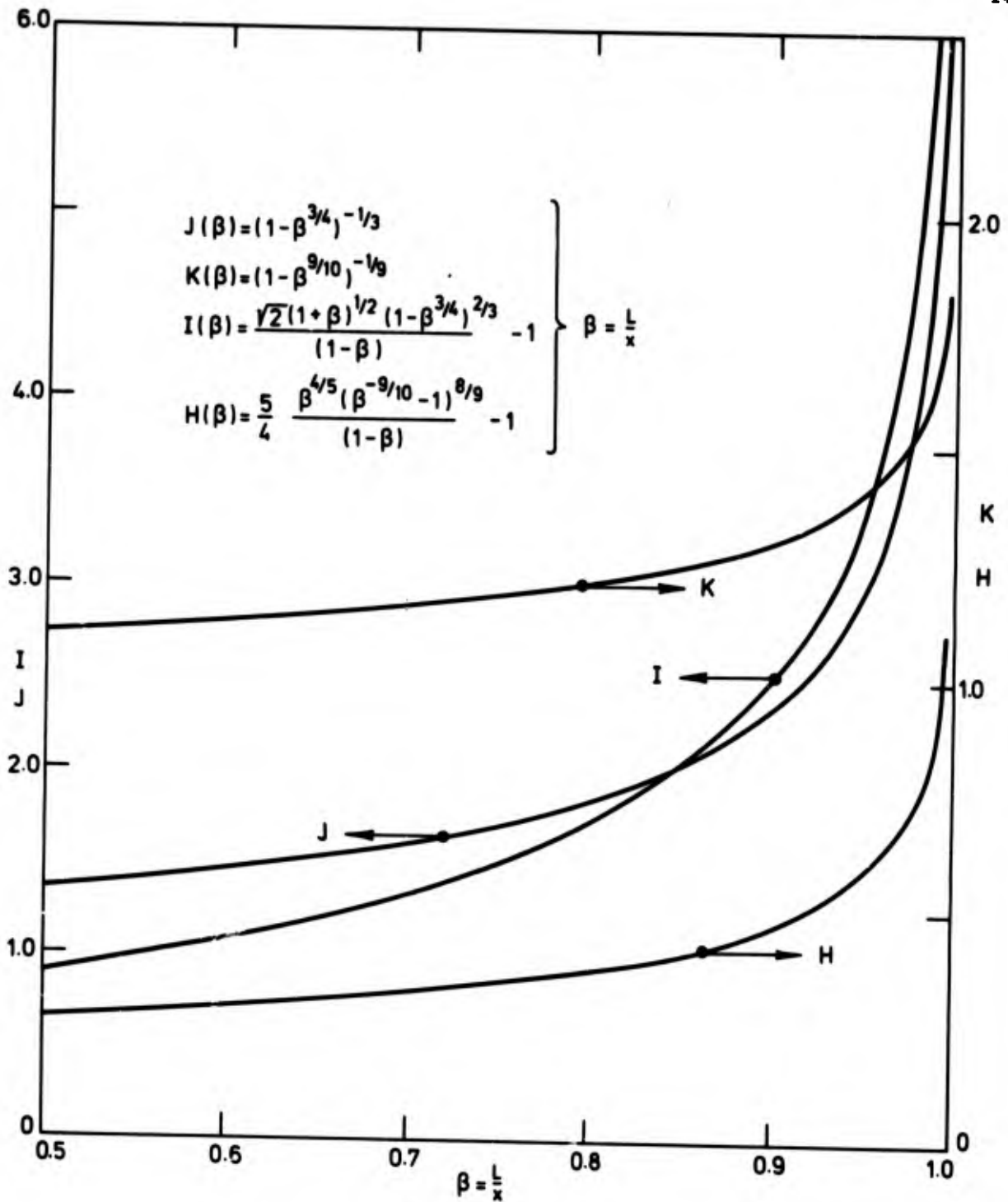


Fig.84

The functions $J(L/x)$, $K(L/x)$, $I(L/x)$ and $H(L/x)$ which enable the change in flat plate heat transfer coefficient due to a step function in surface temperature to be derived from Eqs (170, 171, 172, 173).

$$\frac{h}{h_0} = \frac{T_0 - T_{w1}}{T_0 - T_{w2}} + \frac{T_{w1} - T_{w2}}{T_0 - T_{w2}} J(L/x), \quad \frac{h_m}{h_{0(L+x)}} = 1 + \frac{T_{w1} - T_{w2}}{T_0 - T_{w2}} I(L/x) \quad (\text{laminar})$$

$$\frac{h}{h_0} = \frac{T_0 - T_{w1}}{T_0 - T_{w2}} + \frac{T_{w1} - T_{w2}}{T_0 - T_{w2}} K(L/x), \quad \frac{h_m^2}{h_{0(L+x)}^2} = 1 + \frac{T_{w1} - T_{w2}}{T_0 - T_{w2}} H(L/x) \quad (\text{turbulent})$$

The nomenclature is illustrated in Fig.83, h_m being the mean heat transfer coefficient between stations L and x and $h_{0, (L+x)/2}$ the heat transfer coefficient at a position $(L+x)/2$ in the absence of the temperature discontinuity.